NASA CR-134993
FR-7033



# SINGLE-STAGE EXPERIMENTAL EVALUATION OF LOW ASPECT RATIO, HIGHLY LOADED BLADING FOR COMPRESSORS

## PART IX - FINAL REPORT, STAGE F AND STAGE G

## VOLUME I

by J. G. Cheatham, J. D. Smith, and D. L. Wright

PRATT & WHITNEY AIRCRAFT
DIVISION OF UNITED TECHNOLOGIES CORPORATION
FLORIDA RESEARCH AND DEVELOPMENT CENTER

Prepared for
NATIONAL AERONAUTICS AND SPACE ADMINISTRATION

NASA Lewis Research Center
Contract NAS3-11158

| 1. Report No. | 2. Government Accession No. | 3. Recipient's Catalog No. |
|---|---|---|
| NASA CR-134993 | | |

| 4. Title and Subtitle | 5. Report Date |
|---|---|
| "SINGLE-STAGE EXPERIMENTAL EVALUATION OF LOW ASPECT RATIO, HIGHLY LOADED BLADING FOR COMPRESSORS", PART IX FINAL REPORT, STAGE F AND STAGE G, VOLUME I | May 1976 |
| | 6. Performing Organization Code |

| 7. Author(s) | 8. Performing Organization Report No. |
|---|---|
| J. G. Cheatham, J. D. Smith, and D. L. Wright | PWA FR 7033 |
| | 10. Work Unit No. |

| 9. Performing Organization Name and Address | 11. Contract or Grant No. |
|---|---|
| Pratt & Whitney Aircraft<br>Division of United Technologies Corporation<br>Florida Research and Development Center<br>West Palm Beach, Florida 33402 | NAS3-11158 |
| | 13. Type of Report and Period Covered |
| 12. Sponsoring Agency Name and Address<br>National Aeronautics and Space Administration<br>Washington, D. C. 20546 | Contractor Report |
| | 14. Sponsoring Agency Code |

15. Supplementary Notes

Project Manager, Dr. Wojciech Rostafinski, Fluid System Components Division, NASA-Lewis Research Center, Cleveland, Ohio 44135

16. Abstract

Two single-stage, 0.77 hub/tip ratio axial-flow compressors were tested to evaluate the effectiveness of low aspect ratio blading as a means of obtaining higher stage loadings. One compressor, designated Stage F, was comprised of circular arc blading with an aspect ratio of 0.9 for both the rotor and stator. This compressor was tested with uniform inlet flow, hub radial, tip radial, and 180° arc circumferential inlet distortion. The second compressor, designated Stage G, was comprised of multiple circular arc blading with an aspect ratio of 1.0 for both the rotor and stator. This compressor was tested with uniform inlet flow only. Design rotor tip speeds for Rotor F and Rotor G were 285 m/sec (934 ft/sec) and 327 m/sec (1074 ft/sec) respectively.

Both stages operated at high loading levels with adequate efficiency and operating range. The peak efficiencies and corresponding average stage diffusion factors for Stages F and G at design rotor speed were 86.4% and 84.1% and 0.59 and 0.55, respectively. The surge margin at peak efficiency for Stage F was 12.6% and the corresponding value for Stage G was 16.5%. Both stages experienced a loss in efficiency with increasing rotor speed; however, the multiple circular arc rotor delayed the characteristic loss in efficiency with increasing Mach number to higher Mach number.

Imposition of hub radial, tip radial, and circumferential distortion decreased, did not change, and increased Stage F surge flow, respectively; while stage surge pressure ratio remained relatively unchanged. Both radial distortions were substantially attenuated by the compressor but the circumferential distortion was only slightly attenuated at the walls.

| 17. Key Words (Suggested by Author(s)) | 18. Distribution Statement |
|---|---|
| Compressor<br>Low Aspect Ratio<br>Highly Loaded Blading | Unclassified - unlimited |

| 19. Security Classif. (of this report) | 20. Security Classif. (of this page) | 21. No. of Pages | 22. Price |
|---|---|---|---|
| Unclassified | Unclassified | 249 | $3.00 |

## FOREWORD

This report was prepared by the Pratt & Whitney Aircraft Division of United Technologies Corporation, West Palm Beach, Florida, to present the design and performance for Stage F and Stage G, which were tested under Task IV and Task V of Contract NAS3-11158, Single-Stage Experimental Evaluation of Low Aspect Ratio, Highly Loaded Blading for Compressors. Dr. Wojciech Rostafinski, NASA - Lewis Research Center, Fluid System Components Division, was Project Manager.

CONTENTS

CONTENTS (Continued)

## ILLUSTRATIONS

ILLUSTRATIONS (Continued)

ILLUSTRATIONS (Continued)

ILLUSTRATIONS (Continued)

ILLUSTRATIONS (Continued)

ILLUSTRATIONS (Continued)

ILLUSTRATIONS (Continued)

ILLUSTRATIONS (Continued)

ILLUSTRATIONS (Continued)

ILLUSTRATIONS (Continued)

ILLUSTRATIONS (Continued)

# TABLES

## SUMMARY

Two single-stage, axial flow compressors were designed and tested to evaluate the effectiveness of long chord low aspect ratio blading as a means of obtaining higher stage loadings. One compressor, designated Stage F, was comprised of circular arc blading with an aspect ratio of 0.9 for both the rotor and stator. This compressor, with a design weight flow of 17.11 kg/sec (37.73 lb/sec), was tested with uniform inlet flow, hub and tip radial inlet distortion and 180 deg arc circumferential inlet distortion. The second compressor, designated Stage G, was comprised of multiple circular arc blading with an aspect ratio of 1.0 for both the rotor and stator. This compressor, with a design weight flow of 16.72 kg/sec (36.86 lb/sec), was tested with uniform inlet flow only. A mean-line inlet prewhirl of 11 and 22 deg was generated for Stage F and Stage G, respectively, with a 63 series inlet guide vane set at two different chord angles. Both compressors were tested in a 0.77 hub/tip ratio, rotating drum/cantilevered stator compressor test rig. The specific flow and rotor inlet Mach numbers were consistent with design practice for middle stages of multistage compressors, but the blade loadings were appreciably higher.

At design equivalent rotor speed and flow conditions, Rotor F and Rotor F-Stator F pressure ratios were 1.595 and 1.561 for uniform inlet flow as compared to the design values of 1.614 and 1.565. The corresponding measured adiabatic efficiencies were 91.8 and 86.7% compared to design values of 94.5 and 87.8%. Imposition of hub radial, tip radial and circumferential distortion resulted in respective changes of -3.7, -1.4 and -4.5% in adiabatic efficiency and -0.047, +0.008 and -0.021 changes in pressure ratio for the rotor-stator relative to the uniform inlet flow values at design equivalent rotor speed and flow. At design equivalent rotor speed, compressor surge occurred at 4.2% lower flow with hub radial distortion, 1.4% higher flow with tip radial distortion, and 3.8% higher flow with circumferential distortion when compared to the uniform inlet surge flow. Both the hub radial and tip radial inlet flow distortions were substantially attenuated by the compressor but the circumferential inlet flow distortion was only slightly attenuated at the endwalls.

Rotor G and Rotor G-Stator G pressure ratios at design equivalent rotor speed and flow conditions were 1.640 and 1.585 as compared to performance goals of 1.657 and 1.604. The corresponding measured adiabatic efficiencies were 89.9 and 83.5% and the performance goals were 90.6 and 84.14%.

Comparison of the performance for Stage F and Stage G shows that both stages operated at high loading levels with adequate efficiency and operating range. The peak efficiencies and corresponding average stage diffusion factors for Stages F and G at design rotor speed were 86.4% and 84.1% and 0.59 and 0.55, respectively. The surge margin at peak efficiency for Stage F was 12.6% and the corresponding value for Stage G was 16.5%.

The peak pressure rise coefficient for Stage F at design rotor speed was approximately 30% higher than that of Stage G. Both stages exhibited substantial degradation in efficiency as the rotor speed was increased; however, Rotor G (multiple circular arc) delayed the onset of the rapid loss in efficiency with increasing Mach number to higher Mach numbers.

# INTRODUCTION

Advanced commercial and military gas turbines must emphasize fuel economy as well as minimize initial and maintenance costs. Toward this end, compressor technology leading to high stage pressure ratio with high efficiency is a prime requirement. The objective of this program is to provide this technology. During the initial phases, the performance potential of highly loaded tandem bladed compressor stages was investigated. Recent studies performed at Pratt & Whitney Aircraft have shown that another promising approach to obtaining higher stage loadings is through the use of low aspect ratio blading. Toward demonstration of this objective, two single-stage compressor programs, designated Task IV and Task V of Contract NAS3-11158, were undertaken to experimentally evaluate the performance of low aspect ratio blading configurations as a means of achieving high diffusion loading.

The stage evaluated in Task IV had circular arc blading and was designated Stage F, whereas, the stage evaluated in Task V, designated Stage G, had multiple circular arc blading. Stage F was tested with uniform inlet flow, hub and tip radial distortion, and circumferential distortion of the inlet flow. Stage G was tested with uniform inlet flow.

This two-volume Final Report presents the design of Stage F and the overall and blade element performance of Stage F and Stage G. Volume I is divided into three parts: Part I contains the aerodynamic and mechanical design and overall and blade element performance for Stage F, Part II contains the overall and blade element performance for Stage G, and Part III is a comparison of the two compressor stages.

Volume II presents tabulations of airfoil coordinates, overall and blade element performance data and the vector diagrams resulting from the tests of both Stage F and Stage G in SI (Metric) and U. S. Customary units. Throughout Volumes I and II of this report, the symbols defined in Reference 1 have been incorporated.

# PART I

## TASK IV - STAGE F AERODYNAMIC AND MECHANICAL DESIGN, AND OVERALL AND BLADE ELEMENT PERFORMANCE

Part I of this report summarizes the work performed under Task IV of Contract NAS3-11158. Task IV comprised a twelve-month program to design, fabricate and test a highly loaded low aspect ratio single stage compressor utilizing double circular arc (DCA) blading. This stage, designated as Stage F, was tested with uniform inlet flow, hub radial, tip radial and circumferential inlet distortion.

### Aerodynamic Design

#### Stage Selection

A meanline analysis study was performed to define a low aspect ratio, highly loaded multistage compressor from which a stage to be designated Stage F, and satisfying the requirements of table I could be extracted. This was done to ensure that the stage selected for this investigation was typical of one that could be used in an advanced compressor. The study was initiated assuming compressor blade row solidities, inlet Mach number, inlet specific flow, inlet hub-to-tip ratio and exit Mach number consistent with current compressors. The aspect ratio, and number of stages were then varied in a systematic manner to define a compressor of the desired loading level that has approximately the same length as current compressors. The results revealed that a six-stage, 9:1 pressure ratio compressor with an aspect ratio of 0.9 for each blade row would have about the same length as current compressors with a diffusion factor comparable to the values set forth in table I.

Table I. Design Guidelines

| | |
|---|---|
| Rotor Tip Diameter | 0.5 m (19.685 in.) minimum |
| Hub/Tip Ratio | 0.7 to 0.8 |
| Rotor Tip Speed | 285 m/sec (934 ft/sec) |
| Rotor Tip Diffusion Factor | 0.6 minimum |
| Rotor Blade Aspect Ratio | 0.85 to 1.0 |
| Rotor Tip Solidity | 1.3 approximate |
| Stator Hub Diffusion Factor | 0.6 minimum |
| Stator Blade Aspect Ratio | 0.85 to 1.0 |
| Stator Hub Solidity | 1.4 approximate |

The second stage of the 9:1 compressor was selected for this investigation because: (1) it was consistent with the guidelines presented in table I and (2) after slightly modifying the hub diameter while holding inlet specific flow and mean wheel speed constant, the resultant stage was easily adaptable to an existing compressor rig. A summary of the meanline designs for the high pressure compressor (HPC), the second stage of the high pressure compressor, and the comparable single-stage configuration selected for this program are presented in table II.

Table II. Meanline Design Summary

| Parameter | Compressor | | |
|---|---|---|---|
| | 9:1 HPC | Second Stage | Selected Single-Stage Configuration |
| Rotor Aspect Ratio | 0.9 | 0.9 | 0.9 |
| Stator Aspect Ratio | 0.9 | 0.9 | 0.9 |
| Rotor Solidity | 1.30 | 1.31 | 1.36 |
| Stator Solidity | 1.35 | 1.34 | 1.39 |
| Inlet Hub/Tip Ratio | 0.725 | 0.791 | 0.766 |
| $N/\sqrt{\theta}$, rpm | 10,676 | 9,805 | 9,936 |
| $U_{tip}/\sqrt{\theta}$, m/sec (ft/sec) | 336 (1,101) | 282 (926) | 285 (934) |
| Stage Pressure Ratio, PR | 9.0:1 | 1.56:1 | 1.56:1 |
| Inlet Specific Flow $W\sqrt{\theta}/A\delta$, kg/sec/m$^2$ ($lb_m$/sec/ft$^2$) | 1.453 (34.49) | 1.156 (27.43) | 1.156 (27.43) |
| Flow $W\sqrt{\theta}/\delta$, kg/sec (lb/sec) | 24.69 (54.44) | 17.42 (38.41) | 17.11 (37.73) |

Design Velocity Diagrams

The velocity diagrams were calculated by means of an iteration procedure using a streamline analysis computer program and the loss-loading correlations shown in figures 1 and 2 for the rotor and stator, respectively. This correlation was derived from test data of a similar low aspect ratio stage. The calculation procedure solved the continuity, energy, and radial equilibrium equations, which included the effects of streamline curvature and radial gradients of enthalpy and entropy. Since an existing inlet guide vane was selected for use in this program, loss and turning (i.e., rotor inlet total pressure and air angle) distributions used for the velocity diagram calculations were obtained from test data. The flow path dimensions for the existing drum rotor/cantilevered stator compressor rig, a rotor tip speed of 284.7 m/sec (934 ft/sec) and a stage inlet equivalent flow of 17.11 kg/sec (37.73 lb/sec) were maintained for the velocity diagram calculations. Blockage estimates of approximately 3, 6 and 8% at the rotor inlet, rotor exit and stator exit, respectively, were determined from test data for a similar compressor stage.

The velocity diagram calculation results for Stage F are shown in tables III, IV and V for the inlet guide vane, rotor and stator, respectively, along streamlines that pass through 5, 10, 15, 30, 50, 70, 85, 90 and 95% span at the rotor exit. Spanwise distributions of total pressure, axial velocity and absolute air angle for the rotor inlet, rotor exit and stator exit are shown in figures 3 through 5. Rotor relative air angle distributions are shown in figure 6. Spanwise loss coefficient and diffusion factor distributions are shown in figures 7 and 8 for Rotor F and Stator F, respectively. The predicted average rotor-only pressure ratio and adiabatic efficiency are 1.614 and 94.5%, respectively, at a rotor tip speed of 284.7 m/sec (934 ft/sec). The predicted average IGV - rotor pressure ratio and efficiency are 1.608 and 93.6%, respectively. The predicted average pressure ratio and efficiency for the stage (IGV - rotor-stator) at design rotor speed are 1.559 and 87.2%, respectively.

Table III. Stage F Inlet Guide Vane Vector Diagram Calculation Results

SI (Metric) Units

Equivalent Rotor Speed = 9936 rpm

Equivalent Weight Flow = 17.11 kg/sec

| | Percent Span From Tip | | | | | | | | | | |
|---|---|---|---|---|---|---|---|---|---|---|---|
| | Leading Edge | Trailing Edge | $V_{1e}$ (m/sec) | $V_{zle}$ (m/sec) | $V_{\theta le}$ (m/sec) | $\beta_{1e}$ (deg) | $V_{te}$ (m/sec) | $V_{zte}$ (m/sec) | $V_{\theta te}$ (m/sec) | $\beta_{te}$ (deg) | $\alpha$ (deg) |
| Hub | 95.4 | 95.8 | 116.43 | 116.43 | 0.0 | 0.0 | 131.52 | 128.32 | 23.32 | 10.36 | -0.75 |
| | 91.7 | 91.7 | 118.57 | 118.57 | 0.0 | 0.0 | 133.65 | 131.37 | 24.17 | 10.40 | -0.75 |
| | 86.8 | 86.9 | 119.48 | 119.48 | 0.0 | 0.0 | 134.26 | 131.98 | 24.48 | 10.51 | -1.15 |
| | 70.2 | 70.4 | 119.02 | 119.02 | 0.0 | 0.0 | 134.42 | 131.98 | 25.21 | 10.80 | -2.69 |
| | 49.0 | 49.2 | 118.87 | 118.87 | 0.0 | 0.0 | 134.26 | 131.67 | 27.34 | 11.74 | -4.21 |
| | 29.0 | 29.1 | 119.48 | 119.48 | 0.0 | 0.0 | 134.42 | 131.52 | 28.83 | 12.31 | -5.75 |
| | 13.5 | 13.8 | 119.48 | 119.48 | 0.0 | 0.0 | 133.96 | 130.45 | 30.88 | 13.34 | -7.27 |
| | 9.0 | 9.0 | 117.50 | 117.50 | 0.0 | 0.0 | 131.98 | 128.32 | 30.39 | 13.34 | -7.27 |
| Tip | 4.7 | 4.7 | 113.08 | 113.05 | 0.0 | 0.0 | 128.02 | 124.97 | 28.65 | 12.85 | -7.65 |

| | Percent Span From Tip | | | | |
|---|---|---|---|---|---|
| | Leading Edge | Trailing Edge | $M_{1e}$ | $\bar{\omega}$ | $P_{1e}$ ($N/cm^2$) |
| Hub | 95.4 | 95.8 | 0.3480 | 0.0765 | 10.148 |
| | 91.7 | 91.7 | 0.3527 | 0.0725 | 10.177 |
| | 86.8 | 86.9 | 0.3560 | 0.0668 | 10.190 |
| | 70.2 | 70.4 | 0.3539 | 0.0496 | 10.183 |
| | 49.0 | 49.2 | 0.3531 | 0.0395 | 10.185 |
| | 29.0 | 29.1 | 0.3559 | 0.0444 | 10.198 |
| | 13.5 | 13.8 | 0.3559 | 0.0527 | 10.201 |
| | 9.0 | 9.0 | 0.3495 | 0.0560 | 10.172 |
| Tip | 4.7 | 4.7 | 0.3360 | 0.0593 | 10.108 |

Table III. Stage F Inlet Guide Vane Vector Diagram Calculation Results

U. S. Customary Units

Equivalent Rotor Speed = 9936 rpm

Equivalent Weight Flow = 37.73 lb/sec

| | Percent Span From Tip | | | | | | | | | | |
|---|---|---|---|---|---|---|---|---|---|---|---|
| | Leading Edge | Trailing Edge | $V_{1e}$ (ft/sec) | $V_{zle}$ (ft/sec) | $V_{\theta le}$ (ft/sec) | $\beta_{1e}$ (deg) | $V_{te}$ (ft/sec) | $V_{zte}$ (ft/sec) | $V_{\theta te}$ (ft/sec) | $\beta_{te}$ (deg) | $\alpha$ (deg) |
| Hub | 95.4 | 95.8 | 382.0 | 382.0 | 0.0 | 0.0 | 431.5 | 421.0 | 76.5 | 10.36 | -0.75 |
| | 91.7 | 91.7 | 389.0 | 389.0 | 0.0 | 0.0 | 438.5 | 431.0 | 79.3 | 10.40 | -0.75 |
| | 86.8 | 86.9 | 392.0 | 392.0 | 0.0 | 0.0 | 440.5 | 433.0 | 80.3 | 10.51 | -1.15 |
| | 70.2 | 70.4 | 390.5 | 390.5 | 0.0 | 0.0 | 441.0 | 433.0 | 82.7 | 10.80 | -2.69 |
| | 49.0 | 49.2 | 390.0 | 390.0 | 0.0 | 0.0 | 440.5 | 432.0 | 89.7 | 11.74 | -4.21 |
| | 29.0 | 29.1 | 392.0 | 392.0 | 0.0 | 0.0 | 441.0 | 431.5 | 94.6 | 12.31 | -5.75 |
| | 13.5 | 13.8 | 392.0 | 392.0 | 0.0 | 0.0 | 439.5 | 428.0 | 101.3 | 13.34 | -7.27 |
| | 9.0 | 9.0 | 385.5 | 385.5 | 0.0 | 0.0 | 433.0 | 421.0 | 99.7 | 13.34 | -7.27 |
| Tip | 4.7 | 4.7 | 371.0 | 371.0 | 0.0 | 0.0 | 420.0 | 410.0 | 94.0 | 12.85 | -7.65 |

| | Percent Span From Tip | | | | |
|---|---|---|---|---|---|
| | Leading Edge | Trailing Edge | $M_{1e}$ | $\bar{\omega}$ | $P_{1e}$ (psia) |
| Hub | 95.4 | 95.8 | 0.3480 | 0.0765 | 14.718 |
| | 91.7 | 91.7 | 0.3527 | 0.0725 | 14.760 |
| | 86.8 | 86.9 | 0.3560 | 0.0668 | 14.779 |
| | 70.2 | 70.4 | 0.3539 | 0.0496 | 14.768 |
| | 49.0 | 49.2 | 0.3531 | 0.0395 | 14.771 |
| | 29.0 | 29.1 | 0.3559 | 0.0444 | 14.791 |
| | 13.5 | 13.8 | 0.3559 | 0.0527 | 14.795 |
| | 9.0 | 9.0 | 0.3495 | 0.0560 | 14.753 |
| Tip | 4.7 | 4.7 | 0.3360 | 0.0593 | 14.660 |

## Table IV. Rotor F Vector Diagram Calculation Results

SI (Metric) Units

Equivalent Rotor Speed = 9936 rpm

Equivalent Weight Flow = 17.11 kg/sec

| | Percent Span From Tip | | | | | | | | | | | | | |
|---|---|---|---|---|---|---|---|---|---|---|---|---|---|---|
| | Leading Edge | Trailing Edge | $V'_{1e}$ (m/sec) | $V_{zle}$ (m/sec) | $V'_{\theta le}$ (m/sec) | $\beta'_{le}$ (deg) | $\beta_{le}$ (deg) | $U_{le}$ (m/sec) | $V'_{te}$ (m/sec) | $V_{zte}$ (m/sec) | $V'_{\theta te}$ (m/sec) | $\beta'_{te}$ (deg) | $U_{te}$ (m/sec) | $\alpha$ (deg) |
| Hub | 96.0 | 95.0 | 259.38 | 168.55 | 197.36 | 49.40 | 7.90 | 220.68 | 154.90 | 150.88 | -36.00 | -13.55 | 220.95 | 0.21 |
| | 92.0 | 90.0 | 262.19 | 171.05 | 199.03 | 49.30 | 8.00 | 223.30 | 171.11 | 169.16 | -19.32 | - 6.10 | 223.88 | 0.43 |
| | 86.8 | 85.0 | 265.18 | 171.94 | 201.99 | 49.60 | 8.20 | 226.71 | 180.81 | 180.90 | - 5.70 | - 1.80 | 226.80 | 0.0 |
| | 70.8 | 70.0 | 272.80 | 172.52 | 211.38 | 50.80 | 8.60 | 237.20 | 191.11 | 190.80 | 19.78 | 6.00 | 235.58 | -1.35 |
| | 48.3 | 50.0 | 282.85 | 172.49 | 224.33 | 52.40 | 9.20 | 251.98 | 189.49 | 184.86 | 42.70 | 13.00 | 247.28 | -4.20 |
| | 28.2 | 30.0 | 291.85 | 172.67 | 235.40 | 53.70 | 9.90 | 265.18 | 185.99 | 175.41 | 62.27 | 19.40 | 258.99 | -5.69 |
| | 13.7 | 15.0 | 297.33 | 171.75 | 242.62 | 54.80 | 10.60 | 274.69 | 176.30 | 161.85 | 70.71 | 23.60 | 267.74 | -6.59 |
| | 9.0 | 10.0 | 299.62 | 170.75 | 246.13 | 55.50 | 10.50 | 277.76 | 170.99 | 155.30 | 71.96 | 24.90 | 270.66 | -6.76 |
| Tip | 4.0 | 5.0 | 302.51 | 167.94 | 251.46 | 56.60 | 9.90 | 281.06 | 163.98 | 147.68 | 72.21 | 26.20 | 273.59 | -7.20 |

| | Percent Span From Tip | | | | | | | | | | |
|---|---|---|---|---|---|---|---|---|---|---|---|
| | Leading Edge | Trailing Edge | $M'_{1e}$ | D | $\varpi'$ | Loss Parameter | Momentum Thickness Parameter | $P_{1e}$ ($N/cm^2$) | $T_{1e}$ (°K) | $P_{te}$ ($N/cm^2$) | $T_{te}$ (°K) |
| Hub | 96.0 | 95.0 | 0.782 | 0.690 | 0.268 | 0.0840 | 0.1876 | 10.046 | 288.17 | 16.272 | 339.61 |
| | 92.0 | 90.0 | 0.790 | 0.620 | 0.178 | 0.0578 | 0.1345 | 10.112 | 288.17 | 16.417 | 337.0 |
| | 86.8 | 85.0 | 0.800 | 0.578 | 0.111 | 0.0368 | 0.0875 | 10.135 | 288.17 | 16.527 | 335.17 |
| | 70.8 | 70.0 | 0.824 | 0.540 | 0.019 | 0.0066 | 0.0162 | 10.146 | 288.17 | 16.658 | 332.72 |
| | 48.3 | 50.0 | 0.854 | 0.555 | 0.002 | 0.0007 | 0.0018 | 10.144 | 288.17 | 16.493 | 331.61 |
| | 28.2 | 30.0 | 0.881 | 0.580 | 0.034 | 0.0124 | 0.0316 | 10.158 | 288.17 | 16.272 | 331.11 |
| | 13.7 | 15.0 | 0.897 | 0.627 | 0.085 | 0.0314 | 0.0793 | 10.149 | 288.17 | 16.093 | 332.06 |
| | 9.0 | 10.0 | 0.904 | 0.652 | 0.108 | 0.0399 | 0.1023 | 10.120 | 288.17 | 16.024 | 333.00 |
| Tip | 4.0 | 5.0 | 0.911 | 0.686 | 0.145 | 0.0536 | 0.1424 | 10.066 | 288.17 | 15.955 | 334.72 |

# Table IV. Rotor F Vector Diagram Calculation Results

U. S. Customary Units

Equivalent Rotor Speed = 9936 rpm

Equivalent Weight Flow = 37.73 lb/sec

| | Percent Span From Tip | | | | | | | | | | | | | |
|---|---|---|---|---|---|---|---|---|---|---|---|---|---|---|
| | Leading Edge | Trailing Edge | $V'_{1e}$ (ft/sec) | $V_{z1e}$ (ft/sec) | $V'_{\theta 1e}$ (ft/sec) | $\beta'_{1e}$ (deg) | $\beta_{1e}$ (deg) | $U_{1e}$ (ft/sec) | $V'_{te}$ (ft/sec) | $V_{zte}$ (ft/sec) | $V'_{\theta te}$ (ft/sec) | $\beta'_{te}$ (deg) | $U_{te}$ (ft/sec) | $\alpha$ (deg) |
| Hub | 96.0 | 95.0 | 851.0 | 553.0 | 647.5 | 49.40 | 7.90 | 724.0 | 508.2 | 495.0 | -118.1 | -13.55 | 724.9 | 0.21 |
| | 92.0 | 90.0 | 860.2 | 561.2 | 653.0 | 49.30 | 8.00 | 732.6 | 561.4 | 555.0 | - 63.4 | - 6.10 | 734.5 | 0.43 |
| | 86.8 | 85.0 | 870.0 | 564.1 | 662.7 | 49.60 | 8.20 | 743.8 | 593.2 | 593.5 | - 18.7 | - 1.80 | 744.1 | 0.0 |
| | 70.8 | 70.0 | 895.0 | 566.0 | 693.5 | 50.80 | 8.60 | 778.2 | 627.0 | 626.0 | 64.9 | 6.00 | 772.9 | -1.35 |
| | 48.3 | 50.0 | 928.0 | 565.9 | 736.0 | 52.40 | 9.20 | 826.7 | 621.7 | 606.5 | 140.1 | 13.00 | 811.3 | -4.20 |
| | 28.2 | 30.0 | 957.5 | 566.5 | 772.3 | 53.70 | 9.90 | 870.0 | 610.2 | 575.5 | 204.3 | 19.40 | 849.7 | -5.69 |
| | 13.7 | 15.0 | 975.5 | 563.5 | 796.0 | 54.80 | 10.60 | 901.2 | 578.4 | 531.0 | 232.0 | 23.60 | 878.4 | -6.59 |
| | 9.0 | 10.0 | 983.0 | 560.2 | 807.5 | 55.50 | 10.50 | 911.3 | 561.0 | 509.5 | 236.1 | 24.90 | 888.0 | -6.76 |
| Tip | 4.0 | 5.0 | 992.5 | 551.0 | 825.0 | 56.60 | 9.90 | 922.1 | 538.0 | 484.5 | 236.9 | 26.20 | 897.6 | -7.20 |

| | Percent Span From Tip | | | | | | | | | | |
|---|---|---|---|---|---|---|---|---|---|---|---|
| | Leading Edge | Trailing Edge | $M'_{1e}$ | D | $\bar{\omega}'$ | Loss Parameter | Momentum Thickness Parameter | $P_{1e}$ (psia) | $T_{1e}$ (°R) | $P_{te}$ (psia) | $T_{te}$ (°R) |
| Hub | 96.0 | 95.0 | 0.782 | 0.690 | 0.268 | 0.0840 | 0.1876 | 14.570 | 518.7 | 23.600 | 611.3 |
| | 92.0 | 90.0 | 0.790 | 0.620 | 0.178 | 0.0578 | 0.1345 | 14.665 | 518.7 | 23.810 | 606.6 |
| | 86.8 | 85.0 | 0.800 | 0.578 | 0.111 | 0.0368 | 0.0875 | 14.699 | 518.7 | 23.970 | 603.3 |
| | 70.8 | 70.0 | 0.824 | 0.540 | 0.019 | 0.0066 | 0.0162 | 14.715 | 518.7 | 24.160 | 598.9 |
| | 48.3 | 50.0 | 0.854 | 0.555 | 0.002 | 0.0007 | 0.0018 | 14.712 | 518.7 | 23.920 | 596.9 |
| | 28.2 | 30.0 | 0.881 | 0.580 | 0.034 | 0.0124 | 0.0316 | 14.733 | 518.7 | 23.600 | 596.0 |
| | 13.7 | 15.0 | 0.897 | 0.627 | 0.085 | 0.0314 | 0.0793 | 14.720 | 518.7 | 23.340 | 597.7 |
| | 9.0 | 10.0 | 0.904 | 0.652 | 0.108 | 0.0399 | 0.1023 | 14.678 | 518.7 | 23.240 | 599.4 |
| Tip | 4.0 | 5.0 | 0.911 | 0.686 | 0.145 | 0.0536 | 0.1424 | 14.599 | 518.7 | 23.140 | 602.5 |

Table V. Stator F Vector Diagram Calculation Results

SI (Metric) Units

Equivalent Rotor Speed = 9936 rpm

Equivalent Weight Flow = 17.11 kg/sec

| | Percent Span From Tip | | | | | | | | | | |
|---|---|---|---|---|---|---|---|---|---|---|---|
| | Leading Edge | Trailing Edge | $V_{le}$ (m/sec) | $V_{zle}$ (m/sec) | $V_{\theta le}$ (m/sec) | $\beta_{le}$ (deg) | $V_{te}$ (m/sec) | $V_{zte}$ (m/sec) | $V_{\theta te}$ (m/sec) | $\beta_{te}$ (deg) | $\alpha$ (deg) |
| Hub | 95.0 | 95.8 | 296.42 | 145.54 | 256.95 | 59.00 | 168.86 | 167.64 | 28.35 | 9.70 | 0.79 |
| | 90.0 | 92.0 | 297.64 | 171.30 | 243.84 | 54.30 | 174.04 | 171.30 | 28.96 | 9.70 | 1.70 |
| | 84.9 | 86.2 | 298.25 | 186.69 | 232.56 | 51.00 | 179.53 | 175.72 | 30.18 | 9.70 | 1.70 |
| | 69.7 | 69.9 | 295.96 | 202.08 | 215.95 | 46.90 | 187.76 | 184.86 | 31.70 | 9.70 | 2.34 |
| | 48.9 | 49.2 | 285.90 | 199.95 | 204.37 | 45.80 | 191.41 | 188.82 | 32.00 | 9.70 | 3.75 |
| | 30.0 | 29.5 | 274.62 | 191.26 | 197.21 | 46.10 | 185.93 | 183.49 | 31.09 | 9.70 | 4.80 |
| | 14.7 | 14.1 | 265.94 | 178.31 | 197.51 | 48.25 | 182.88 | 180.29 | 30.78 | 9.70 | 5.84 |
| | 9.8 | 9.3 | 263.35 | 172.21 | 199.19 | 49.50 | 182.58 | 179.98 | 30.48 | 9.70 | 6.21 |
| Tip | 4.8 | 4.5 | 260.91 | 163.98 | 202.08 | 51.10 | 182.58 | 179.98 | 30.48 | 9.70 | 6.73 |

| | Percent Span From Tip | | | | | | | |
|---|---|---|---|---|---|---|---|---|
| | Leading Edge | Trailing Edge | $M_{le}$ | D | $\bar{\omega}$ | Loss Parameter | Momentum Thickness Parameter | $P_{te}$ ($N/cm^2$) |
| Hub | 95.0 | 95.8 | 0.861 | 0.673 | 0.127 | 0.0401 | 0.1468 | 15.459 |
| | 90.0 | 92.0 | 0.868 | 0.652 | 0.125 | 0.0399 | 0.1139 | 15.583 |
| | 84.9 | 86.2 | 0.873 | 0.627 | 0.120 | 0.0390 | 0.0956 | 15.734 |
| | 69.7 | 69.9 | 0.868 | 0.581 | 0.097 | 0.0327 | 0.0681 | 16.038 |
| | 48.9 | 49.2 | 0.836 | 0.549 | 0.062 | 0.0220 | 0.0440 | 16.121 |
| | 30.0 | 29.5 | 0.800 | 0.554 | 0.069 | 0.0256 | 0.0255 | 15.879 |
| | 14.7 | 14.1 | 0.770 | 0.562 | 0.072 | 0.0277 | 0.0607 | 15.734 |
| | 9.8 | 9.3 | 0.760 | 0.564 | 0.068 | 0.0265 | 0.0610 | 15.679 |
| Tip | 4.8 | 4.5 | 0.749 | 0.567 | 0.065 | 0.0256 | 0.0631 | 15.631 |

Table V. Stator F Vector Diagram Calculation Results

U. S. Customary Units

Equivalent Rotor Speed = 9936 rpm

Equivalent Weight Flow = 37.73 lb/sec

| | Percent Span From Tip | | | | | | | | | | |
|---|---|---|---|---|---|---|---|---|---|---|---|
| | Leading Edge | Trailing Edge | $V_{le}$ (ft/sec) | $V_{zle}$ (ft/sec) | $V_{\theta le}$ (ft/sec) | $\beta_{le}$ (deg) | $V_{te}$ (ft/sec) | $V_{zte}$ (ft/sec) | $V_{\theta te}$ (ft/sec) | $\beta_{te}$ (deg) | $\alpha$ (deg) |
| Hub | 95.0 | 95.8 | 972.5 | 477.5 | 843.0 | 59.00 | 554.0 | 550.0 | 93.0 | 9.70 | 0.79 |
| | 90.0 | 92.0 | 976.5 | 562.0 | 800.0 | 54.30 | 571.0 | 562.0 | 95.0 | 9.70 | 1.70 |
| | 84.9 | 86.2 | 978.5 | 612.5 | 763.0 | 51.00 | 589.0 | 576.5 | 99.0 | 9.70 | 1.70 |
| | 69.7 | 69.9 | 971.0 | 663.0 | 708.5 | 46.90 | 616.0 | 606.5 | 104.0 | 9.70 | 2.34 |
| | 48.9 | 49.2 | 938.0 | 656.0 | 670.5 | 45.80 | 628.0 | 619.5 | 105.0 | 9.70 | 3.75 |
| | 30.0 | 29.5 | 901.0 | 627.5 | 647.0 | 46.10 | 610.0 | 602.0 | 102.0 | 9.70 | 4.80 |
| | 14.7 | 14.1 | 872.5 | 585.0 | 648.0 | 48.25 | 600.0 | 591.5 | 101.0 | 9.70 | 5.84 |
| | 9.8 | 9.3 | 864.0 | 565.0 | 653.5 | 49.50 | 599.0 | 590.5 | 100.0 | 9.70 | 6.21 |
| Tip | 4.8 | 4.5 | 856.0 | 538.0 | 663.0 | 51.10 | 599.0 | 590.5 | 100.0 | 9.70 | 6.73 |

| | Percent Span From Tip | | | | | | | |
|---|---|---|---|---|---|---|---|---|
| | Leading Edge | Trailing Edge | $M_{le}$ | D | $\bar{\omega}$ | Loss Parameter | Momentum Thickness Parameter | $P_{te}$ (psia) |
| Hub | 95.0 | 95.8 | 0.861 | 0.673 | 0.127 | 0.0401 | 0.1468 | 22.420 |
| | 90.0 | 92.0 | 0.868 | 0.652 | 0.125 | 0.0399 | 0.1139 | 22.600 |
| | 84.9 | 86.2 | 0.873 | 0.627 | 0.120 | 0.0390 | 0.0956 | 22.820 |
| | 69.7 | 69.9 | 0.868 | 0.581 | 0.097 | 0.0327 | 0.0681 | 23.260 |
| | 48.9 | 49.2 | 0.836 | 0.549 | 0.062 | 0.0220 | 0.0440 | 23.380 |
| | 30.0 | 29.5 | 0.800 | 0.554 | 0.069 | 0.0256 | 0.0255 | 23.030 |
| | 14.7 | 14.1 | 0.770 | 0.562 | 0.072 | 0.0277 | 0.0607 | 22.820 |
| | 9.8 | 9.3 | 0.760 | 0.564 | 0.068 | 0.0265 | 0.0610 | 22.740 |
| Tip | 4.8 | 4.5 | 0.749 | 0.567 | 0.065 | 0.0256 | 0.0631 | 22.670 |

Stage F Geometry

Inlet Guide Vane - An existing inlet guide vane, comprised of NACA Series 63-($C_{1_0}A_4K_6$) 06 sections, was used to obtain the desired rotor relative inlet air angle distribution. The metal geometries for inlet guide vane airfoil sections on planes tangent to conic surfaces that approximate the design streamlines of revolution are summarized in table VI.

Rotor F and Stator F - Simulated double-circular arc airfoils (i.e., the mean camber line and the suction and pressure surface lines of each blade element are lines with a constant rate of angle change with path distance on a specified conical streamline surface) were selected for the rotor and stator. The chord lengths, the number of blades, and the number of vanes evolved from the existing flowpath dimensions, the requirement for an aspect ratio of 0.9 in both blade rows, and the solidity required to obtain the specified loading for each blade row. Thickness-to-chord ratio distributions were selected to give the minimum airfoil cross sections consistent with safe mechanical design practices.

The blade element geometries for Stage F were selected in a manner similar to the procedure used in the design of Rotor D of NASA Contract NAS3-11158, Task III (Reference 2). First, the two-dimensional turning that combines with axial velocity ratio and secondary flow effects to produce the required blade row exit conditions was calculated using the procedure outlined in Reference 2. The two-dimensional turning was then used to calculate incidence and camber angles from a P&WA correlation of cascade minimum-loss incidence angle.

The double-circular-arc (DCA) airfoil sections selected for the rotor and stator were positioned on conic surfaces that approximate the design streamlines of revolution, and the resulting Rotor F and Stator F metal geometries on these conic surfaces are summarized in tables VII and VIII, respectively. Definition of the symbols used in tables VI through VIII are given in Appendix A and are shown in figure 9. The radial distributions of camber, incidence, and deviation angles are shown in figures 10 and 11 for Rotor F and figures 12 and 13 for Stator F. The design velocity diagram turning given in table IV and the camber incidence angles given in table VI were used to calculate the rotor deviation angle (i.e., $\delta^\circ = \phi - \Delta\beta + i_m$). The stator deviation angle was calculated in the same manner using the corresponding values given in tables VII and VIII. As previously stated, the Rotor F and Stator F airfoil sections were designed on conic surfaces which approximate design streamlines of revolution. For manufacturing purposes, however, the rotor and stator airfoil coordinates were given on planes tangent to cylindrical surfaces normal to a radial line termed the stacking line. The airfoil sections were positioned such that the stacking line passed through the center of gravity of the sections. A computer program provided a smooth fit of the airfoil properties and produced a set of coordinates for manufacturing purposes. Coordinates for redefined sections, which were used for manufacturing purposes, are given in Appendix A of Volume II. A photograph of the blade and vane is presented in figure 14.

Table VI. Stage F Inlet Guide Vane Geometry Data*

No. of Vanes: 42

Airfoil: NACA 63 ($C1_0A_4K_6$) 06 Average Chord Length: 3.886 cm (1.530 in.)

| | Percent Span From Tip | | | | | | | | |
|---|---|---|---|---|---|---|---|---|---|
| | Leading Edge | Trailing Edge | $\kappa_{le}$ | $\kappa_{te}$ | $\phi$ | $\gamma°$ | $\sigma$ | t/c | $\delta°$ |
| Hub | 95.4 | 95.8 | -5.90 | 17.00 | -22.90 | 5.70 | 1.220 | 0.06 | 6.64 |
| | 91.7 | 91.7 | -5.92 | 17.30 | -23.22 | 5.85 | 1.203 | 0.06 | 6.90 |
| | 86.8 | 86.9 | -5.97 | 17.68 | -23.65 | 6.00 | 1.182 | 0.06 | 7.17 |
| | 70.2 | 70.4 | -6.25 | 18.80 | -25.05 | 6.40 | 1.118 | 0.06 | 8.00 |
| | 49.0 | 49.2 | -6.66 | 20.24 | -26.90 | 6.95 | 1.043 | 0.06 | 8.50 |
| | 29.0 | 29.1 | -7.00 | 21.61 | -28.61 | 7.40 | 0.982 | 0.06 | 9.00 |
| | 13.5 | 13.8 | -7.32 | 22.70 | -30.02 | 7.85 | 0.939 | 0.06 | 9.36 |
| | 9.0 | 9.0 | -7.42 | 23.05 | -30.47 | 7.90 | 0.927 | 0.06 | 9.71 |
| Tip | 4.7 | 4.7 | -7.42 | 23.28 | -30.70 | 7.95 | 0.916 | 0.06 | 10.43 |

*Information included in this table is defined on planes tangent to conic surfaces which approximate design streamlines of revolution. The geometries were interpolated from existing vane sections designed on planes tangent to cylindrical surfaces.

Table VII. Rotor F Geometry Data*

No. of Blades: 31

Airfoil: Simulated Double-Circular-Arc**

Average Chord Length: 6.629 cm (2.61 in.)

| | Percent Span From Tip | | | | | | | | | |
|---|---|---|---|---|---|---|---|---|---|---|
| | Leading Edge | Trailing Edge | $\kappa'_{le}$ | $\kappa'_{te}$ | $\phi$ | $\gamma°$ | $\sigma$ | t/c | $i_m$ | $\delta°$ |
| Hub | 96.0 | 95.0 | 55.65 | -33.90 | 89.55 | 10.88 | 1.550 | 0.0686 | -6.25 | 20.35 |
| | 92.0 | 90.0 | 54.40 | -26.10 | 80.50 | 14.15 | 1.530 | 0.0673 | -5.10 | 20.00 |
| | 86.8 | 85.0 | 54.00 | -20.00 | 74.00 | 17.00 | 1.507 | 0.0658 | -4.40 | 18.20 |
| | 70.8 | 70.0 | 53.82 | - 8.00 | 61.82 | 22.91 | 1.442 | 0.0611 | -3.02 | 14.00 |
| | 48.3 | 50.0 | 54.45 | 2.20 | 52.25 | 28.32 | 1.360 | 0.0547 | -2.05 | 10.80 |
| | 28.2 | 30.0 | 55.45 | 9.50 | 45.95 | 32.48 | 1.290 | 0.0487 | -1.75 | 9.90 |
| | 13.7 | 15.0 | 56.67 | 11.30 | 45.37 | 33.99 | 1.242 | 0.0443 | -1.87 | 12.30 |
| | 9.0 | 10.0 | 57.55 | 10.90 | 46.65 | 34.22 | 1.228 | 0.0428 | -2.05 | 14.00 |
| Tip | 4.4 | 5.0 | 59.00 | 9.60 | 49.40 | 34.30 | 1.214 | 0.0414 | -2.40 | 16.60 |

*Information included in this table is defined on planes tangent to the conic surfaces, which approximate design streamlines of revolution.

**Mean camber line and suction and pressure surface lines of each blade element are lines with a constant rate of angle change with path distance on the conic surface, which approximates the design streamline of revolution.

Table VIII. Stator F Geometry Data*

No. of Vanes: 36

Airfoil: Simulated Double-Circular-Arc**

Average Chord Length: 5.715 cm (2.25 in.)

| | Percent Span From Tip | | | | | | | | | |
|---|---|---|---|---|---|---|---|---|---|---|
| | Leading Edge | Trailing Edge | $\kappa_{le}$ | $\kappa_{te}$ | $\phi$ | $\gamma°$ | $\sigma$ | t/c | $i_m$ | $\delta°$ |
| Hub | 95.0 | 95.8 | 65.00 | -5.25 | 70.25 | 29.88 | 1.562 | 0.0509 | -6.00 | 14.95 |
| | 90.0 | 92.0 | 59.40 | -6.00 | 65.40 | 26.70 | 1.543 | 0.0518 | -5.10 | 15.70 |
| | 84.9 | 86.2 | 55.80 | -5.80 | 61.60 | 25.00 | 1.517 | 0.0529 | -4.80 | 15.50 |
| | 69.7 | 69.9 | 52.30 | -4.75 | 57.05 | 23.78 | 1.461 | 0.0560 | -5.40 | 14.45 |
| | 48.9 | 49.2 | 52.60 | -4.10 | 56.70 | 24.25 | 1.388 | 0.0602 | -6.80 | 13.80 |
| | 30.0 | 29.5 | 54.55 | -4.00 | 58.55 | 25.28 | 1.326 | 0.0640 | -8.45 | 13.70 |
| | 14.7 | 14.1 | 57.50 | -4.00 | 61.50 | 26.75 | 1.280 | 0.0671 | -9.25 | 13.70 |
| | 9.8 | 9.3 | 58.70 | -3.20 | 61.90 | 27.75 | 1.266 | 0.0681 | -9.20 | 12.90 |
| Tip | 4.8 | 4.5 | 60.20 | -2.30 | 62.50 | 28.95 | 1.252 | 0.0691 | -9.10 | 12.00 |

*Information included in this table is defined on planes tangent to the conic surfaces, which approximate design streamlines of revolution.

**Mean camber line and suction and pressure surface lines of each blade element are lines with a constant rate of angle change with path distance on the conic surface, which approximates the design streamline of revolution.

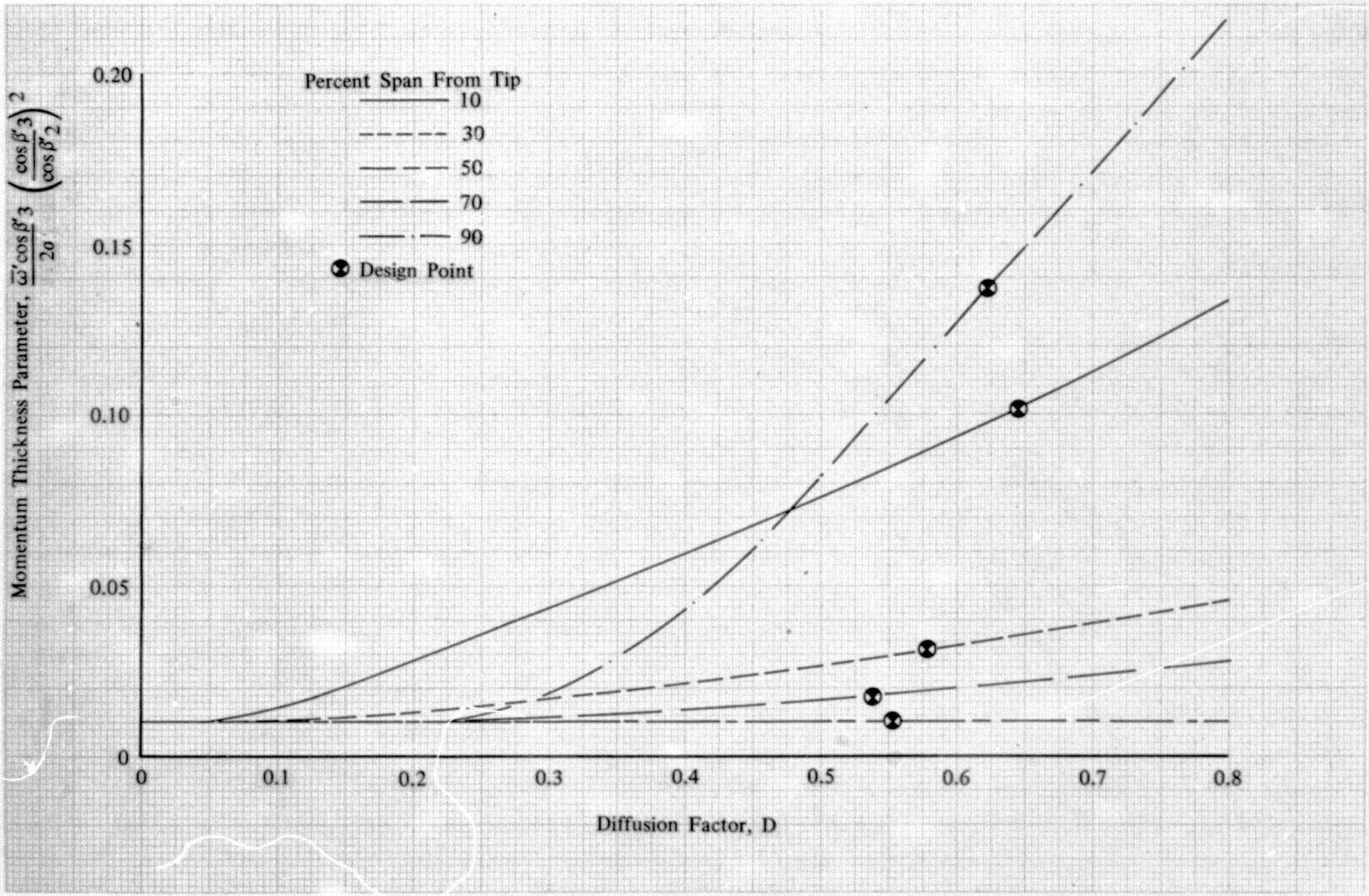


Figure 1. Rotor F Momentum Thickness Parameter vs Diffusion Factor

DF 102089

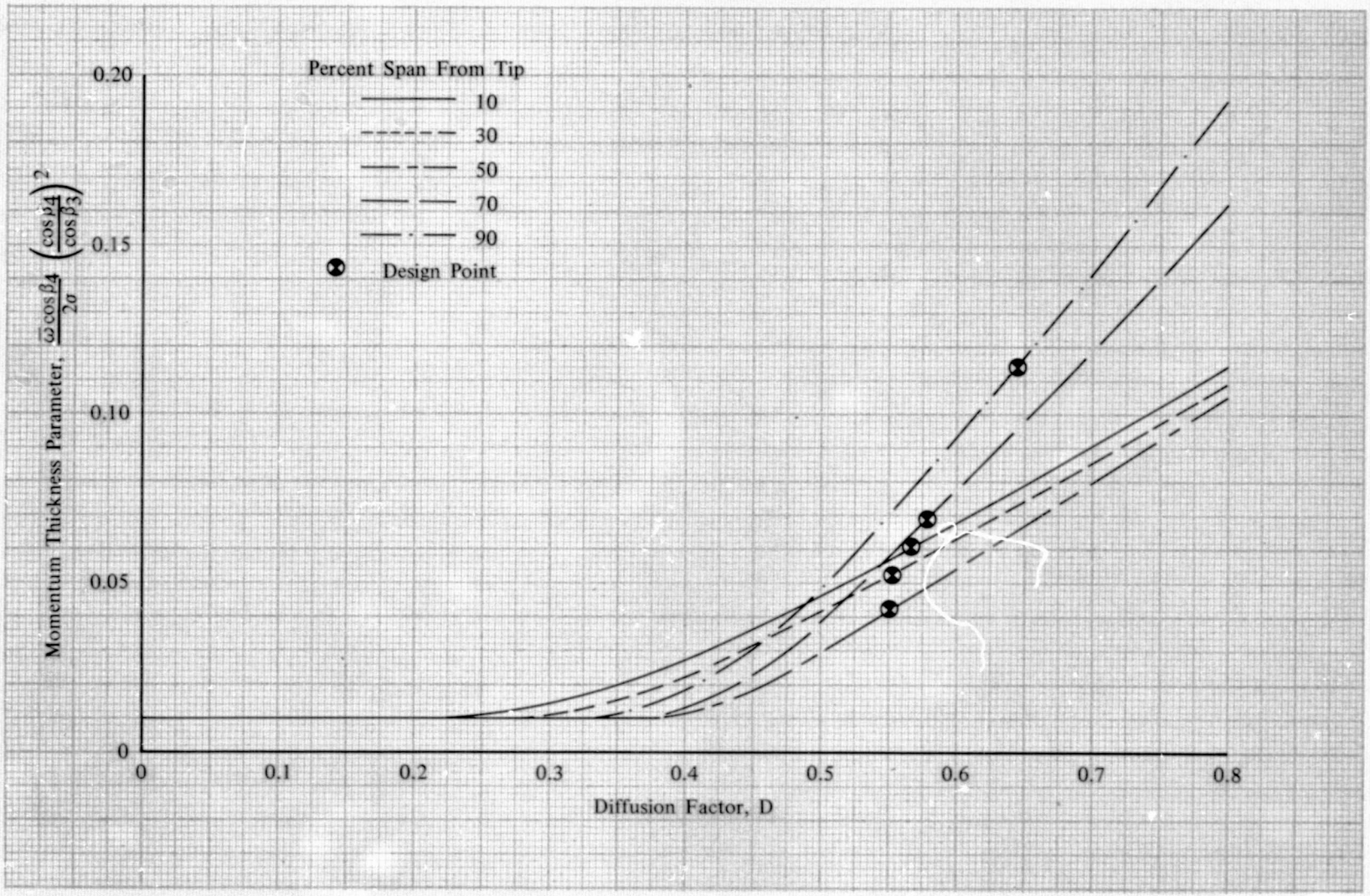


Figure 2. Stator F Momentum Thickness Parameter vs Diffusion Factor

DF 102090

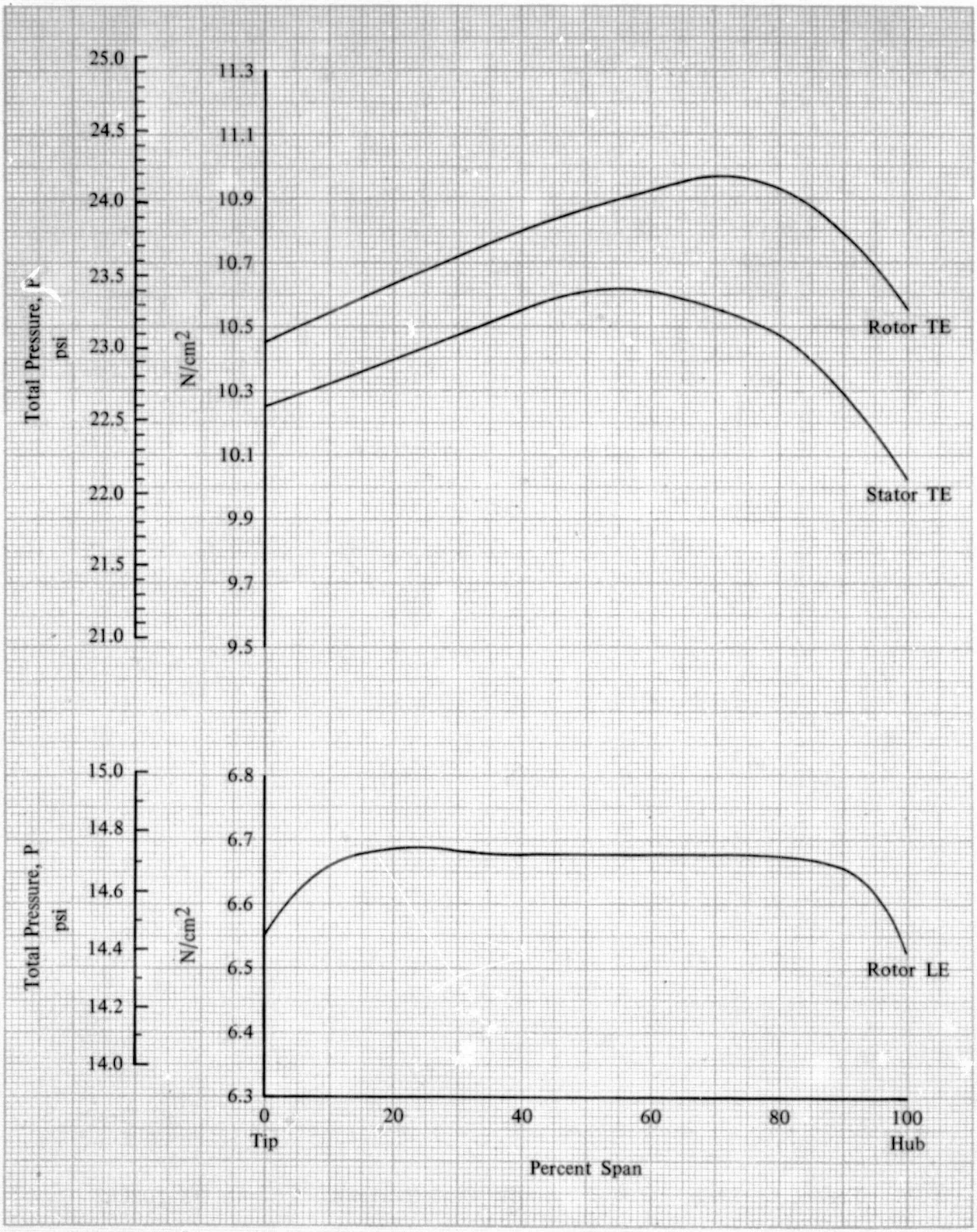


Figure 3. Stage F Total Pressure Distributions DF 102091

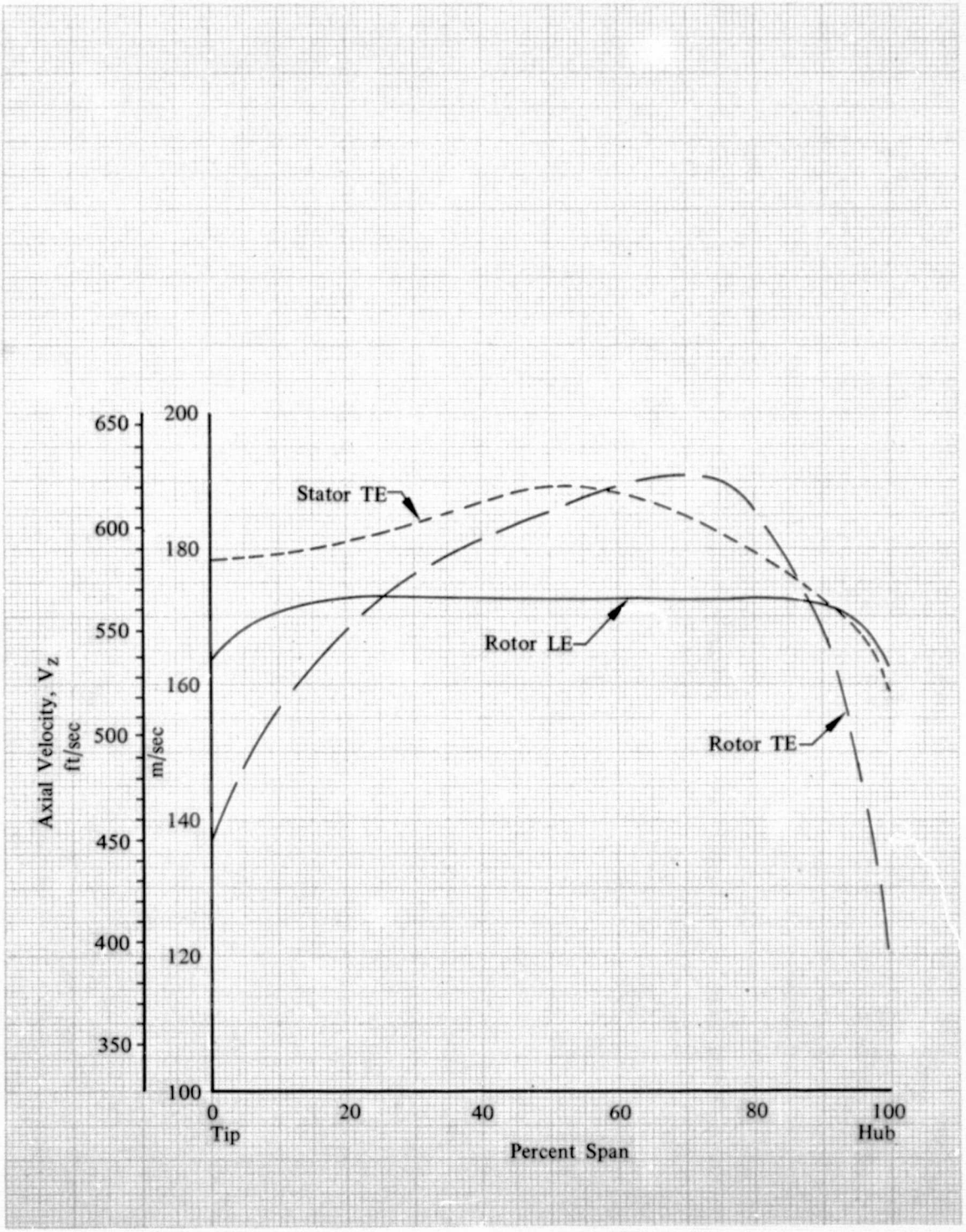


Figure 4. Stage F Axial Velocity Distributions DF 102092

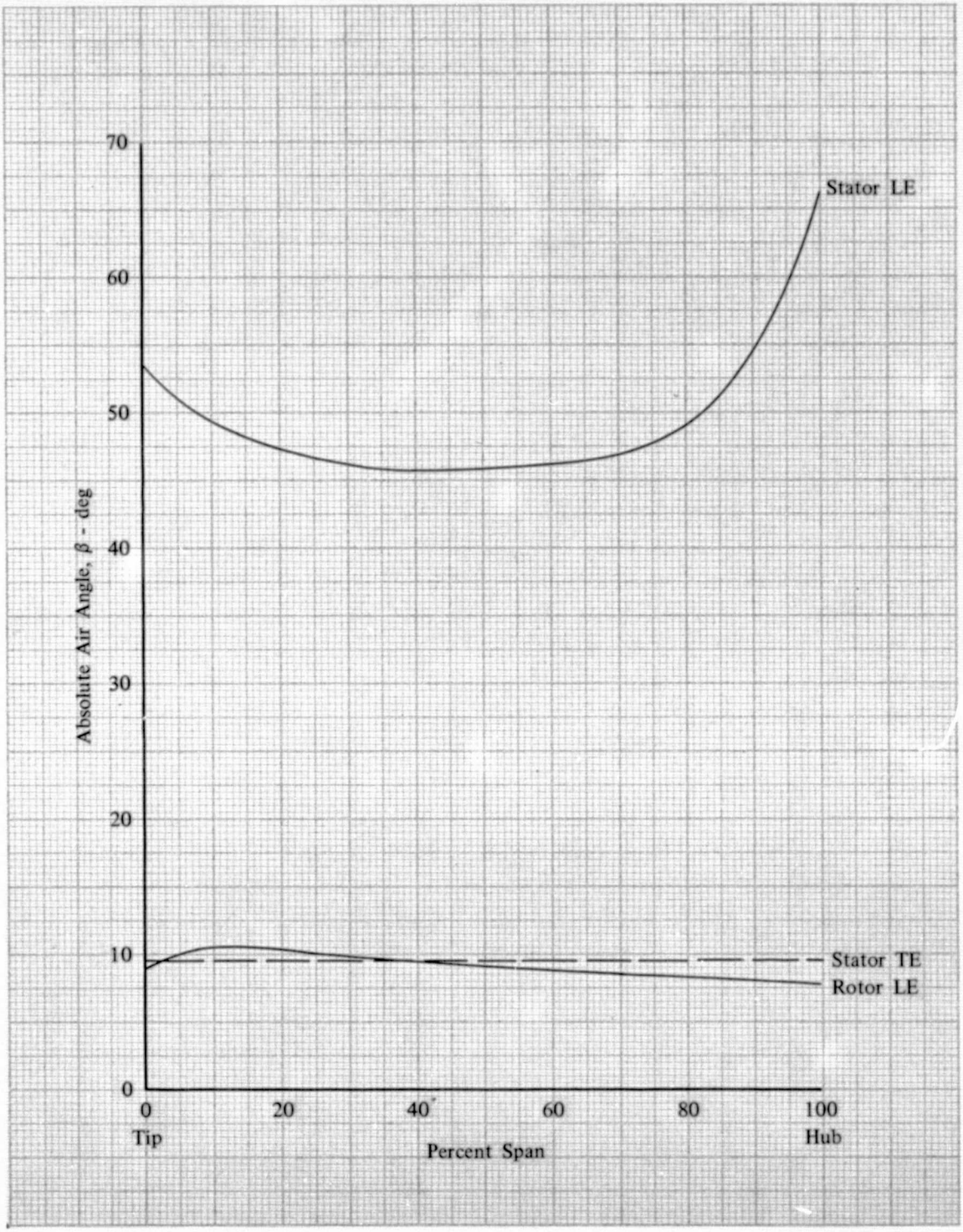


Figure 5. Stage F Absolute Air Angle Distributions DF 102093

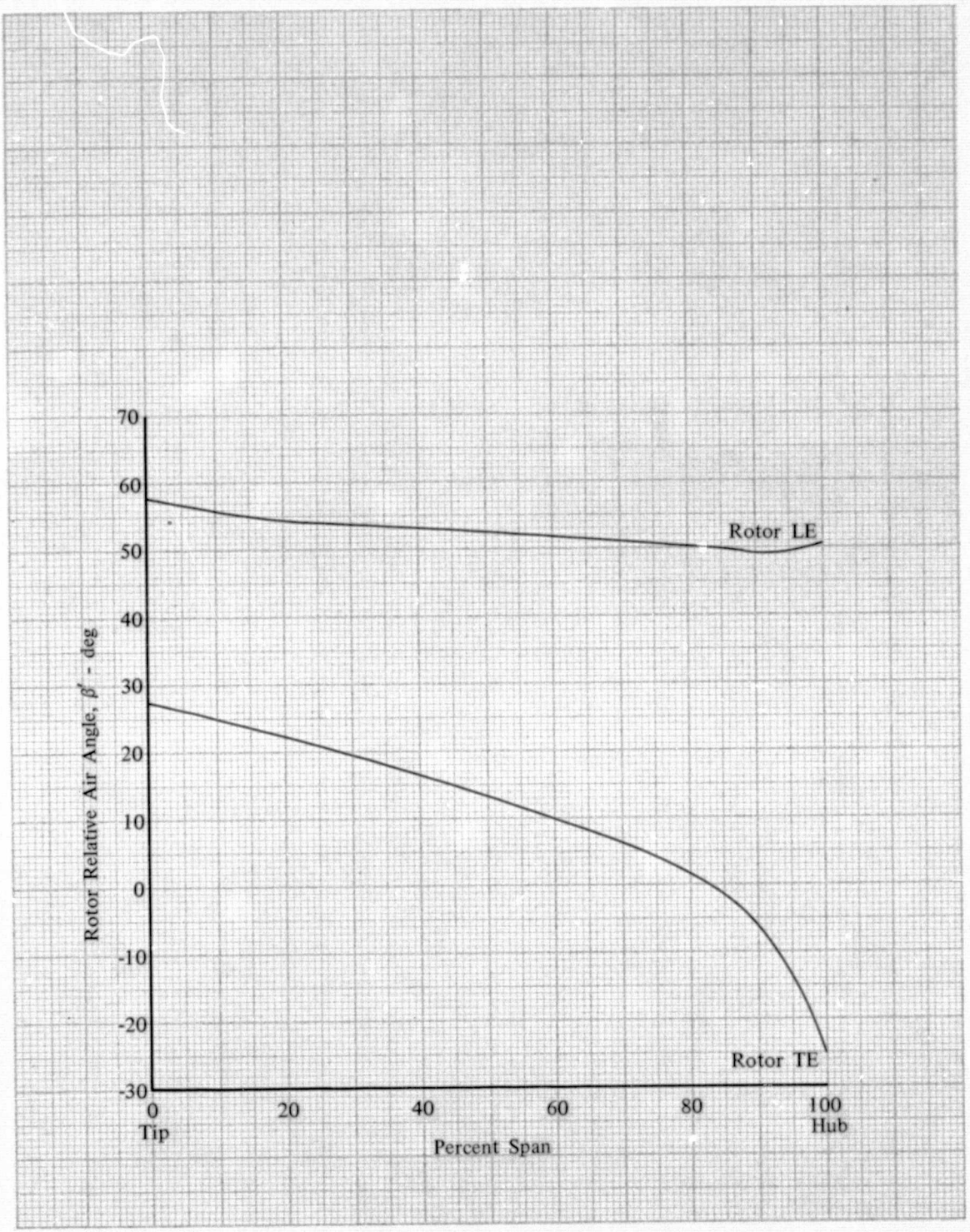


Figure 6. Rotor F Relative Air Angle Distributions DF 102094

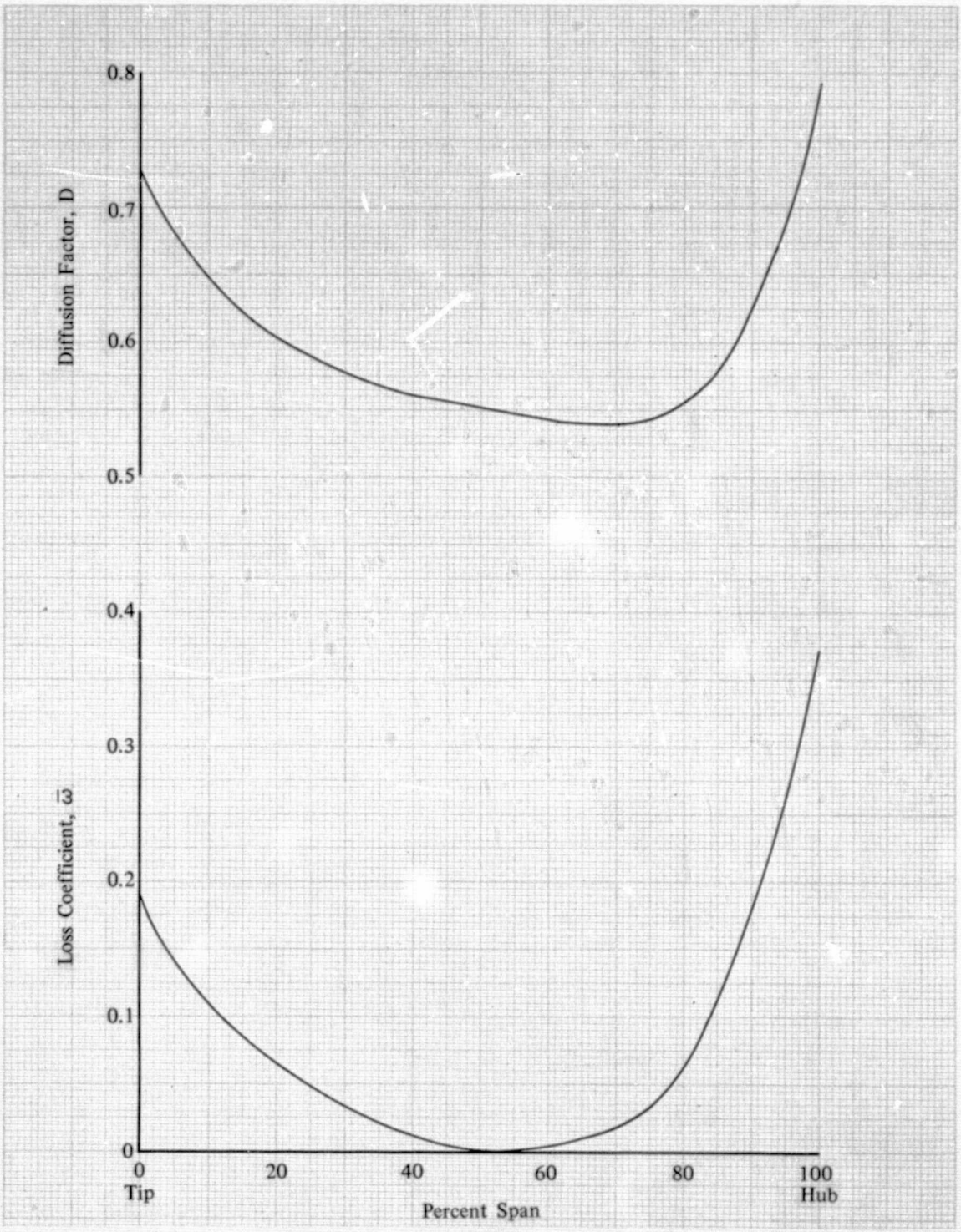


Figure 7. Rotor F Loss Coefficient and Diffusion Factor Distributions DF 102095

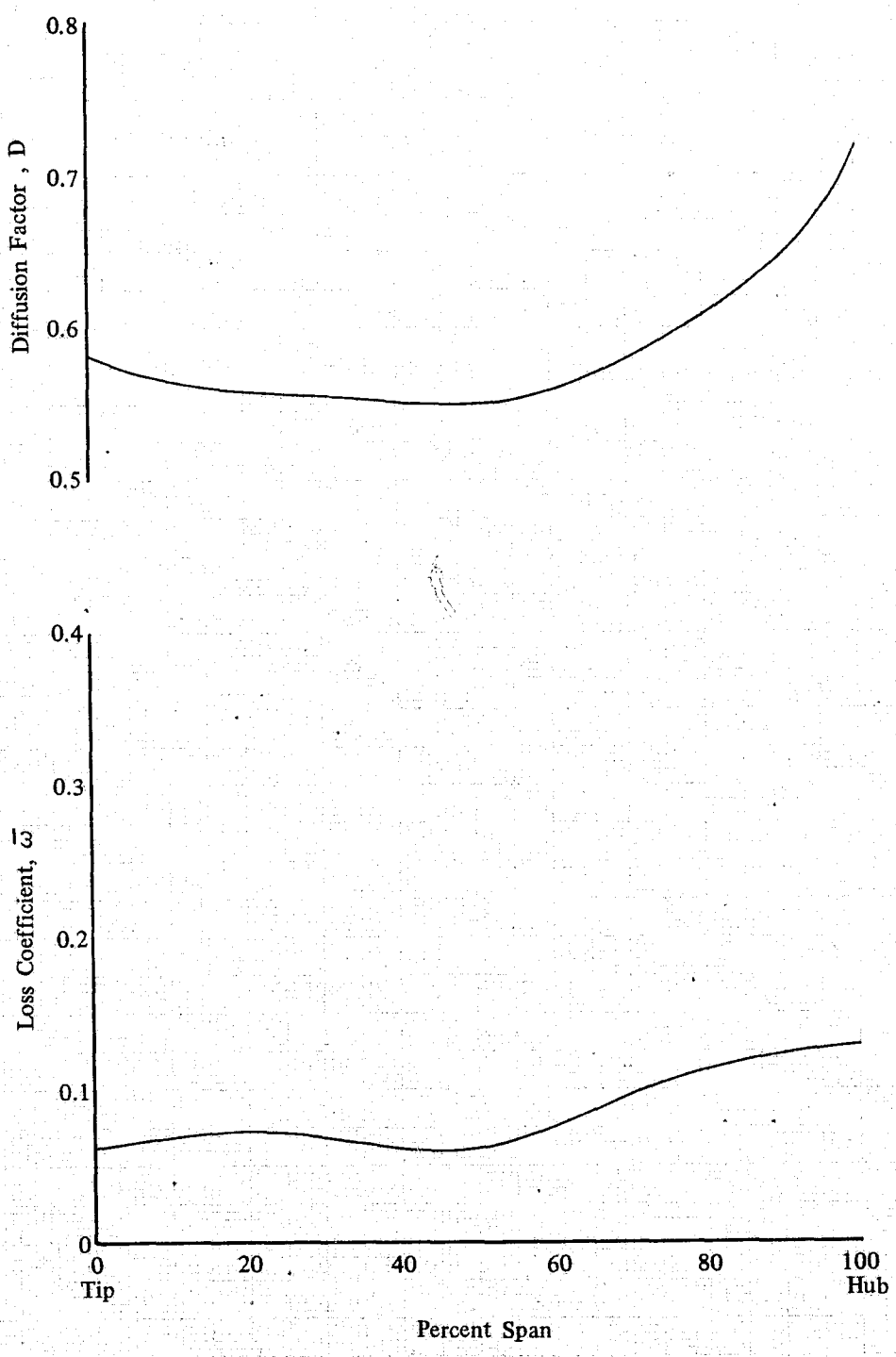


Figure 8. Stator F Loss Coefficient and Diffusion Factor Distributions DF 102096

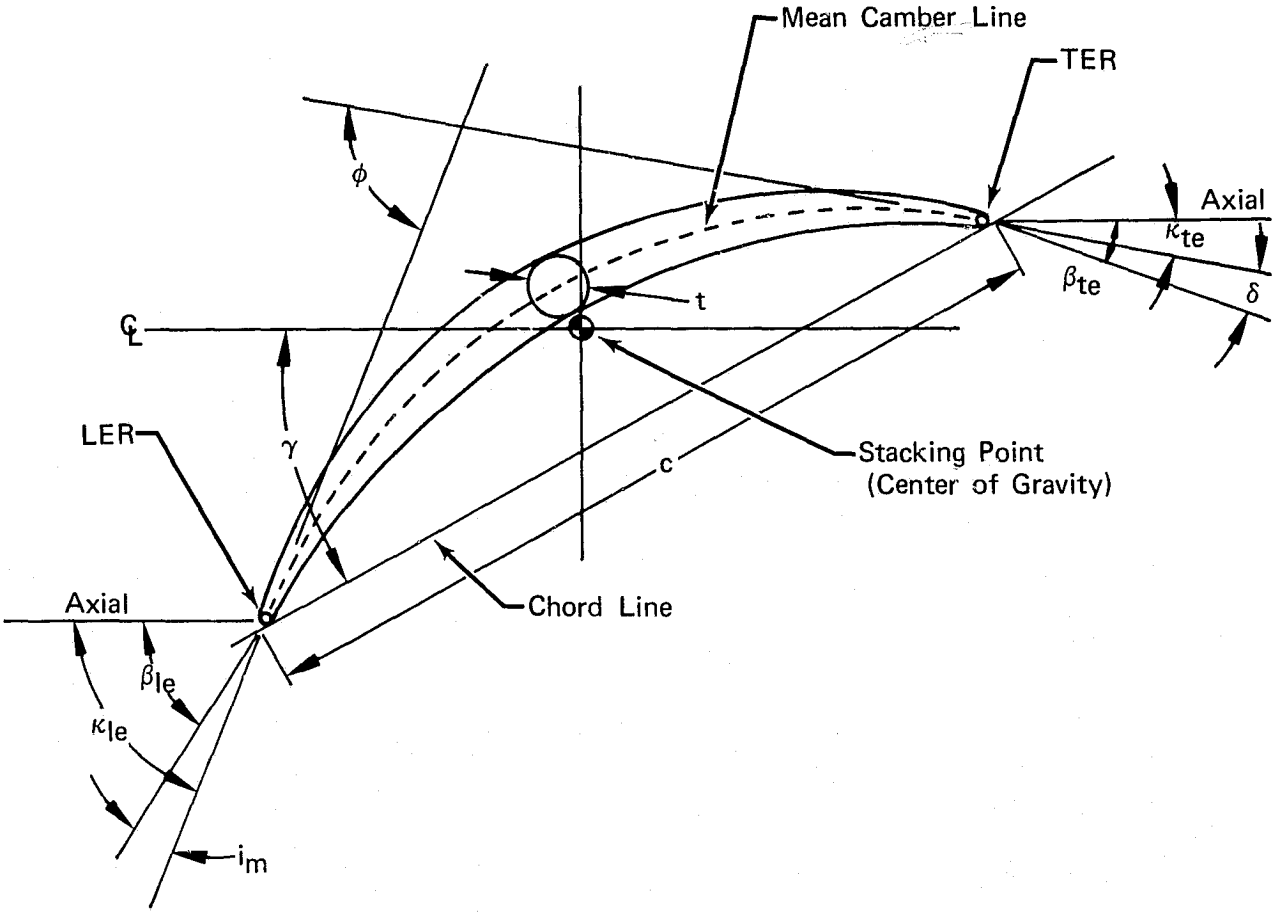


Definitions

| | |
|---|---|
| c | Chord Length, cm (in.) |
| $i_m$ | Incidence Angle, deg |
| LER | Leading Edge Radius, cm (in.) |
| t | Maximum Thickness, cm (in.) |
| TER | Trailing Edge Radius, cm (in.) |
| $\beta_{le}$ | Air Angle - Leading Edge, deg |
| $\beta_{te}$ | Air Angle - Trailing Edge, deg |
| $\gamma$ | Chord Angle, deg |
| $\delta$ | Deviation Angle, deg |
| $\kappa_{le}$ | Metal Angle - Leading Edge, deg |
| $\kappa_{te}$ | Metal Angle - Trailing Edge, deg |
| $\phi$ | Camber, deg |

Figure 9. Double Circular Arc Airfoil Definitions FD 97769

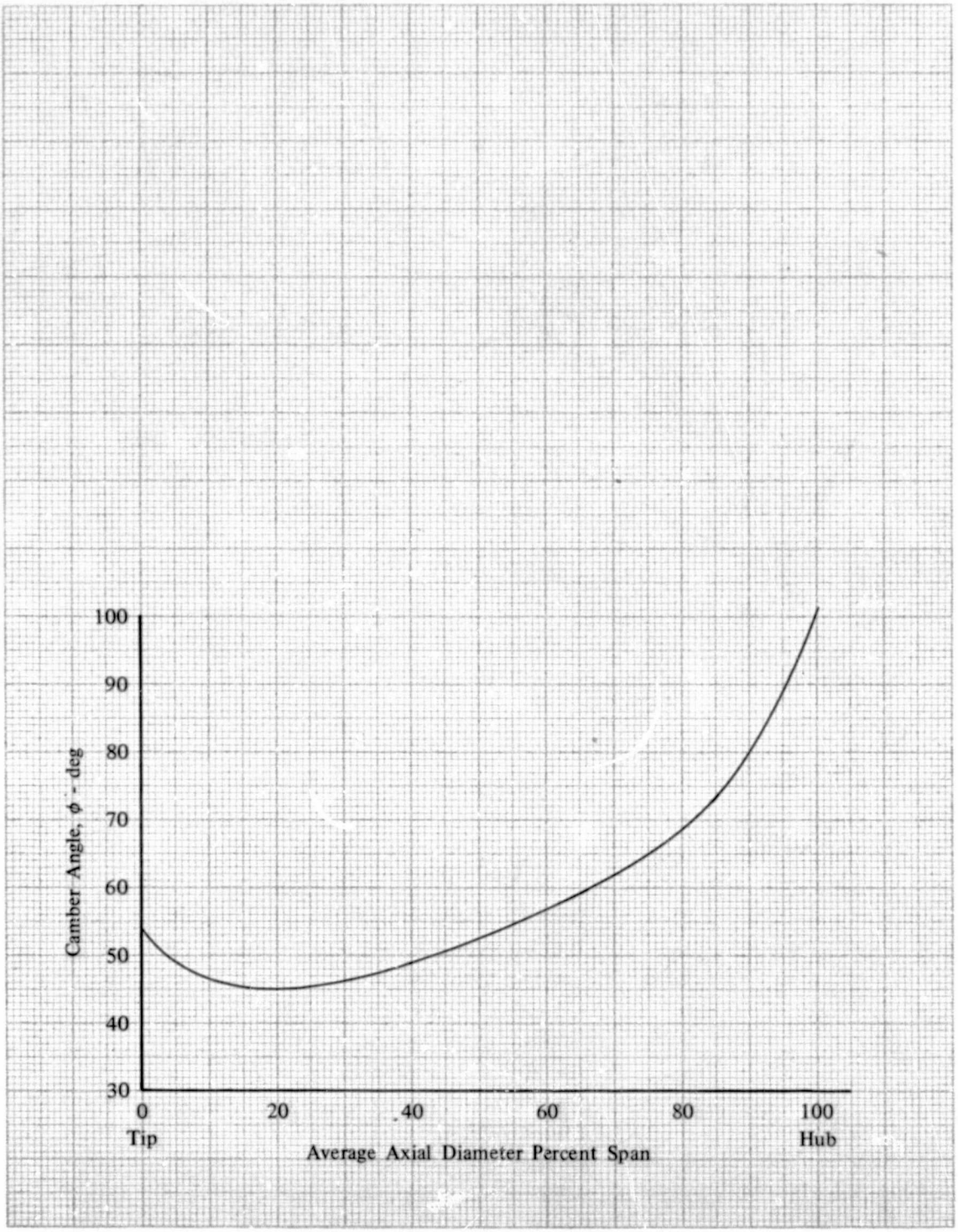


Figure 10. Rotor F Camber Angle Distribution DF 102098

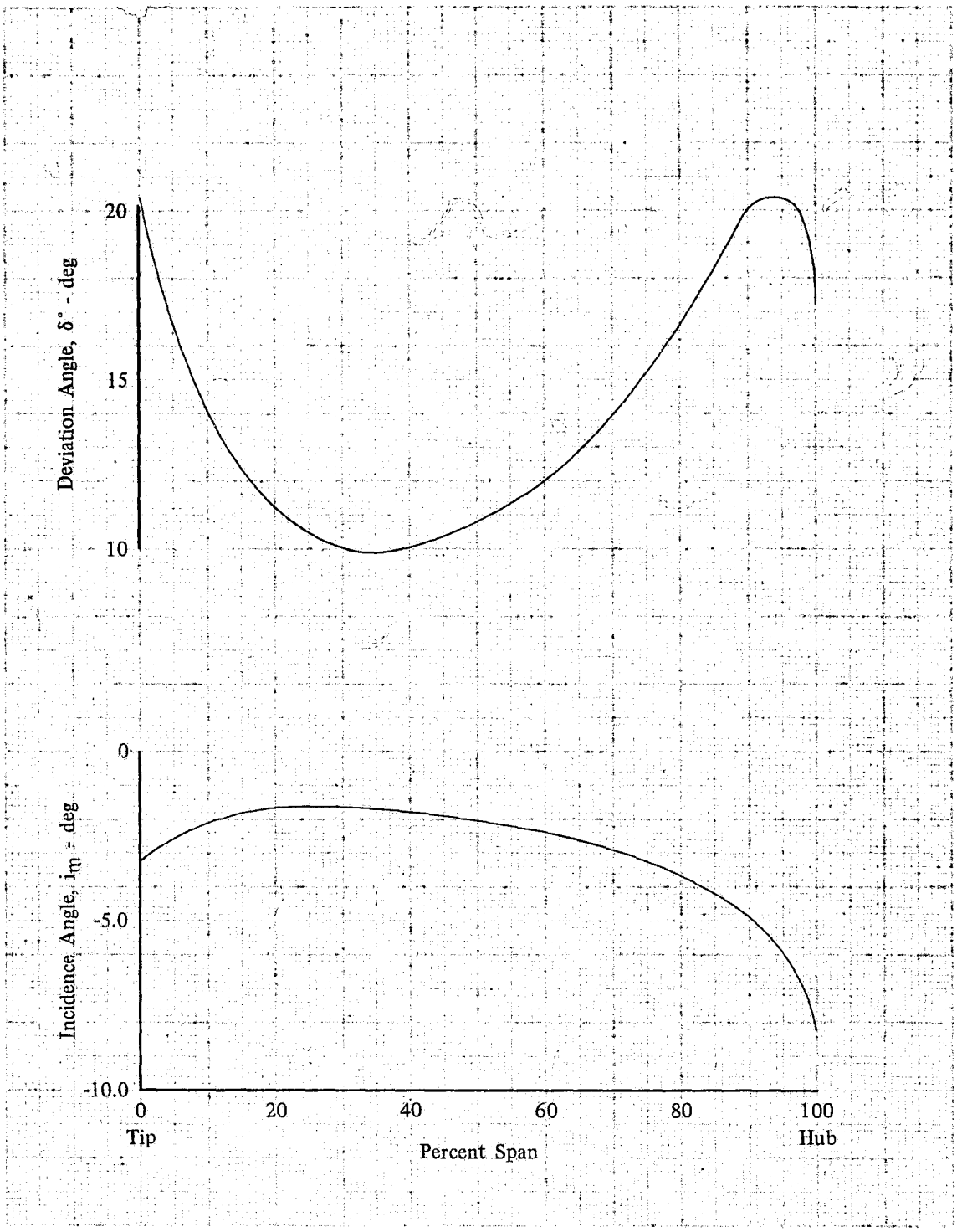


Figure 11. Rotor F Incidence and Deviation Angle Distributions DF 102097

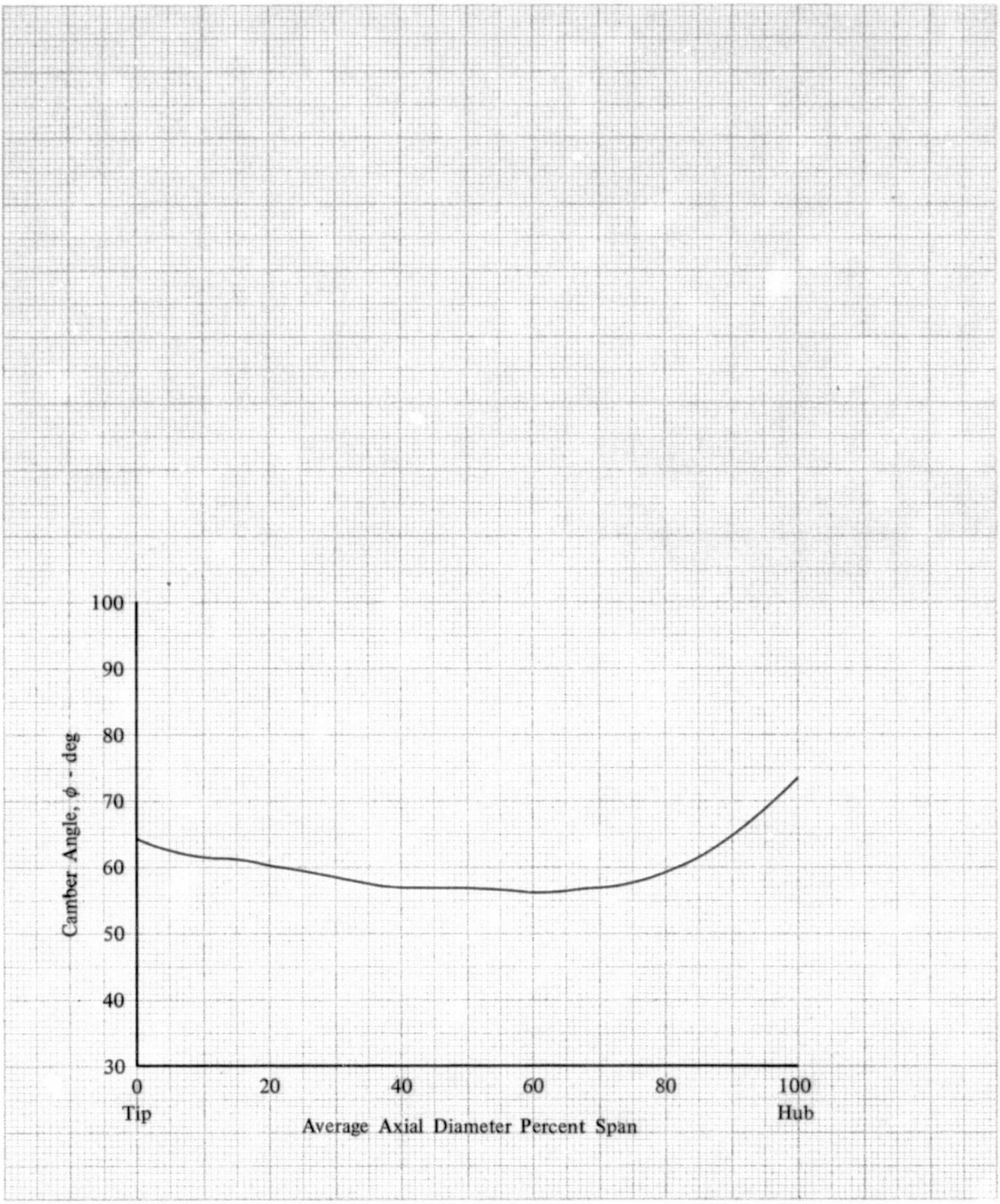


Figure 12. Stator F Camber Angle Distributions DF 102100

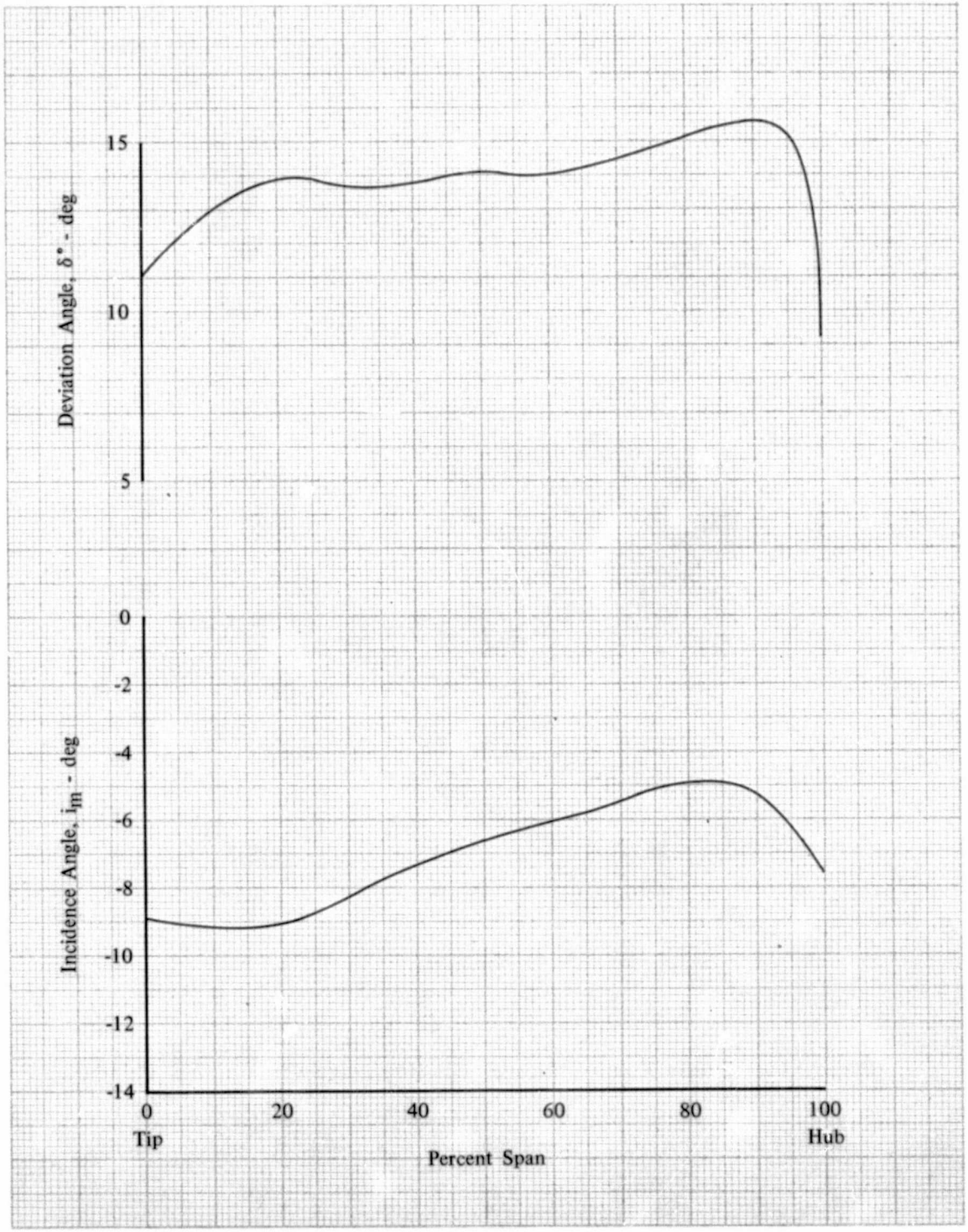


Figure 13. Stator F Incidence and Deviation Angle Distributions DF 102099


Figure 14. Rotor F and Stator F Leading Edge View FE 144161

## Mechanical Design

### Steady-State Stress Analysis

The steady-state airfoil stresses due to centrifugal loads and/or gas bending loads were calculated at design equivalent rotor speed and flow at the leading and trailing edges and on the convex surface at the point of maximum thickness for both Rotor F and Stator F. The results are shown in figure 15. The maximum calculated Rotor F stress was 12,273 $N/cm^2$ (17,800 psi) and occurred at the hub leading edge. The maximum Stator F stress of 2,137 $N/cm^2$ (7,070 psi) was calculated at the junction of the Stator F airfoil and the attachment trunnion. Since the maximum stresses for both airfoils were considerably below the 0.2% yield strength of 75,845 $N/cm^2$ (110,000 psi) of the material selected for the blading, no airfoil stress problems were anticipated.

### Vibratory Analysis

The calculated bending and torsional vibratory frequencies for Stage F airfoils are shown in terms of frequency versus rotor speed in figure 16. Rotor F first bending and first torsion frequencies of 1560 and 3260 Hz, respectively, were calculated at design equivalent rotor speed. Lines representing multiples of rotor frequency (E) are shown to permit identification of resonant operating conditions due to upstream support struts, rotating stall zones or instrumentation that might possibly be encountered during testing. Although the first bending frequency approaches the 8E line at 110% design speed, no resonant condition was expected because the 8E excitation produced by the eight upstream struts will be sufficiently dissipated at the rotor leading edge. Stator F first bending and first torsion natural frequencies of 1750 and 2450 Hz, respectively, were calculated for a cantilevered stator configuration. These frequencies were sufficiently high to preclude a resonant vibratory problem during testing.

Because of the relatively high resonant frequencies shown in figure 16 and the large vibratory stress margin available as indicated by the Goodman diagrams of figure 17, i.e., 36,544 and 38,612 $N/cm^2$ (53,000 and 56,000 psi) based on smooth fatigue strength for Rotor F and Stator F, respectively, no Stage F airfoil vibratory problem was anticipated.

### Flutter Analysis

Reduced velocity and incidence parameters were calculated for Rotor F at the design operating condition and for the estimated negative and positive incidence angle operating limits between 50 and 110% design equivalent rotor speed and compared to correlated flutter data in figure 18.

The reduced velocity parameter was defined as

$$K = \frac{12V}{\pi c \omega}$$

and the incidence parameter was defined as

$$f(i_m) = \frac{i_m - i_{m_{ref}}}{\text{low-loss incidence range}}$$

where V, c, $i_{m_{ref}}$, and low-loss incidence range are the values for airfoil sections located at 25% span from the tip. The loss incidence range and $i_{m_{ref}}$ were determined from an unpublished P&WA cascade data correlation. The bending and torsional mode flutter calculations were made at Mach numbers of 0.4 and 0.6, respectively, so that the values obtained could be compared with the correlated data. The calculated operating envelope does not overlap the stall flutter region and consequently no flutter problem was anticipated. A reduced velocity parameter versus average stage pressure ratio was calculated for Stator F and compared to correlated flutter data for a cantilevered stator configuration in figure 19.

The reduced velocity parameter was as defined for the rotor and the average row pressure ratio was defined as:

$$\left[(P_{le} + P_{te})/2\right]/P_{inlet}$$

The values of velocity and chord used to calculate the stator reduced velocity parameter are the values at 50% span. As shown, the design point was at a sufficient distance from the flutter region to preclude a flutter problem.

Disk and Attachment Stress

Rotor F and disk lug tension, bending, shear, and bearing stresses were calculated at a rotor speed of 11,480 rpm or approximately 115% of design speed. The results of these calculations are presented in table IX. The combined tension and bending lug stresses calculated for Rotor F and the disk were 32,338 and 45,024 N/cm$^2$ (46,900 and 65,300 psi), respectively. These calculated stresses are well within the 0.2% yield strength of 75,845 N/cm$^2$ (110,000 psi) of the stainless steels (AMS 5616 and 5613) selected for the rotor and disk. The maximum allowed stress presented in table IX was based on current P&WA engine design practice.

As shown, none of the stresses present in the Stage F design exceed the maximum stress permitted and no attachment stress problems were anticipated.

Table IX. Stage F Attachment Stresses

| Configuration | Type of Stress, $N/cm^2$ (psi) | | | | | |
|---|---|---|---|---|---|---|
| | Tension | Bearing | Bending | Shear | Combined Tension and Bending | Torsion |
| Rotor F Lug AMS 5616 | 12,135 (17,600) | 36,337 (52,700) | 20,202 (29,300) | 12,756 (18,500) | 32,338 (46,900) | NA |
| *Maximum Allowed Stress | 22,754 (33,000) | 68,261 (99,000) | 37,923 (55,000) | 18,617 (27,000) | 44,128 (64,000) | NA |
| % Calculated Stress of Maximum Allowed Stress | 53 | 53 | 53 | 68 | 73 | NA |
| Disk Lug AMS 5613 | 19,996 (29,000) | 36,337 (52,700) | 25,029 (36,300) | 11,584 (16,800) | 45,024 (65,300) | 5,750 (8,340) |
| *Maximum Allowed Stress | 33,786 (49,000) | 68,261 (99,000) | 37,923 (55,000) | 26,201 (38,000) | 49,782 (72,200) | 30,338 (44,000) |
| % Calculated Stress of Maximum Allowed Stress | 59 | 53 | 66 | 44 | 90 | 19 |

*The maximum allowed stress is based on current P&WA engine design practice.

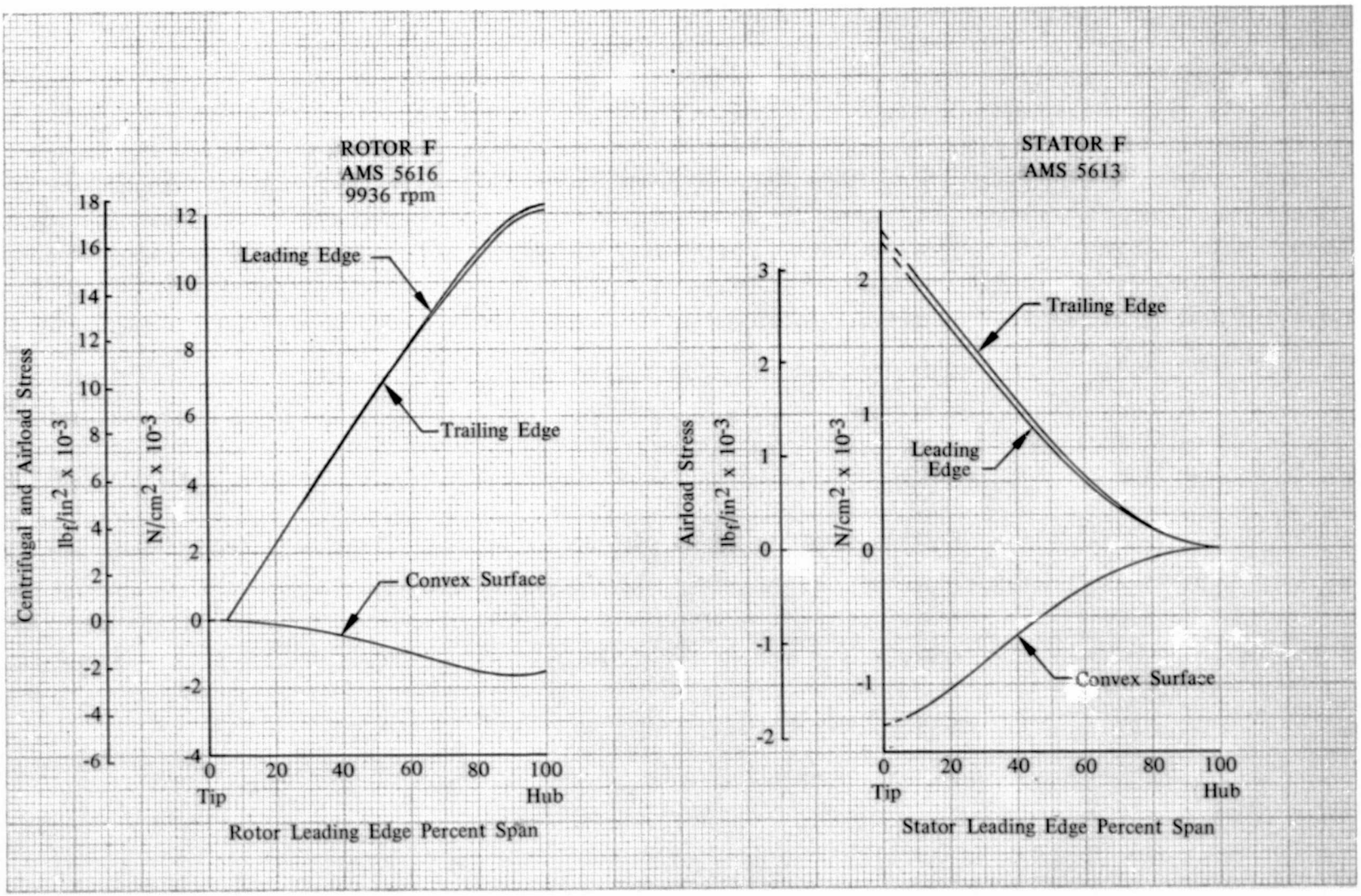


Figure 15. Stage F Airfoil Stress Distribution

DF 102101

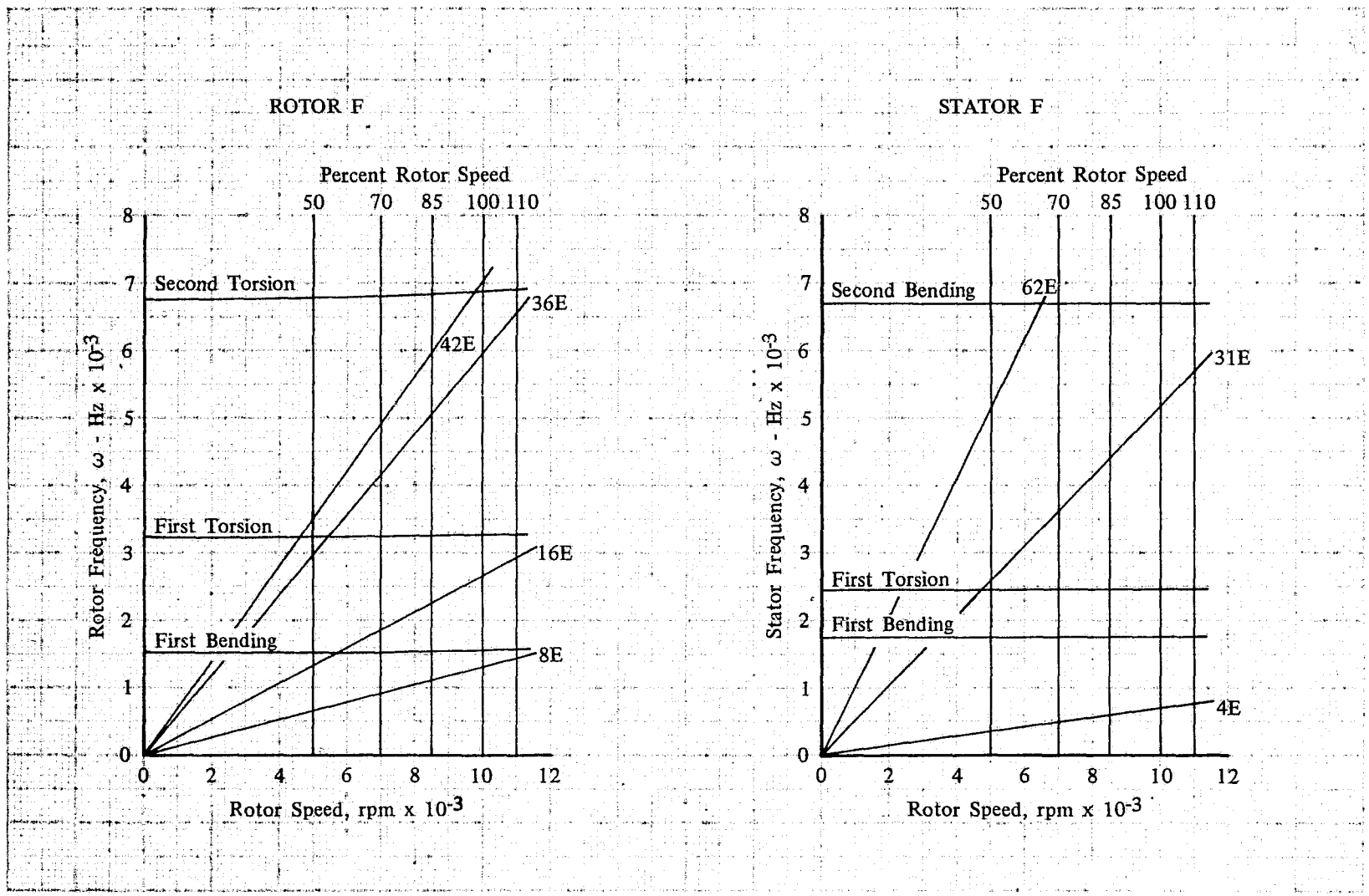


Figure 16. Stage F Airfoil Resonance Diagrams

DF 102102

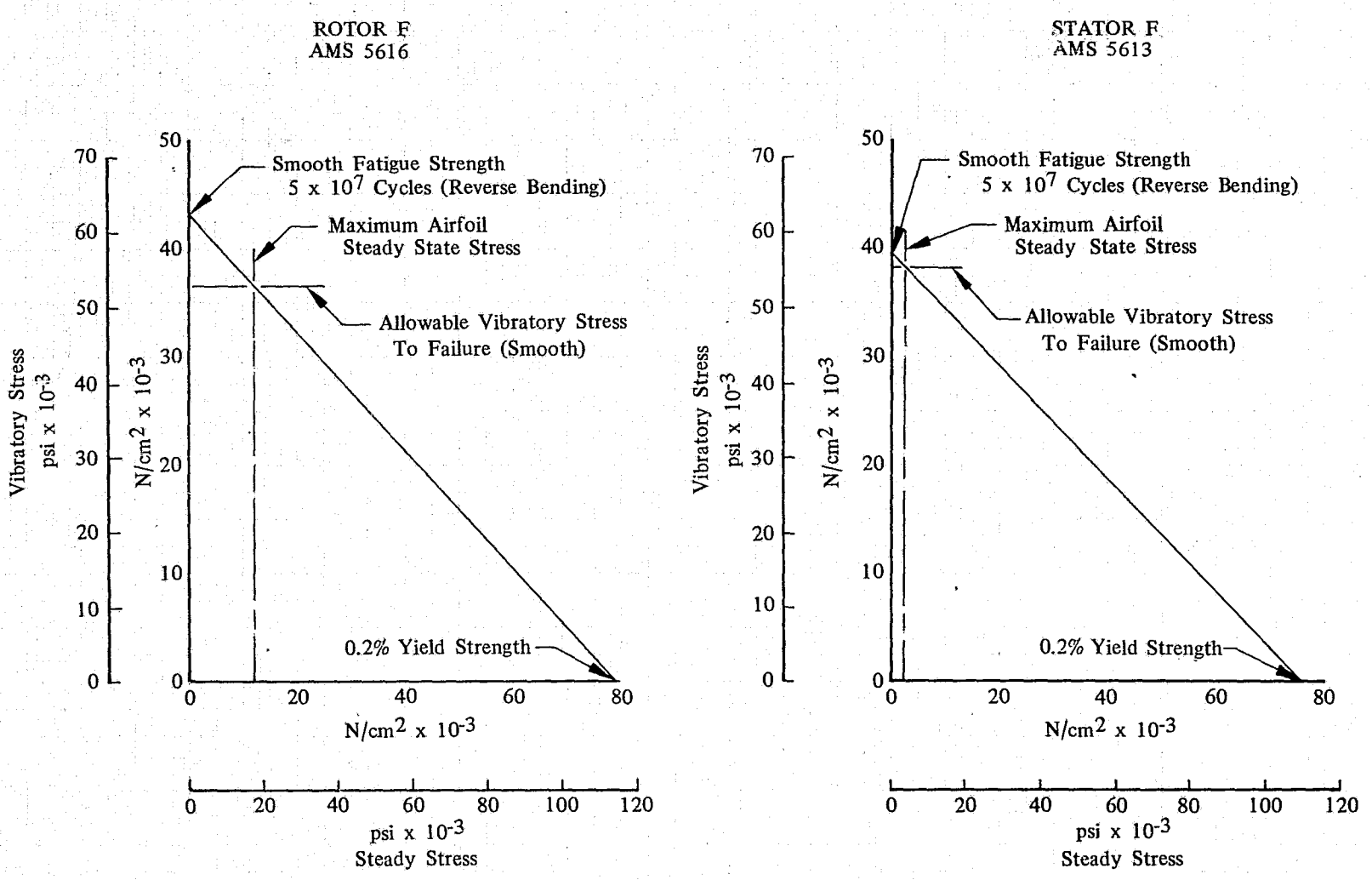


Figure 17. Stage F Airfoil Material Goodman Diagrams

DF 102103

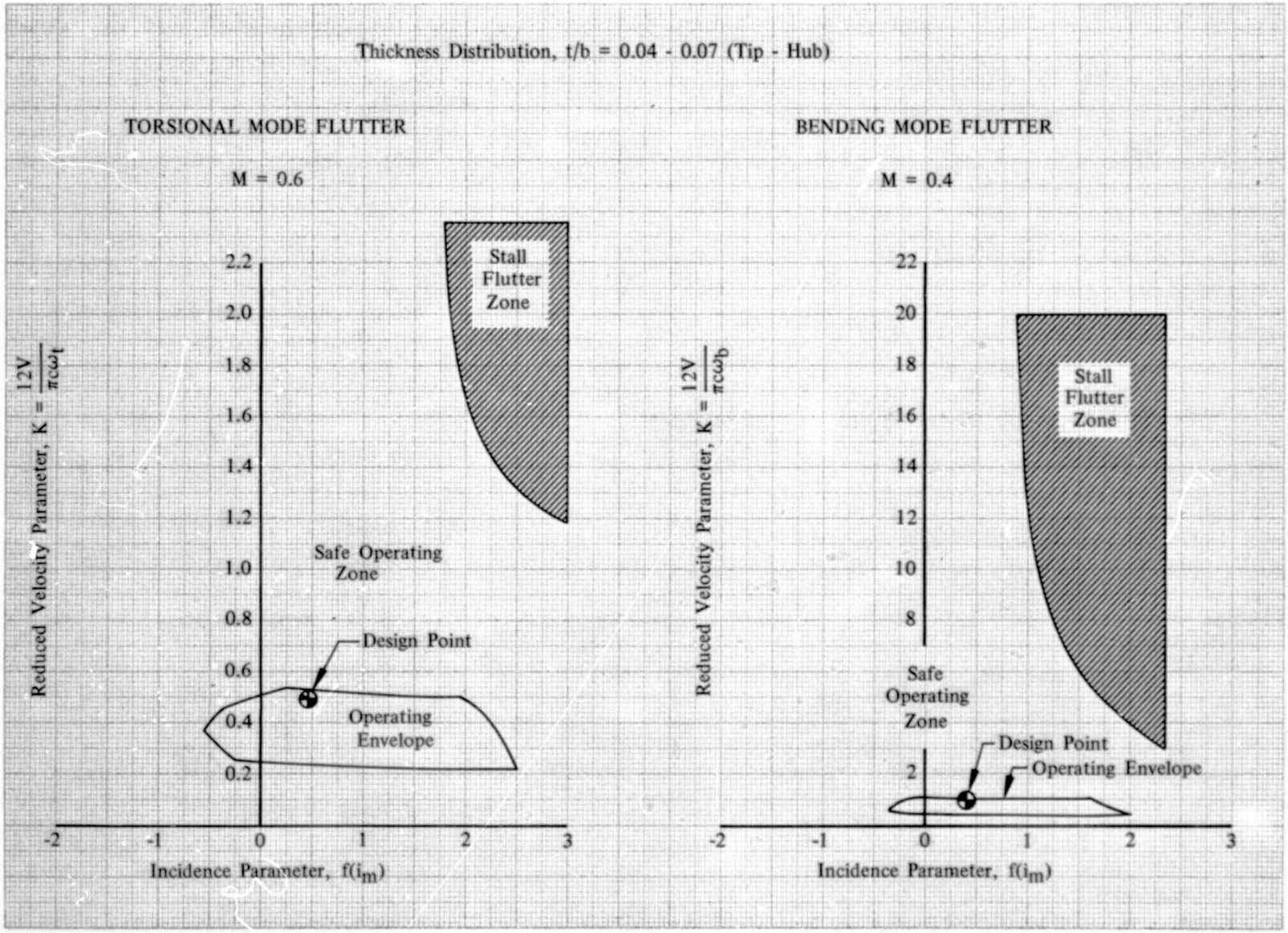


Figure 18. Rotor F First Bending and First Torsional Mode Flutter Characteristics

DF 102104

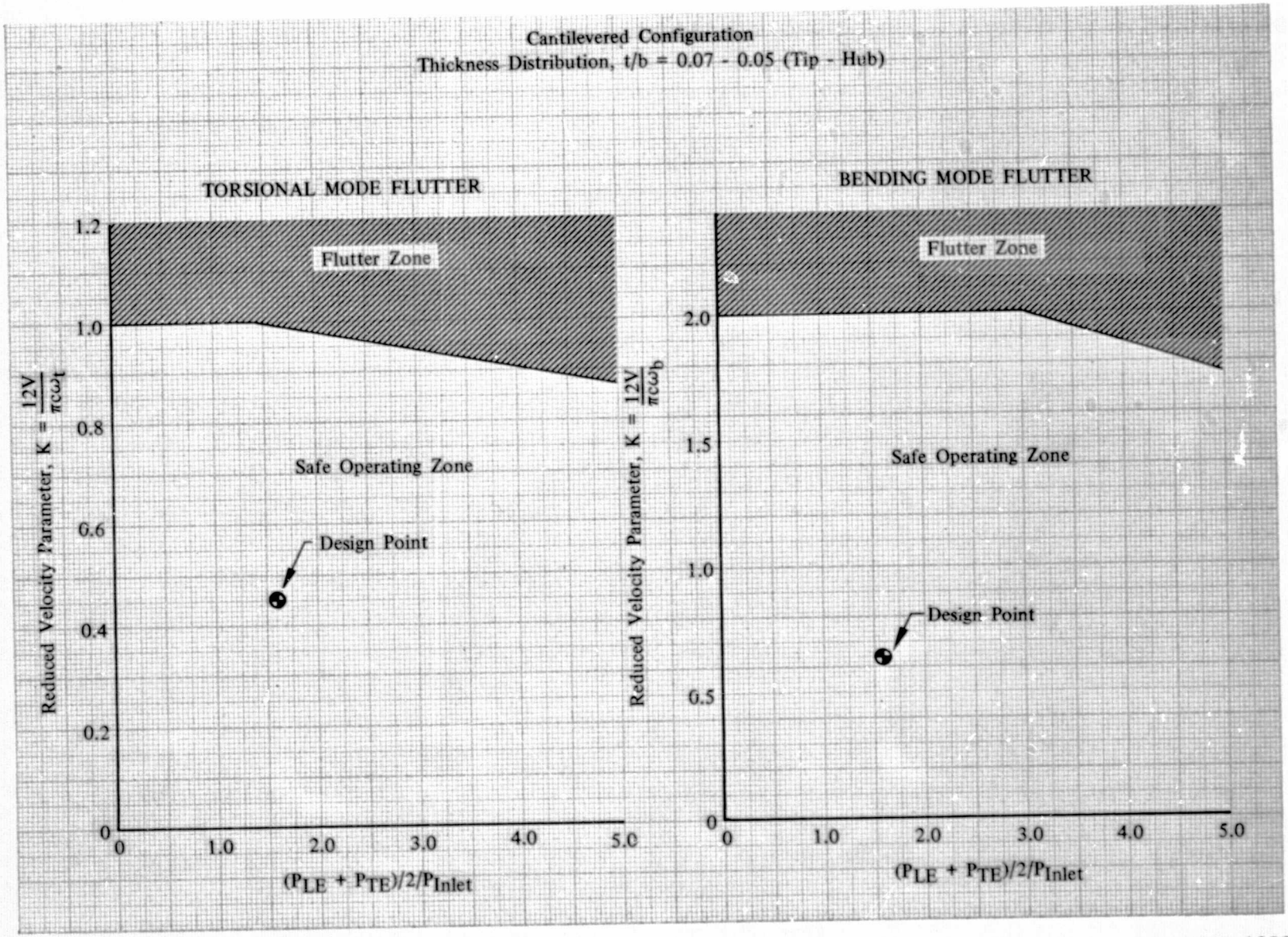


Figure 19. Stator F First Bending and First Torsional Mode Flutter Characteristics

DF 102105

## Test Equipment

### Compressor Test Facility

An elevation view of the compressor research facility is shown in figure 20. The compressor was driven by a 1,119 kw (1500 hp) constant speed (1800 rpm) electric motor through a dynamatic clutch and a 7.7:1 ratio speed-increasing gearbox. The maximum horsepower available at a constant gearbox input speed was limited by the torque capability of the dynamatic clutch.

Air entered the compressor through a 15.54 m (51 foot) long, 0.762 m (30 in.) diameter inlet duct designed to ASME standards for flow measuring with thin plate orifices. Low velocity uniform air was provided at the rig inlet bellmouth by a 1.27 m (50 in.) diameter plenum. Transition from the 0.762 m (30 in.) diameter duct to the plenum was accomplished with a four-deg half-angle transition duct. At maximum flowrate for the test configuration, the Mach number at the bellmouth inlet was 0.03.

### Compressor Test Rig

The general configuration of the single-stage rig is shown in figure 21. Flowpath dimensions are presented in figure 22. The hub/tip ratio at the rotor inlet is 0.768. The test section had a constant hub diameter of 0.419 m (16.50 in.) and the outer wall converged from a diameter of 0.582 m (22.900 in.) at the inlet guide vane leading edge to a 0.513 m (20.182 in.) diameter at the stator trailing edge.

As shown in figure 21, the rotor disk/drum assembly is overhung on the drive shaft ahead of the bearing support package. The inlet assembly is supported by eight struts located upstream of the inlet guide vanes. Approximately 11 deg of rotor prewhirl was provided by the IGV. Stator discharge was 10 deg from axial and no exit guide vanes were incorporated. Flowrate was varied by a sliding sleeve discharge valve which regulated stage discharge pressure.

Compressor airflow was measured with a 0.445 m (17.5 in.) diameter ASME standard thin plate orifice located 8.534 m (28 feet) from the inlet duct bellmouth. The orifice was instrumented with two upstream and two differential static pressure taps to permit redundant flowrate calculations. Compressor rotor speed was measured with electromagnetic sensors monitoring blade tip and gear tooth passing frequency.

### Instrumentation

Uniform and Radially Distorted Inlet Flow Tests - Instrumentation typical of that provided to obtain overall and blade element performance data for each blade or vane row is shown in figure 23a, b and c. The circumferential locations of instrumentation are shown in figure 24 for instrumentation Stations 0, 1, 2, 3 and 4. These instrumentation stations are located axially as shown in figure 22. Table X presents a summary of the instrumentation positioned at each axial station. Where possible, dual instrumentation was provided at each axial station to provide redundant measurements. Inlet total temperature was measured in the inlet plenum with four half-shielded total temperature probes and a Rosemount temperature probe; inlet total pressure was measured in the inlet plenum with five Kiel total pressure probes. Four equally spaced static pressure orifices were located on both the inner and outer walls at instrumentation Station 0.

Radial distributions of total and static pressure at the inlet guide vane inlet and static pressure and air angle at the inlet guide vane and stator exit were measured by means of 30 deg wedge probes, shown in figure 23a. Wall static pressure at the inlet guide vane inlet and exit was measured with four inner and four outer diameter wall static pressure orifices equally spaced circumferentially. However, since the static pressures, measured with the 30 deg wedge traverse instrumentation, failed to agree with the values measured with the wall static pressure orifices, the static pressure data measured with the 30 deg wedge probes were not used in the data reduction and analysis.

The inlet guide vane exit total pressure profile was measured with a pair of five-span radial rakes circumferentially traversed through a 14 deg arc. These probes, shown in figure 23b, provided sensors at nine radial locations, i.e., 4.1, 14.1, 22.7, 32.7, 42.1, 52.1, 72.3, 83.8 and 93.8% span from the tip. The circumferential location and sweep of these probes is shown in figure 24. Rotor exit (i.e., stator inlet) and stator exit outer diameter wall static pressures were measured with four equally spaced mid-channel and four cross-gap static pressure orifices located at 10, 30, 70 and 90% of stator gaps. Because of close spacing of the rotor and stator, measurements other than wall static pressure were precluded. Rotor performance was calculated through analysis of the stator discharge data as described in the data reduction procedures.

Total pressure and total temperature profiles of the stator exit were measured with two pairs of five-span radial rakes circumferentially traversed through a 16 deg arc. Each pair of probes, shown in figure 23c, provided sensors at ten radial locations, i.e., 4.1, 14.1, 22.7, 32.7, 42.1, 52.1, 62.3, 72.3, 83.8 and 93.8% span from the tip. The circumferential location and sweep of these probes during traversing are shown in figure 24.

Pressure data from stationary probes were recorded on magnetic tape utilizing a pneumatic scanner system. Traverse probe pressure and air angle data, temperature data, and stall transient data were recorded on magnetic tape utilizing a microsadic data recording system capable of recording at approximately 60 samples per minute.

Stator exit total pressure at surge was measured with the circumferential traverse probes positioned on stator exit mid-channel streamline and close coupled to transducers for fast response to change in total pressure. The time at which total pressure decreased during surge determined which inlet static pressure scan was to be used to calculate weight flow at the initiation of surge. A high response pressure transducer was mounted over the rotor tip and used to measure high-frequency total pressure oscillations and to indicate the initiation of rotating stall and/or surge. The high response transducer output was recorded on magnetic tape and correlated in time with the transient recording of the plenum and Station 0 static pressures.

Four blades and four vanes were instrumented with strain gages to provide vibratory stress data. Gage locations were determined from bench vibrator tests with the aid of stresscoat, and selected locations were verified by fatigue tests. The gage outputs were displayed on oscilloscopes and usually monitored during tests.

Circumferentially Distorted Inlet Flow Tests - The instrumentation used for the uniform inlet and radial inlet flow distortion tests was inadequate to provide (1) overall performance data within and outside the circumferentially distorted region without moving the screen and (2) a uniform spacing of flow distribution data at twelve locations relative to the distortion screen with a maximum of six screen positions. Consequently, the instrumentation was revised as shown by the numbers in parentheses in Table X. The redundant transient instrumentation and the previously recorded and not used traverse static pressure instrumentation (see page 49) was eliminated to provide recording channels for an additional air angle traverse probe at Station 1 and two total pressure rakes at Station 2. The circumferential locations of the revised instrumentation are shown in figure 25. A description of the required changes at each instrumentation station is presented below.

| | |
|---|---|
| Plenum: | The plenum wall static pressure (transient) at 300° was deleted. |
| Station 0: | The OD wall static pressure (transient) at 270° was deleted. |
| Station 1 - IGV Inlet: | A 30 deg wedge probe was added at 141° 30', i.e., 180 deg from the location of the 30 deg wedge probe at 321° 30', to measure air angle. The wedge probe at 321° 30' was to measure air angle only, whereas it previously measured total and static pressure. |
| Station 2 - IGV Exit: | An additional pair of five-span total pressure rakes were added at 18° 47' and 198° 47'. These probes and the pair at 104° 29' and 284° 29' ensured a representative radial distribution of total pressure inside and outside the distorted region. The 30 deg wedge probes located at 7° 29' and 187° 29' were used to record only air angle, whereas previously they had also recorded static pressure. |
| Station 4 - Stator Exit: | The 30 deg wedge probes at 107° 25' and 287° 25' were used to record only air angle, whereas previously they had also recorded static pressure. |

Distortion Screens

Twenty-mesh, 0.051 cm (0.020 in.) diameter wire was used for the hub radial, tip radial and circumferential distortion screens. The hub and tip radial distortion screens covered 40 and 35% of the inlet annulus area, respectively, and the circumferential distortion screen covered a 180 deg sector of the inlet annulus area. For the overall performance test points the screen was positioned between 295° and 115°, i.e., the approximate top half of the annulus area (figure 25).

For the two flow conditions for which flow distribution data were obtained (100% design equivalent rotor speed near surge and mid-flow), the screen was indexed five times in 30 deg increments to the right, i.e., screen position 2 extended from 325° to 145°, thus providing data for a total of six screen positions. The radial and circumferential distortion screens were mounted on a 2.54 cm (1.0 in.) mesh 0.318 cm (0.125 in.) diameter wire support screen located approximately one rotor diameter upstream of the rotor leading edge. The support screen spanned the entire annulus and was installed for all Stage F tests.

Table X. Instrumentation Summary for Stage F

| Axial Location | Type of Instrumentation | No. of Probes | Total Pressure | Air Angle | Static Pressure | Total Temperature | Radial Travel |
|---|---|---|---|---|---|---|---|
| Inlet Duct ASME Orifice | *Wall Static | 2 (2) | | | 2 (2) | | |
| | *Wall Static | 2 (2) | | | Δ2 (2) | | |
| Plenum | Shielded Thermocouple | 4 (4) | | | | 4 (4) | |
| | OD Wall Static (Transient) | 1 | | | 1 (0) | | |
| | Rosemount Temperature Probe | | | | | | 1 (1) |
| | *Kiel Probe | 5 (5) | 5 (5) | | | | |
| Support Strut Exit (Instrumentation Station 0) | OD Wall Static (Transient) | 2 (1) | | | 2 (1) | | |
| | *OD Wall Static | 2 (2) | | | 2 (2) | | |
| IGV Inlet (Instrumentation Station 1) | 30-deg Wedge (Traverse) | 1 (2) | 1 | (2) | 1 (0) | | 1 (2) |
| | *OD Wall Static | 4 (4) | | | 4 (4) | | |
| | *ID Wall Static | 4 (4) | | | 4 (4) | | |
| IGV Exit - Rotor Inlet (Instrumentation Station 2) | 30-deg Wedge (Traverse) | 2 (2) | | 2 (2) | 2 (0) | | 2 (2) |
| | 5 Sensor Radial Rake | 2 (4) | 9 (15) | | | | |
| | *OD Wall Static | 4 (4) | | | 4 (4) | | |
| | *ID Wall Static | 4 (4) | | | 4 (4) | | |
| Rotor Exit - Stator Inlet (Instrumentation Station 3) | High Response Transducer (Transient) | 1 (1) | 1 (1) | | | | |
| | *OD Wall Static | 4 (4) | | | 4 (4) | | |
| | *OD Wall Static (Cross-Gap) | 4 (4) | | | 4 (4) | | |
| Stator - Stage Exit (Instrumentation Station 4) | 5 Sensor Radial Rake | 4 (4) | 20 (20) | | | 20 (20) | |
| | 30-deg Wedge (Traverse) | 2 (2) | | 2 (2) | 4 (0) | | 2 (2) |
| | *OD Wall Static | 4 (4) | | | 4 (4) | | |
| | *OD Wall Static (Cross-Gap) | 4 (4) | | | 4 (4) | | |

*Indicates instrumentation connected to Scanivalve Transducer
( ) Indicates instrumentation utilized for circumferential inlet flow distortion tests

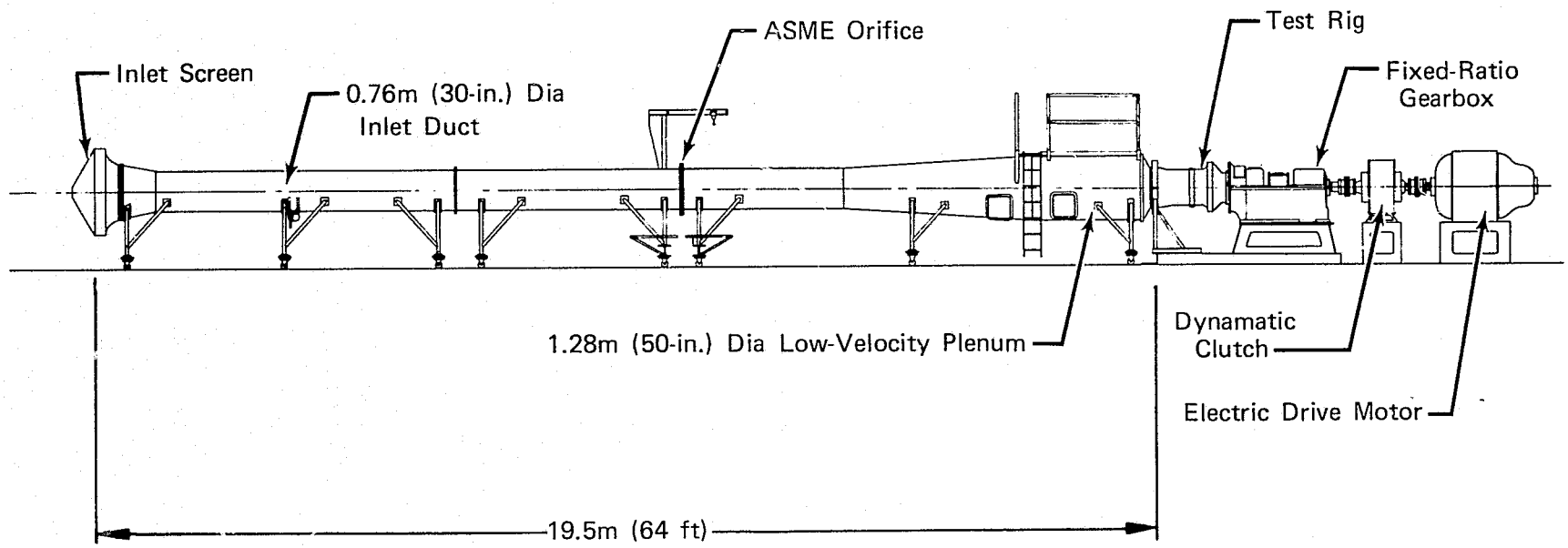


Figure 20. Compressor Research Facility

FD 97763

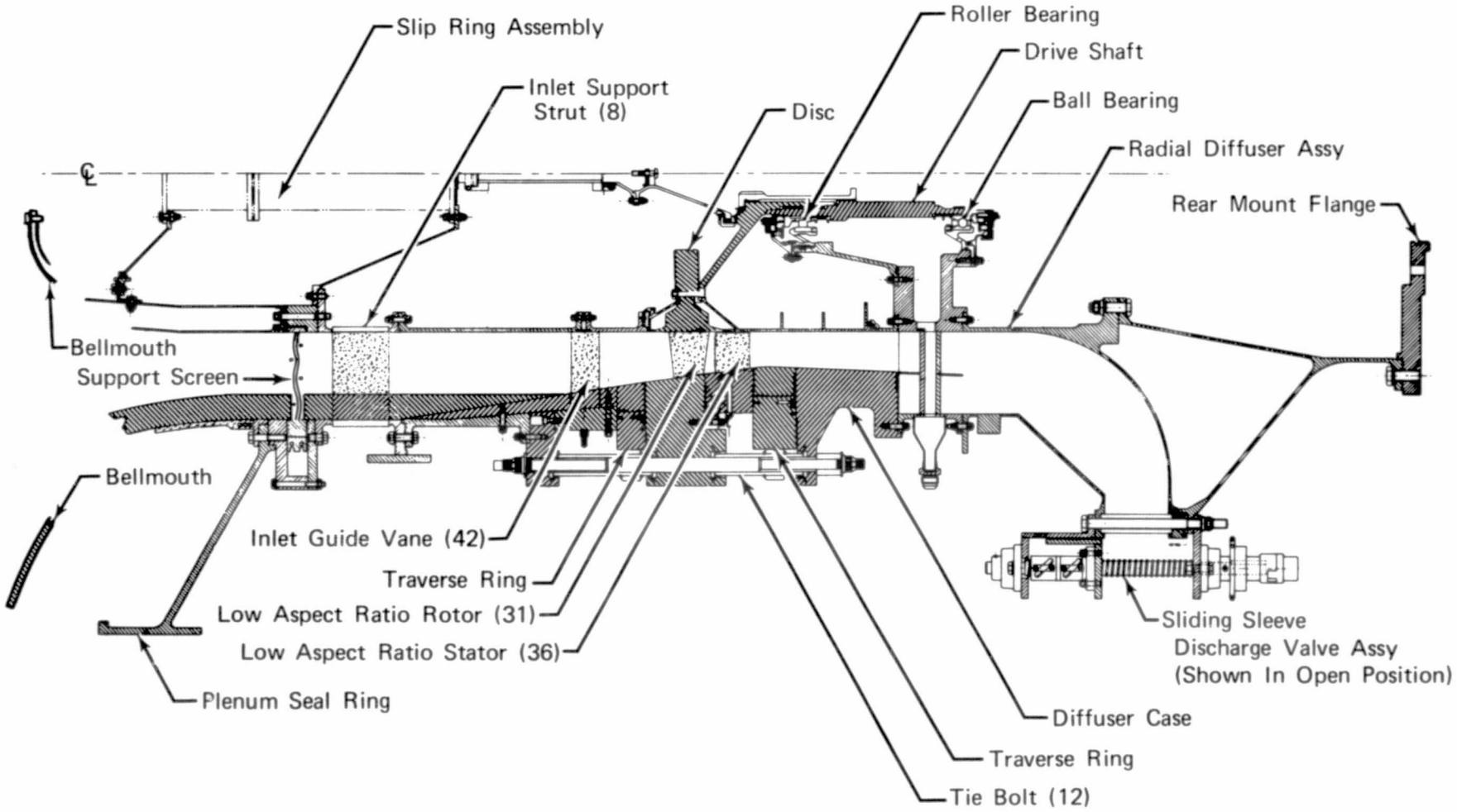


Figure 21. Single Stage Drum Rotor Cantilevered Stator Compressor Rig - Stage F Configuration FD 97764

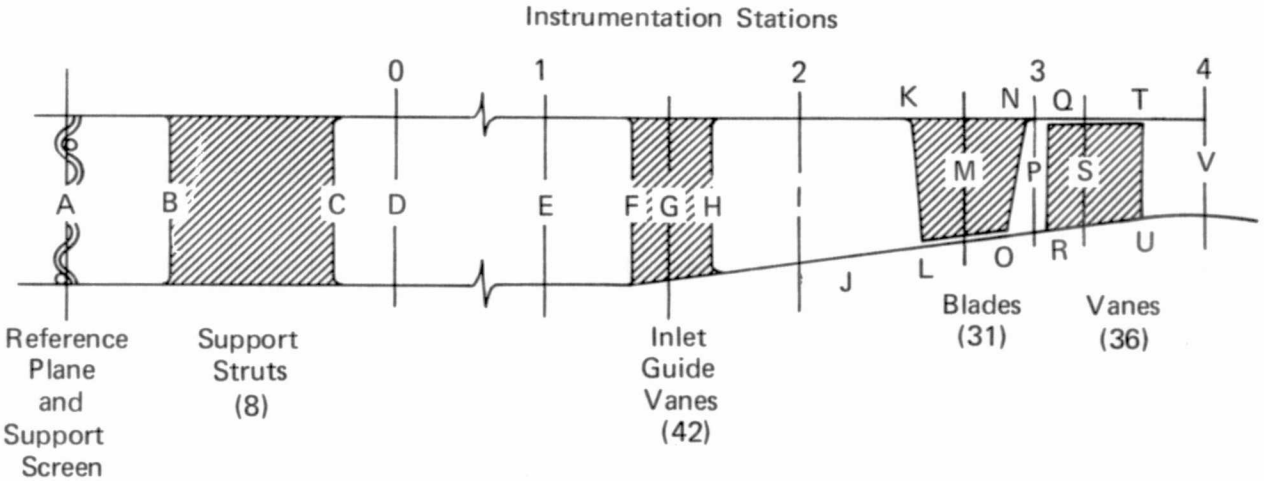


| Flowpath Location | Location Description | Inner Wall Diameter | | Outer Wall Diameter | | Axial Distance from Reference Plane | |
|---|---|---|---|---|---|---|---|
| | | cm | in. | cm | in. | cm | in. |
| A | Reference Screen and Support Screen ℄ | 41.950 | 16.500 | 58.166 | 22.900 | 0.0 | 0.0 |
| B | Support Strut Leading Edge | 41.950 | 16.500 | 58.166 | 22.900 | 5.822 | 2.292 |
| C | Support Strut Trailing Edge | 41.950 | 16.500 | 58.166 | 22.900 | 13.441 | 5.292 |
| D | Instrumentation Station 0 | 41.950 | 16.500 | 58.166 | 22.900 | 21.519 | 8.472 |
| E | Instrumentation Station 1 | 41.950 | 16.500 | 58.166 | 22.900 | 34.066 | 13.412 |
| F | Inlet Guide Vane Leading Edge | 41.950 | 16.500 | 58.103 | 22.875 | 37.876 | 14.912 |
| G | Inlet Guide Vane Stacking Line | 41.950 | 16.500 | 57.556 | 22.660 | 39.649 | 15.610 |
| H | Inlet Guide Vane Trailing Edge | 41.950 | 16.500 | 56.934 | 22.415 | 41.661 | 16.402 |
| I | Instrumentation Station 2 | 41.950 | 16.500 | 55.771 | 21.957 | 45.994 | 18.108 |
| J | Flowpath Wall Angle Change | 41.950 | 16.500 | 55.270 | 21.760 | 47.879 | 18.850 |
| K | Rotor Hub Leading Edge | 41.950 | 16.500 | — | — | 50.416 | 19.849 |
| L | Rotor Tip Leading Edge | — | — | 54.480 | 21.449 | 51.161 | 20.142 |
| M | Rotor Stacking Line | 41.950 | 16.500 | 53.899 | 21.220 | 53.574 | 21.092 |
| N | Rotor Hub Trailing Edge | 41.950 | 16.500 | — | — | 56.990 | 22.437 |
| O | Rotor Tip Trailing Edge | — | — | 53.162 | 20.930 | 56.622 | 22.292 |
| P | Instrumentation Station 3 | 41.950 | 16.500 | 53.023 | 20.875 | 57.150 | 22.500 |
| Q | Stator Hub Leading Edge | 41.950 | 16.500 | — | — | 58.108 | 22.877 |
| R | Stator Tip Leading Edge | — | — | 52.786 | 20.782 | 58.082 | 22.867 |
| S | Stator Stacking Line | 41.950 | 16.500 | 52.268 | 20.578 | 60.140 | 23.677 |
| T | Stator Hub Trailing Edge | 41.950 | 16.500 | — | — | 62.934 | 24.777 |
| U | Stator Tip Trailing Edge | — | — | 51.575 | 20.305 | 62.883 | 24.757 |
| V | Instrumentation Station 4 | 41.950 | 16.500 | 51.262 | 20.182 | 65.004 | 25.592 |

Figure 22. Stage F Flowpath Dimensions

FD 97765

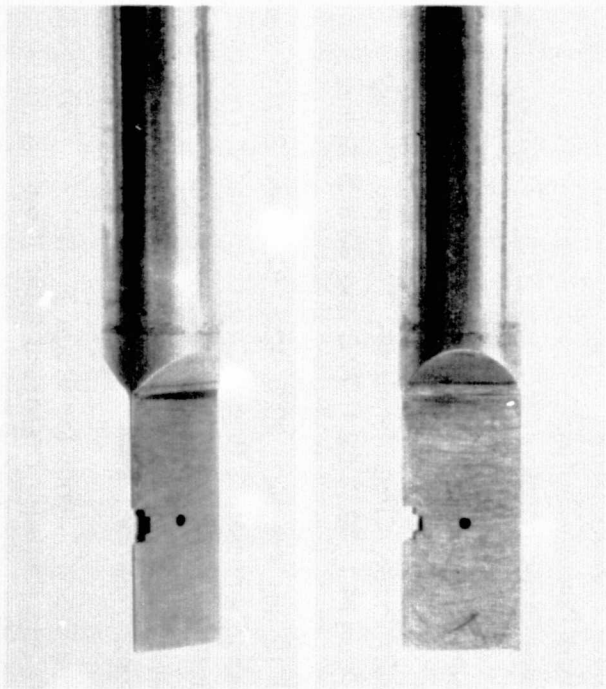

FE 136197

a. IGV Inlet Total and Static Pressure, Rotor Inlet, Stator Exit Air Angle and Static Pressure 30-deg Wedge Probe, Radial Traverse

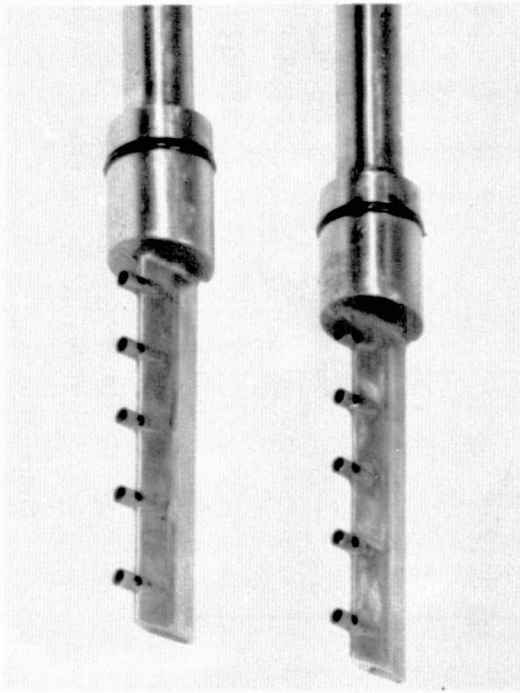

FE 133428

b. IGV Exit Total Pressure, Five Sensor Radial Rakes, Circumferential Traverse

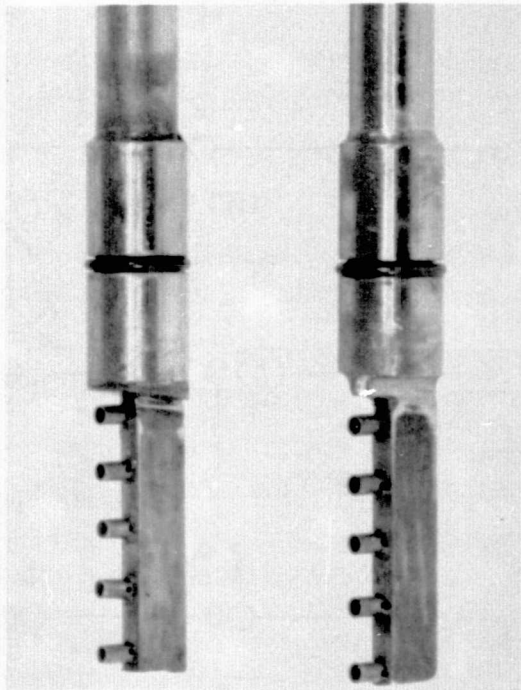

FE 133427

c. Stator Exit Total Pressure, Total Temperature, Five Sensor Radial Rakes, Circumferential Traverse

Figure 23. Traverse Instrumentation for Stage F

FD 97766

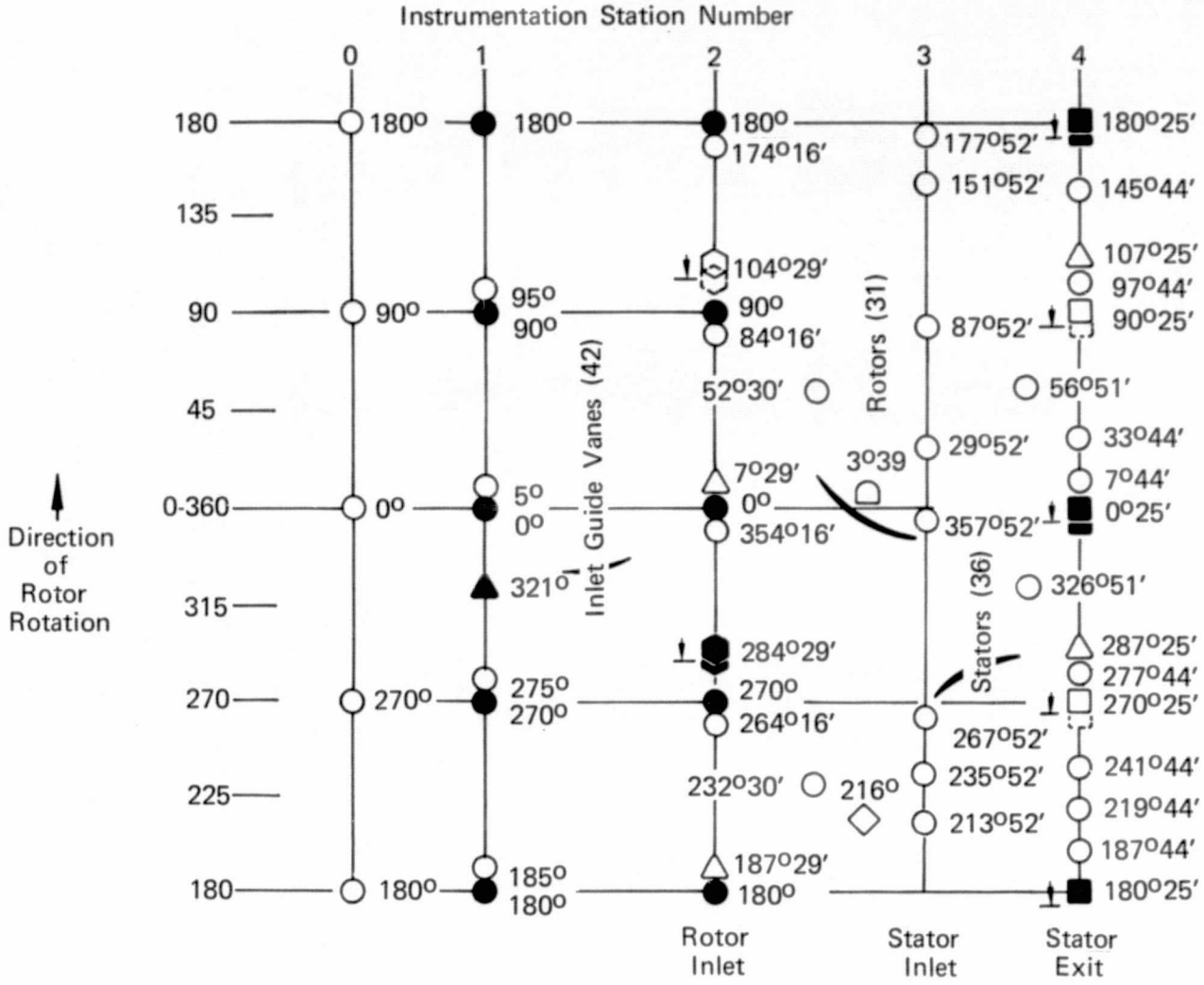


| Symbols | Description |
|---|---|
| ○ | OD Wall Static Pressure Orifice |
| ● | ID Wall Static Pressure Orifice |
| △ | 30 deg Wedge Static Pressure/Air Angle Radial Traverse Probe |
| ▲ | 30 deg Wedge Total/Static Pressure Radial Traverse Probe |
| ⬡ | Total Pressure Probe, Circumferentially Traversed Through 14 deg Arc, (4.1, 22.7, 42.1, and 83.8% Spans) |
| ⬢ | Total Pressure Probe, Circumferentially Traversed Through 14 deg Arc (14.1, 32.7, 52.1, 72.3 and 93.8 % Spans) |
| □ | Total Pressure/Temperature Probe, Circumferentially Traversed Through 16 deg Arc (4.1, 22.7, 42.1, 62.3, and 83.8 % Spans) |
| ■ | Total Pressure/Temperature Probe, Circumferentially Traversed Through 16 deg Arc (14.1, 32.7, 52.1, 72.3, and 93.8 % Spans) |
| ◇ | Speed Sensor |
| ▱ | High Response Pressure Sensor |

Figure 24. Instrumentation Layout for Stage F with Uniform and Radially Distorted Inlet Flow FD 97767

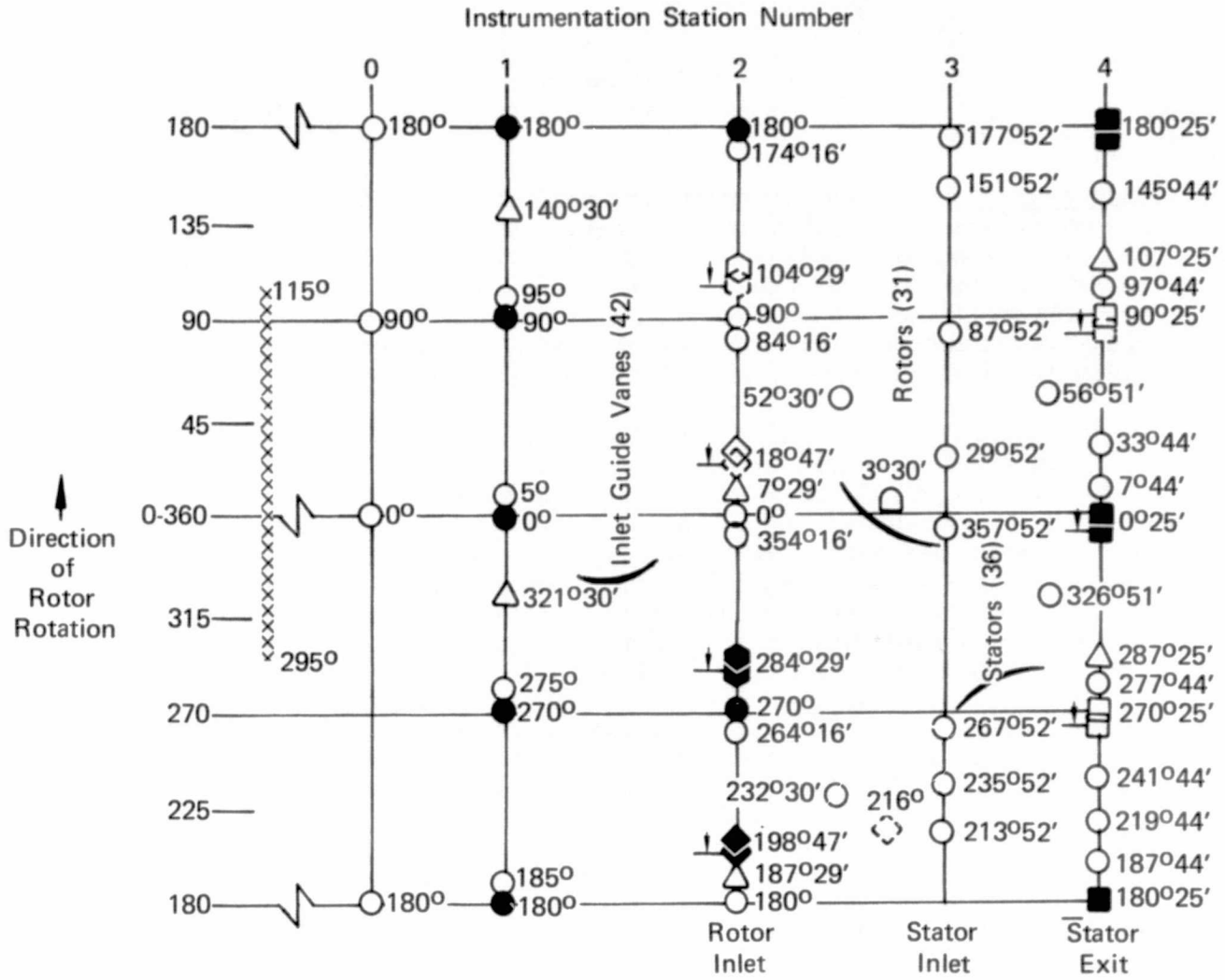


| Symbols | Description |
|---|---|
| ○ | OD Wall Static Pressure Orifice |
| ● | ID Wall Static Pressure Orifice |
| △ | 30 deg Wedge Air Angle Radial Traverse Probe |
| ⬡ | Total Pressure Probe, Circumferentially Traversed Through 14 deg Arc (4.1, 22.7, 42.1 and 83.8% Spans) |
| ⬢ | Total Pressure Probe, Circumferentially Traversed Through 14 deg Arc (4.1, 22.7 and 83.8% Spans) |
| ◇ | Total Pressure Probe, Circumferentially Traversed Through 14 deg Arc (14.1, 52.1, 72.3 and 93.8% Spans) |
| ◆ | Total Pressure Probe, Circumferentially Traversed Through 14 deg Arc (14.1, 52.1, 72.3 and 93.8% Spans) |
| □ | Total Pressure/Temperature Probe, Circumferentially Traversed Through 16 deg Arc (4.1, 22.7, 42.1, 62.3, and 83.8% Spans) |
| ■ | Total Pressure/Temperature Probe, Circumferentially Traversed Through 16 deg Arc (14.1, 32.7, 52.1, 72.3, and 93.8 % Spans) |
| ◇ | Speed Sensor |
| ◌ | High Response Pressure Sensor |

Figure 25. Instrumentation Layout for Stage F with 180 deg Arc Circumferentially Distorted Inlet Flow

FD 97768

## Procedures

### Test Procedures

Shakedown Tests - A shakedown test was performed to establish the mechanical integrity of the test rig, determine typical stress and vibration levels over the operating range, and obtain five overall and blade element data points and a surge transient at near design rotor speed to check out instrumentation and data reduction programs. In addition, data were obtained to determine the magnitude and extent of distortion that could be achieved at design rotor speed and maximum weight flow with the selected hub and tip radial distortion screens.

Performance Tests - Overall performance, blade element performance, flow distribution and surge transient data were obtained during the uniform inlet flow tests at 50, 70, 85, 95 and 100% of design equivalent rotor speed. Six data points (defined as a combination of flow and speed) were recorded at each rotor speed to define stage performance between maximum obtainable flow and near surge. The near-surge point was determined on the basis of flow and rotor exit pressure. Overall performance, blade element performance and flow distribution data were obtained at three flow conditions, including maximum and near-surge flow at 70, 85 and 100% of design equivalent rotor speed for the hub radial and tip radial distortion of the inlet flow. With circumferential distortion of the inlet flow, overall performance data were obtained for five flow conditions at design rotor speed and three flow conditions each at 70 and 85% of design rotor speed. The maximum and near surge flow conditions comprised two of the data points on each speedline. Blade element and flow distribution data were also obtained for the near surge and near design weight flow conditions at design rotor speed. To obtain an approximately uniform spacing of flow distribution data around the compressor annulus, data were recorded for six screen positions for each of these two data points. Only one screen position was required to assure a sampling of the overall performance in both the distorted and undistorted zones of the flow field for the remaining nine data points.

At each data point, recording of fixed pressure and temperature instrumentation data was followed by the recording of radial and then circumferential traverse instrumentation data. Blade stresses and rig vibrations were monitored during steady-state and surge transient operation at all rotor speeds.

Transient measurements of orifice pressure, plenum pressure, bellmouth static pressure, rotor speed, and rotor exit total pressure were recorded 10 times per second to define surge characteristics as the stage was operated into and out of surge. The output from a high response pressure transducer flush-mounted over the rotor tip was also recorded as the stage was operated into and out of surge. These high response probe data were correlated in time with the other transient measurements.

### Data Reduction Procedures

Data reduction was accomplished in three steps. The first step involved the use of two computer programs: (1) to convert millivolt readings to appropriate engineering units, and (2) to provide a tabulated and plotted array of pressures, temperature, and air angle at instrumentation stations. Conversion of data to absolute values, appropriate Mach number corrections, and adjustment of pressures and temperature to equivalent NASA standard day conditions was performed in the second computer program.

The second step in the planned data reduction procedures involved a third computer program which was to calculate the rotor exit static pressure and air angle distributions from the compressor geometry, airflow, rotor speed and rotor inlet and stator exit total pressures, temperatures and air angles using continuity, energy, and radial equilibrium equations. The original intent was to use the measured static pressure distributions at the inlet guide vane inlet, rotor exit and stator exit, but the values measured with the 30 deg wedge traverse instrumentation failed to agree with measured wall static pressures. Consequently, the radial distributions of static pressure at these locations were determined in the following manner: A straight line static pressure distribution between the average measured OD and ID wall static pressure was assumed at the inlet guide vane inlet and rotor inlet. A static pressure profile was calculated for the stator exit with the program which calculated the rotor exit static pressure distribution by adjusting the boundary layer displacement factor to achieve agreement between calculated and measured static pressure at the rotor and stator exit outer wall. The radial distributions of rotor exit air angle and rotor exit and stator exit static pressure, so calculated by this program, were than input into the final performance program.

The third and final step in the data reduction procedure involved a fourth computer program to calculate overall and blade element performance variables for the inlet guide vane, rotor, and stator. The array of data provided in step one and the rotor exit air angles and rotor exit and stator exit static pressures calculated in step two were analyzed for the selection of radial distributions of pressures, temperatures, and air angles at each axial station for input into this computer program. The selection of the radial distributions of the data in step one was straightforward except for the rotor exit total pressure which was selected as the freestream total pressure from the stator exit circumferential traverse data. These traverse data exhibited a circumferential variation in total pressure superimposed on the stator wake profile that was cyclic and repeated across each vane gap. Similar gapwise variations in stator exit total temperature circumferential traverse data were also present which consistently followed the total pressure values over a range of flows and speeds. Typical examples of these gapwise variations in total pressure and total temperature at 14, 52 and 84% span from the tip are shown in figure 26. These cyclic variations in total pressure and temperature were more pronounced at the hub region and diminished significantly toward the tip as the interblade spacing increased, indicating the variation was sensitive to the distance between the rotor trailing edge and the stator leading edge. It was therefore concluded that the gapwise variations were attributable to a stator leading edge back pressure effect on the rotor. Consequently, the rotor exit freestream total pressure was obtained by taking an area average of the stator exit total pressure data after fairing a gapwise profile across the stator wake profile.

Overall Performance

Total pressure ratios and adiabatic efficiencies were calculated for the rotor, rotor-stator and inlet guide vane-rotor-stator, i.e., stage. The inlet guide vane, rotor, and stator exit total pressures and total temperatures were weighted according to local mass flow to obtain average values. The mass-averaged stator exit total temperatures were used for rotor, rotor-stator and stage efficiency calculations.

The inlet guide vane and stator wake total pressures and total pressures at each radial measuring station were mass averaged using the local total pressure in the wake, the local total temperature in the wake, and the calculated local static pressure in the wake. Mach number was determined from the local measured total and calculated static pressure. The local mass flow was then obtained from the relationship

$$\frac{W\sqrt{T}}{PA} = \sqrt{\frac{\gamma g_c}{R}}\ M\left[1 + \frac{\gamma - 1}{2}\ M^2\right]^{\frac{1+\gamma}{2(1-\gamma)}}$$

where A is the flow area associated with each radial measurement increment.

For the circumferential distortion data, the mass flow averaged values of total pressure and total temperature measured within and outside the 180 deg arc circumferentially distorted flow region were averaged to calculate the performance. This is equivalent to assuming that the relative extent of the distorted and undistorted flow remained unchanged through the compressor.

Blade Element Performance and Flow Distribution Data

Blade element performance and flow distribution data were calculated for each blade row for uniform and radially distorted inlet flow. Calculations were made along design streamlines that pass through 5, 10, 15, 30, 50, 70, 85, 90 and 95% span at the rotor exit instrumentation Station 3. The calculations were performed at the instrumentation stations and at the inlet guide vane, rotor, and stator leading and trailing edges. The pressures, temperatures, and air angles at the blade row leading and trailing edges were obtained by translating the measured values from the instrumentation stations assuming conservation of angular momentum, conservation of energy, continuity, and flow along design streamlines. A description of the translation method is presented in Reference 3. For circumferentially distorted inlet flow, only flow distribution data are presented (i.e., total and static pressure, total temperature, flow angle, axial velocity, Mach number and turning) and all data are at the instrumentation stations and not translated to the blade row leading and trailing edges.

Surge Transient Data

The point of incipient surge at each rotor speed tested was determined from examination of the orifice pressure drop, plenum pressure, bellmouth pressure and rotor exit pressure data that were recorded at 10 scans per second. Typical relationship of these variables during an excursion into surge is shown in figure 27.

Orifice pressure drop was determined at the incipient surge point and the corresponding weight flow was determined from the correlation of orifice pressure drop and orifice weight flow shown in figure 28. Similar correlations were also made for the hub and tip radial distortion and the circumferential distortion data. The steady-state pressure ratio data were extrapolated to the stall flow using the shape of the steady-state data curve as a guideline.

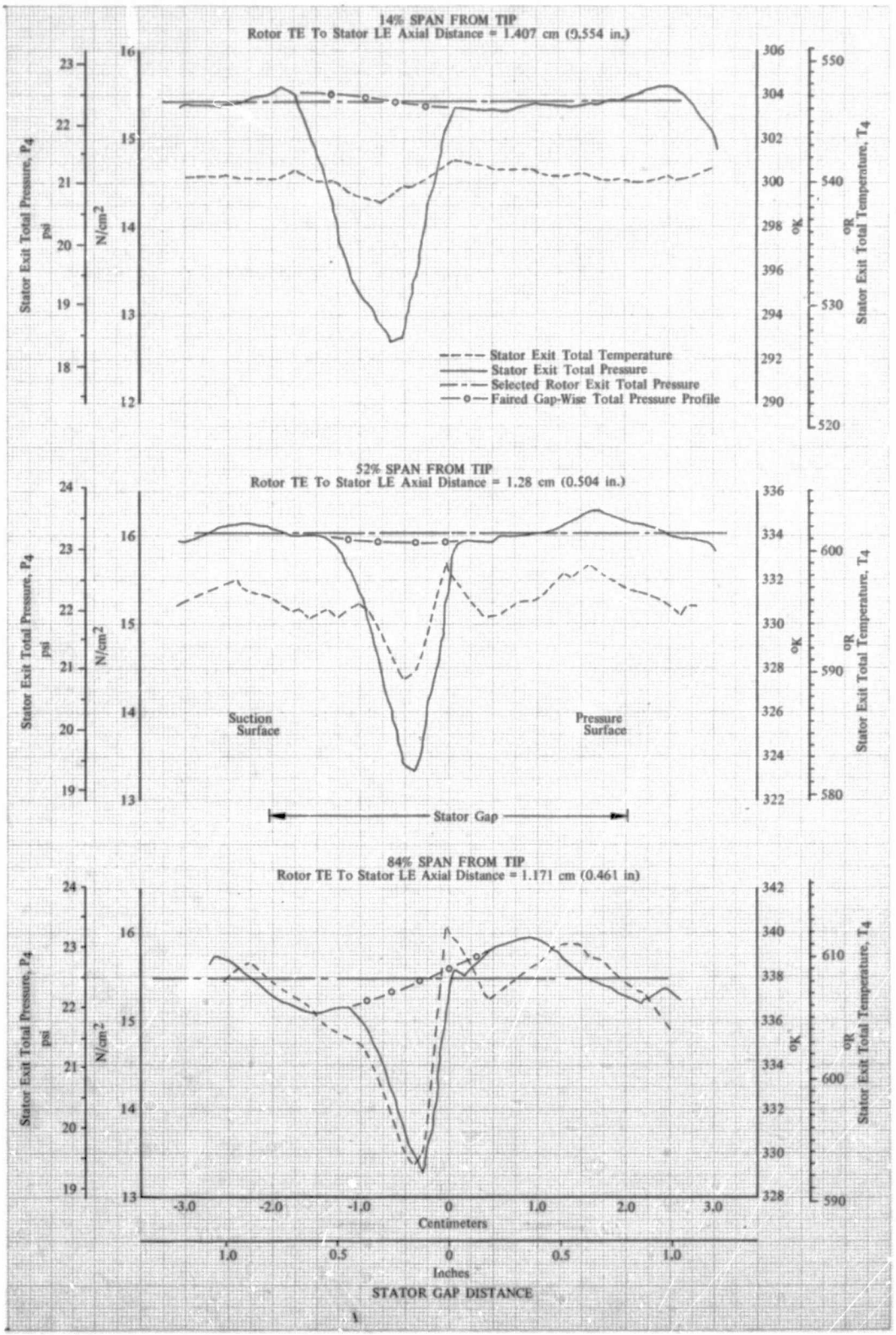


Figure 26. Typical Gapwise Variations in Stator F DF 102158
Wake Total Pressure and Total Temperature; 100% Design Equivalent Rotor Speed; Equivalent Weight Flow = 17.26 kg/sec (38.04 lb/sec); Uniform Inlet Flow

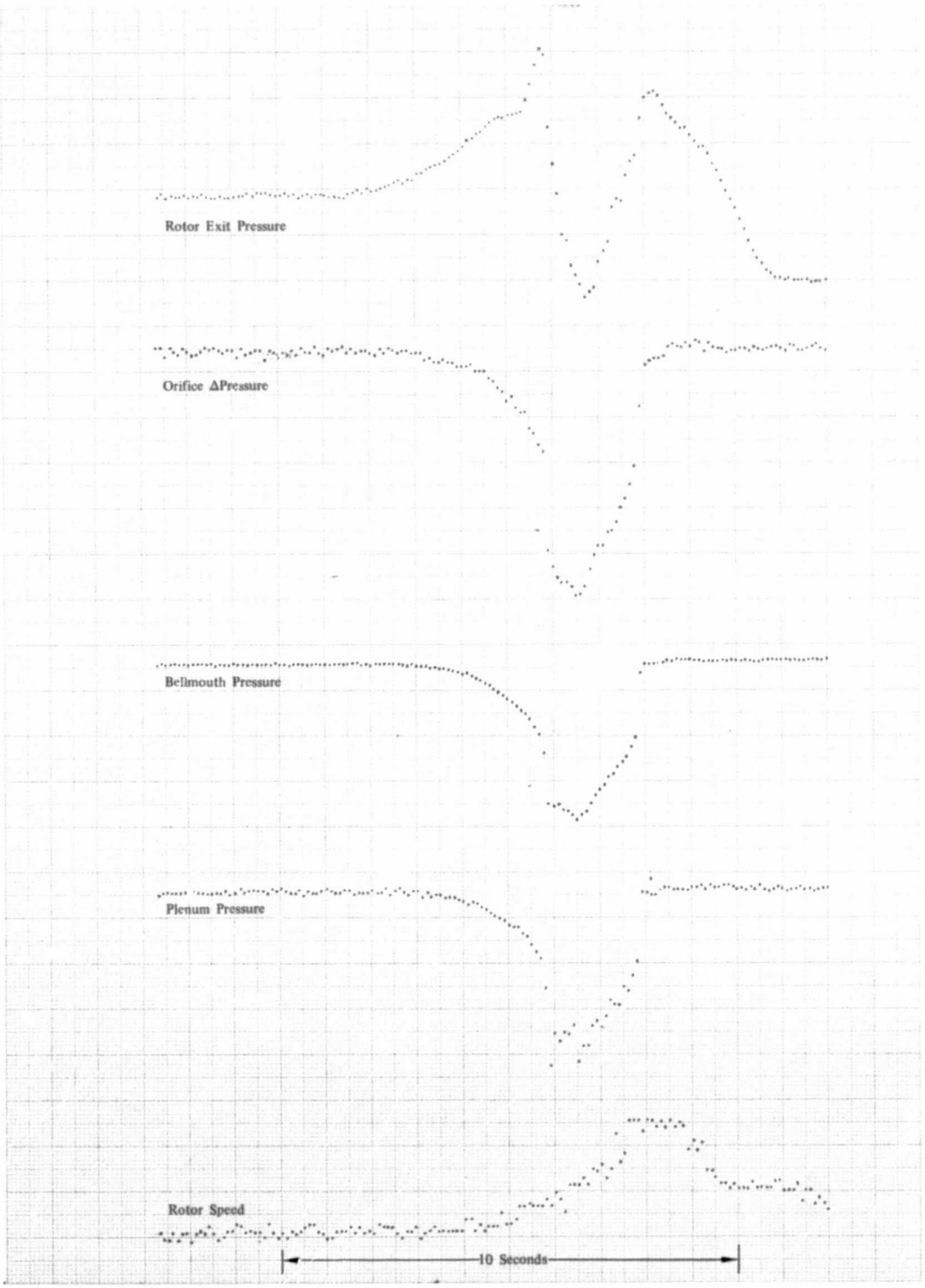


Figure 27. Typical Surge Transient Data DF 102212

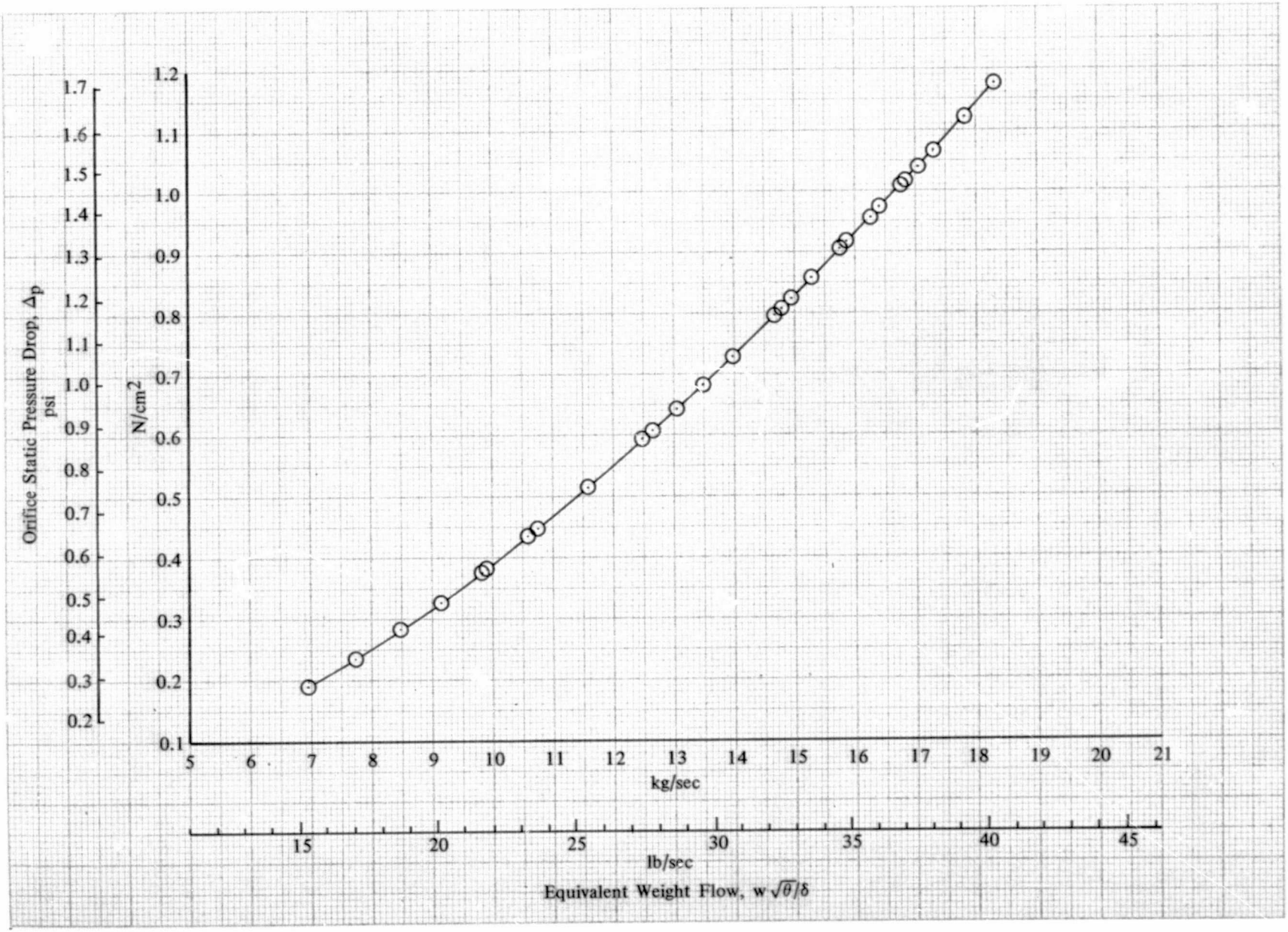


Figure 28. Orifice Static Pressure Drop vs Equivalent Weight Flow for Stage F Flowpath With Support Screen

DF 102106

## Presentation of Data

### Uniform Inlet

Overall Performance - Overall performance data are presented in terms of total pressure ratio and adiabatic efficiency as functions of equivalent weight flow ($W\sqrt{\theta}/\delta$) and equivalent rotor speed ($N/\sqrt{\theta}$) for the rotor in figure 29, rotor-stator in figure 30 and the IGV-rotor-stator (stage) in figure 31. The design total pressure ratio and adiabatic efficiency for the rotor were 1.614 and 94.5%, respectively, at design flow. The corresponding design values for the rotor-stator were 1.565 and 87.8% and for the stage were 1.559 and 87.2%. The design point is shown on each figure for comparison with the performance results. The dashed stall line in figures 29 through 31 passes through surge points determined from the transient data. Pressure ratio, adiabatic efficiency, and polytropic efficiency for the rotor, rotor-stator, and IGV-rotor-stator (stage) are tabulated for the steady-state data points in table XI and repeated in Appendix B of Volume II.

Based on a curve faired through the data points, the rotor achieved an adiabatic efficiency of 91.8% and a total pressure of 1.595 at design equivalent rotor speed and flow. At the same flow and rotor speed, the rotor-stator achieved an adiabatic efficiency of 86.7% and a total pressure ratio of 1.561 and the stage achieved an adiabatic efficiency of 86.3% and a total pressure ratio of 1.560. At design equivalent rotor speed, maximum rotor, rotor-stator, and stage adiabatic efficiencies of 91.9, 86.7, and 86.4%, respectively, were reached at approximately 100.8, 100.9, and 101.1% design equivalent flow; corresponding surge margins were 12.9, 13.1, and 12.6%.

Blade Element Performance and Flow Distribution Data - As discussed on page 50, the blade element performance and flow distribution data were calculated for the instrumentation stations and for the IGV, rotor and stator leading and trailing edges. Table B-2 of Appendix B, Volume II, presents the data at the instrumentation stations at the near design point operating condition and is included to illustrate the differences at the near design point between values calculated from the data at the instrumentation stations and the values calculated from the data that have been translated to the IGV, rotor and stator leading and trailing edges. The differences are small except for the values translated to the IGV trailing edge and the rotor leading edge. These differences are caused by the convergence of the OD wall between the IGV and rotor which results in a reduction of approximately 18% in annulus area. Only the translated values are given in tables B-3 and B-4 of Appendix B, Volume II, for the remaining uniform inlet compressor test points. The plotted results discussed for the rotor and stator in the following paragraphs are based on the translated data.

Inlet Guide Vane Blade Element Performance - Inlet guide vane exit air angle distributions are presented in figure 32 for the two data points closest to design speed and flow. Air angle data obtained with each of two 30-deg wedge probes are identified by symbol, and the design air angle distribution is shown for comparison. The air angles measured with the two probes agree closely with a maximum difference of approximately one deg. The average of the measured air angles agrees within 1.5 deg of the design air angle across the span except at 5% and 95% of span from the tip where the difference increases to approximately 2.0 deg.

Rotor Blade Element Performance - Rotor diffusion factor, deviation angle, and loss coefficient are shown as functions of incidence angle in figures 33a through 33i. At the design incidence angle and rotor speed, total pressure losses were slightly higher than the design value from 5 to 70% span from the tip and substantially greater than the design value at 85 to 95% span. Deviation angles were one to two deg less than the design value between 5 and 70% span from the tip, seven deg less than the design value at 85 and 90% span and approximately four deg less at 95% span. The diffusion factor at design incidence angle and rotor speed was greater than the design value at all spanwise locations with the maximum differences occurring at 85, 90, and 95% span from the tip.

Loss parameter versus diffusion factor is presented in figures 34a through 34e for 10, 30, 50, 70, and 90% span, respectively. The design value and the data point corresponding to the minimum loss coefficient at design equivalent rotor speed are indicated on each figure. Comparison of these two points shows that the measured data are higher than the design point loss parameter and diffusion factor at each span.

Figure 35 compares the data points corresponding to the minimum loss coefficient points at design equivalent rotor speed to the momentum thickness parameter - diffusion factor design curves. This loss-loading comparison accounts for the influence of the difference between the measured diffusion factor values and the design values on the blade element losses. Figure 35 shows that the measured rotor performance was close to the design curves at all spans.

Stator Blade Element Performance - Stator diffusion factor, deviation angle, and loss coefficient are presented as functions of incidence angle in figures 36a through 36i. For design incidence angle and rotor speed, the stator losses were the same as or less than design at 50 and 70% span from the tip and greater than design at 5, 10, 15, and 30% span. Deviation angles, at design incidence, were greater than the design values at 5 and 10% span and approximately the same as design at 15 to 70% span. Diffusion factors, at design incidence angle and rotor speed, were less than the design value at 5 to 70% span from the tip. Similar comparisons could not be made at 85, 90, and 95% span from the tip because the design incidence at these spanwise locations was from 4.6 to 6.2 deg less than the closest data point at design rotor speed.

Loss parameter versus diffusion factor is shown in figures 37a through 37e for 10, 30, 50, 70, and 90% spans, respectively. The design value and the data point corresponding to the minimum loss coefficient at design equivalent rotor speed are indicated on each figure. Comparison of these two data points shows the measured data have a loss parameter and diffusion factor approximately the same as or less than the design value at each span.

Figure 38 compares the data points corresponding to the minimum loss coefficient points at design equivalent rotor speed to the momentum thickness parameter - diffusion factor design curves. This comparison shows that the measured stator performance was lower than the design curves at 30, 70 and 90% span and higher than the design curves at 10 and 50% span.

Wall Static Pressure - The wall static pressure data at instrumentation Stations 3 and 4 were examined to determine if circumferential and gapwise gradients were significant. As shown in figure 39, the variations of static pressure at different circumferential locations at approximately the same location relative to the stator vane, are small relative to the variations that exist within one stator vane gap. It was therefore concluded that no significant circumferential variation was present in these data but that a substantial gapwise variation was present. This strong pressure field due to the stator vanes is consistent with the substantial gapwise total pressure and temperature gradients noted in the data reduction section.

Table XI. Overall Performance of Stage F
Uniform Inlet

| (IGV Inlet) Equivalent Weight Flow kg/sec | lb/sec | Rotor $\overline{P}_3/\overline{P}_2$ | Rotor $\eta_{ad}$ | Rotor $\eta_p$ | Rotor-Stator $\overline{P}_4/\overline{P}_2$ | Rotor-Stator $\eta_{ad}$ | Rotor-Stator $\eta_p$ | IGV - Rotor-Stator $\overline{P}_4/\overline{P}_1$ | IGV - Rotor-Stator $\eta_{ad}$ | IGV - Rotor-Stator $\eta_p$ |
|---|---|---|---|---|---|---|---|---|---|---|
| | | | | | 100% Design Equivalent Rotor Speed | | | | | |
| 18.25 | 40.23 | 1.490 | 0.796 | 0.807 | 1.419 | 0.691 | 0.706 | 1.415 | 0.685 | 0.700 |
| 17.78 | 39.19 | 1.583 | 0.902 | 0.908 | 1.543 | 0.847 | 0.856 | 1.542 | 0.845 | 0.854 |
| 17.26 | 38.04 | 1.596 | 0.918 | 0.923 | 1.559 | 0.867 | 0.875 | 1.556 | 0.863 | 0.871 |
| 16.75 | 36.94 | 1.587 | 0.908 | 0.914 | 1.554 | 0.862 | 0.871 | 1.552 | 0.860 | 0.868 |
| 16.22 | 35.76 | 1.594 | 0.899 | 0.906 | 1.565 | 0.858 | 0.867 | 1.562 | 0.855 | 0.864 |
| 15.70 | 34.62 | 1.593 | 0.901 | 0.908 | 1.553 | 0.847 | 0.857 | 1.551 | 0.844 | 0.853 |
| | | | | | 95% Design Equivalent Rotor Speed | | | | | |
| 17.75 | 39.13 | 1.430 | 0.820 | 0.829 | 1.372 | 0.717 | 0.729 | 1.368 | 0.709 | 0.722 |
| 17.00 | 37.48 | 1.517 | 0.936 | 0.939 | 1.474 | 0.866 | 0.873 | 1.470 | 0.860 | 0.868 |
| 16.36 | 36.07 | 1.524 | 0.935 | 0.939 | 1.488 | 0.877 | 0.884 | 1.485 | 0.872 | 0.879 |
| 15.75 | 34.72 | 1.515 | 0.915 | 0.920 | 1.483 | 0.864 | 0.871 | 1.479 | 0.858 | 0.866 |
| 15.25 | 33.61 | 1.515 | 0.907 | 0.912 | 1.478 | 0.849 | 0.857 | 1.476 | 0.846 | 0.854 |
| 14.70 | 32.40 | 1.520 | 0.896 | 0.902 | 1.476 | 0.828 | 0.837 | 1.474 | 0.824 | 0.833 |
| | | | | | 85% Design Equivalent Rotor Speed | | | | | |
| 16.70 | 36.81 | 1.332 | 0.864 | 0.869 | 1.299 | 0.784 | 0.791 | 1.297 | 0.778 | 0.786 |
| 15.78 | 34.78 | 1.391 | 0.943 | 0.946 | 1.368 | 0.891 | 0.896 | 1.365 | 0.887 | 0.891 |
| 14.92 | 32.88 | 1.395 | 0.934 | 0.937 | 1.369 | 0.876 | 0.881 | 1.367 | 0.872 | 0.877 |
| 13.95 | 30.75 | 1.397 | 0.913 | 0.917 | 1.376 | 0.869 | 0.875 | 1.374 | 0.865 | 0.871 |
| 13.01 | 28.68 | 1.402 | 0.903 | 0.907 | 1.377 | 0.851 | 0.858 | 1.376 | 0.849 | 0.856 |
| 12.61 | 27.80 | 1.402 | 0.893 | 0.898 | 1.373 | 0.834 | 0.841 | 1.372 | 0.832 | 0.839 |
| | | | | | 70% Design Equivalent Rotor Speed | | | | | |
| 14.61 | 32.22 | 1.236 | 0.950 | 0.952 | 1.214 | 0.865 | 0.869 | 1.211 | 0.856 | 0.860 |
| 13.44 | 29.62 | 1.249 | 0.957 | 0.959 | 1.235 | 0.905 | 0.908 | 1.233 | 0.898 | 0.901 |
| 12.46 | 27.46 | 1.252 | 0.943 | 0.944 | 1.240 | 0.902 | 0.904 | 1.239 | 0.899 | 0.902 |
| 11.57 | 25.50 | 1.252 | 0.938 | 0.940 | 1.241 | 0.898 | 0.902 | 1.239 | 0.892 | 0.895 |
| 10.59 | 23.35 | 1.255 | 0.916 | 0.919 | 1.241 | 0.869 | 0.873 | 1.240 | 0.865 | 0.869 |
| 9.81 | 21.63 | 1.257 | 0.889 | 0.892 | 1.239 | 0.828 | 0.833 | 1.238 | 0.826 | 0.832 |
| | | | | | 50% Design Equivalent Rotor Speed | | | | | |
| 10.73 | 23.65 | 1.116 | 0.950 | 0.951 | 1.108 | 0.890 | 0.890 | 1.107 | 0.881 | 0.882 |
| 9.89 | 21.81 | 1.117 | 0.956 | 0.957 | 1.112 | 0.913 | 0.914 | 1.111 | 0.906 | 0.907 |
| 9.14 | 20.15 | 1.119 | 0.921 | 0.922 | 1.114 | 0.884 | 0.886 | 1.113 | 0.878 | 0.880 |
| 8.47 | 18.67 | 1.120 | 0.916 | 0.917 | 1.115 | 0.875 | 0.877 | 1.114 | 0.869 | 0.871 |
| 7.73 | 17.04 | 1.123 | 0.927 | 0.928 | 1.117 | 0.888 | 0.890 | 1.117 | 0.884 | 0.886 |
| 6.92 | 15.25 | 1.125 | 0.908 | 0.910 | 1.118 | 0.853 | 0.855 | 1.117 | 0.851 | 0.853 |

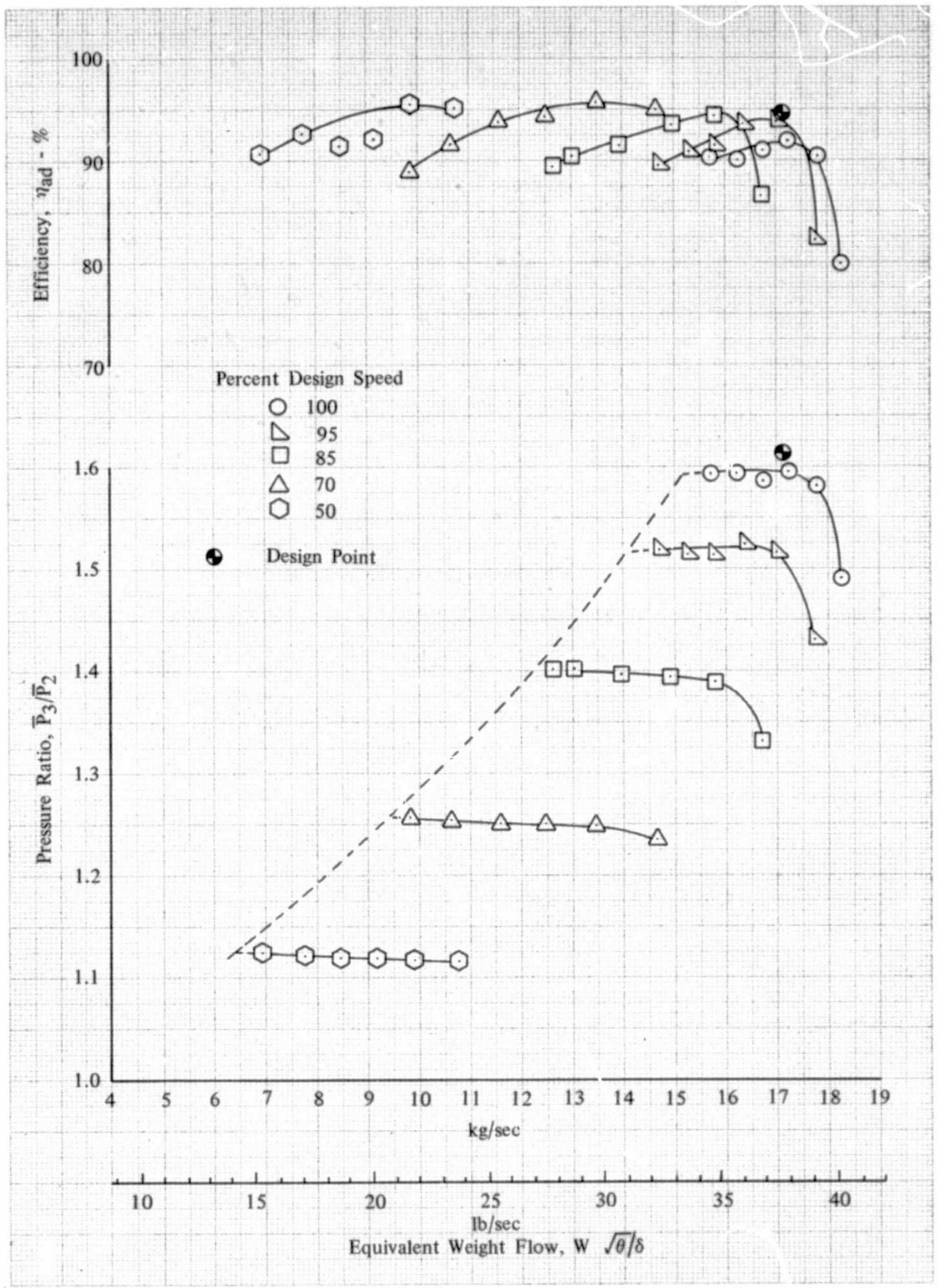


Figure 29. Overall Performance of Rotor F with Uniform Inlet Flow

DF 102107

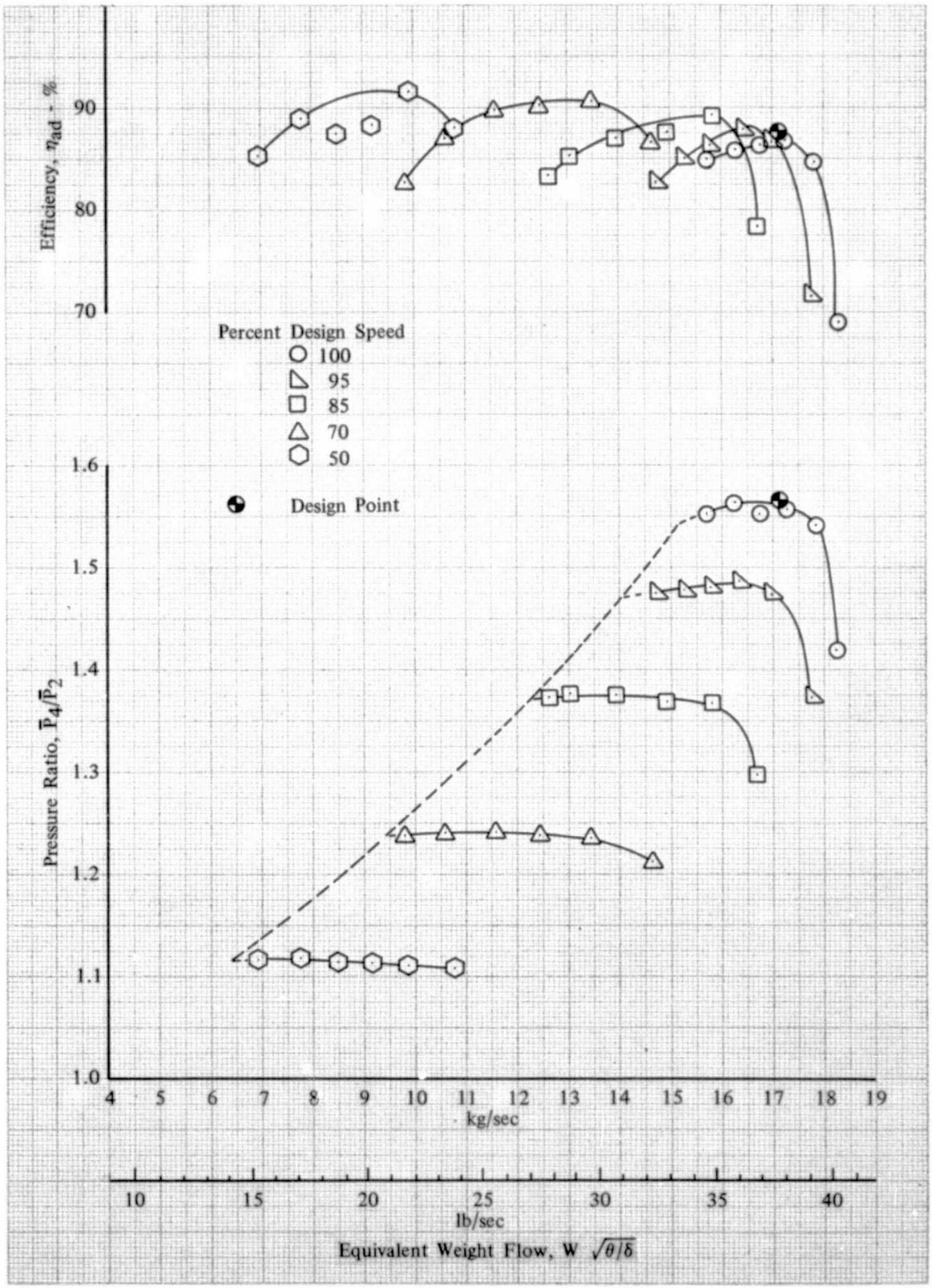


Figure 30. Overall Performance of Rotor F-Stator F with Uniform Inlet Flow DF 102108

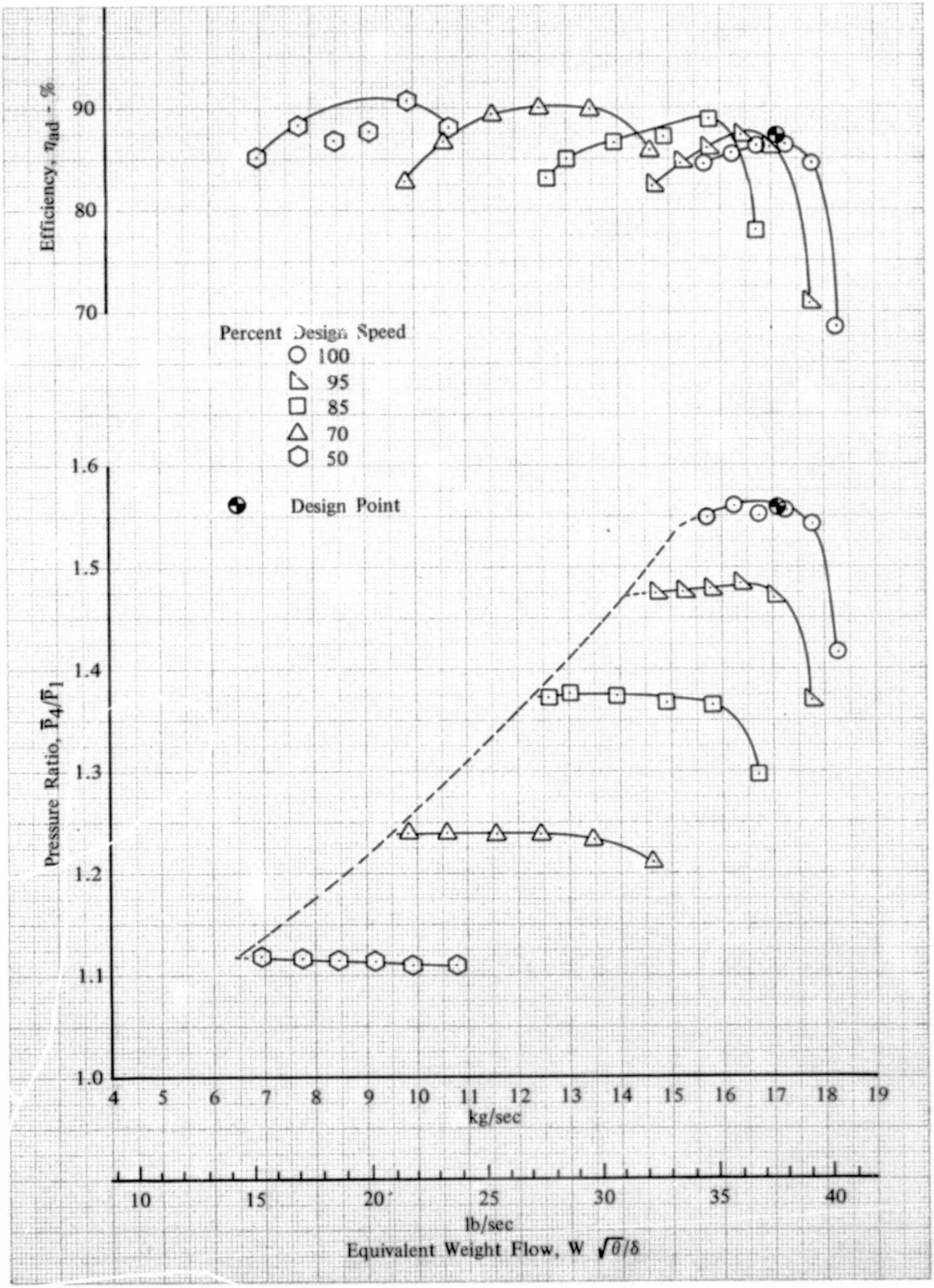


Figure 31. Overall Performance of Stage F with Uniform Inlet Flow DF 102109

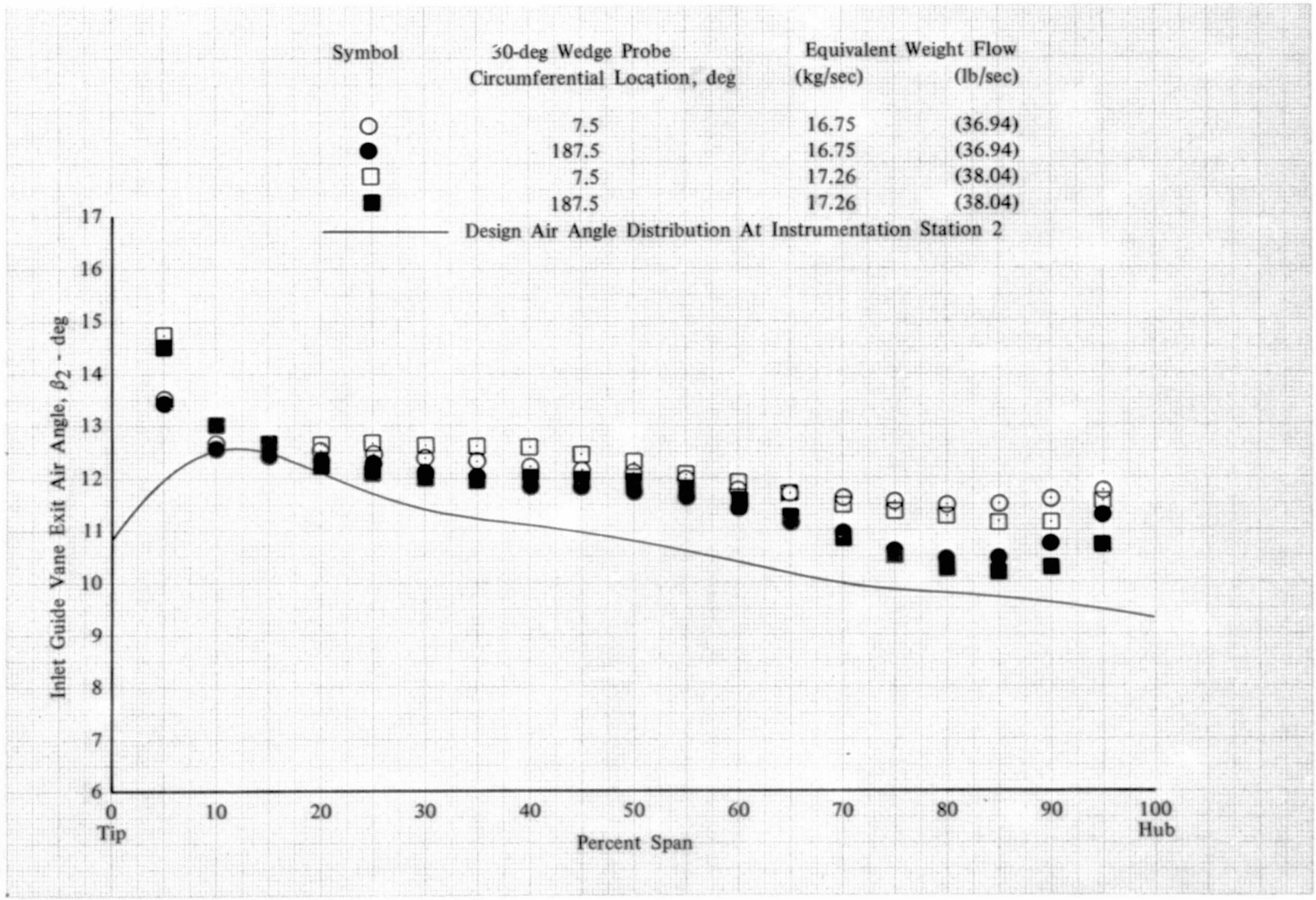


Figure 32. Stage F Inlet Guide Vane Exit Air Angle Distribution

DF 102110

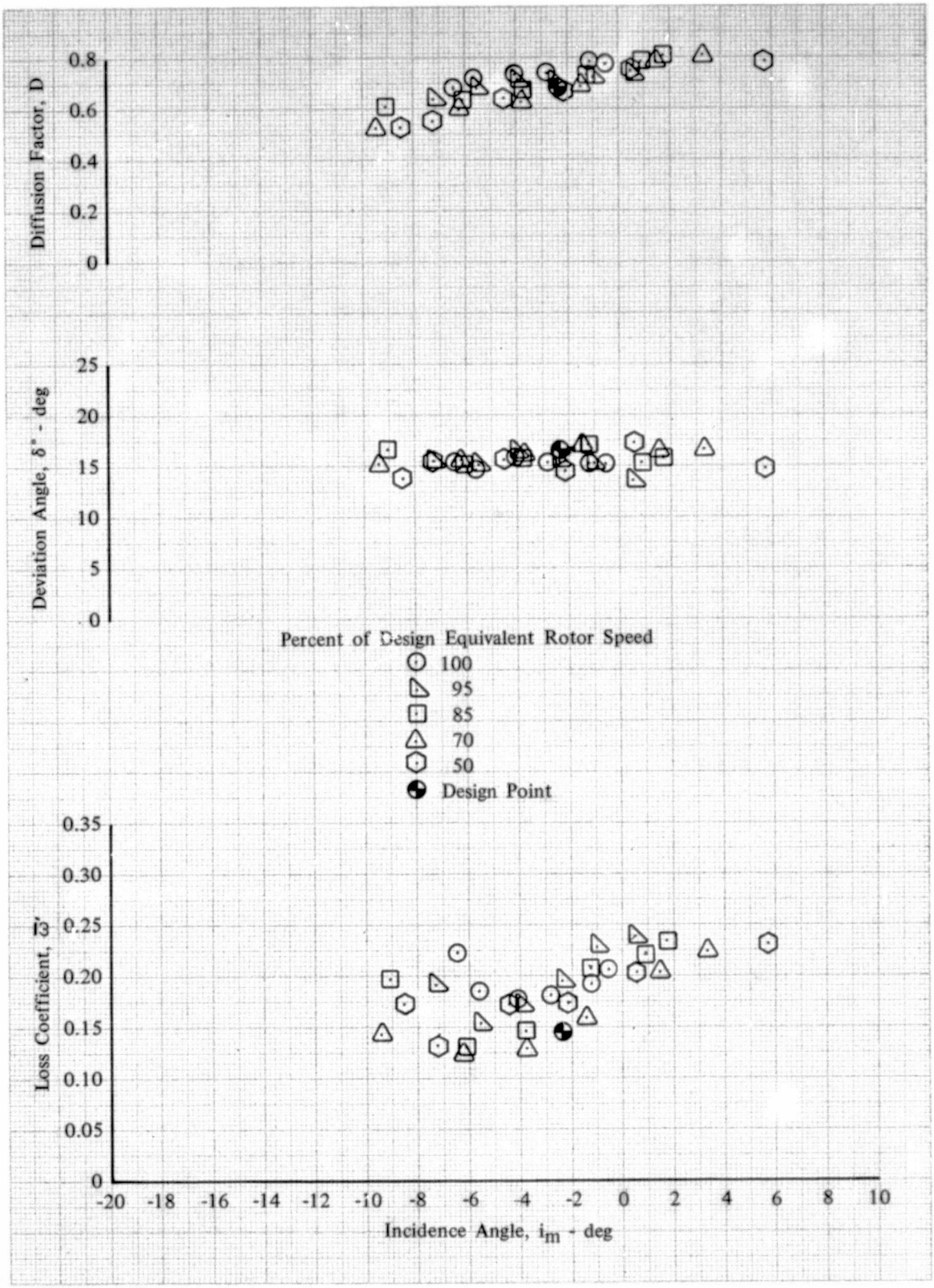


Figure 33a. Rotor F Blade Element Performance, 5% Span from Tip; Uniform Inlet Flow

DF 102111

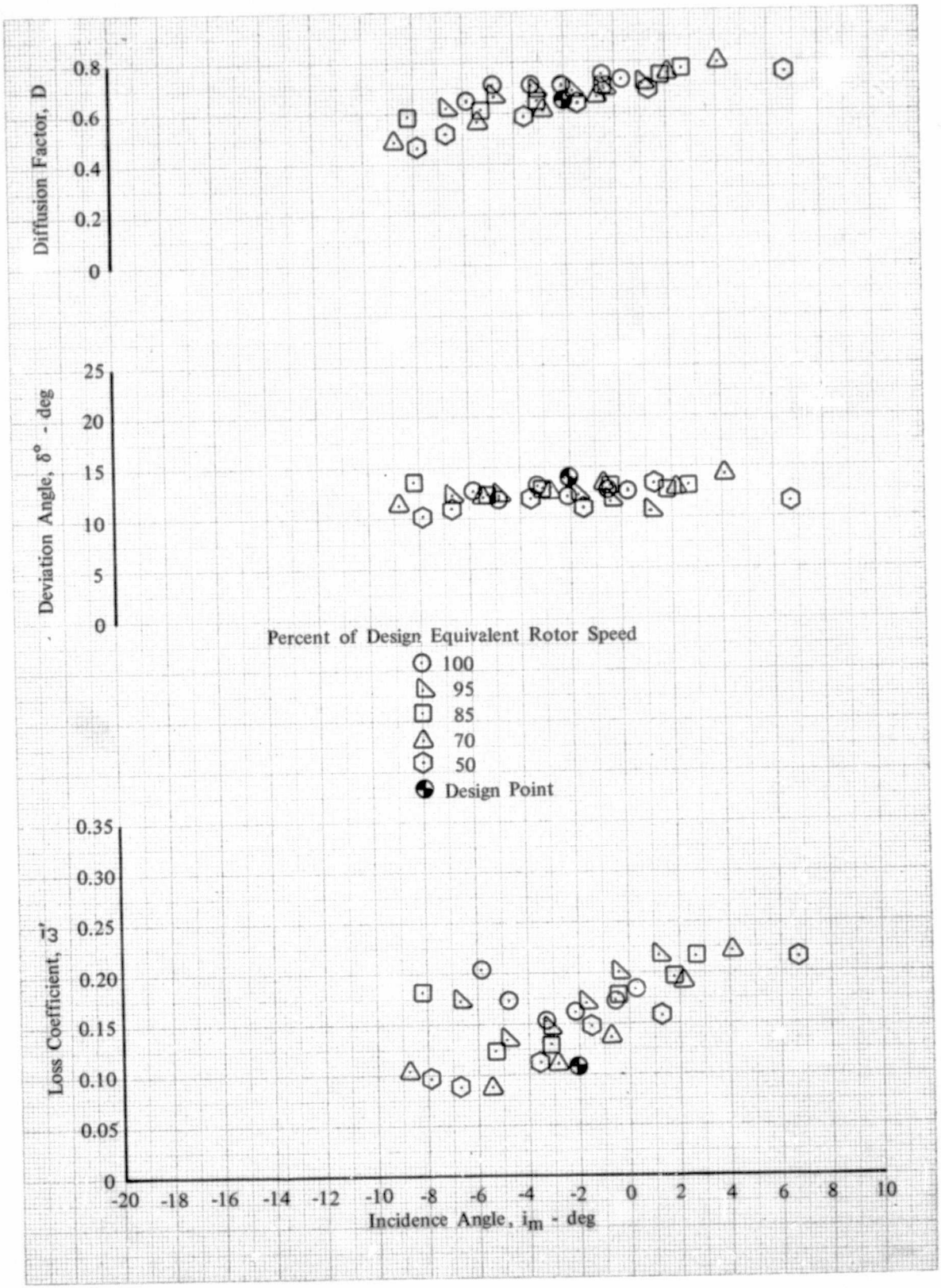


Figure 33b. Rotor F Blade Element Performance, 10% Span from Tip; Uniform Inlet Flow DF 102112

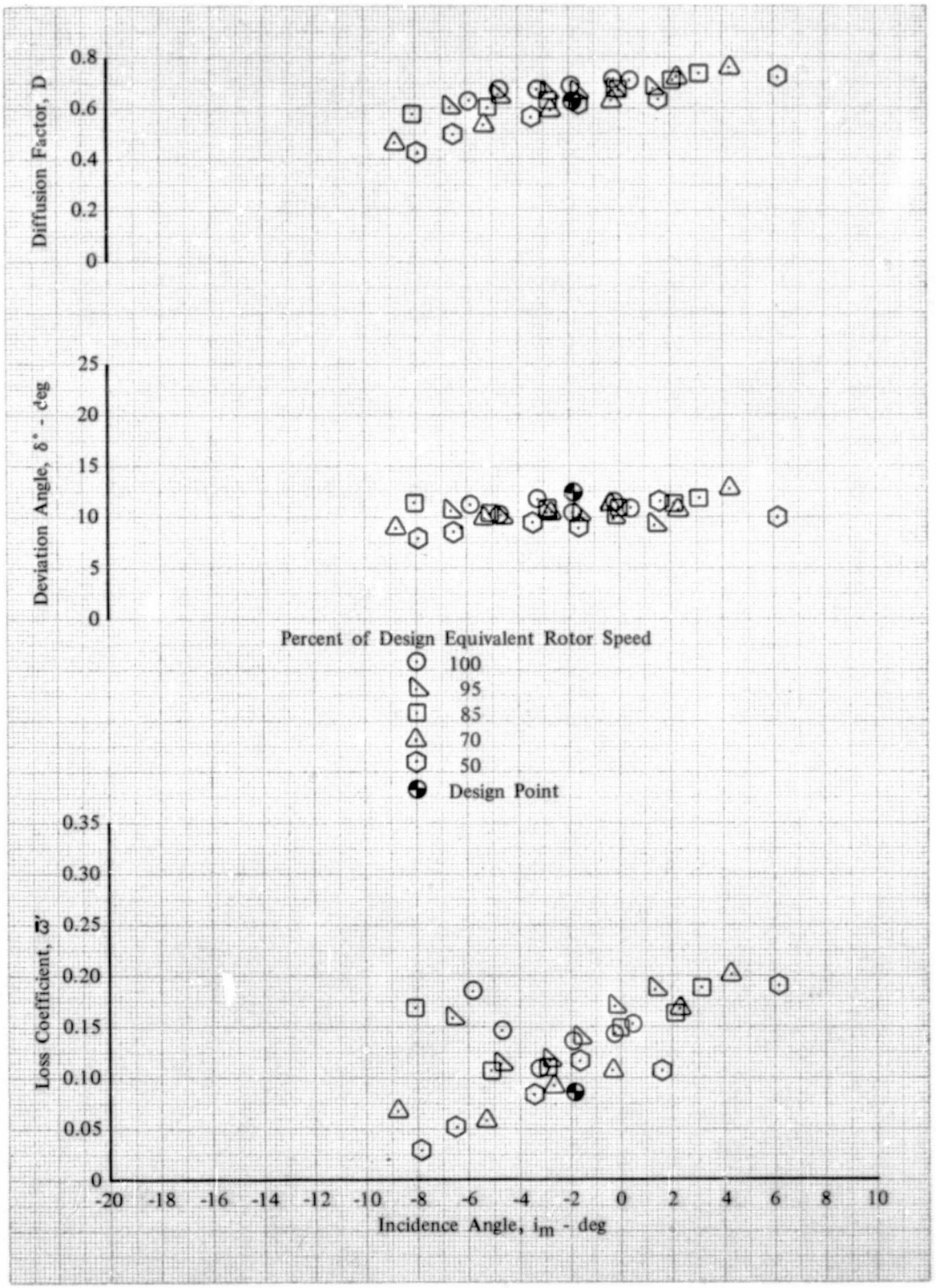


Figure 33c. Rotor F Blade Element Performance, 15% Span from Tip; Uniform Inlet Flow

DF 102113

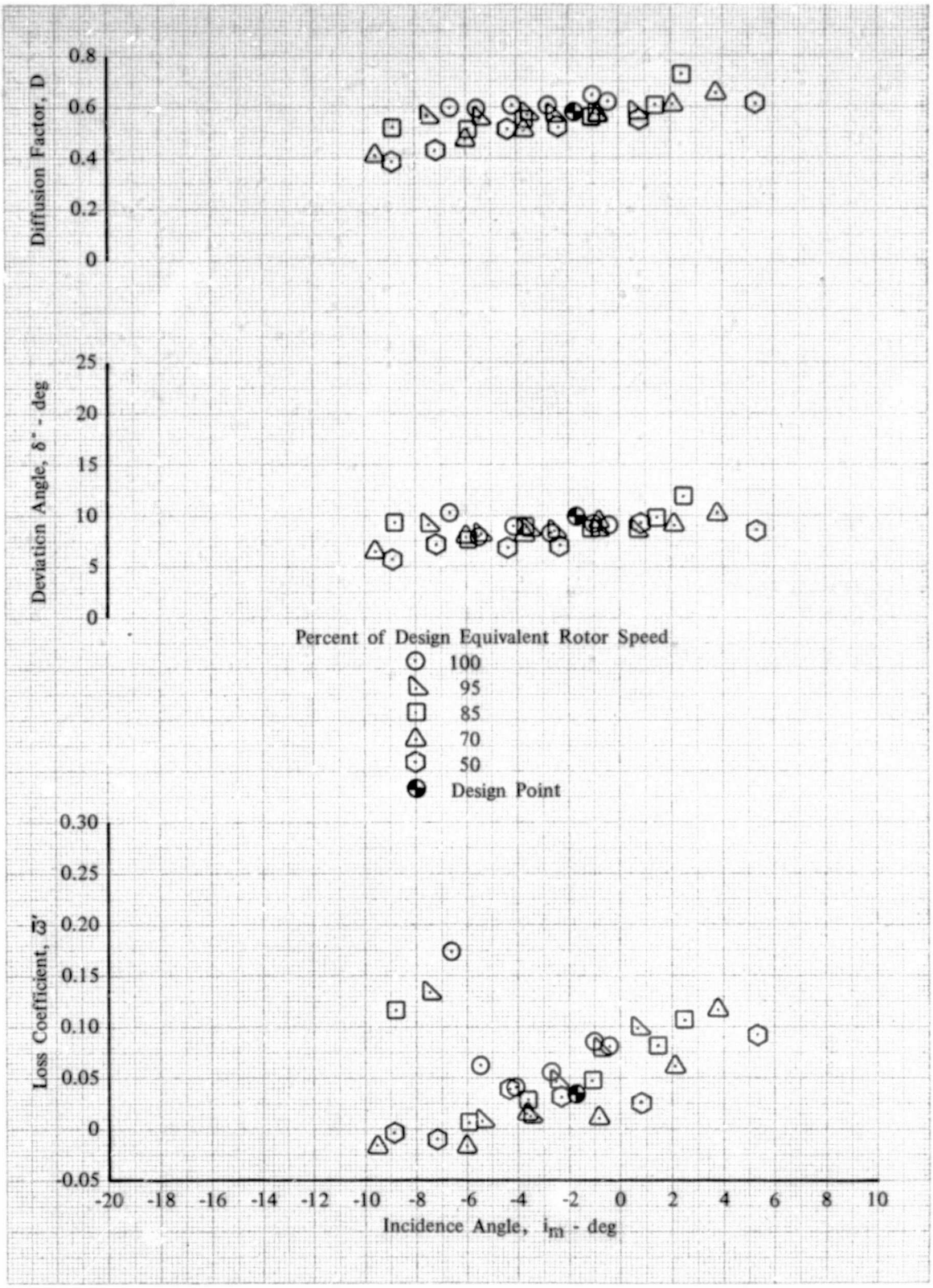


Figure 33d. Rotor F Blade Element Performance, 30% Span from Tip; Uniform Inlet Flow DF 102114

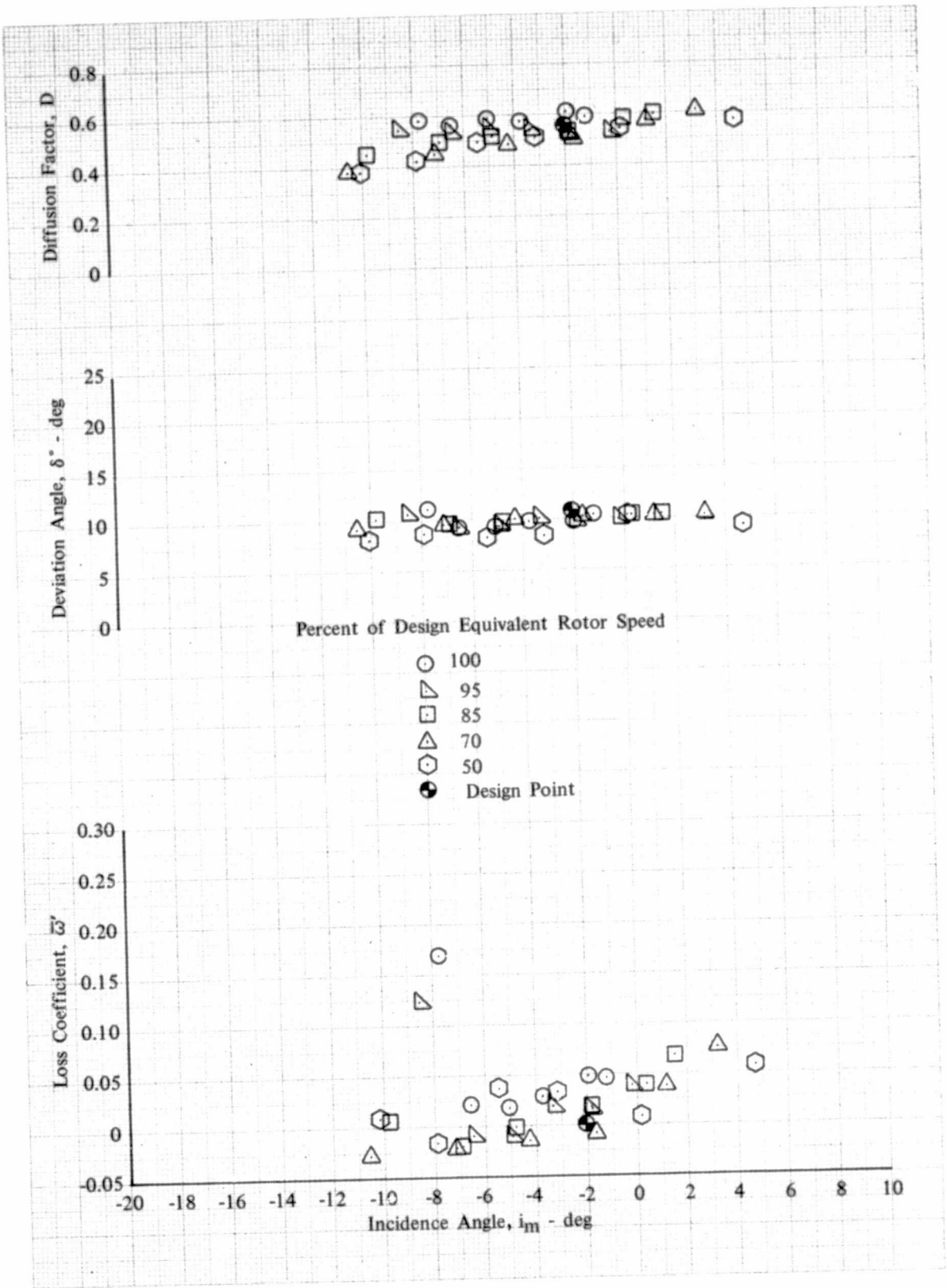


Figure 33e. Rotor F Blade Element Performance, 50% Span; Uniform Inlet Flow

DF 102115

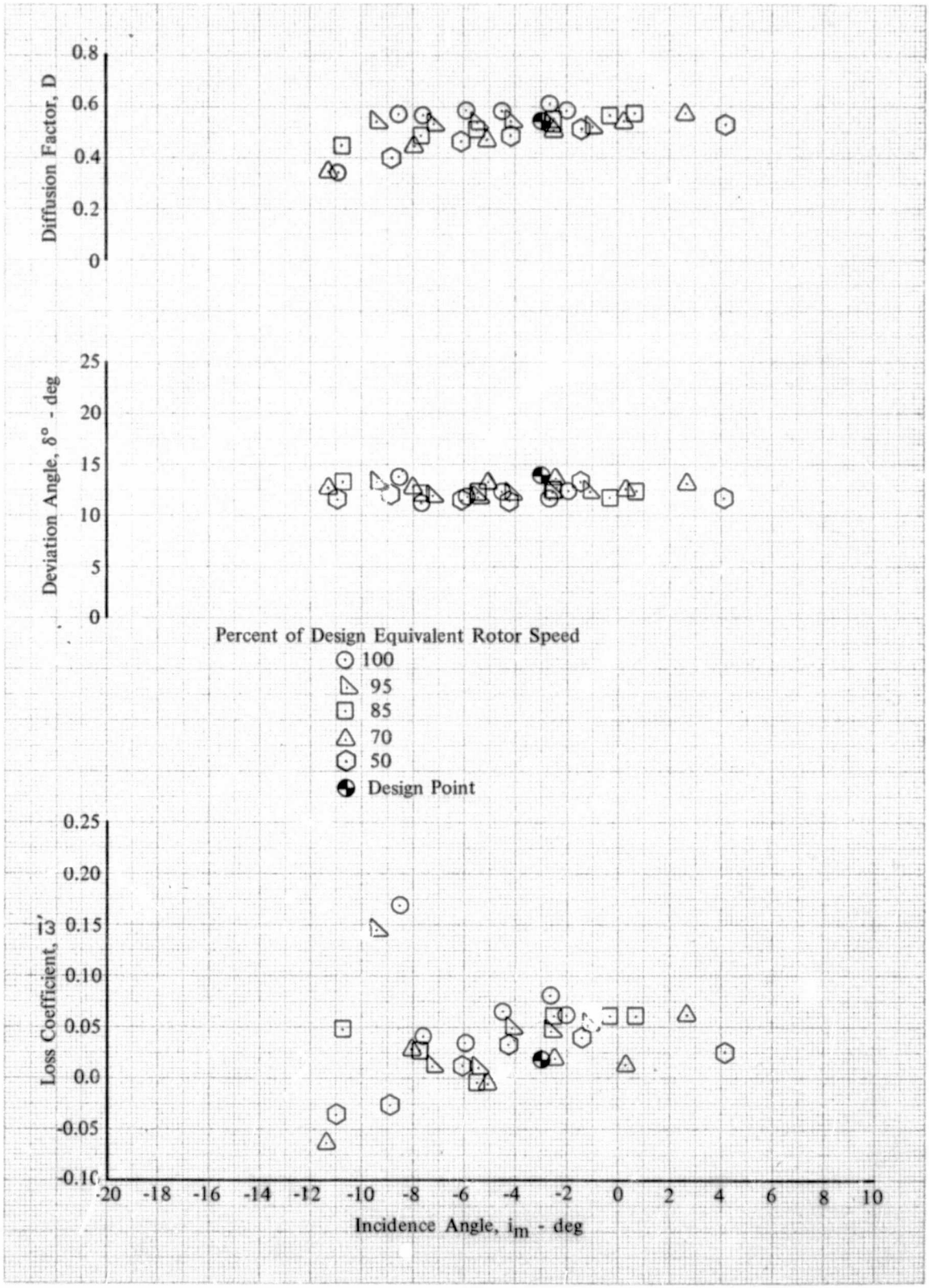


Figure 33f. Rotor F Blade Element Performance, 70% Span from Tip; Uniform Inlet Flow DF 102116

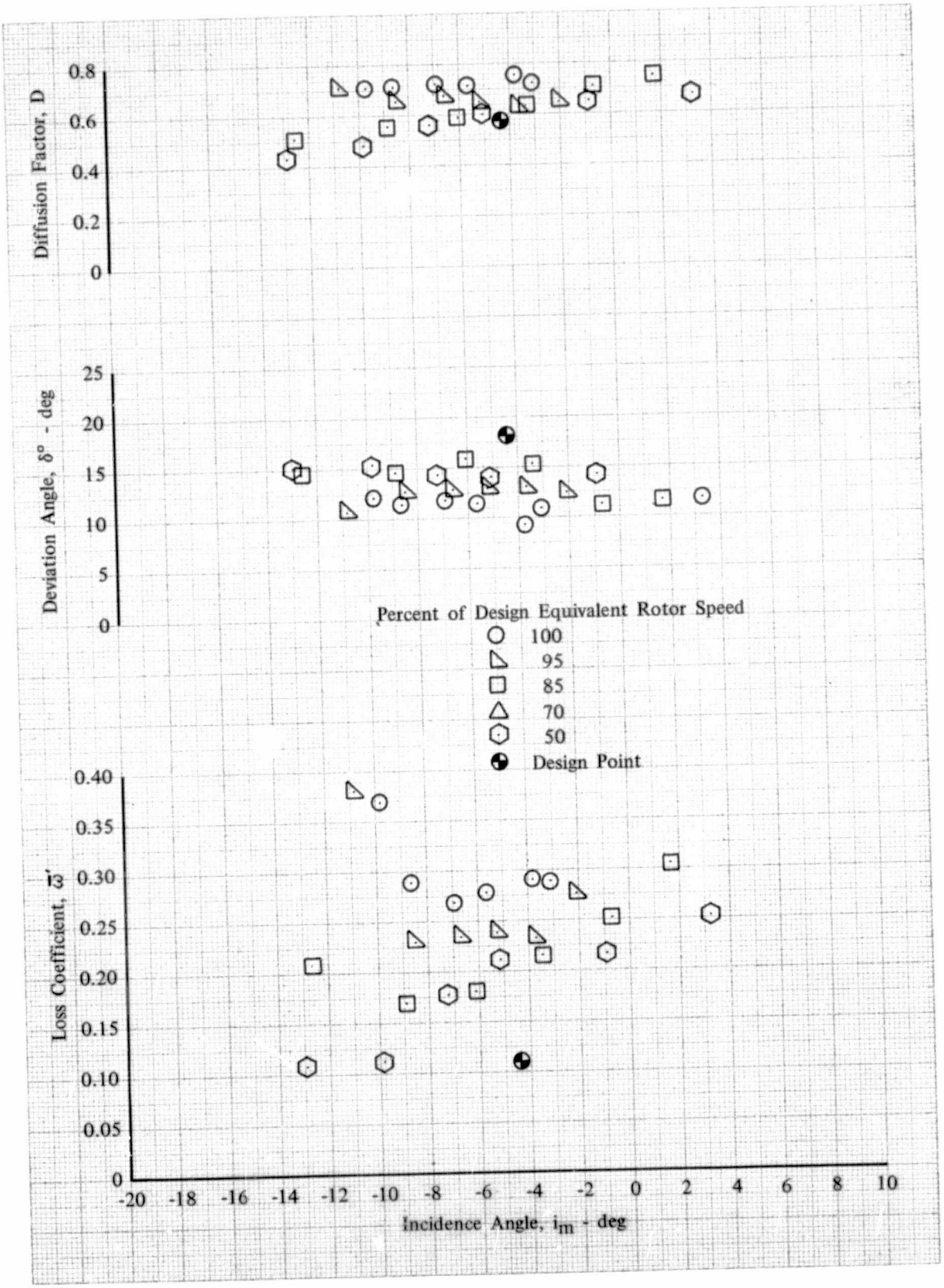


Figure 33g. Rotor F Blade Element Performance, 85% Span from Tip; Uniform Inlet Flow

DF 102117

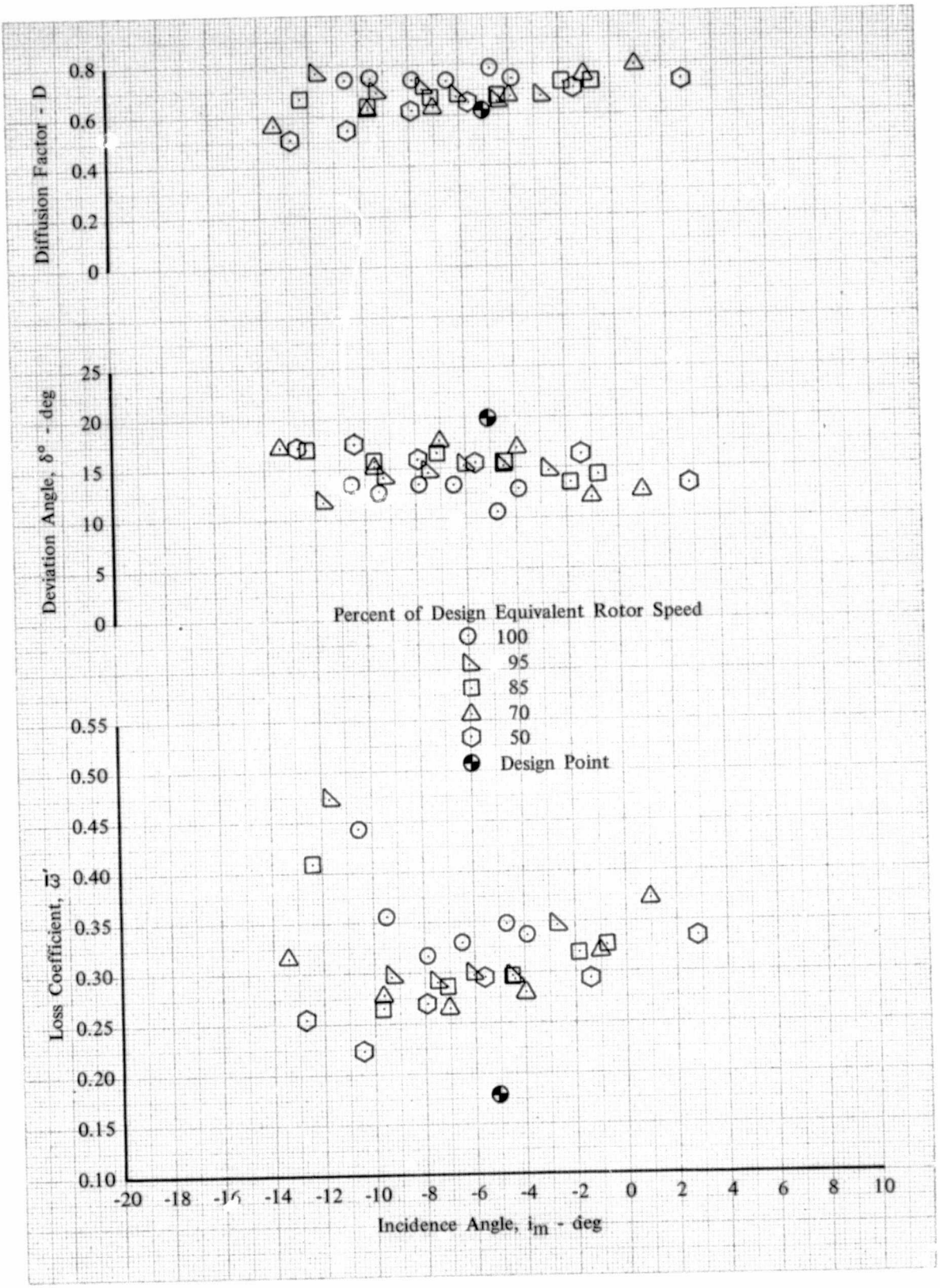


Figure 33h. Rotor F Blade Element Performance, 90% Span from Tip; Uniform Inlet Flow

DF 102118

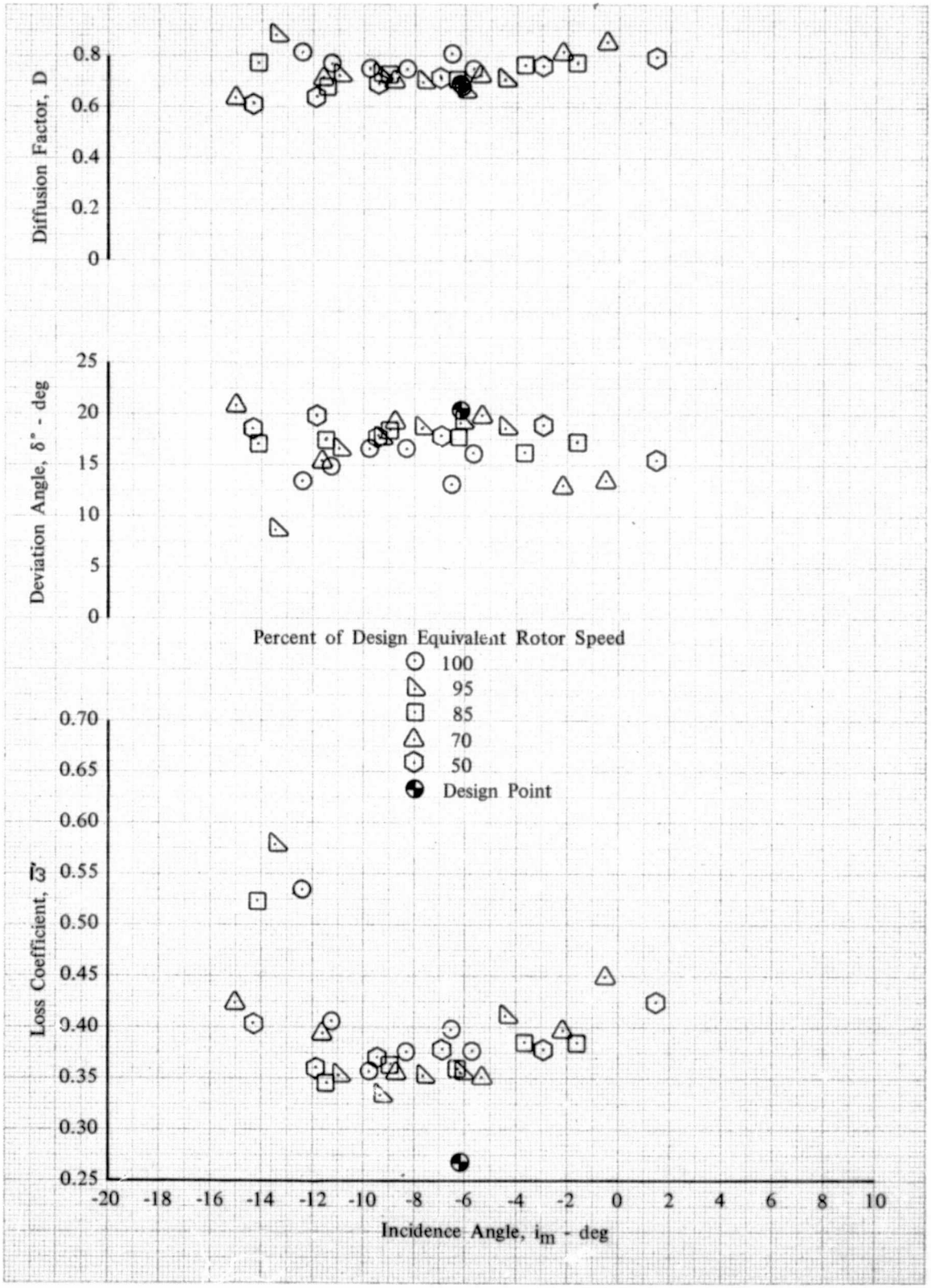


Figure 33i. Rotor F Blade Element Performance, 95% Span from Tip; Uniform Inlet Flow DF 102119

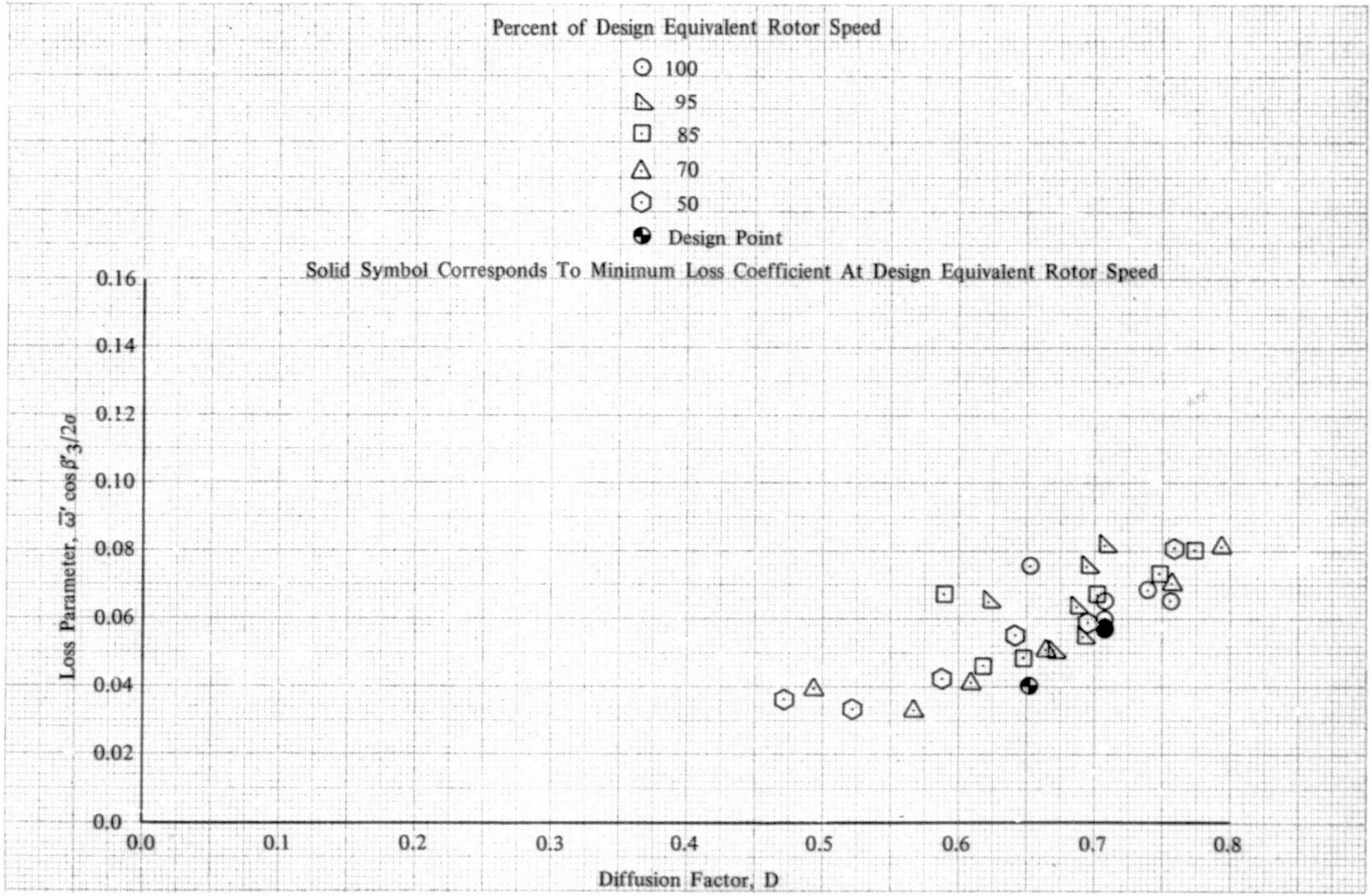


Figure 34a. Rotor F Loss Parameter vs Diffusion Factor, 10% Span from Tip; Uniform Inlet Flow DF 102120

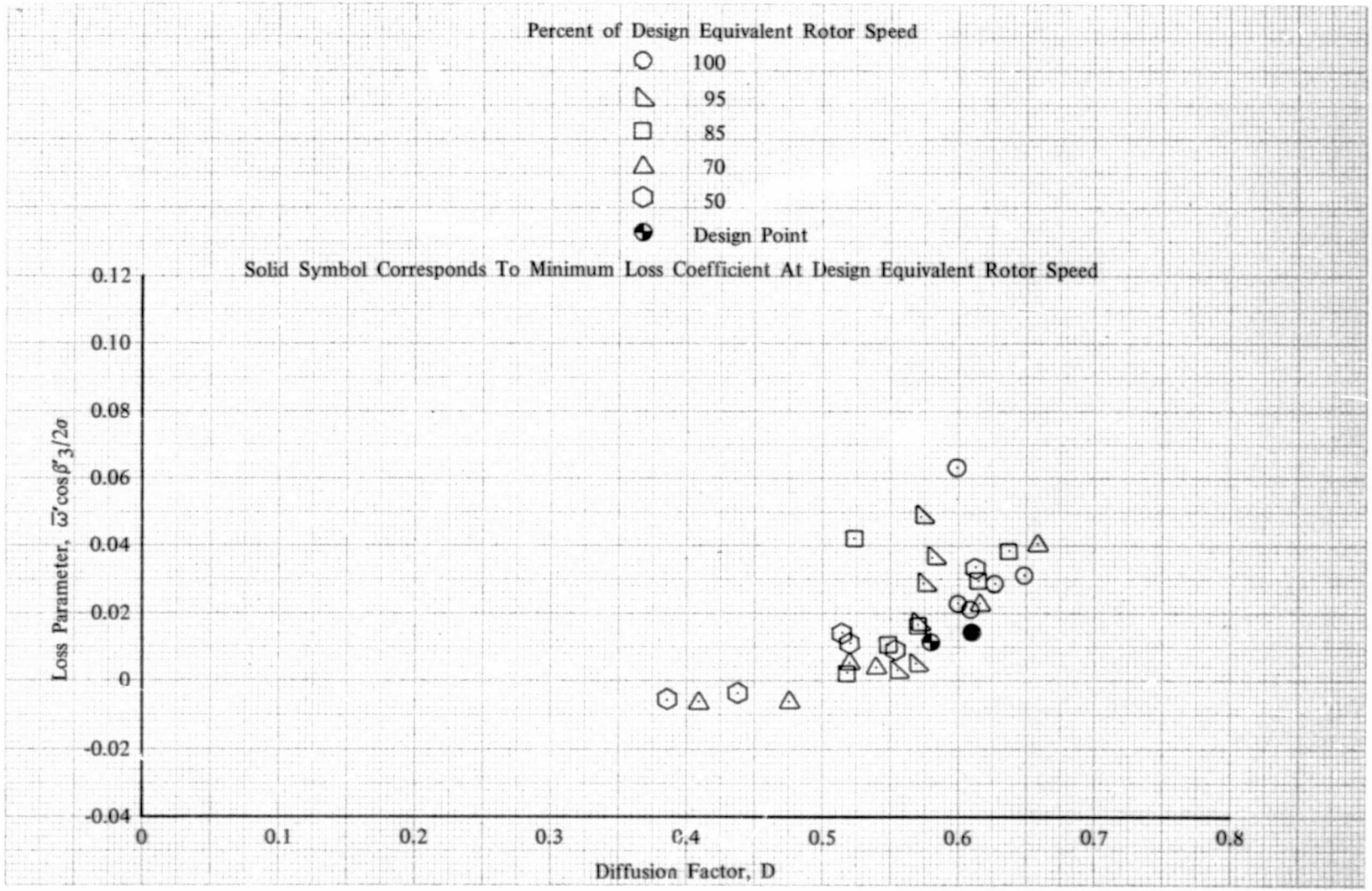


Figure 34b. Rotor F Loss Parameter vs Diffusion Factor, 30% Span from Tip; Uniform Inlet Flow DF 102121

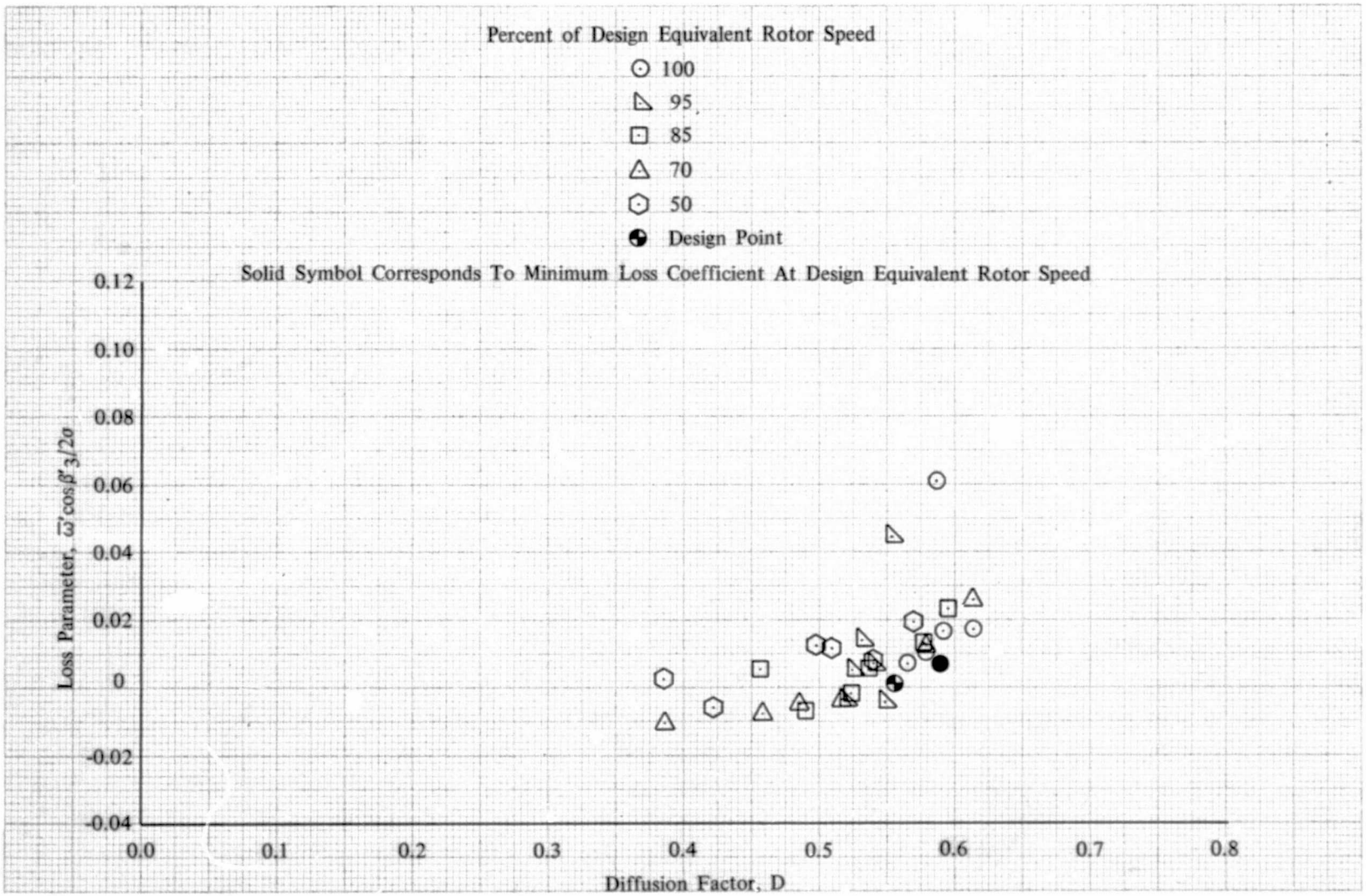


Figure 34c. Rotor F Loss Parameter vs Diffusion Factor, 50% Span; Uniform Inlet Flow DF 102122

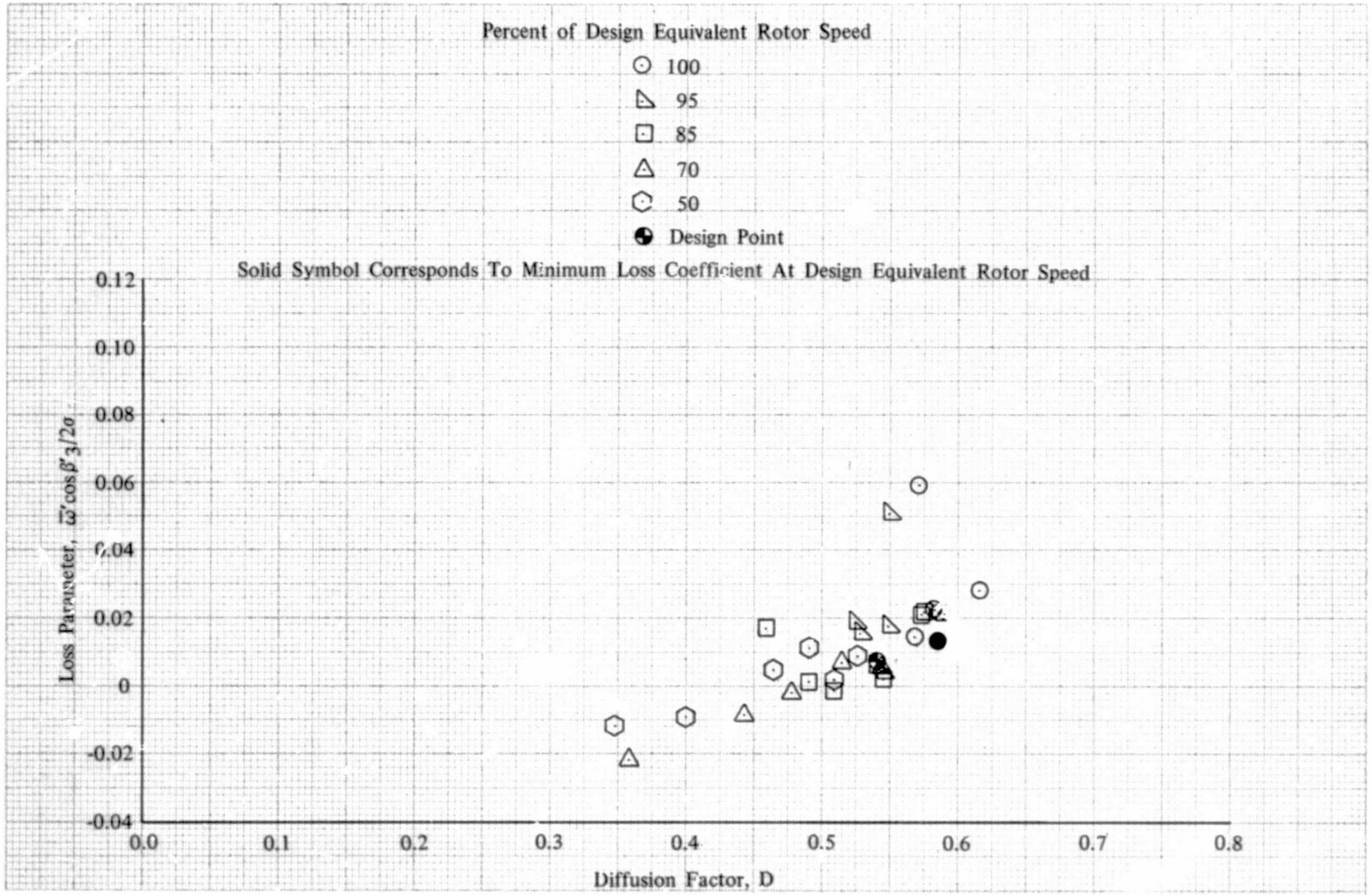


Figure 24d. Rotor F Loss Parameter vs Diffusion Factor, 70% Span from Tip; Uniform Inlet Flow DF 102123

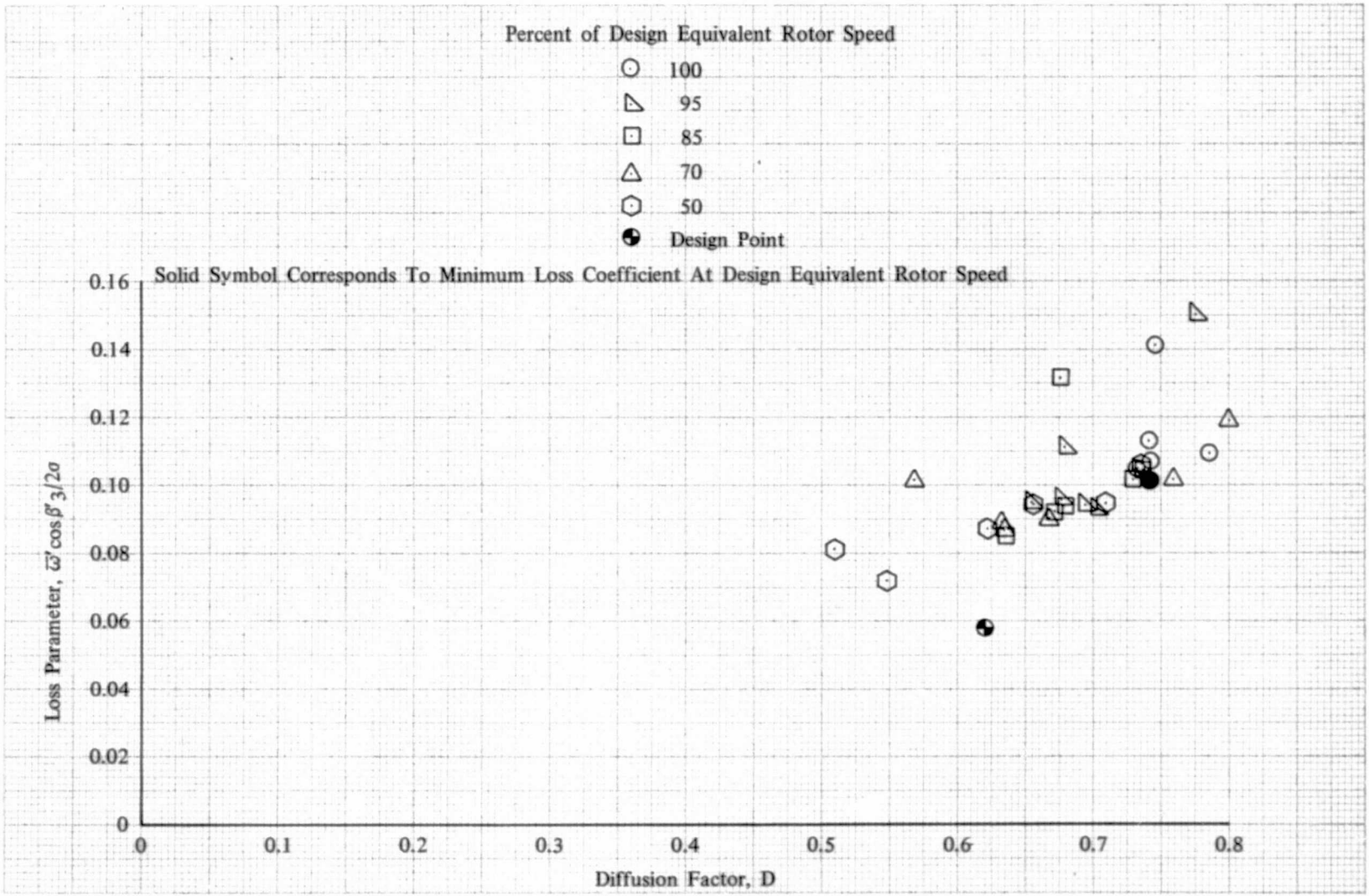


Figure 34e. Rotor F Loss Parameter vs Diffusion Factor, 90% Span from Tip; Uniform Inlet Flow DF 102124

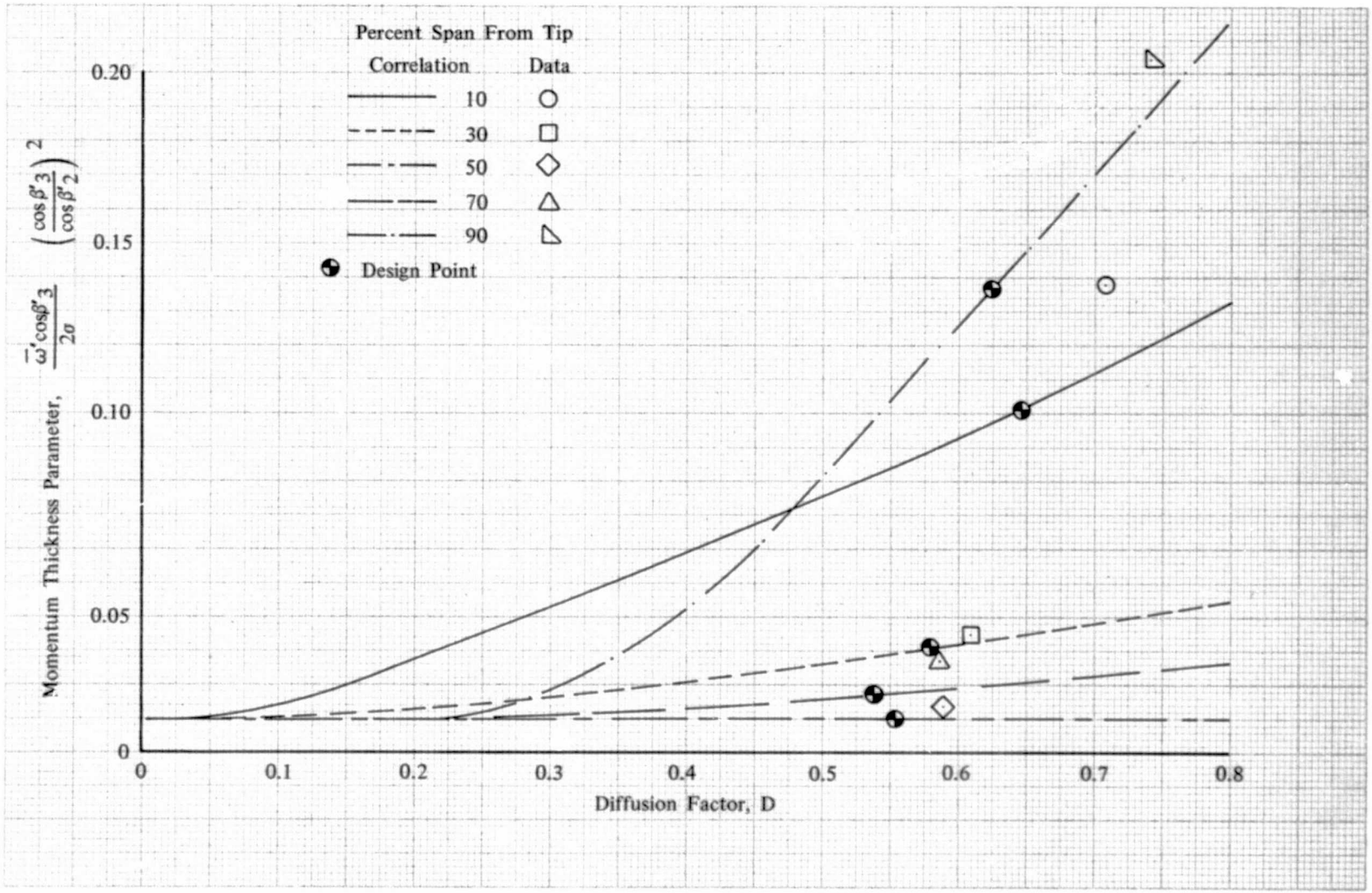


Figure 35. Comparison of Measured Minimum Loss Coefficient Points to Momentum Thickness Parameter for Rotor F at Design Equivalent Rotor Speed; Uniform Inlet

DF 102125

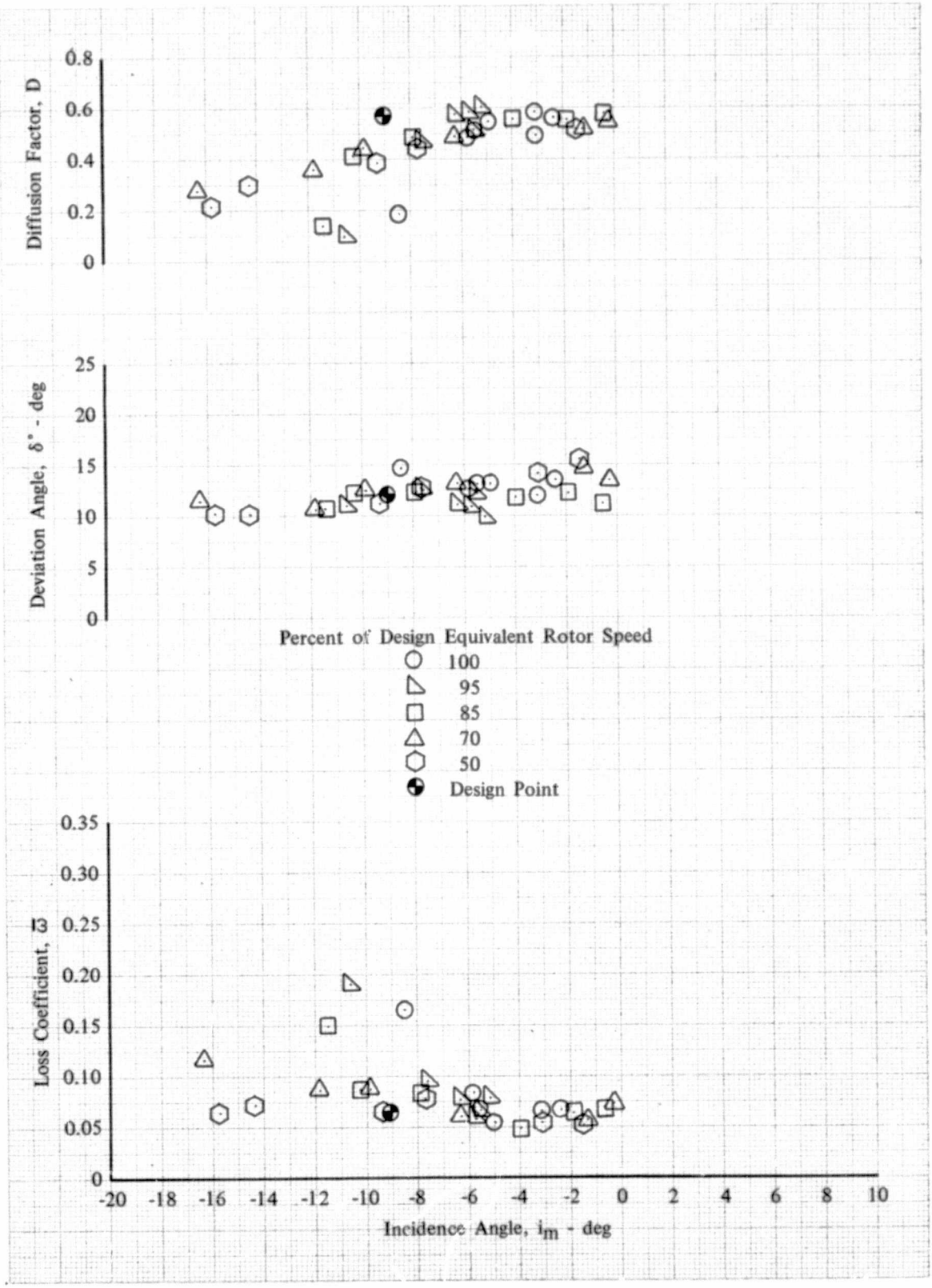


Figure 36a. Stator F Blade Element Performance, 5% Span from Tip; Uniform Inlet Flow DF 102126

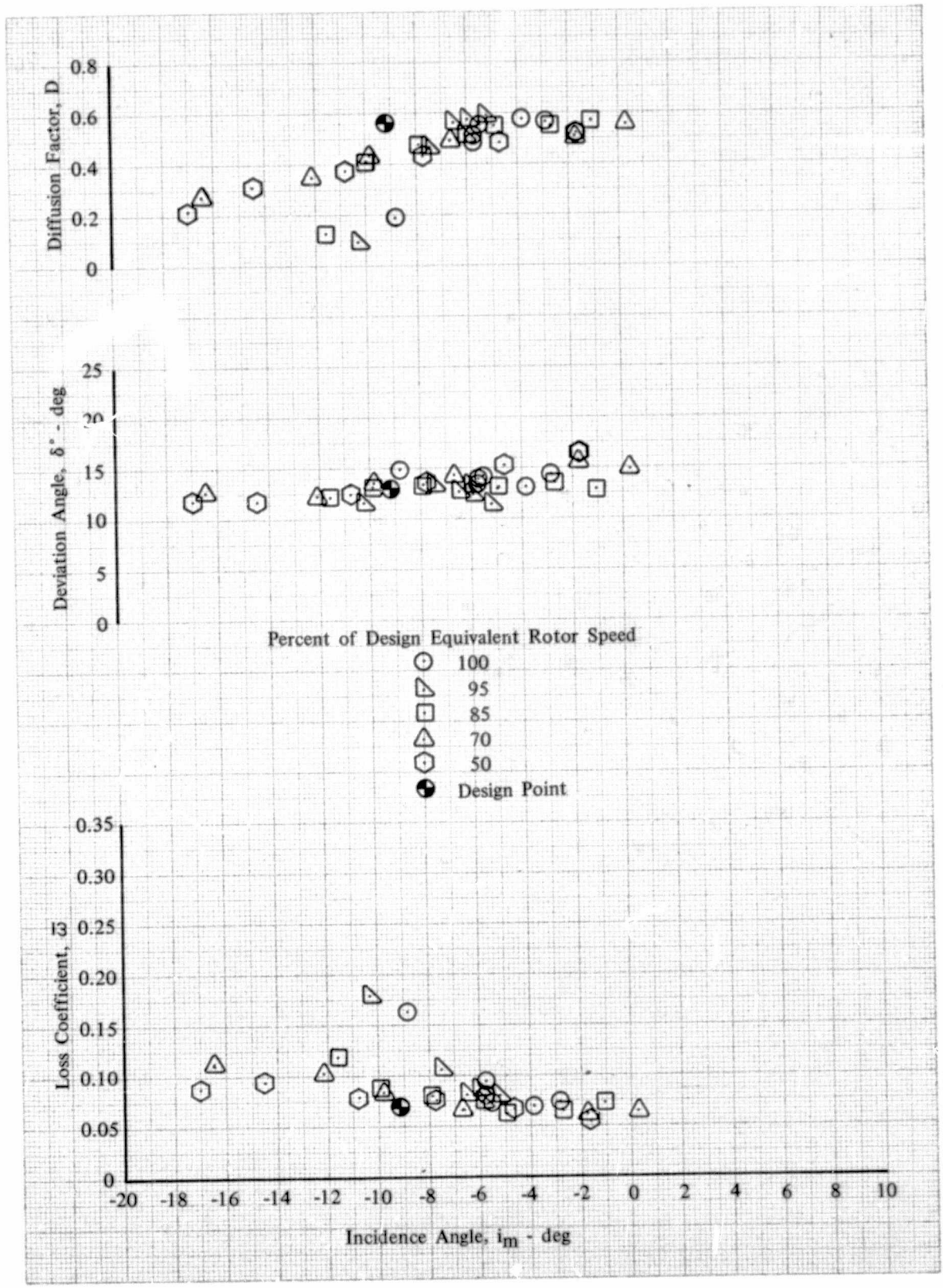


Figure 36b. Stator F Blade Element Performance, 10% Span from Tip; Uniform Inlet Flow

DF 102127

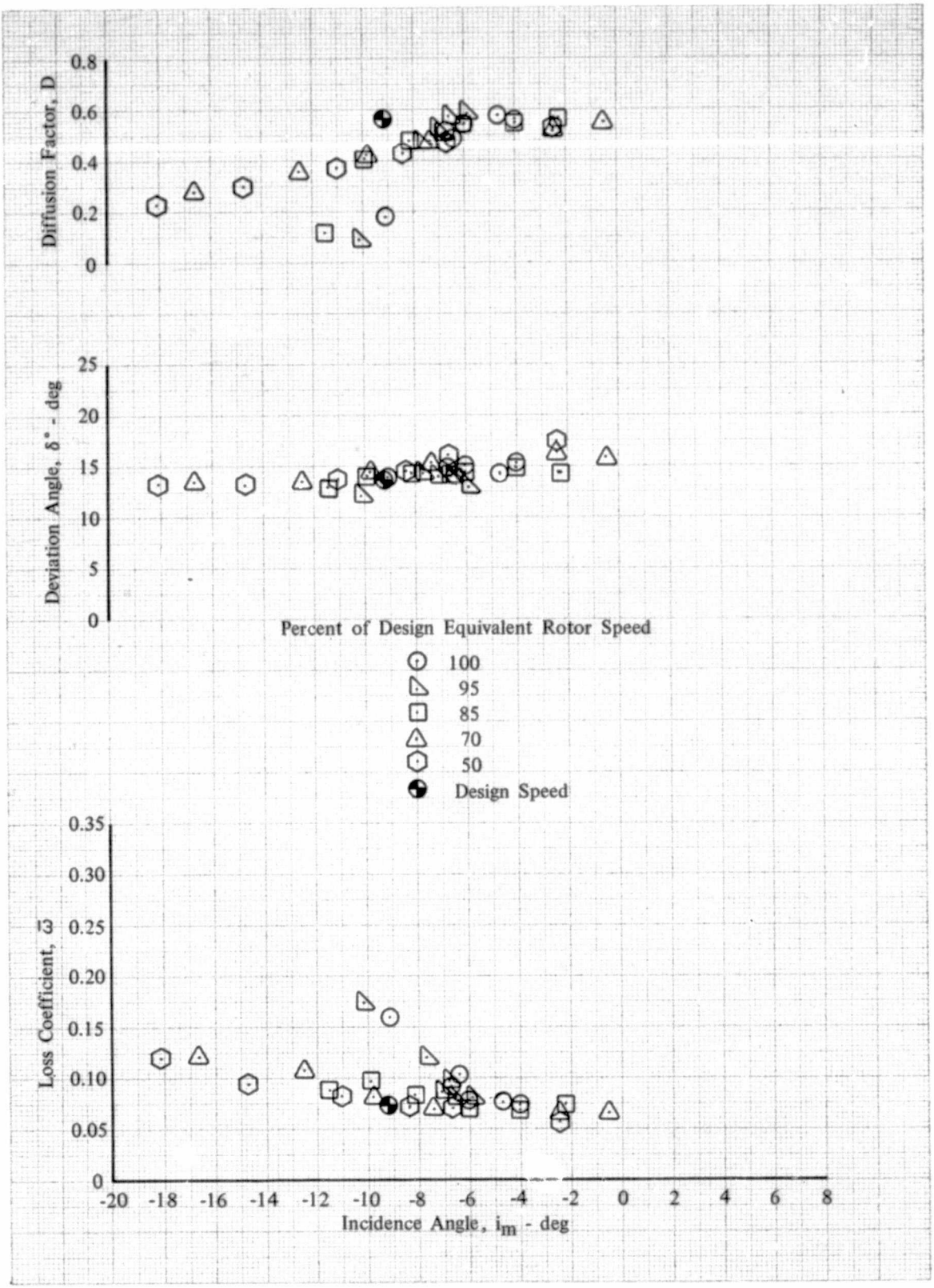


Figure 36c. Stator F Blade Element Performance, 15% Span from Tip; Uniform Inlet Flow DF 102128

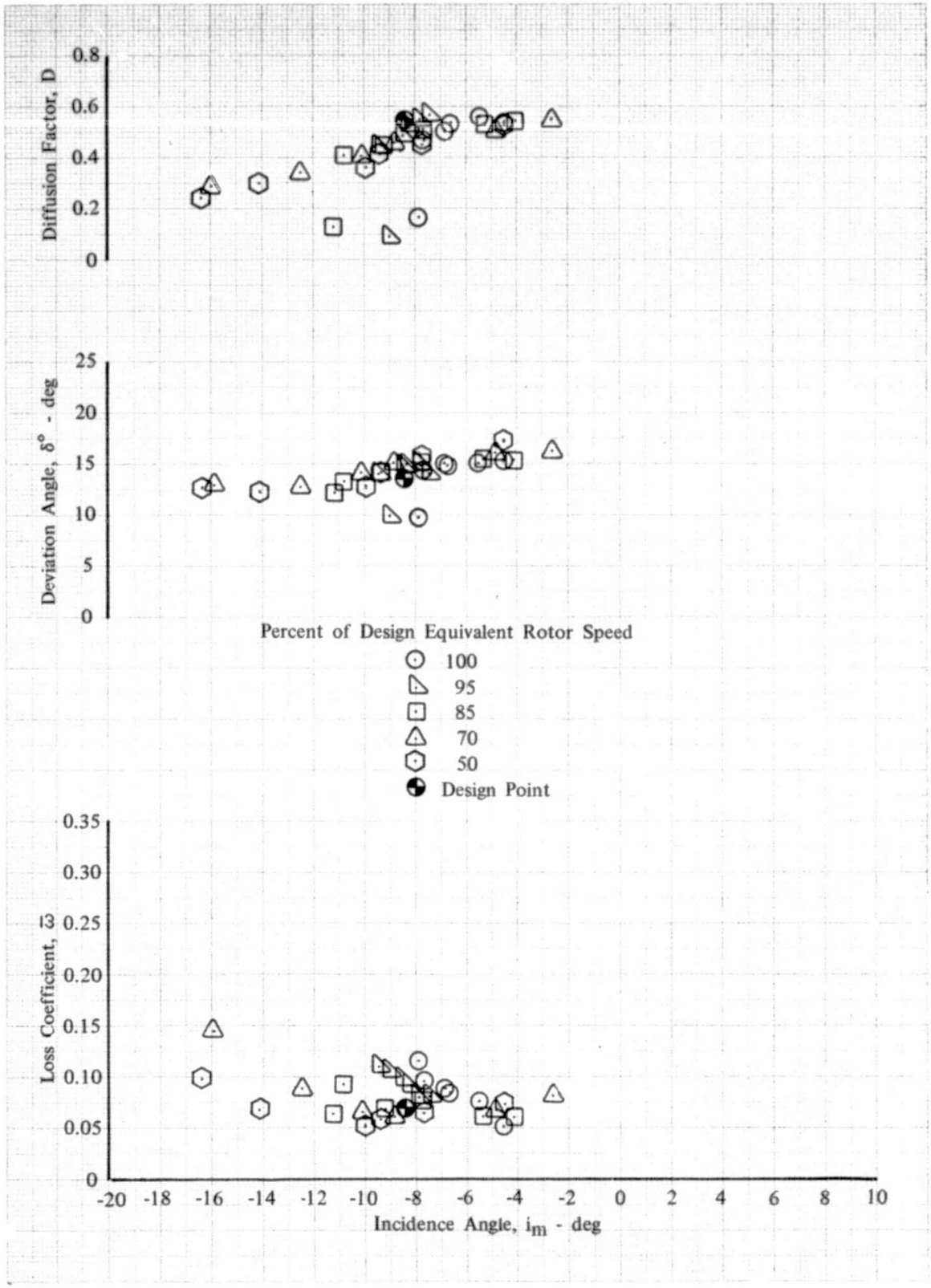


Figure 36d. Stator F Blade Element Performance, 30% Span from Tip; Uniform Inlet Flow DF 102129

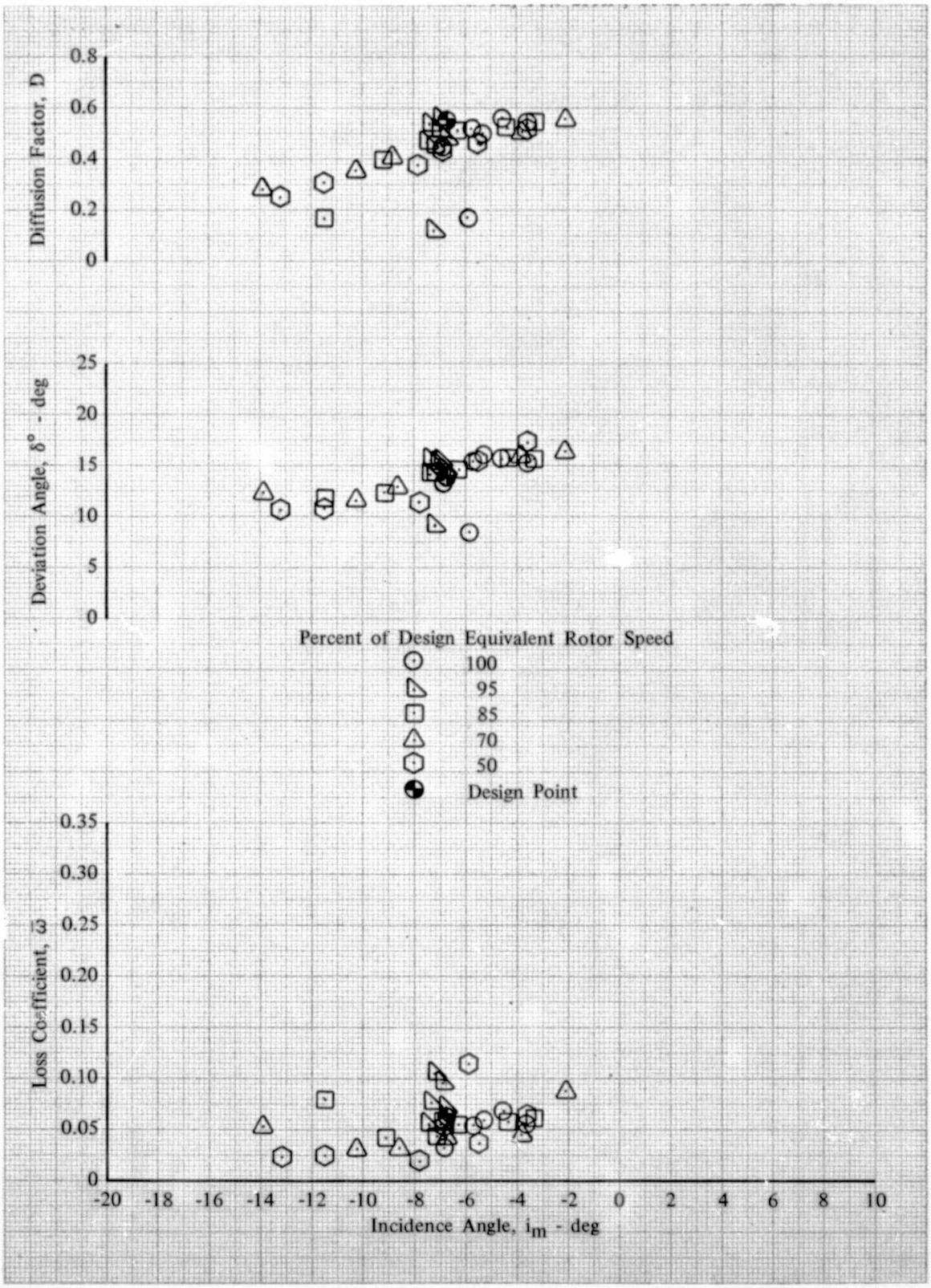


Figure 36e. Stator F Blade Element Performance, 50% Span; Uniform Inlet Flow

DF 102130



C.2

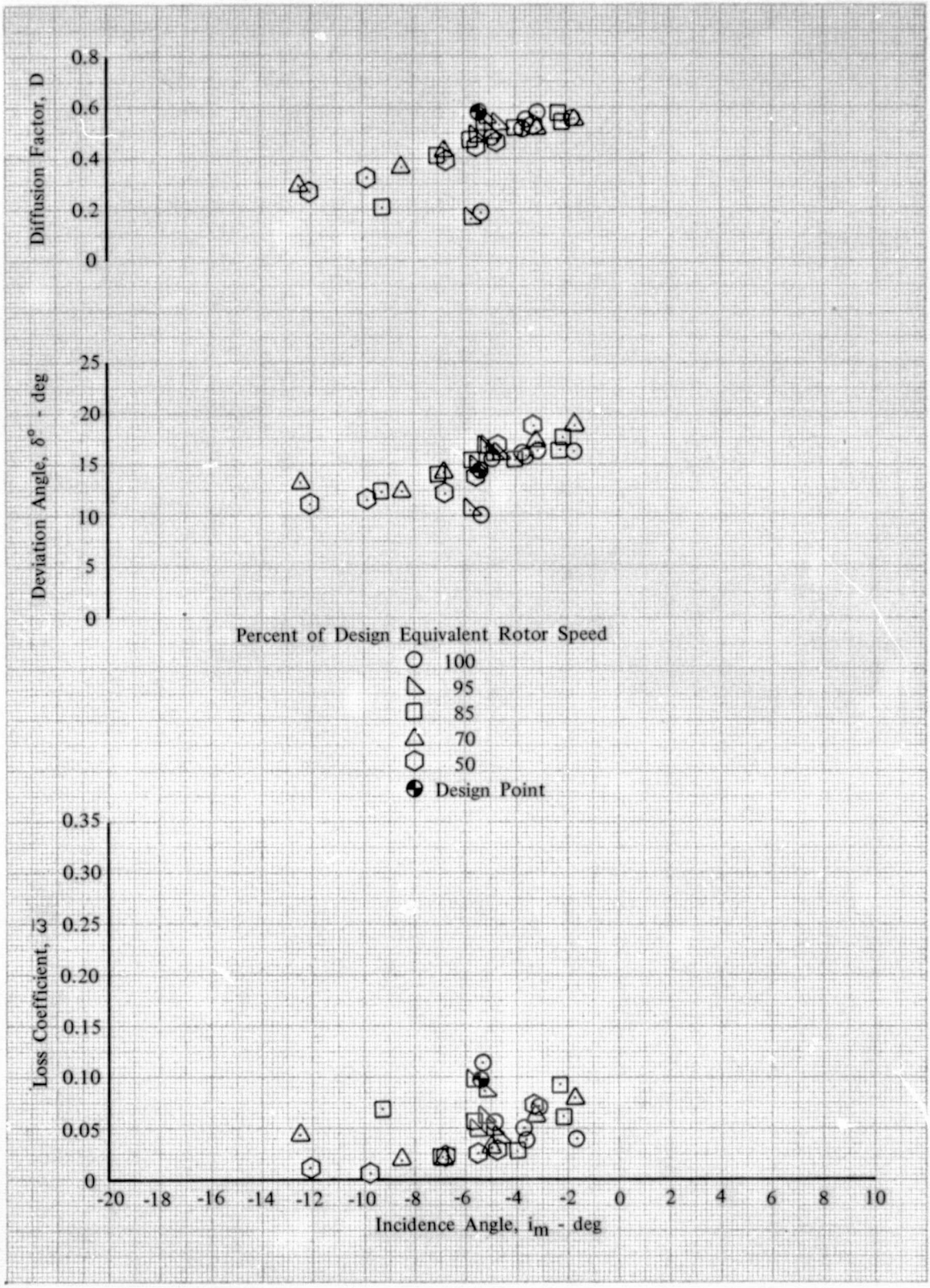


Figure 36f. Stator F Blade Element Performance, 70% Span from Tip; Uniform Inlet Flow DF 102131

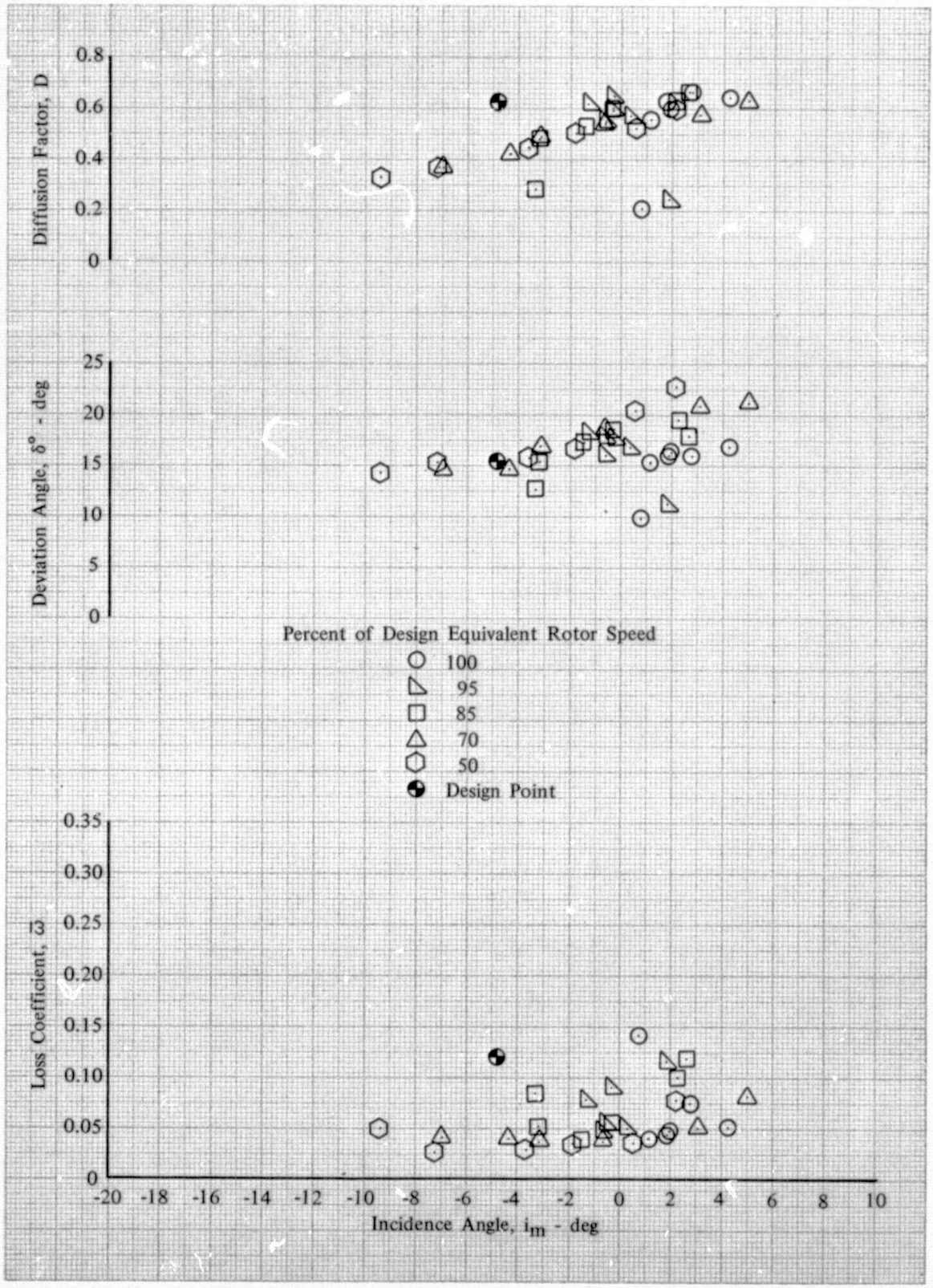


Figure 36g. Stator F Blade Element Performance, 85% Span from Tip; Uniform Inlet Flow DF 102132

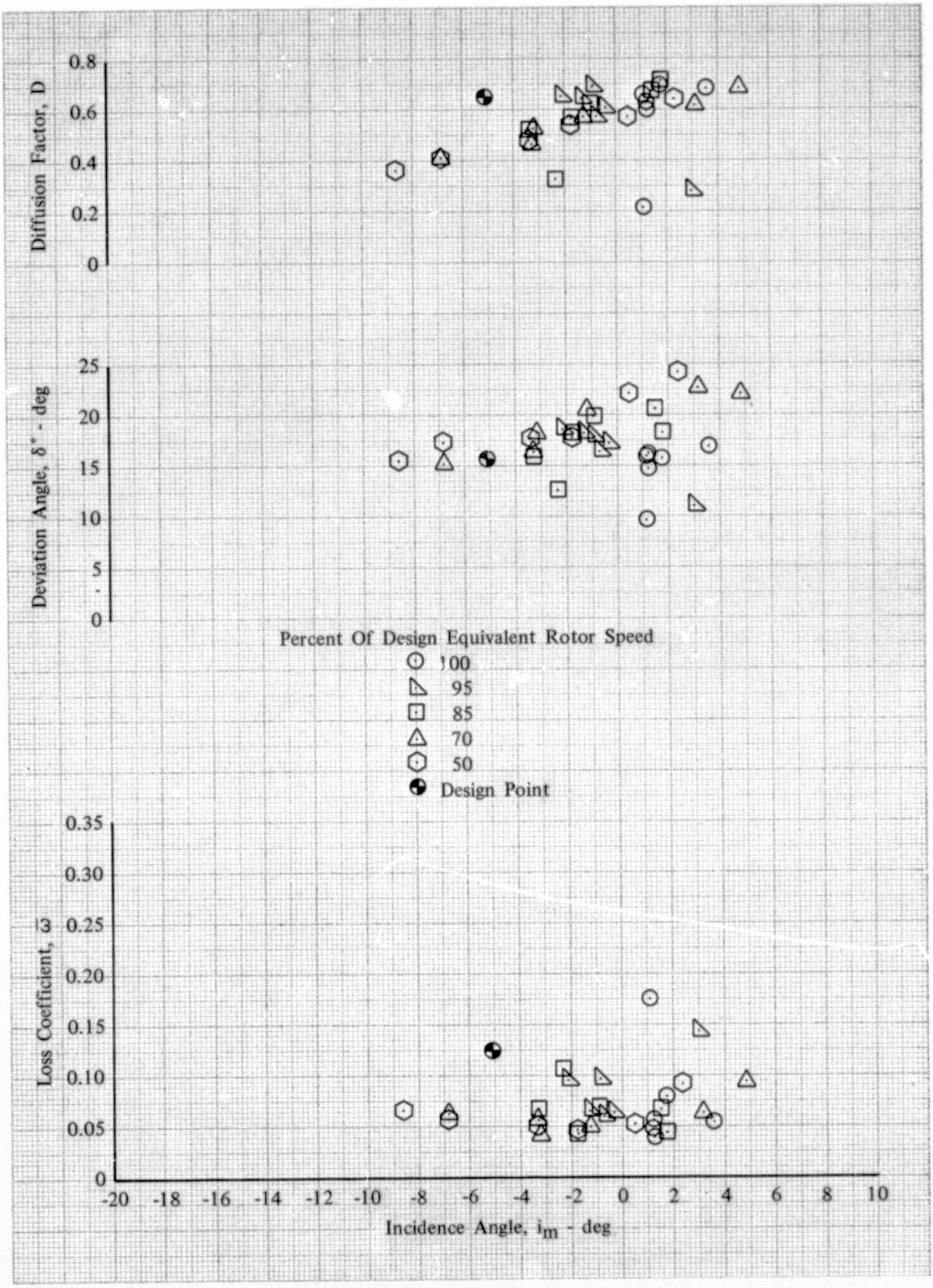


Figure 36h. Stator F Blade Element Performance, 90% Span from Tip; Uniform Inlet Flow DF 102133

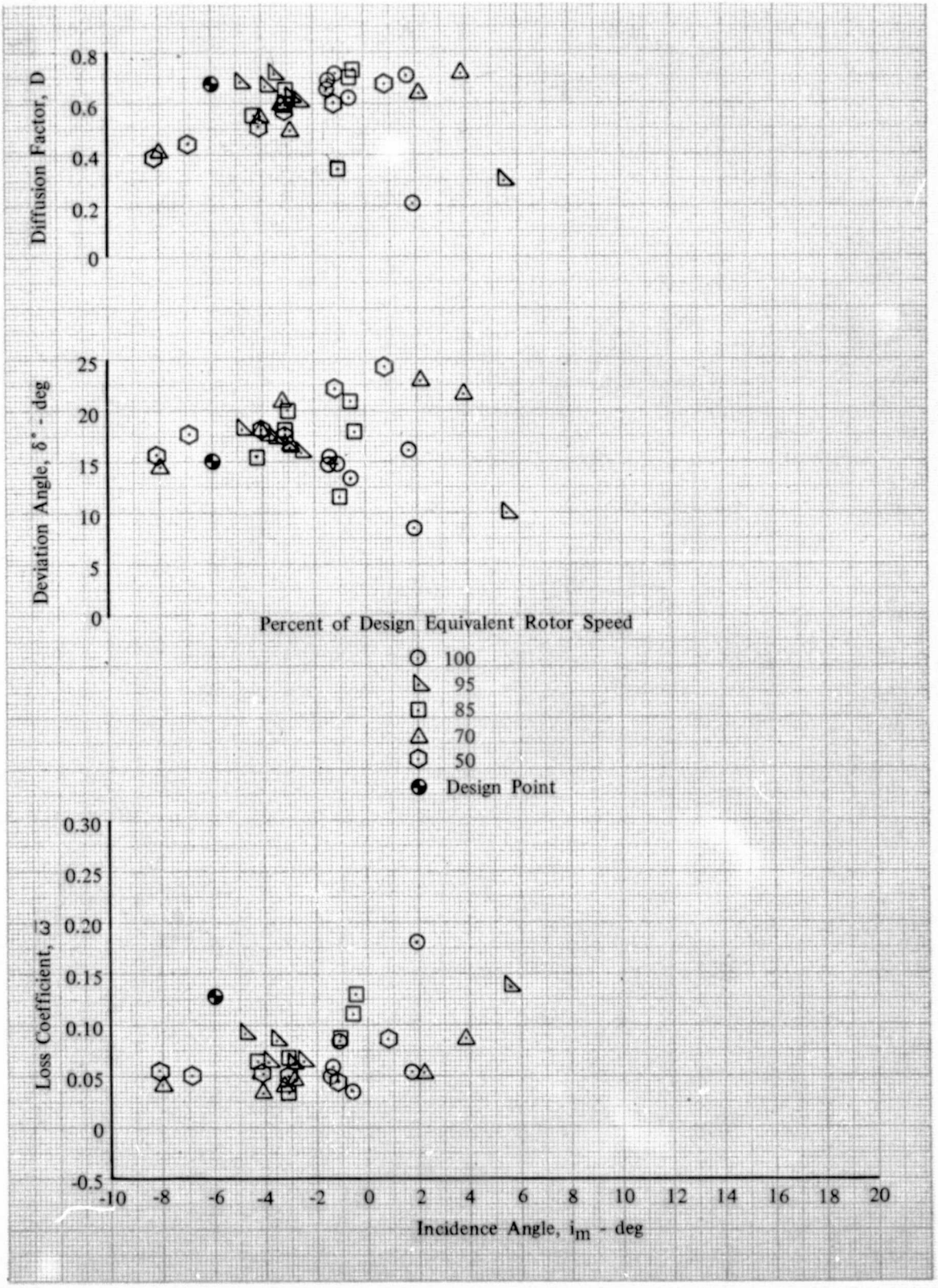


Figure 36i. Stator F Blade Element Performance, 95% Span from Tip; Uniform Inlet Flow

DF 102134

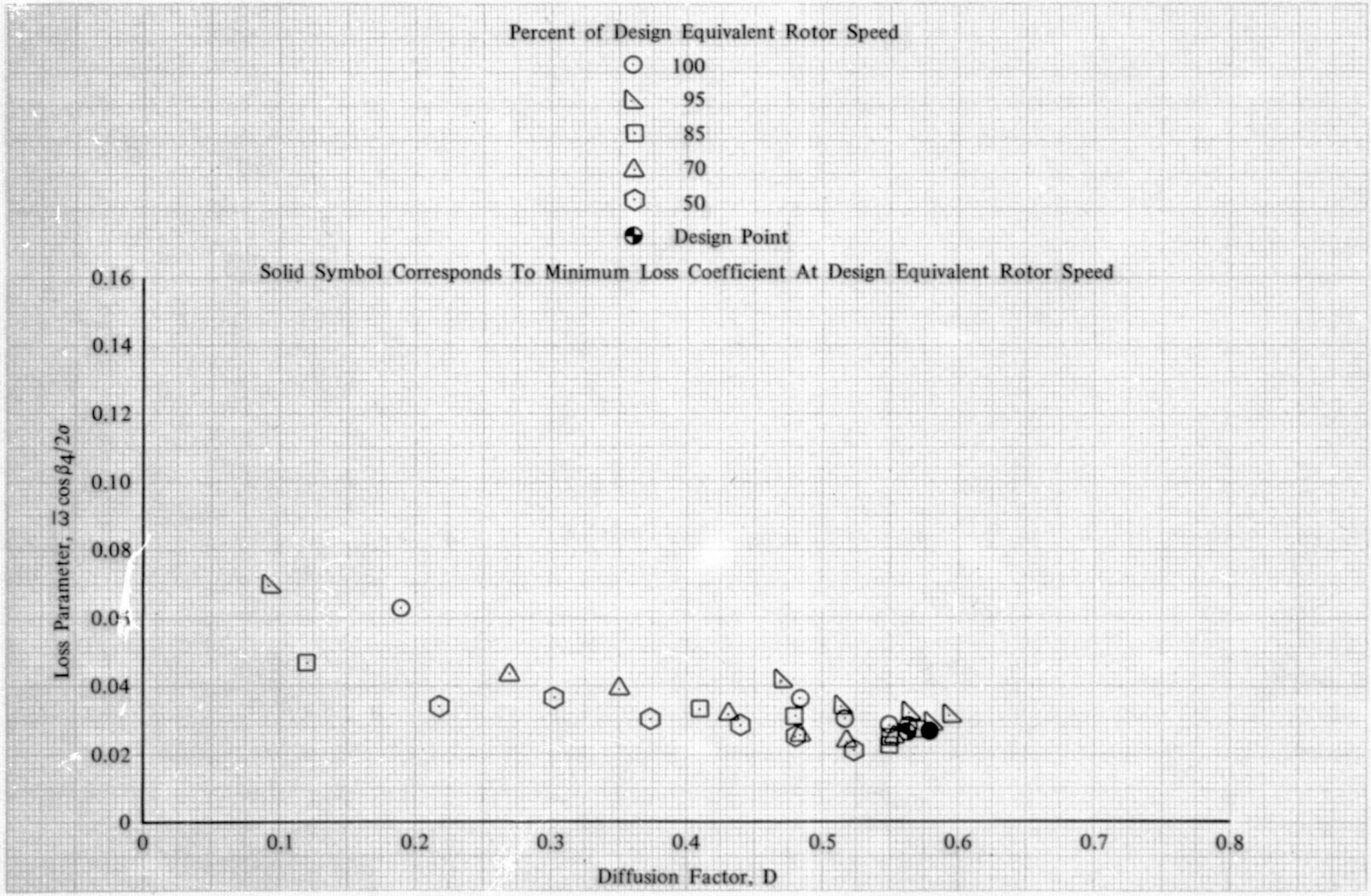


Figure 37a. Stator F Loss Parameter vs Diffusion Factor, 10% Span from Tip; Uniform Inlet Flow DF 102135

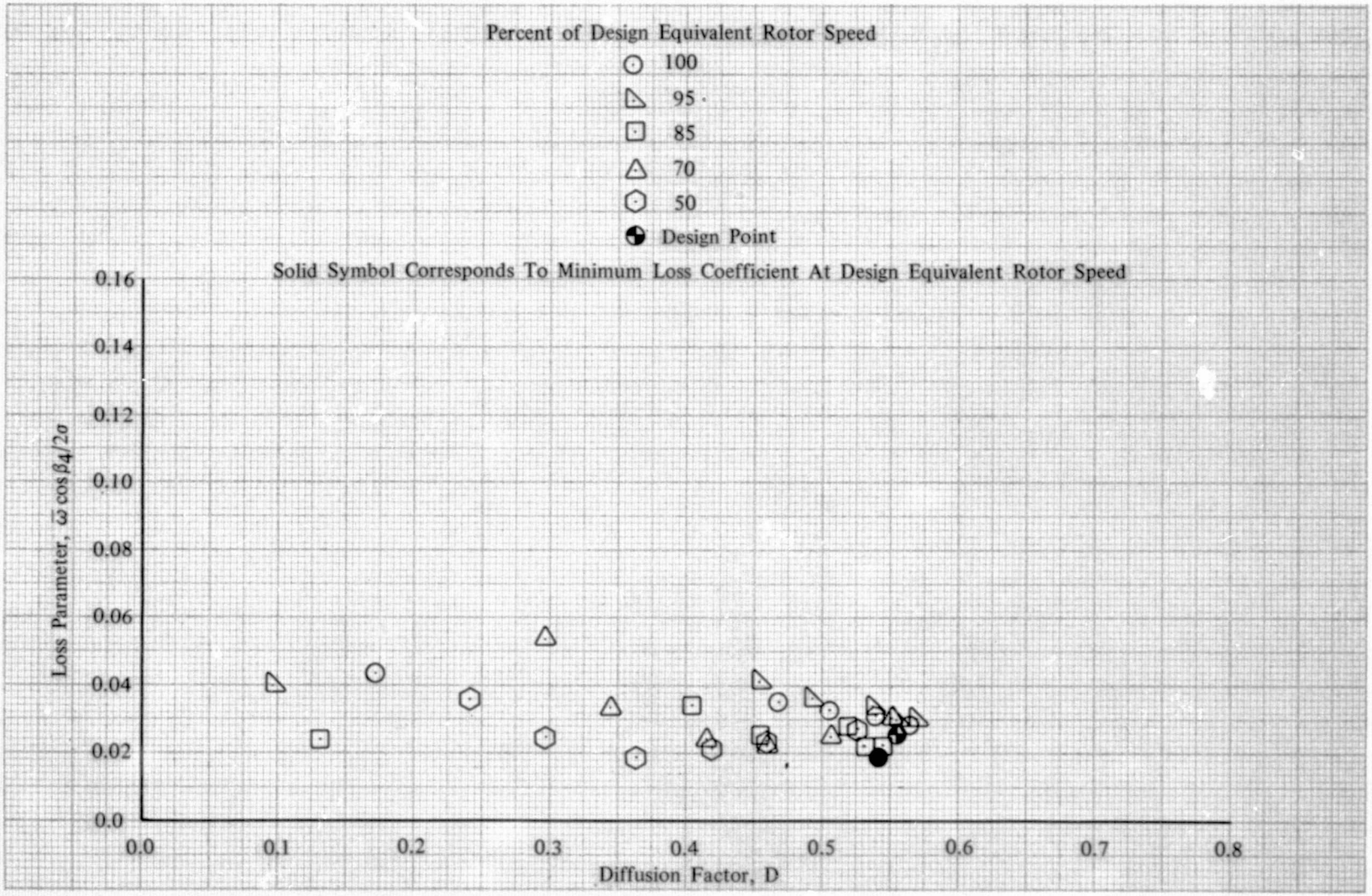


Figure 37b. Stator F Loss Parameter vs Diffusion Factor, 30% Span from Tip; Uniform Inlet Flow DF 102136

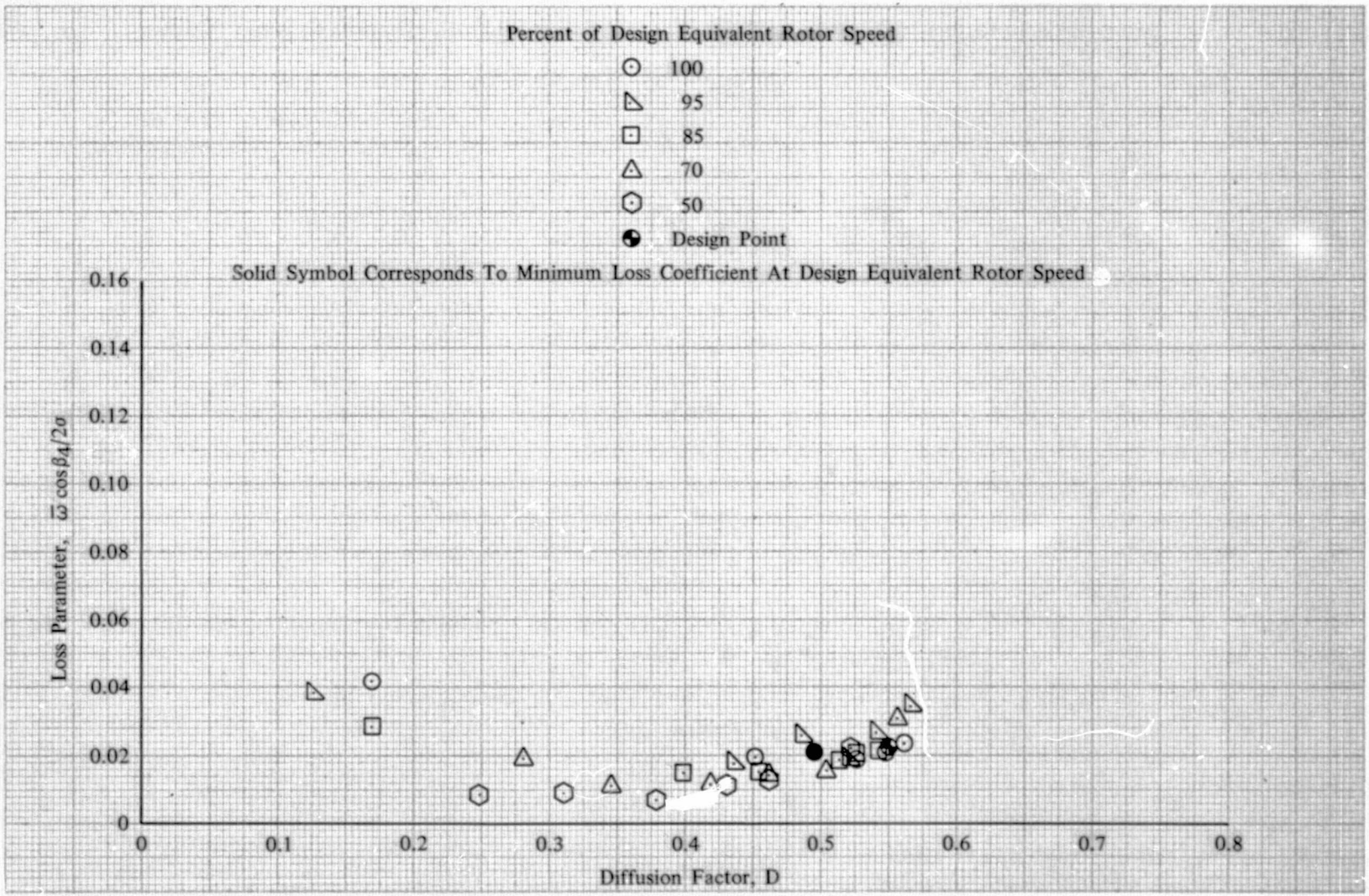


Figure 37c. Stator F Loss Parameter vs Diffusion Factor, 50% Span; Uniform Inlet Flow DF 102137

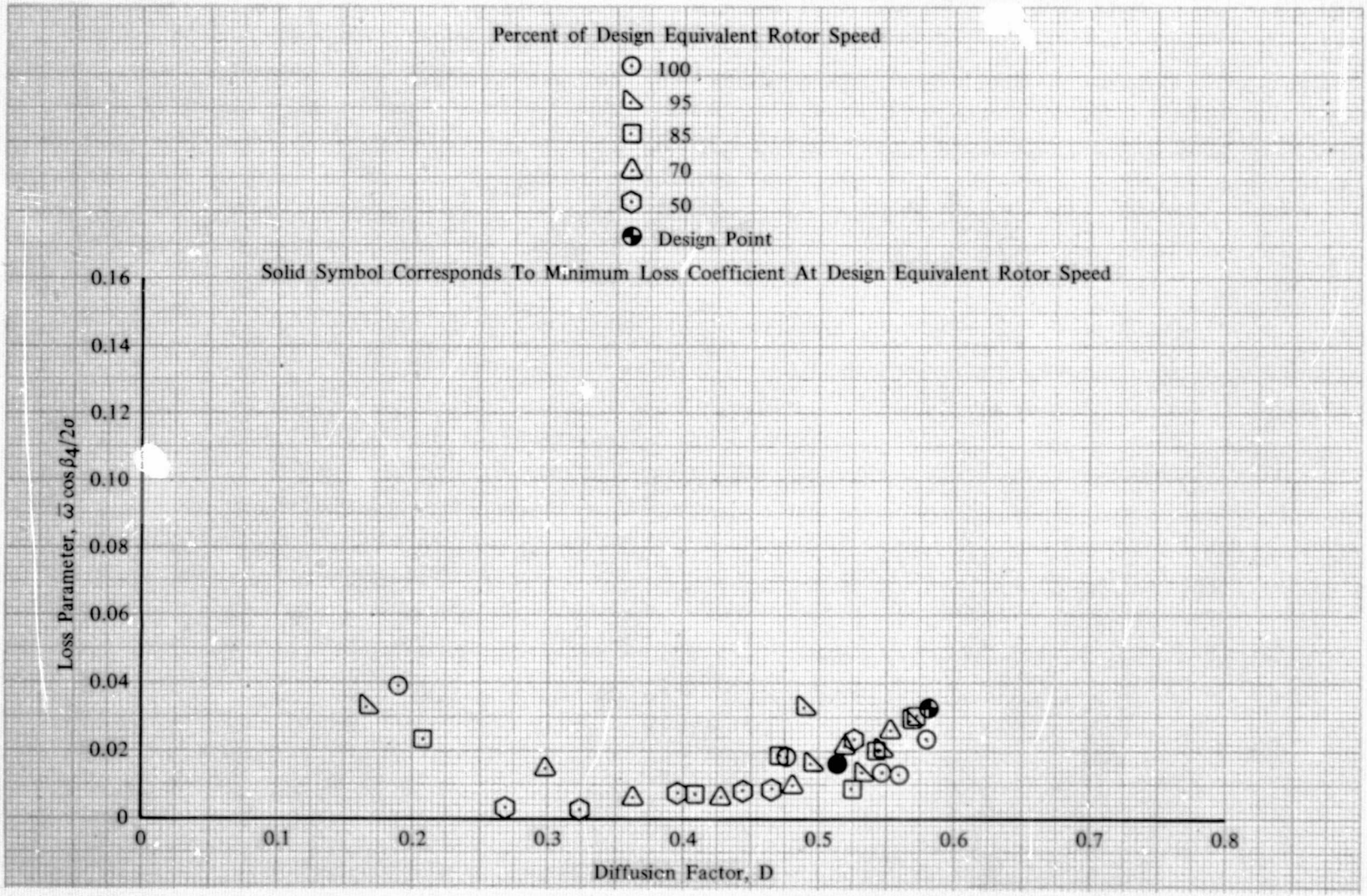


Figure 37d. Stator F Loss Parameter vs Diffusion Factor, 70% Span from Tip; Uniform Inlet Flow DF 102138

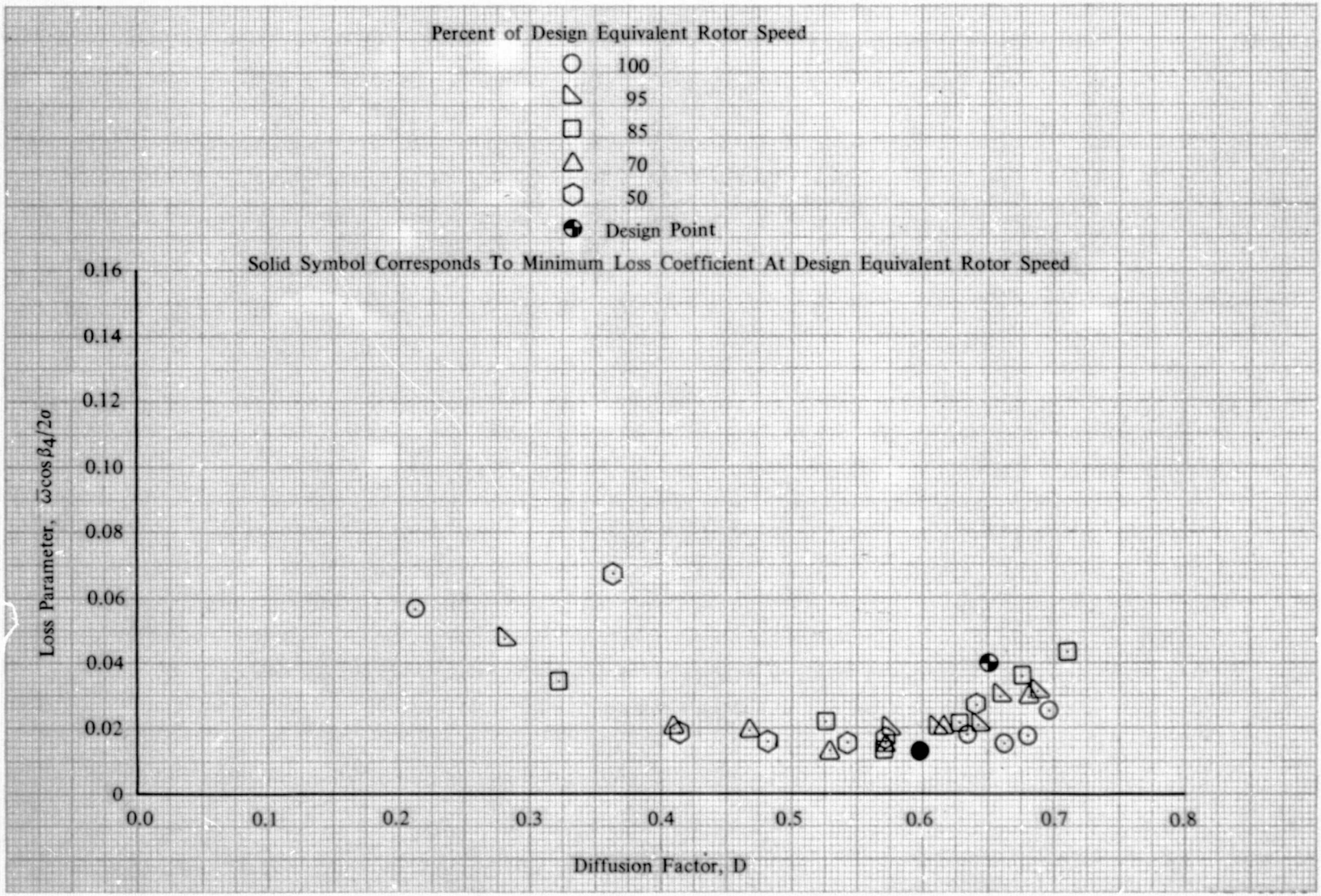


Figure 37e. Stator F Loss Parameter vs Diffusion Factor, 90% Span from Tip; Uniform Inlet Flow DF 102139

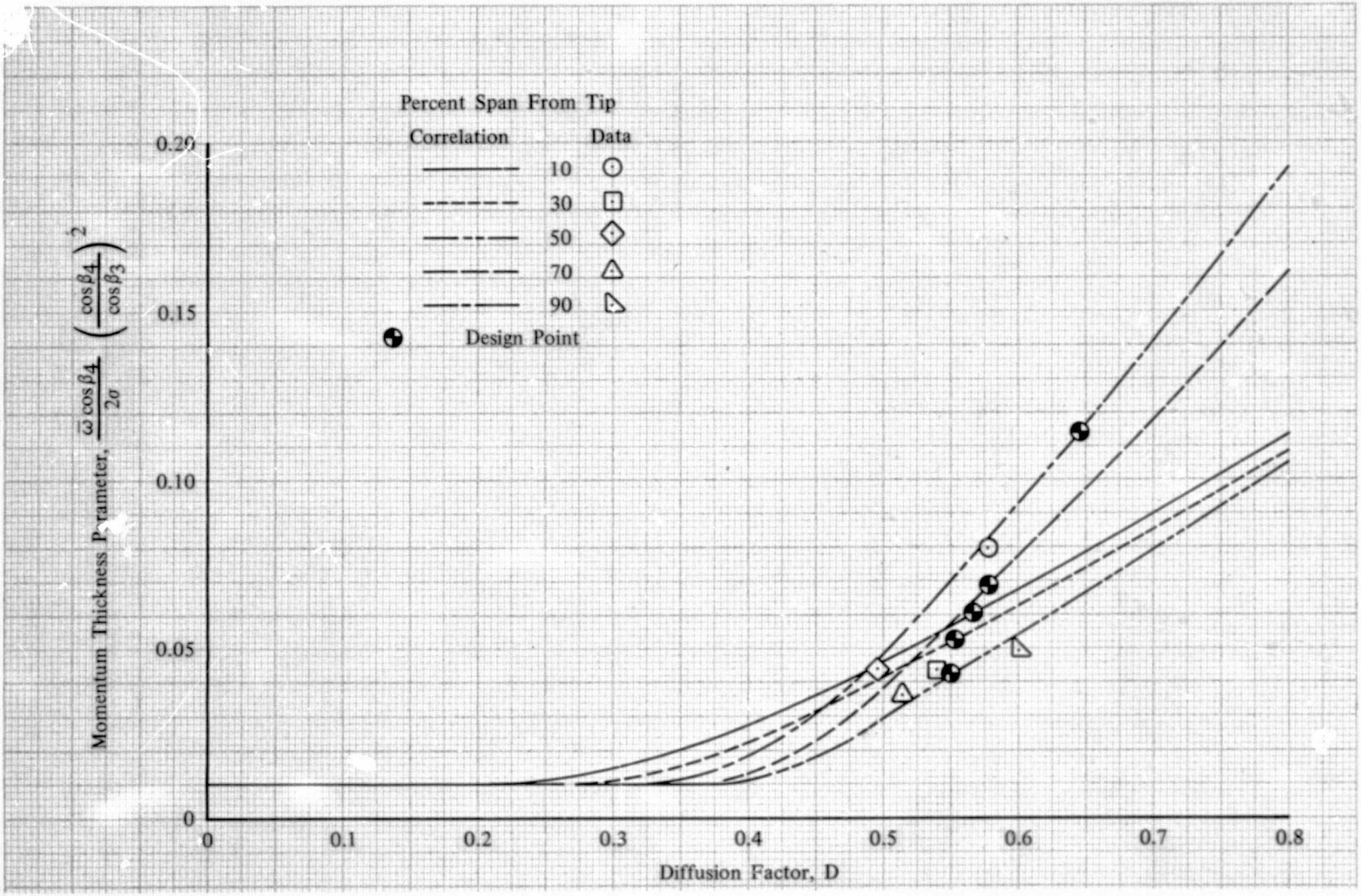


Figure 38. Comparison of Measured Minimum Loss Coefficient Points to Momentum Thickness Parameter for Stator F at Design Equivalent Rotor Speed; Uniform Inlet Flow DF 102140

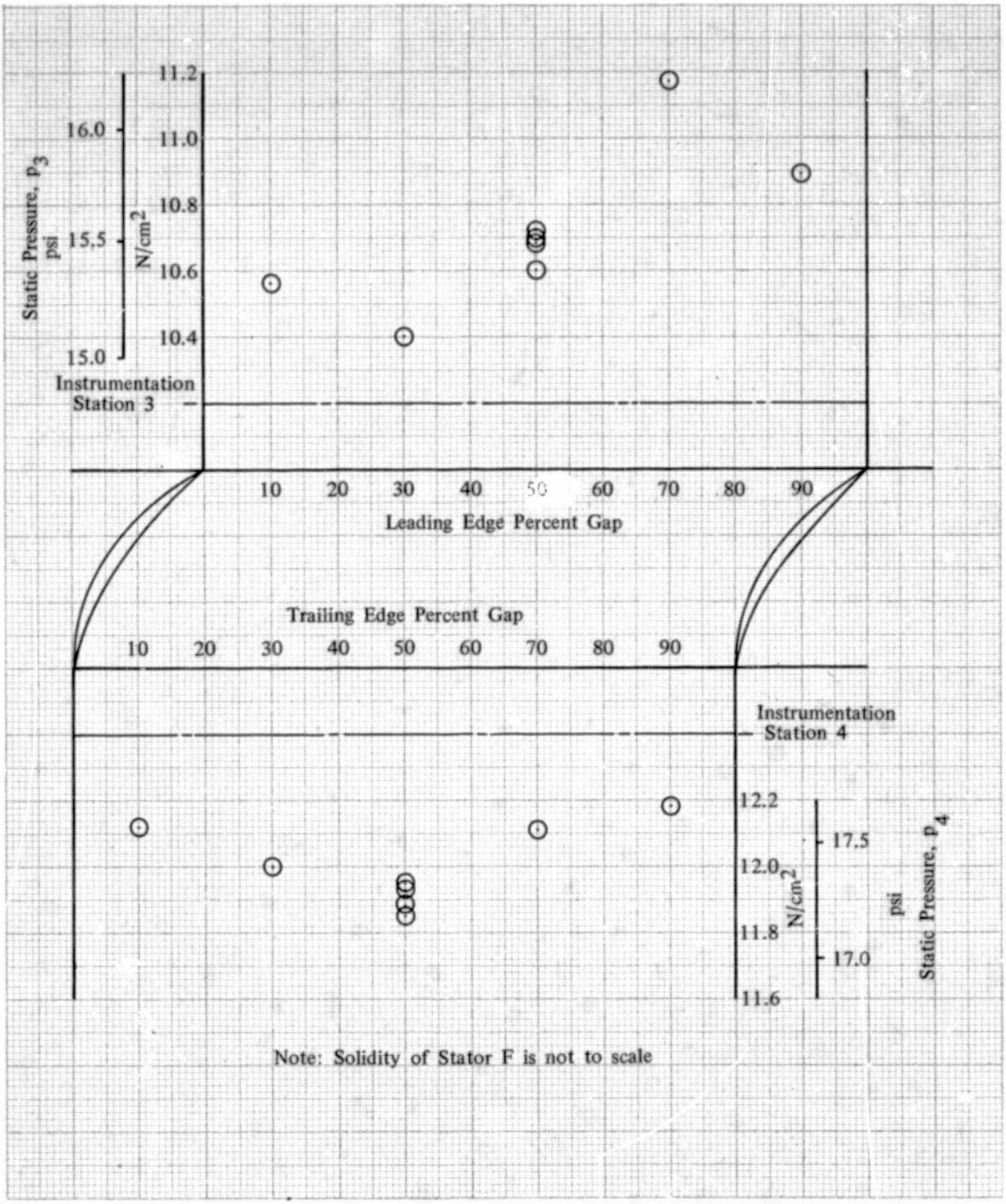


Figure 39. Rotor Exit and Stator Exit Wall Static Pressure Distributions; 100% Design Equivalent Rotor Speed; Equivalent Weight Flow = 17.25 kg/sec (38.04 lb/sec); Uniform Inlet Flow

DF 102141

Hub and Tip Radial Inlet Flow Distortion

Overall performance, blade element performance, and flow distribution data were obtained with hub radial and tip radial distortion of the inlet flow. The screens used to produce the distortion are described on page 39. At flows of approximately 17.69 kg/sec (39 lb/sec, i.e., 103% design equivalent flow), the hub and tip radial distortion screens produced 17.7 and 13.4% total pressure distortion, respectively, i.e., $(Pl_{max} - Pl_{min})/Pl_{max}$. Rotor inlet total pressure profiles are presented in figure 40.

Overall Performance - Overall performance data obtained with hub radial distortion of the inlet flow are presented in terms of pressure ratio and adiabatic efficiency as functions of equivalent weight flow and equivalent rotor speed for the rotor, rotor-stator, and inlet guide vane-rotor-stator (stage) in figures 41 through 43. Similarly, presented in figures 44 through 46 is the overall performance obtained with a tip radial distortion of the inlet flow. Uniform inlet flow data and the rotor, rotor-stator, and stage design points are presented in these figures for comparison with the radially distorted inlet flow data. The surge line shown was determined for surge transient data. Pressure ratio, adiabatic efficiency, and polytropic efficiency for the rotor, rotor-stator, and stage are tabulated for the steady-state data points with radial distortion in table XII and repeated in table B-5 of Appendix B, Volume II.

With hub radial distortion of the inlet flow, rotor pressure ratio, and efficiency at design equivalent flow and rotor speed were 1.525 and 86.4%, compared with 1.595 and 91.8% for uniform inlet flow. Similarly, rotor-stator pressure ratio and efficiency were 1.514 and 83.0% as compared with 1.561 and 86.7% with uniform inlet flow. With the addition of hub radial distortion, the surge flows were 3.8, 5.9, and 4.2% lower than with uniform inlet flow at 70, 85 and 100% design equivalent rotor speed, respectively. Therefore, Stage F performance was adversely affected by hub radial distortion while surge flow was not.

With tip radial distortion of the inlet flow, rotor pressure ratio at design equivalent flow and rotor speed was 1.598 as compared with 1.595 for the uniform inlet flow. Rotor efficiency under the same conditions was 91.0%, compared with 91.8% for uniform inlet flow. The corresponding rotor-stator pressure ratio and efficiency were 1.569 and 85.3% as compared with 1.561 and 86.7% for uniform inlet. Surge occurred at 7.4, 3.5, and 1.4% higher flow at 70, 85, and 100% design equivalent rotor speed, respectively, when compared to the uniform inlet test results. Consequently, Stage F was not substantially affected by tip radial distortion.

Blade Element Performance and Flow Distribution Data - Blade element performance and flow distribution data with radial distortion were calculated for each of the nine design streamline locations, and the results, based on data translated to the blade row leading and trailing edges, are presented in tables B-6 through B-9 of Appendix B, Volume II.

Rotor and Stator Blade Element Performance - Diffusion factor, deviation angle, and loss coefficient with hub radial and tip radial distortion of the inlet flow are presented as functions of incidence angle in figures 47a through 47i for the rotor and in figures 48a through 48i for the stator. The average of the respective uniform inlet data is represented on each of these figures with a line. Comparison of the distortion data to the uniform inlet data shows the rotor data have substantial disagreements between the hub radially distorted, tip radially distorted and uniform inlet flow data whereas the stator data have very good agreement for all data. Agreement of the stator data indicates the perturbation caused by the inlet distortion screens was attenuated within the rotor.

Examination of the rotor inlet data shows good agreement between the air angle data from each of the two traverse probes and good agreement between the static pressure data from the taps on the inner wall and the taps on the outer wall. However, the inlet guide vane exit total pressure data exhibited highly inconsistent behavior for the distortion tests. Typical hub, mean and tip total pressure profiles are presented in figure 49 for uniform inlet and hub and tip radially distorted inlet conditions. These data show the total pressure profiles with distorted inlet flow disagree substantially with the uniform inlet profiles in the distorted regions and agree more closely with the uniform inlet in the undistorted regions. Reexamination of the rotor blade element data shows the same trend, i.e., severe disagreement between the distorted data and the uniform inlet data in the distorted region and no substantial disagreement in the undistorted region. Therefore, it was concluded the inlet guide vane total pressure profiles caused the discrepancies in the rotor blade element data. The instrumentation was insufficient to determine the cause of the unusual profiles typified in figure 49.

Flow Distribution Data - Radial distributions of total and static pressure, total temperature, absolute air angle, and axial velocity for the rotor inlet, stator inlet and stator exit are presented for hub and tip radial distortion of the inlet flow in figures 50 through 58 and 59 through 67, respectively. The values for the nine design streamline locations are also tabulated in tables B-6 through B-9 of Appendix B, Volume II.

Stage inlet and exit total pressure and axial velocity profiles for uniform inlet flow at design rotor speed and 17.25 kg/sec (38.0 lb/sec, i.e., 100.7% design flow) are given in figure 68. Comparison of these uniform inlet profiles to the hub and tip radial distortion profiles in figures 50 and 59 shows there is little difference between the exit profiles for the uniform inlet and hub and tip distortion, thus indicating the rotor substantially attenuates both distortion patterns. This result is typical of the results obtained at other rotor speeds and flows. However, these distortion attenuation capabilities of Rotor F have produced an anomaly.

The ability of a rotor to attenuate inlet distortion is measured by its ability to increase its work level with the decrease in inlet axial velocity caused by the inlet distortion. This ability can be assessed by calculating the relationship between "ideal" rotor pressure ratio and the axial velocity/rotor speed ratio (Vz/U) with the assumption of a constant inlet absolute air angle ($\beta_2$) and constant exit relative air angle ($\beta_3'$). Distortion attenuation capabilities are good if there is a negative gradient, i.e., increasing pressure ratio with decreasing Vz/U, while distortion attenuation capabilities are poor if the gradient is positive or just slightly negative. The pressure ratio - Vz/U relationship for Rotor F

with a constant $\beta_2$ - constant $\beta_3'$ is given in figure 69 at 10 and 90% span from the rotor tip and is compared to values calculated from the data for uniform inlet and hub and tip radially distorted inlet flow. Figure 69 shows that the rotor tip has a steep negative gradient for the constant $\beta_2$ - constant $\beta_3'$ slope which agrees with the data and explains why the tip distortion was attenuated. The rotor hub was essentially a zero gradient for the constant $\beta_2$ - constant $\beta_3'$ slope indicating that the rotor hub should be unable to attenuate any significant distortion. However, the hub did attenuate the distortion as shown above. This distortion attenuation ability is explained by figure 69 which shows the pressure ratio - Vz/U relationship calculated from the hub radial distortion data substantially exceeded the constant $\beta_2$ - constant $\beta_3'$ value, thus allowing the hub to attenuate the distortion. A comparison of the spanwise distributions of rotor deviations with hub radial and tip radial distortion and uniform inlet flow, presented in figure 70, indicates this difference between the predicted and measured pressure ratio - Vz/U relationship resulted from a sharp increase in rotor deviation in the rotor hub region.

## Table XII. Overall Performance of Stage F Radial Distortion

| (IGV Inlet) Equivalent Weight Flow kg/sec | lb/sec | Rotor $\overline{P}_3/\overline{P}_2$ | Rotor $\eta_{ad}$ | Rotor $\eta_p$ | Rotor - Stator $\overline{P}_4/\overline{P}_2$ | Rotor - Stator $\eta_{ad}$ | Rotor - Stator $\eta_p$ | IGV - Rotor - Stator $P_4/P_1$ | IGV - Rotor - Stator $\eta_{ad}$ | IGV - Rotor - Stator $\eta_p$ |
|---|---|---|---|---|---|---|---|---|---|---|
| | | | | | HUB RADIAL DISTORTION | | | | | |
| | | | | | 100% Design Equivalent Rotor Speed | | | | | |
| 17.79 | 39.21 | 1.476 | 0.795 | 0.806 | 1.427 | 0.718 | 0.732 | 1.425 | 0.715 | 0.729 |
| 16.02 | 35.32 | 1.573 | 0.875 | 0.883 | 1.538 | 0.826 | 0.837 | 1.532 | 0.819 | 0.829 |
| 14.98 | 33.06 | 1.600 | 0.880 | 0.887 | 1.547 | 0.813 | 0.824 | 1.542 | 0.806 | 0.818 |
| | | | | | 85% Design Equivalent Rotor Speed | | | | | |
| 16.24 | 35.80 | 1.363 | 0.889 | 0.894 | 1.333 | 0.817 | 0.824 | 1.318 | 0.784 | 0.791 |
| 13.93 | 30.71 | 1.402 | 0.896 | 0.901 | 1.381 | 0.852 | 0.858 | 1.376 | 0.841 | 0.848 |
| 12.21 | 26.92 | 1.415 | 0.876 | 0.882 | 1.379 | 0.807 | 0.816 | 1.372 | 0.793 | 0.802 |
| | | | | | 70% Design Equivalent Rotor Speed | | | | | |
| 13.95 | 30.75 | 1.245 | 0.902 | 0.905 | 1.227 | 0.839 | 0.844 | 1.218 | 0.808 | 0.813 |
| 11.54 | 25.44 | 1.263 | 0.909 | 0.912 | 1.251 | 0.866 | 0.870 | 1.246 | 0.849 | 0.854 |
| 9.97 | 21.99 | 1.270 | 0.883 | 0.887 | 1.250 | 0.819 | 0.825 | 1.244 | 0.802 | 0.808 |
| | | | | | TIP RADIAL DISTORTION | | | | | |
| | | | | | 100% Design Equivalent Rotor Speed | | | | | |
| 17.91 | 39.48 | 1.500 | 0.815 | 0.825 | 1.447 | 0.738 | 0.751 | 1.434 | 0.719 | 0.733 |
| 16.41 | 36.17 | 1.606 | 0.903 | 0.909 | 1.566 | 0.850 | 0.859 | 1.553 | 0.833 | 0.843 |
| 15.52 | 34.21 | 1.614 | 0.894 | 0.901 | 1.560 | 0.827 | 0.837 | 1.546 | 0.810 | 0.821 |
| | | | | | 85% Design Equivalent Rotor Speed | | | | | |
| 16.54 | 36.46 | 1.385 | 0.908 | 0.912 | 1.348 | 0.829 | 0.836 | 1.339 | 0.809 | 0.817 |
| 14.37 | 31.68 | 1.416 | 0.922 | 0.926 | 1.393 | 0.876 | 0.881 | 1.386 | 0.861 | 0.867 |
| 13.15 | 28.99 | 1.414 | 0.895 | 0.900 | 1.387 | 0.839 | 0.847 | 1.383 | 0.832 | 0.839 |
| | | | | | 70% Design Equivalent Rotor Speed | | | | | |
| 14.23 | 31.38 | 1.264 | 0.938 | 0.940 | 1.245 | 0.875 | 0.879 | 1.239 | 0.855 | 0.859 |
| 11.96 | 26.36 | 1.275 | 0.933 | 0.935 | 1.260 | 0.883 | 0.887 | 1.256 | 0.870 | 0.874 |
| 10.82 | 23.85 | 1.271 | 0.888 | 0.892 | 1.254 | 0.835 | 0.840 | 1.252 | 0.829 | 0.834 |

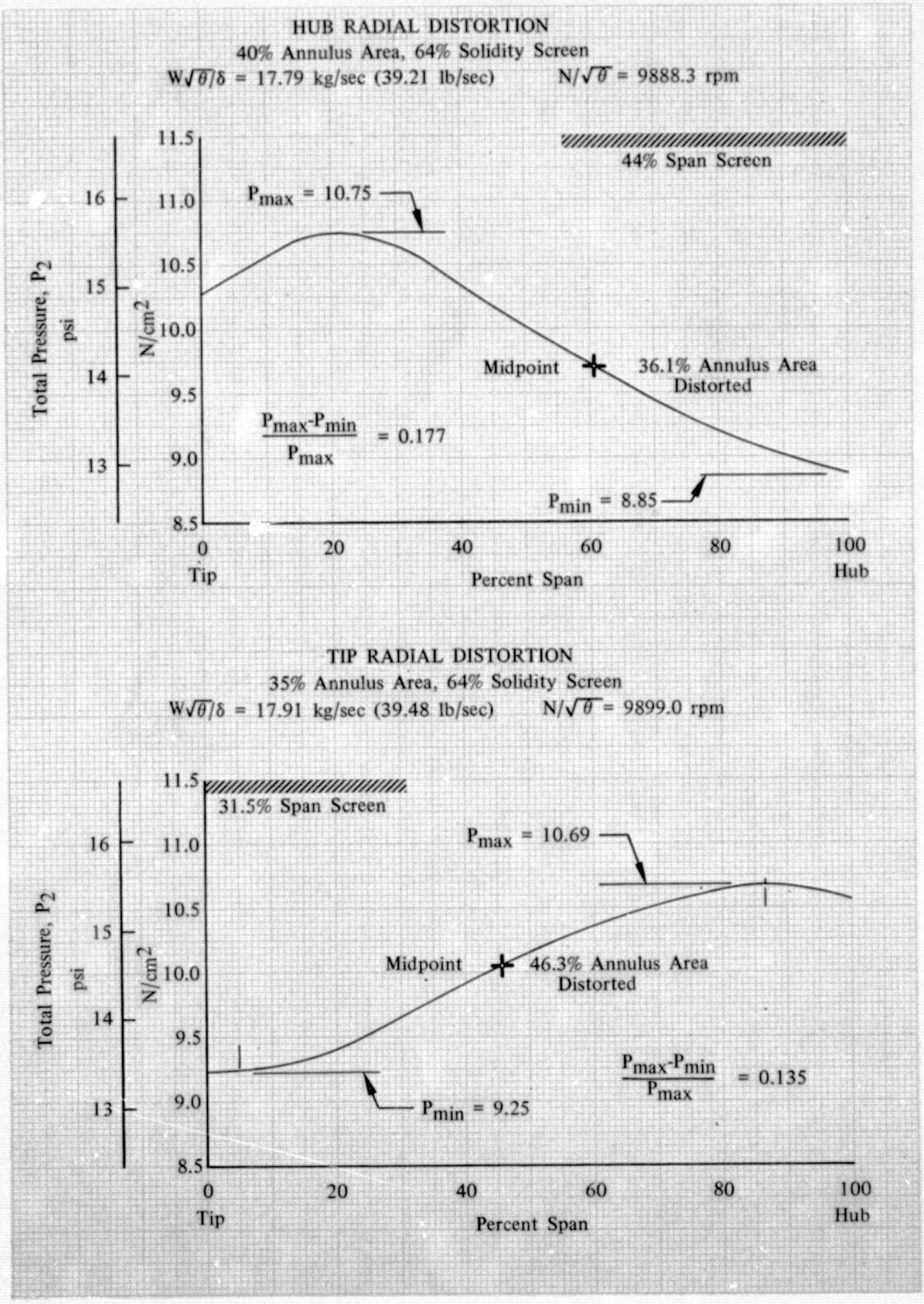


Figure 40. Rotor F Inlet Total Pressure Profiles With Radial Distortion DF 102142

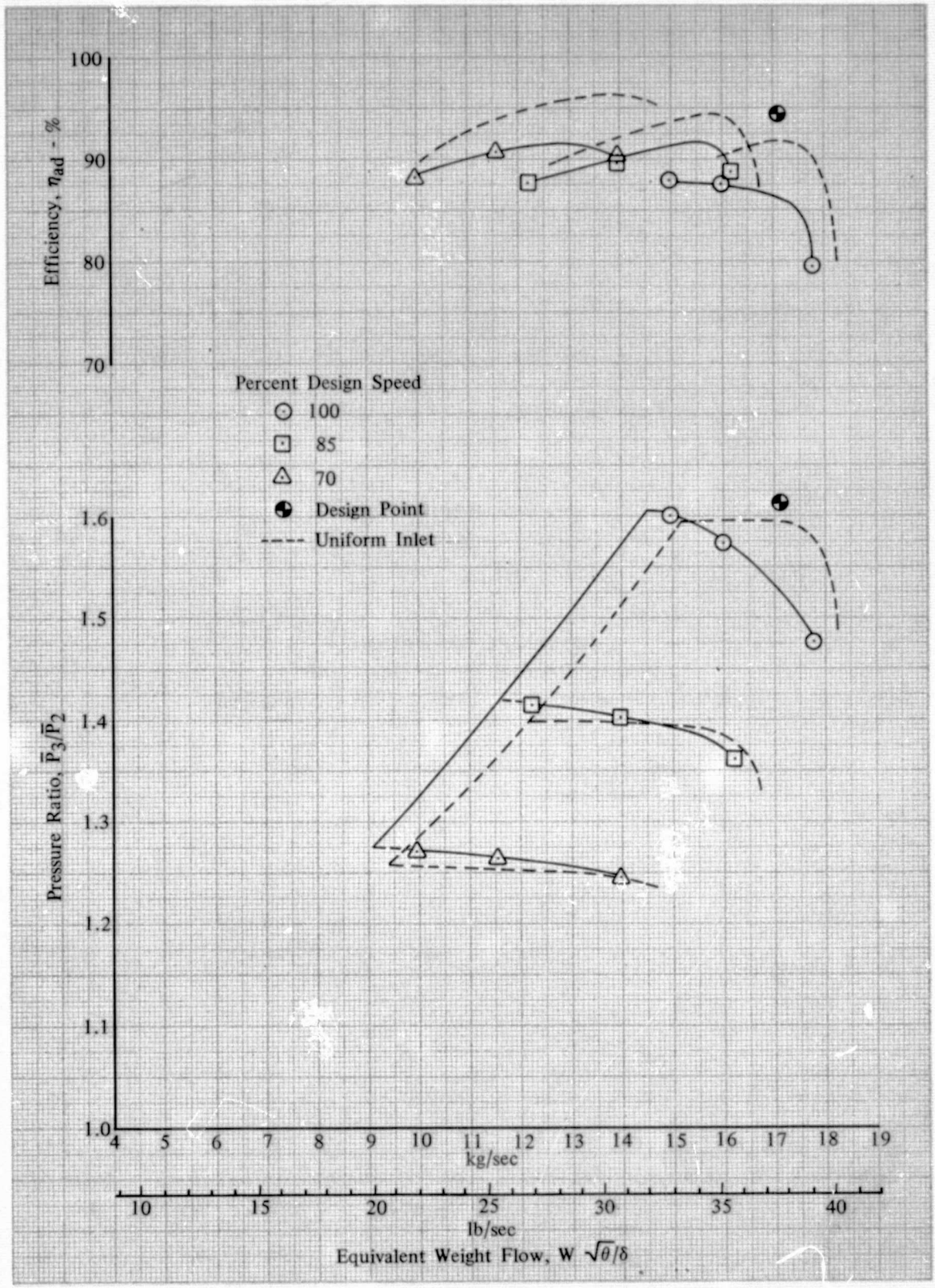


Figure 41. Overall Performance of Rotor F with Hub Radial Distortion DF 102143

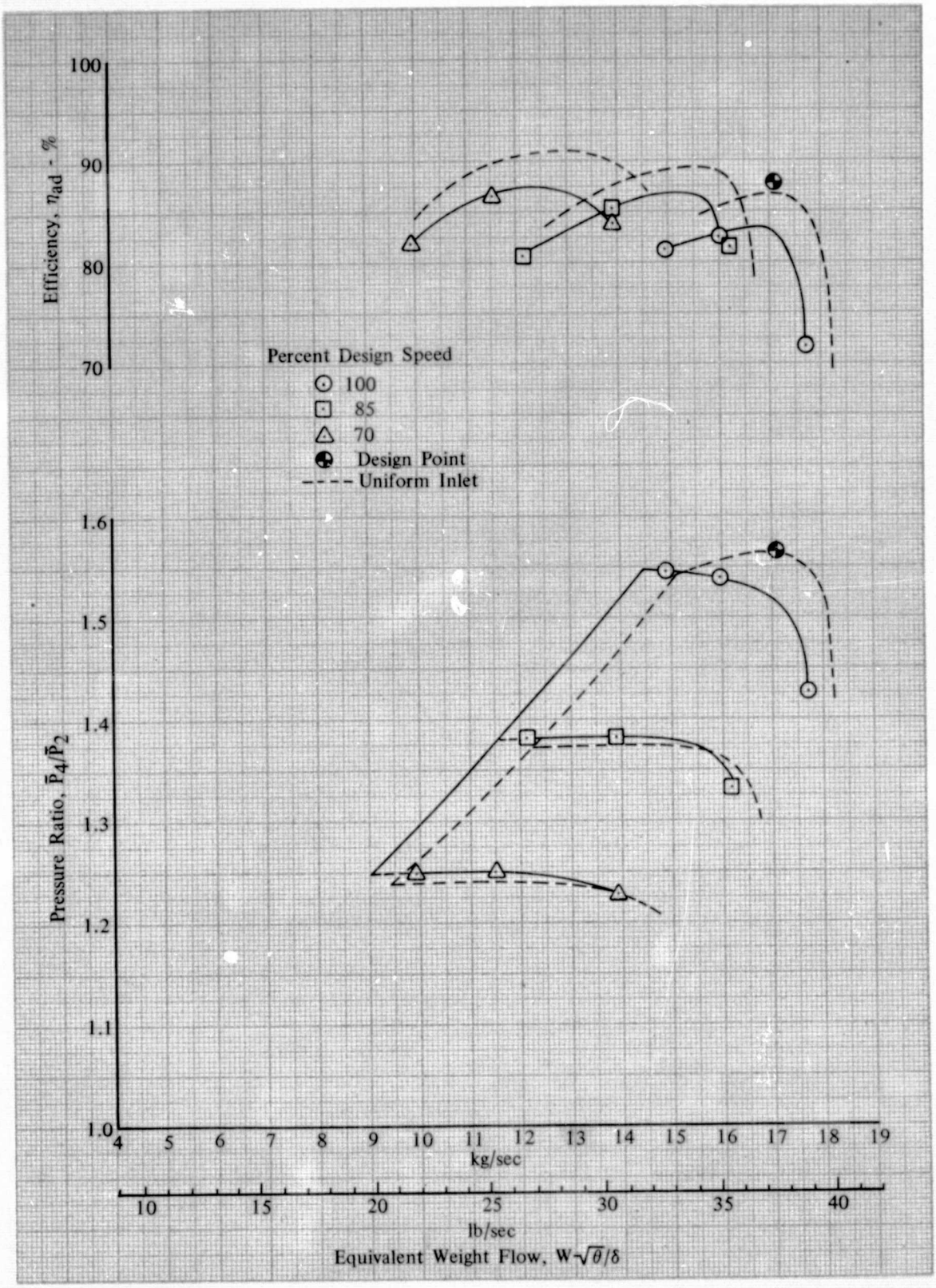


Figure 42. Overall Performance of Rotor F-Stator F with Hub Radial Distortion DF 102144

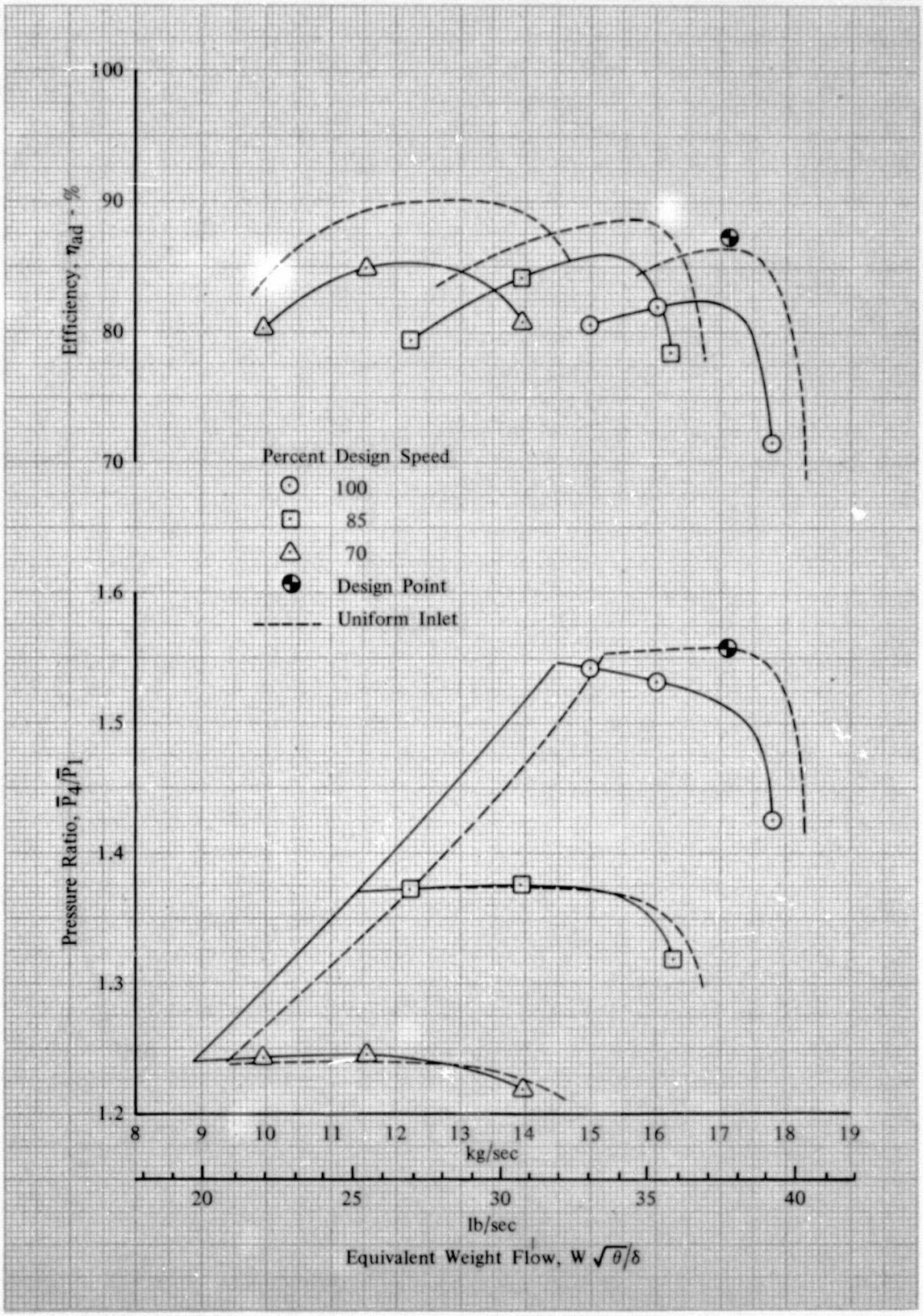


Figure 43. Overall Performance of Stage F with Hub Radial Distortion DF 102145

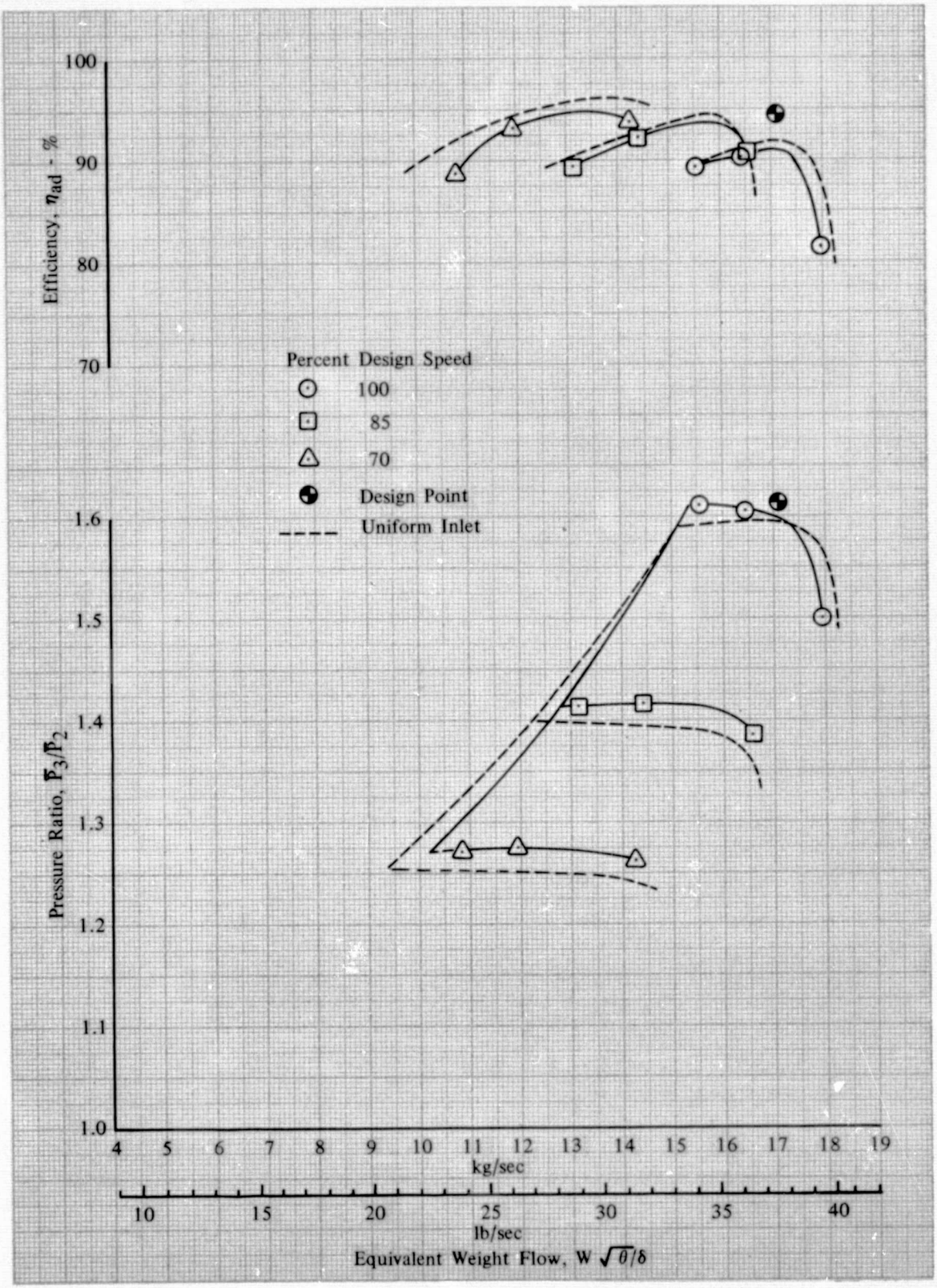


Figure 44. Overall Performance of Rotor F with Tip Radial Distortion DF 102146

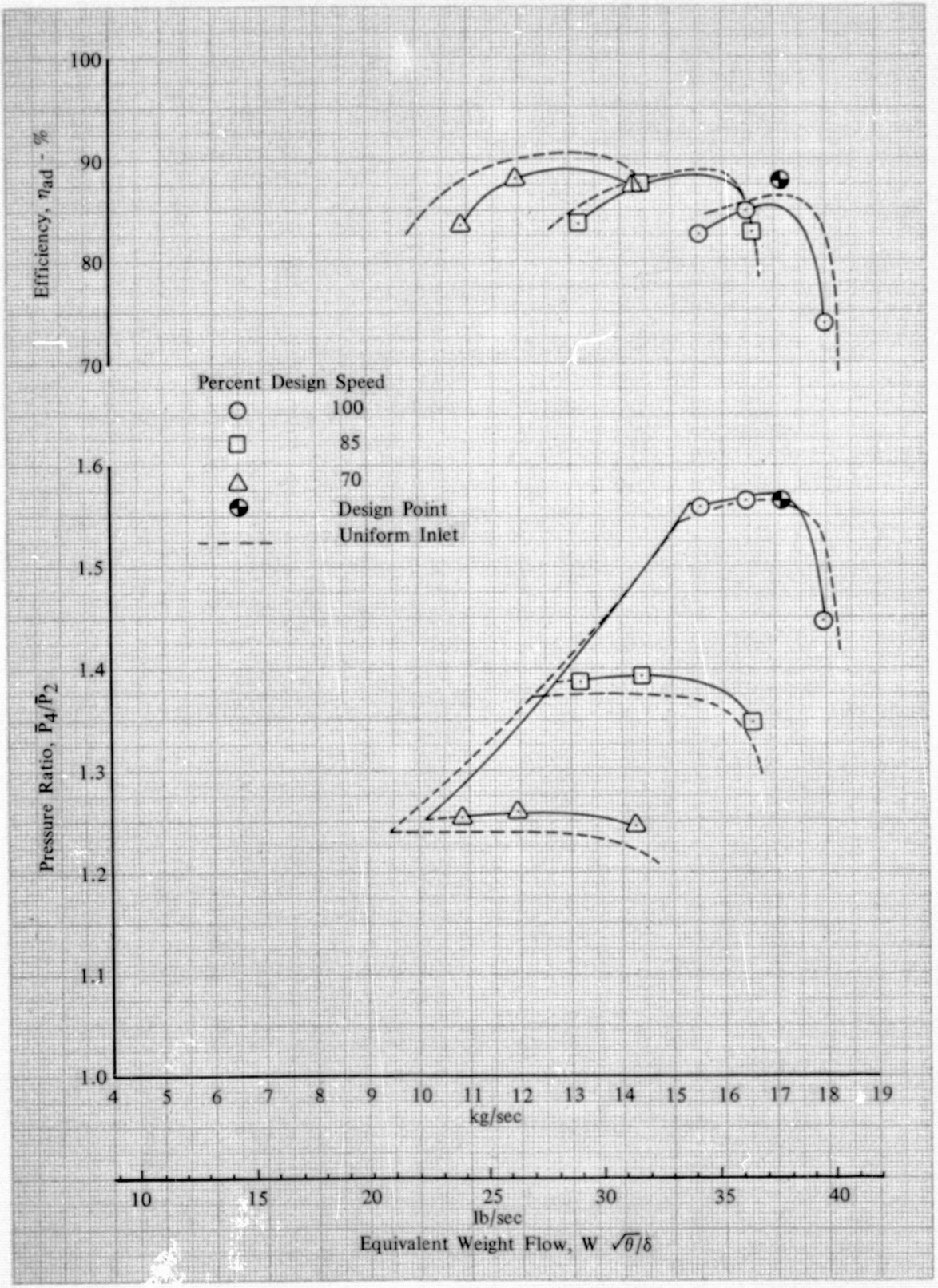


Figure 45. Overall Performance of Rotor F-Stator F with Tip Radial Distortion DF 102147

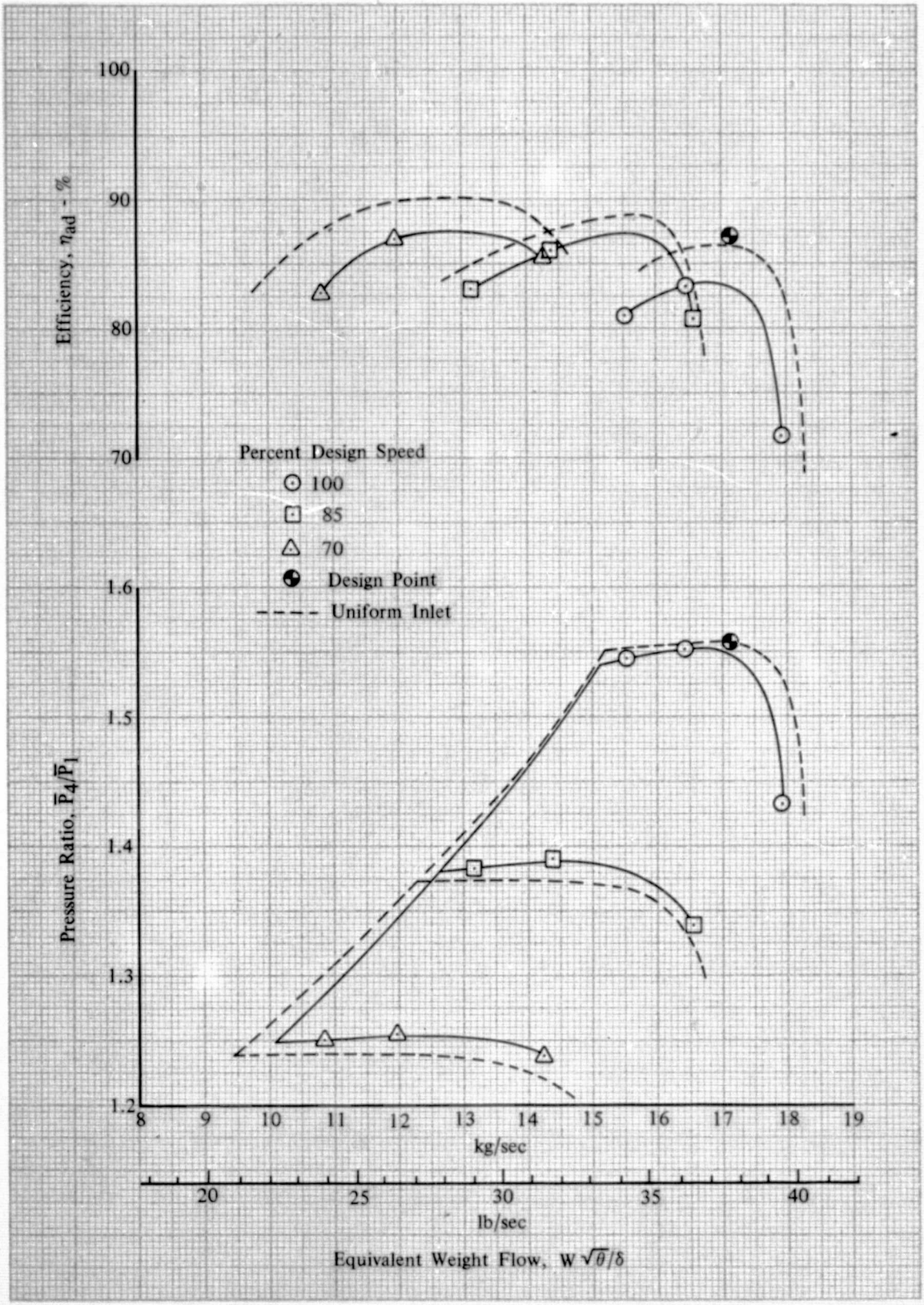


Figure 46. Overall Performance of Stage F with Tip Radial Distortion DF 102148

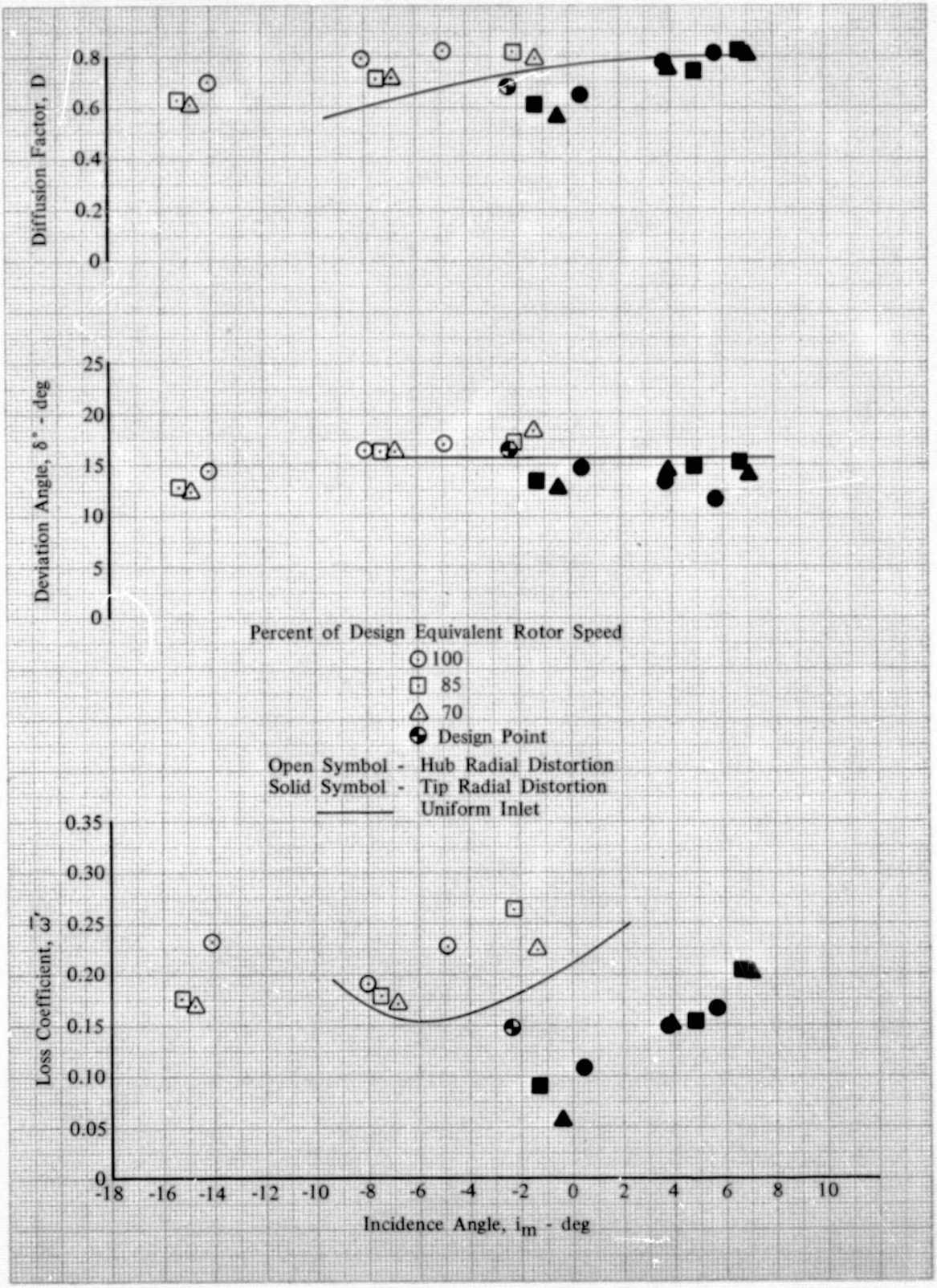


Figure 47a. Rotor F Blade Element Performance; 5% Span from Tip; Hub and Tip Radial Distortion

DF 102149

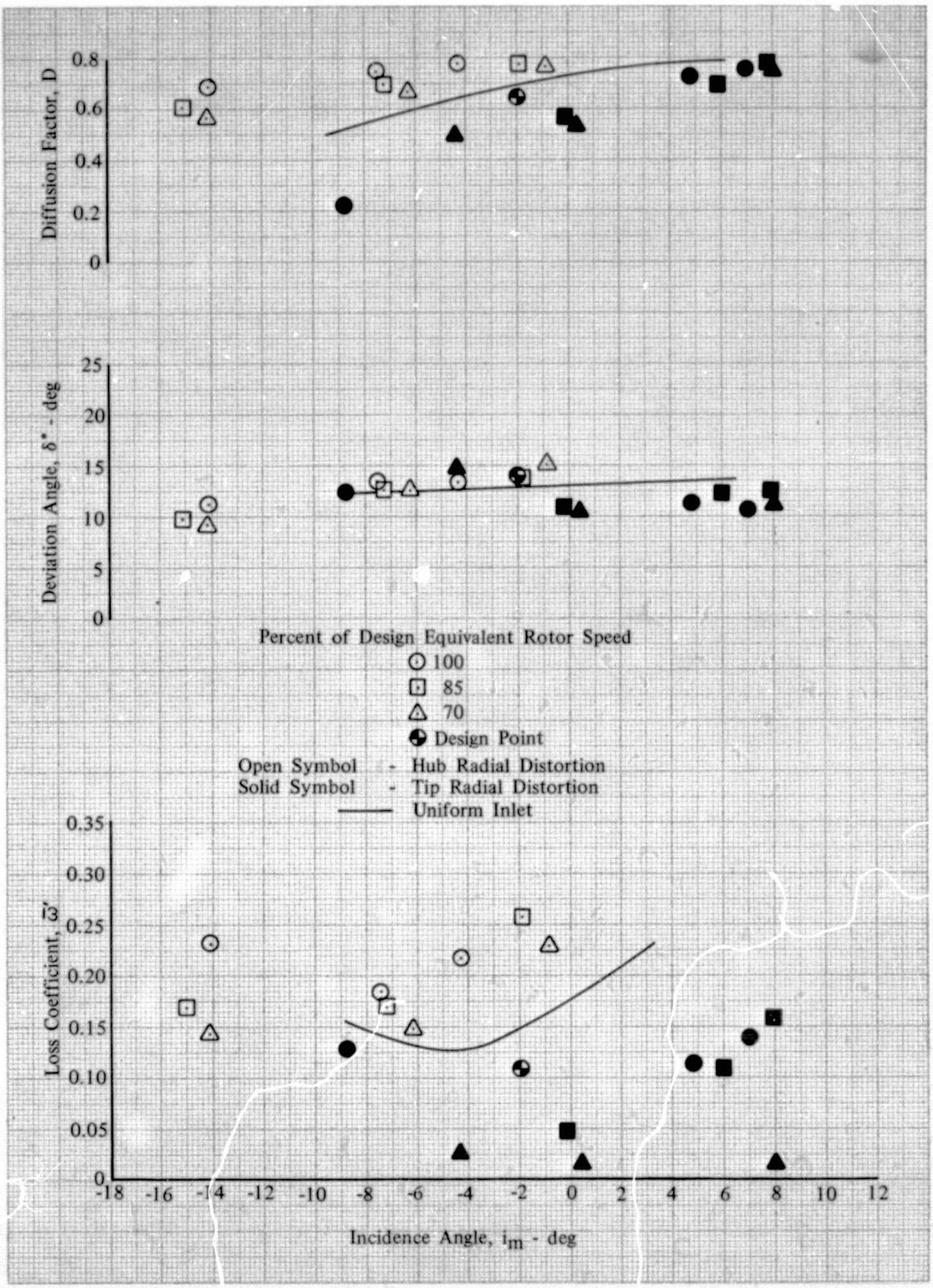


Figure 47b. Rotor F Blade Element Performance; 10% Span from Tip; Hub and Tip Radial Distortion

DF 102150

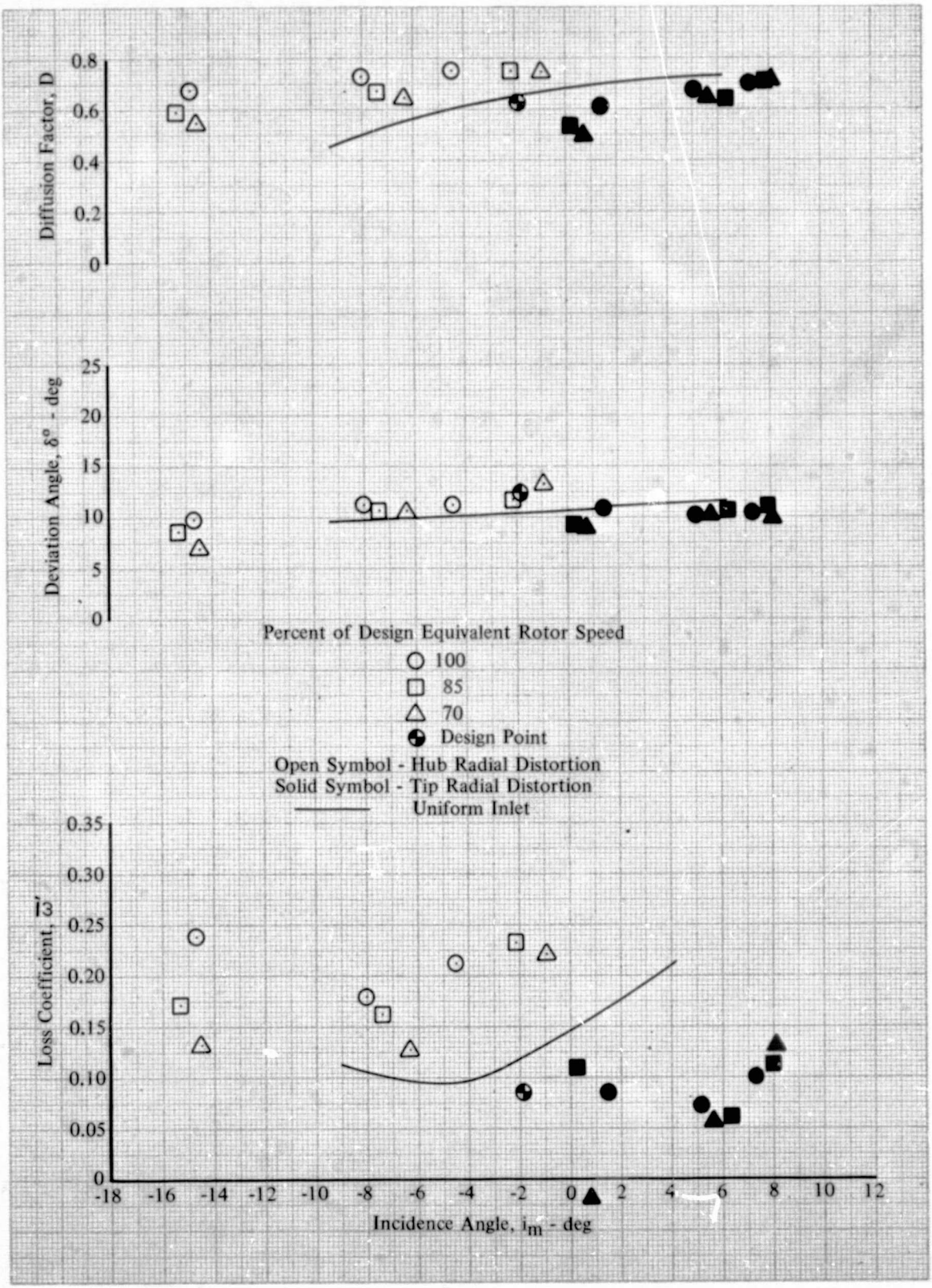


Figure 47c. Rotor F Blade Element Performance; 15% Span from Tip; Hub and Tip Radial Distortion

DF 102151

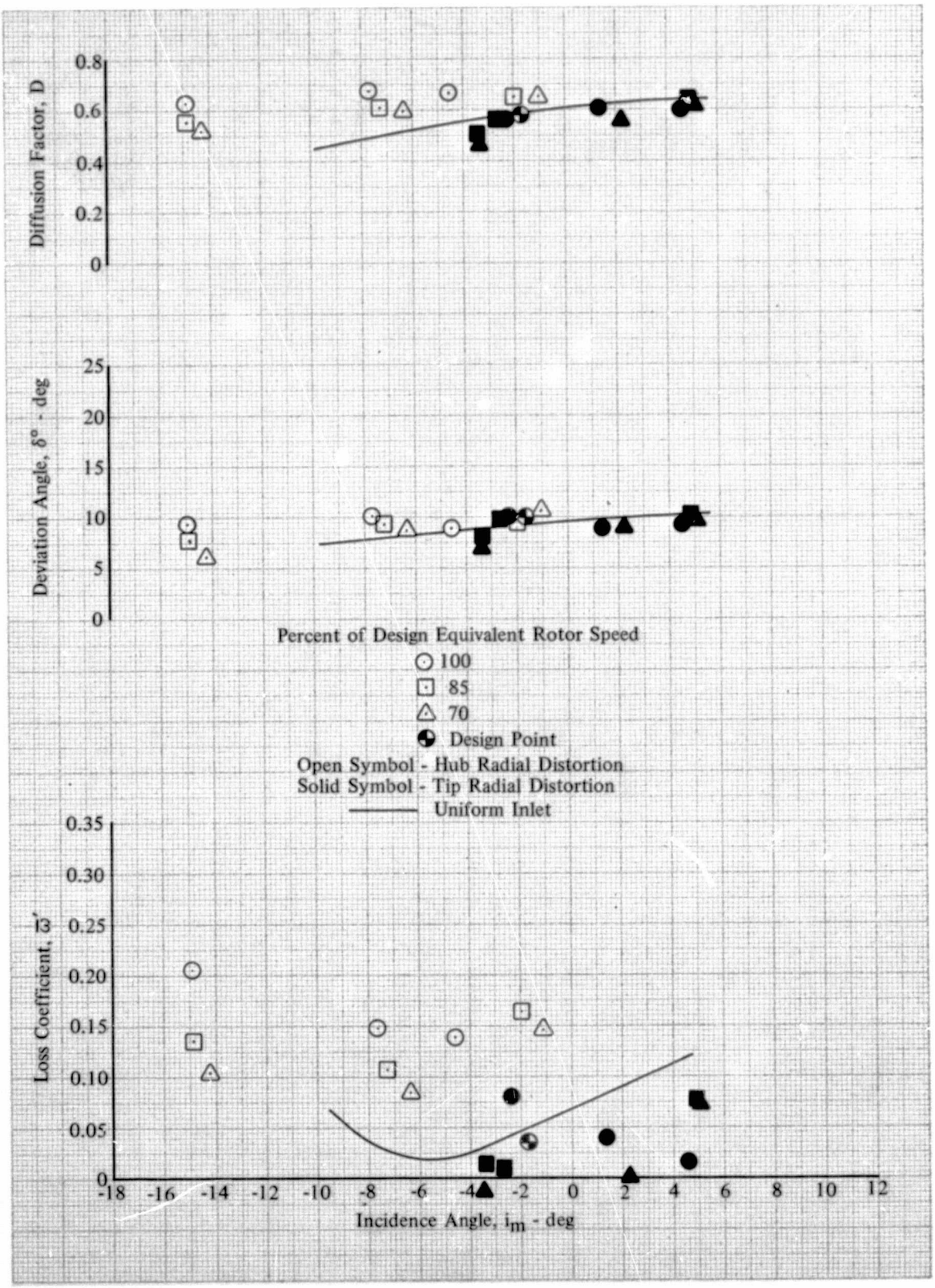


Figure 47d. Rotor F Blade Element Performance; 30% Span from Tip; Hub and Tip Radial Distortion

DF 102152

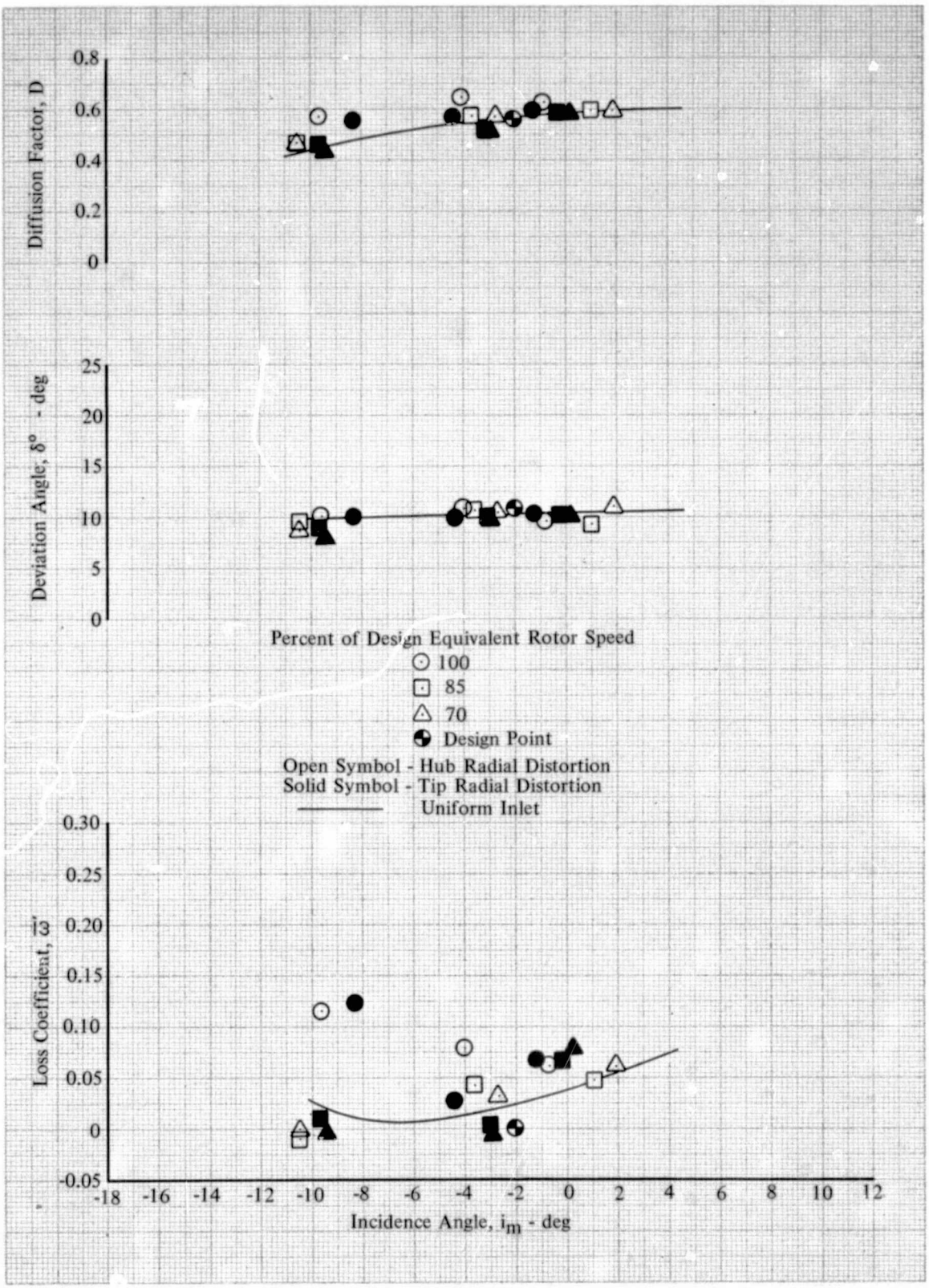


Figure 47e. Rotor F Blade Element Performance; 50% Span; Hub and Tip Radial Distortion DF 102153

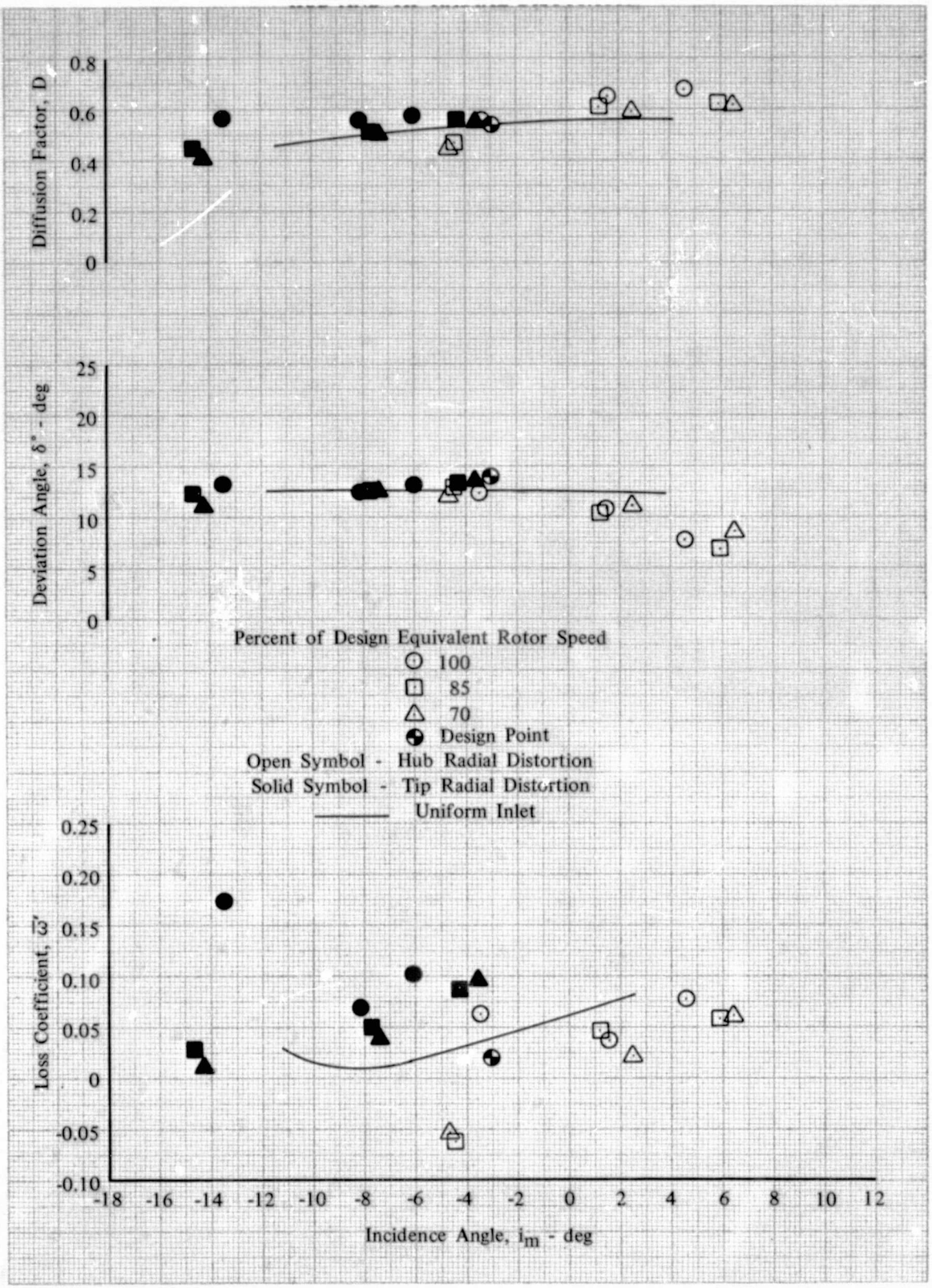


Figure 47f. Rotor F Blade Element Performance; 70% Span from Tip; Hub and Tip Radial Distortion

DF 102154

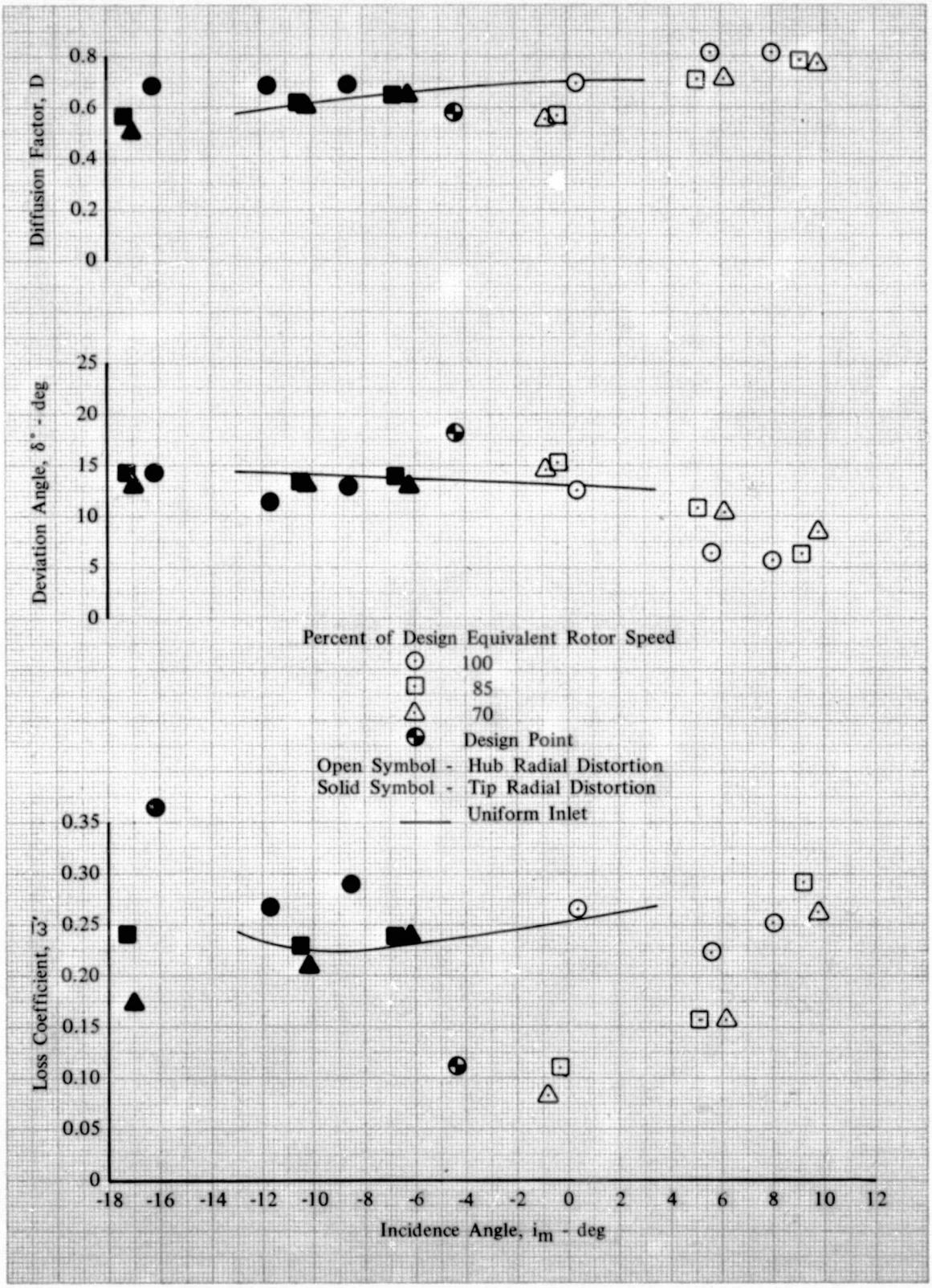


Figure 47g. Rotor F Blade Element Performance; 85% Span from Tip; Hub and Tip Radial Distortion

DF 102155

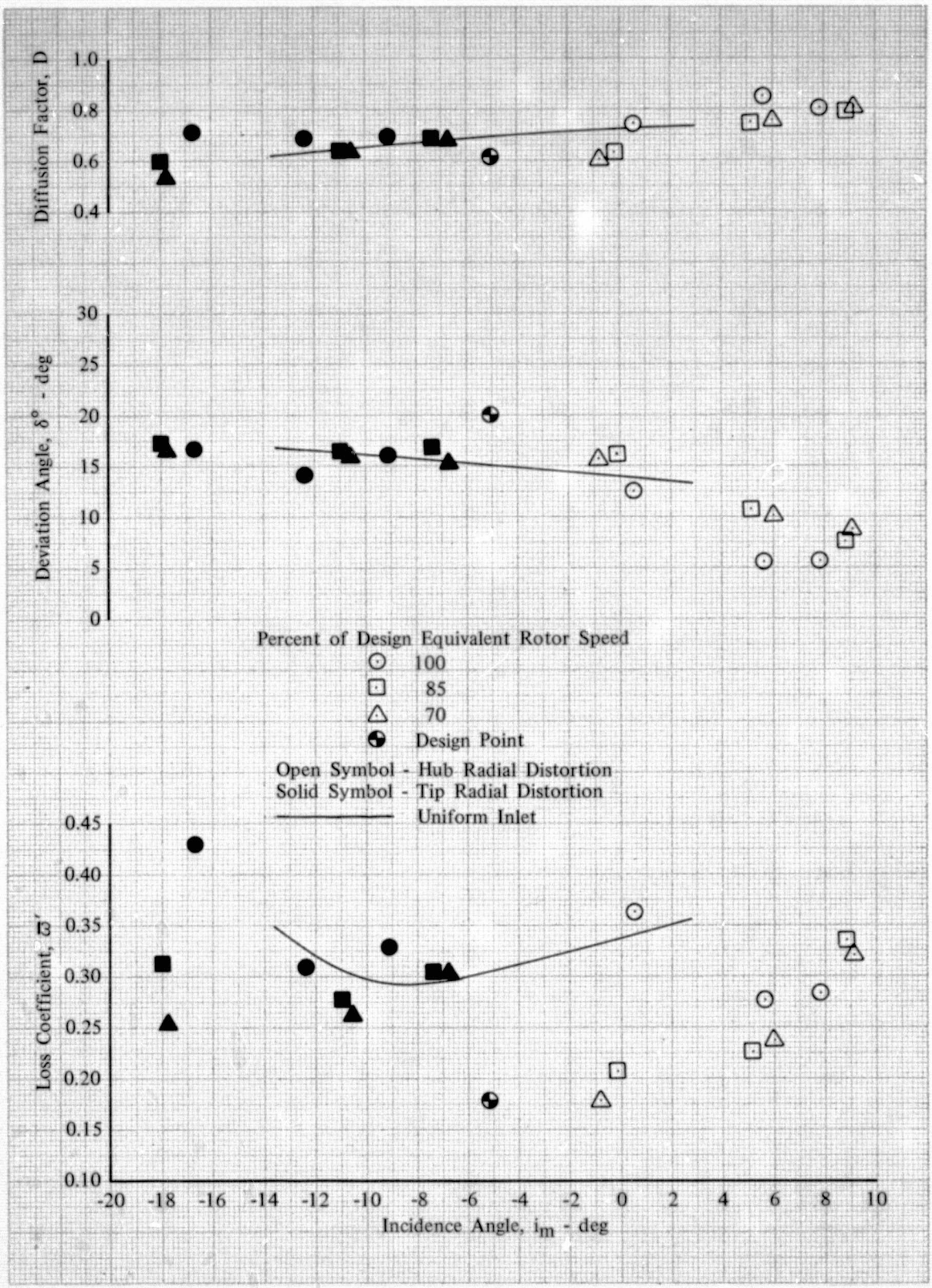


Figure 47h. Rotor F Blade Element Performance; 90% Span from Tip; Hub and Tip Radial Distortion

DF 102156

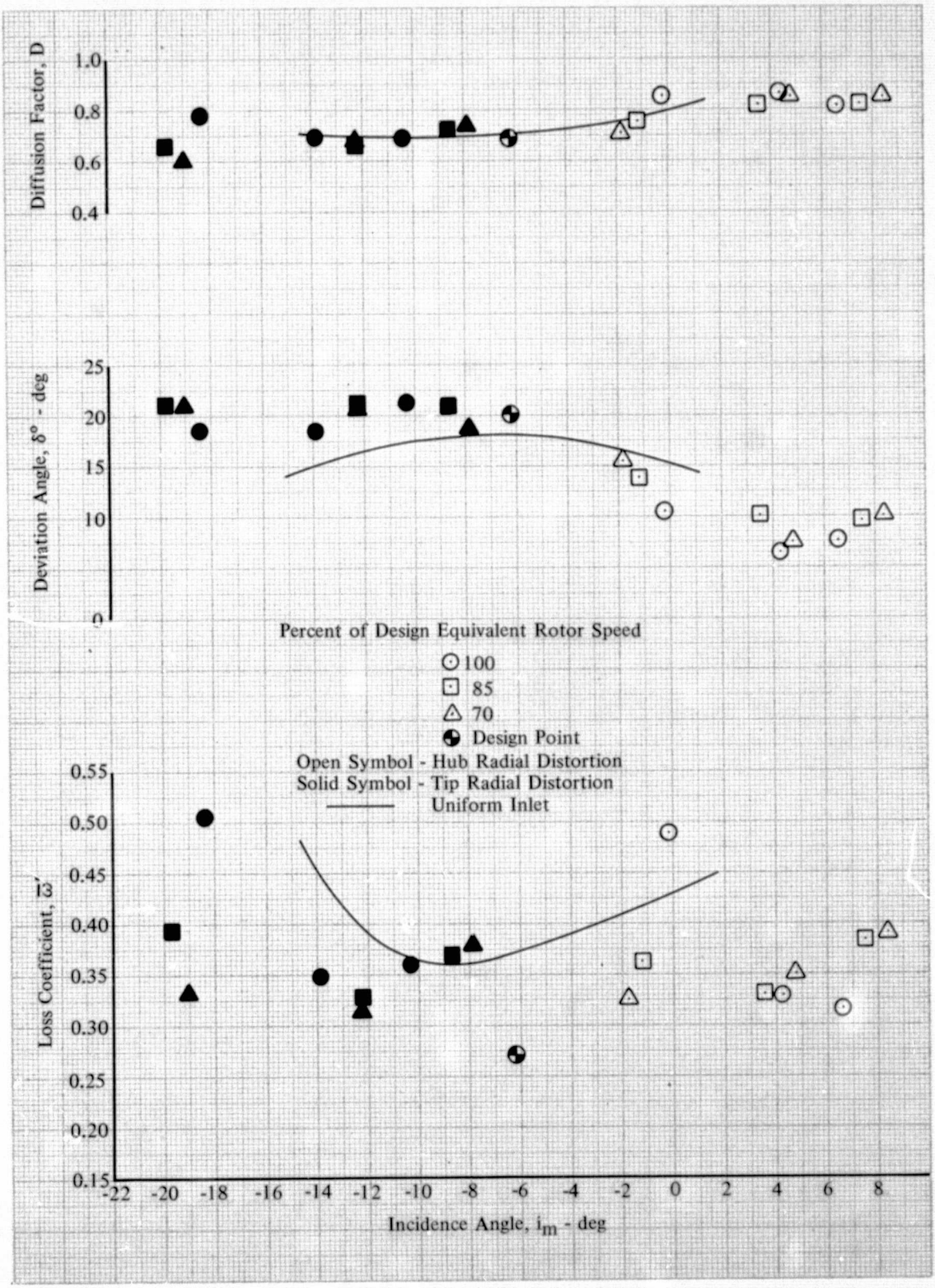


Figure 47i. Rotor F Blade Element Performance; 95% Span from Tip; Hub and Tip Radial Distortion

DF 102157

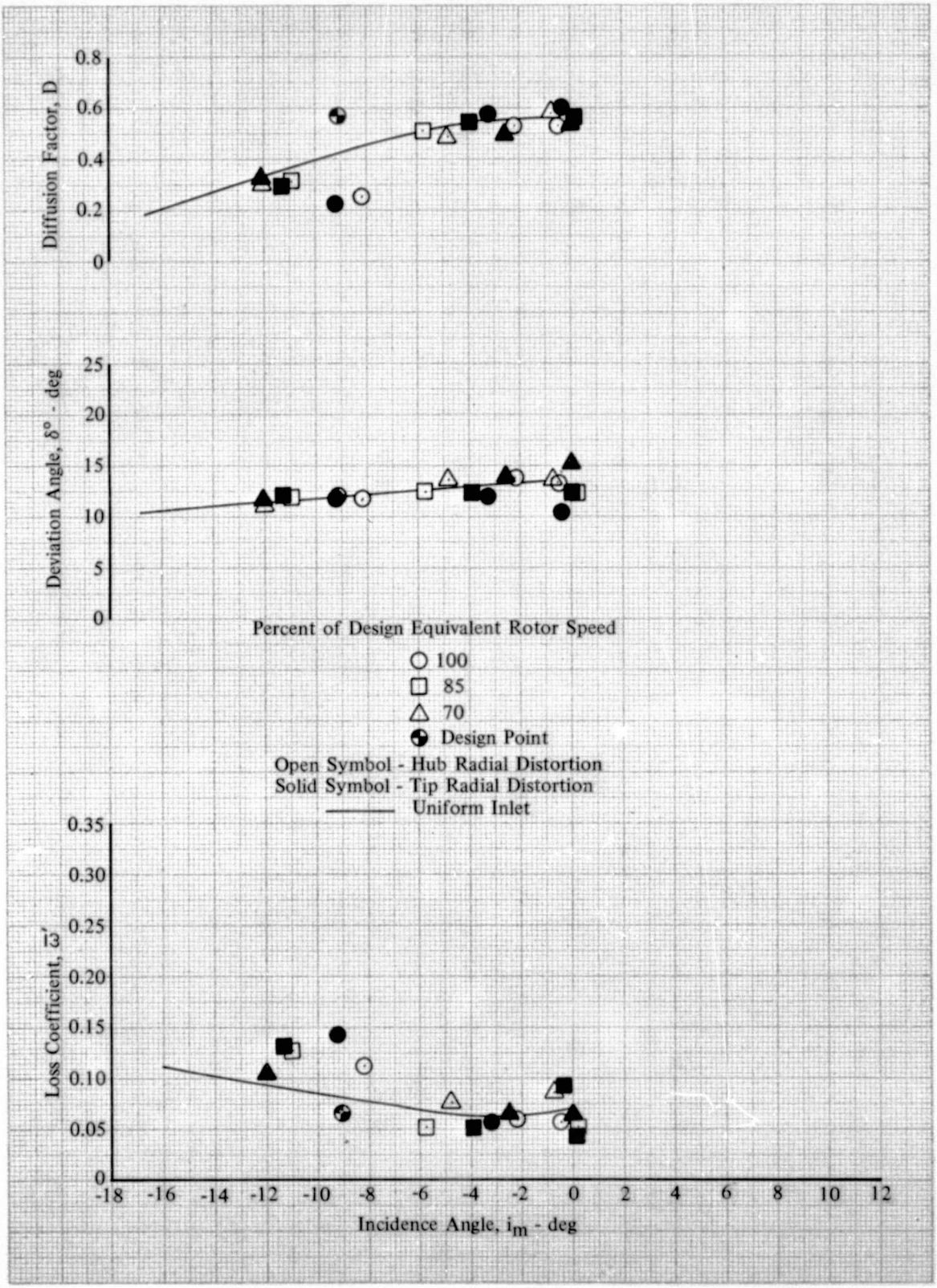


Figure 48a. Stator F Blade Element Performance; 5% Span from Tip; Hub and Tip Radial Distortion

DF 102159

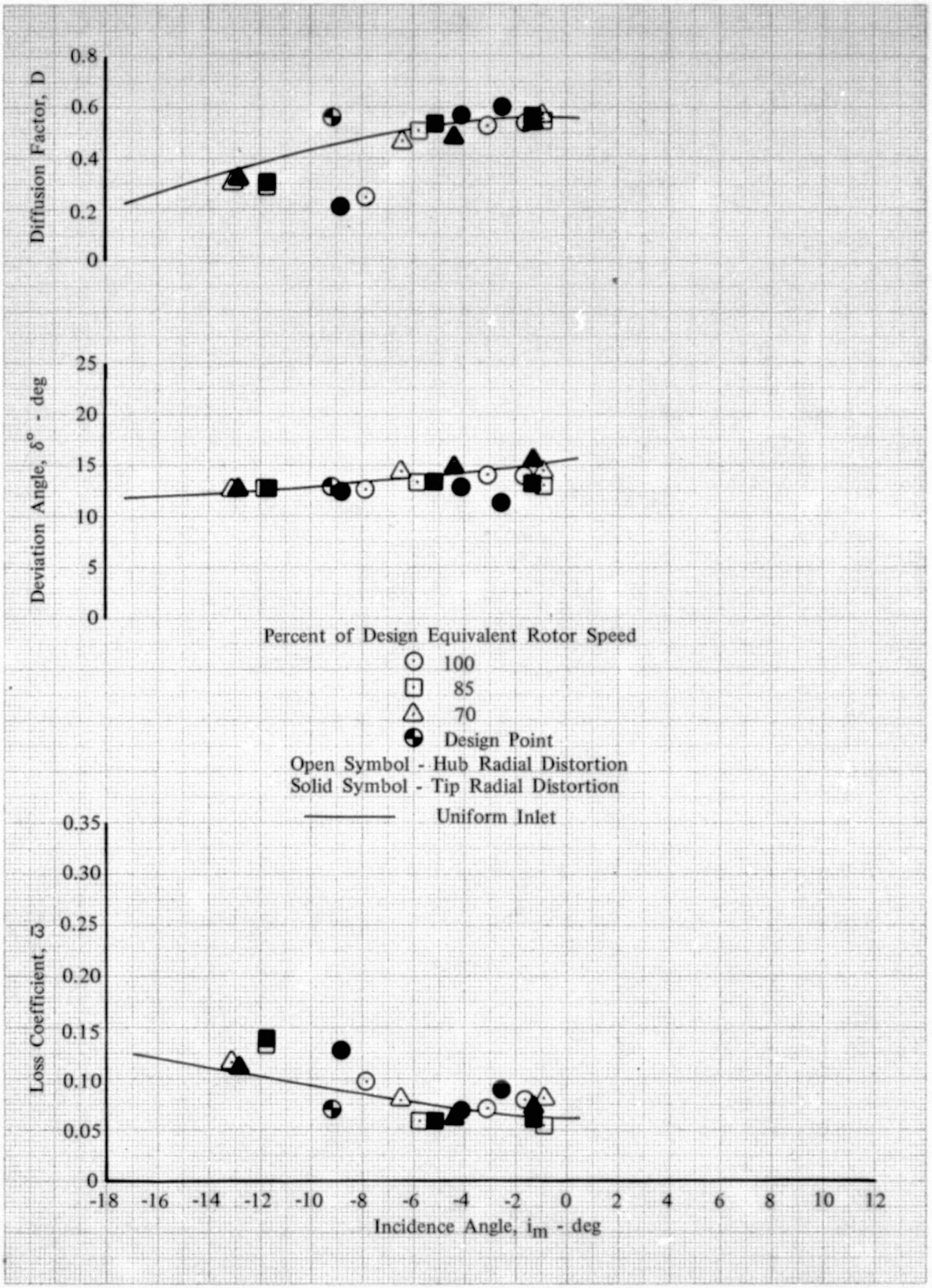


Figure 48b. Stator F Blade Element Performance; 10% Span from Tip; Hub and Tip Radial Distortion

DF 102160

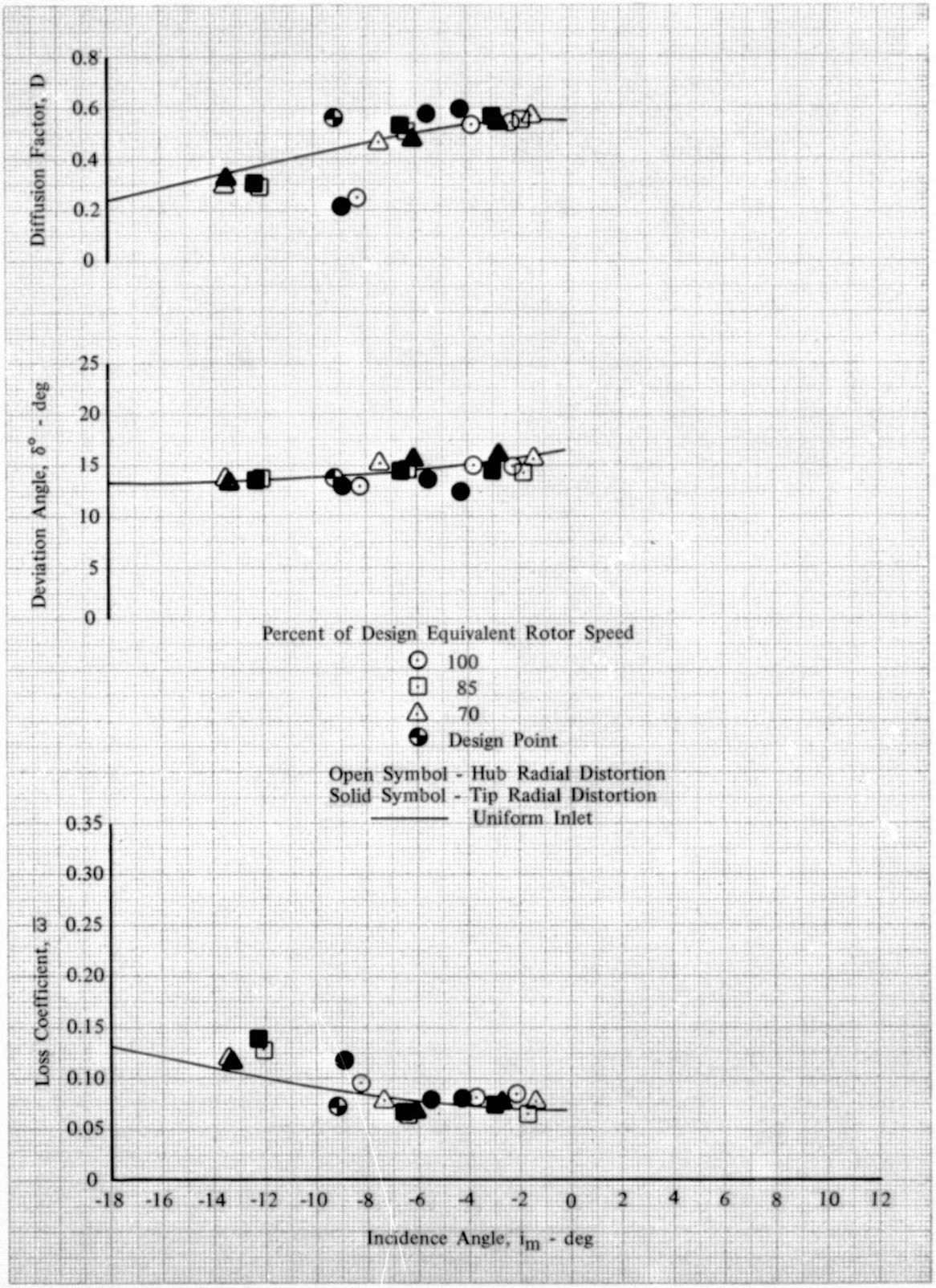


Figure 48c. Stator F Blade Element Performance; 15% Span from Tip; Hub and Tip Radial Distortion

DF 102161

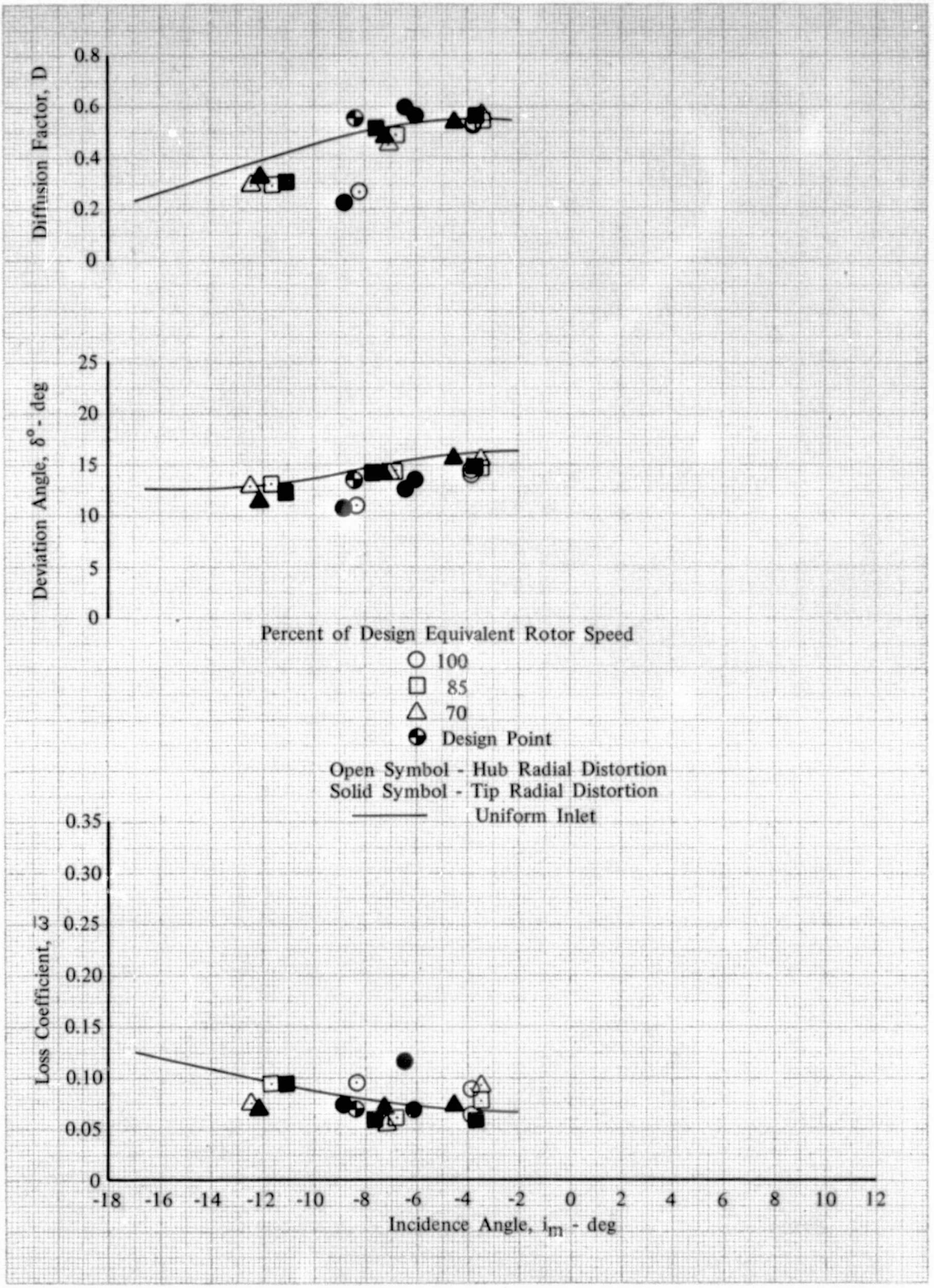


Figure 48d. Stator F Blade Element Performance; 30% Span from Tip; Hub and Tip Radial Distortion

DF 102162

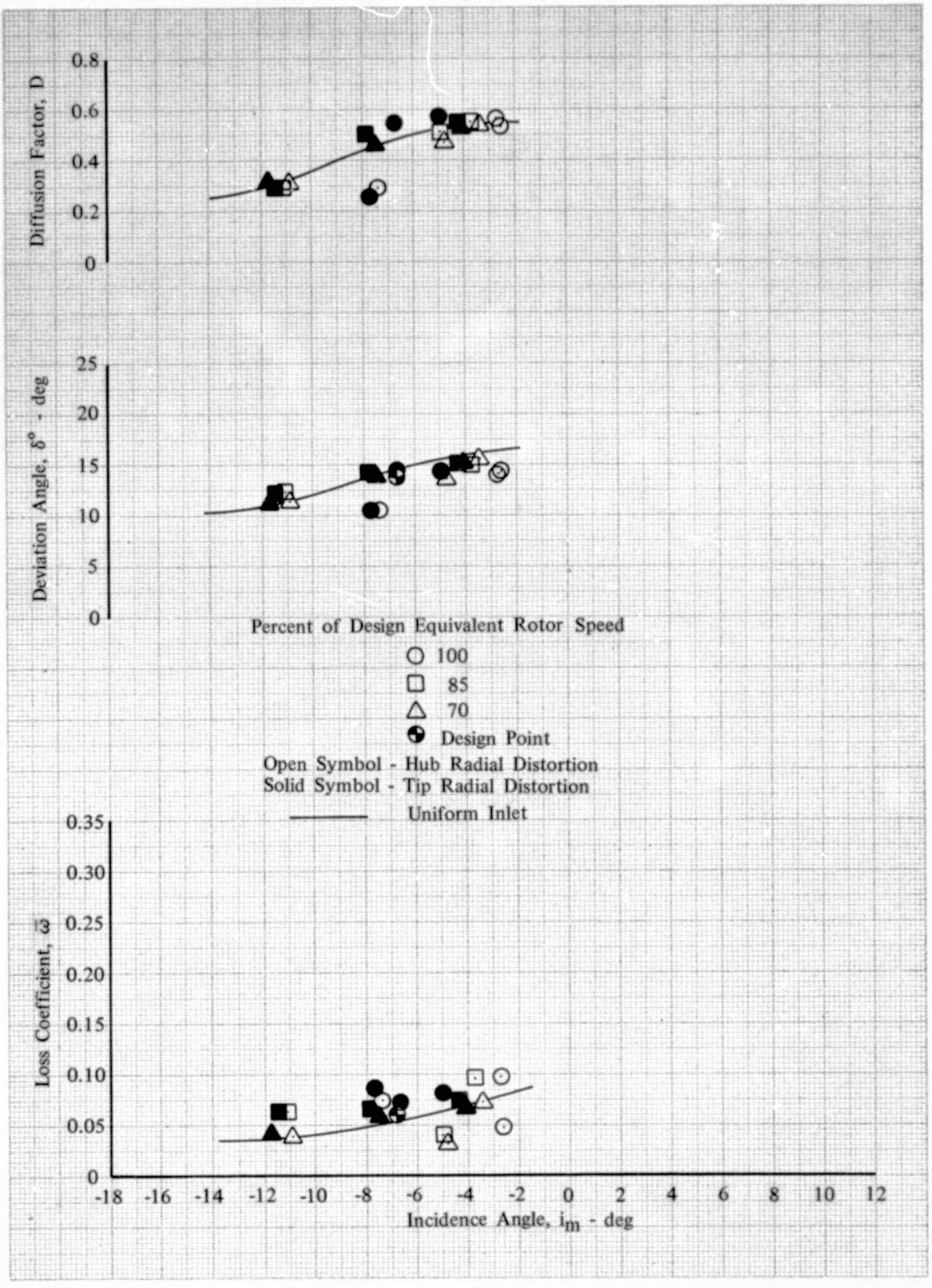


Figure 48e. Stator F Blade Element Performance; 50% Span; Hub and Tip Radial Distortion DF 102163

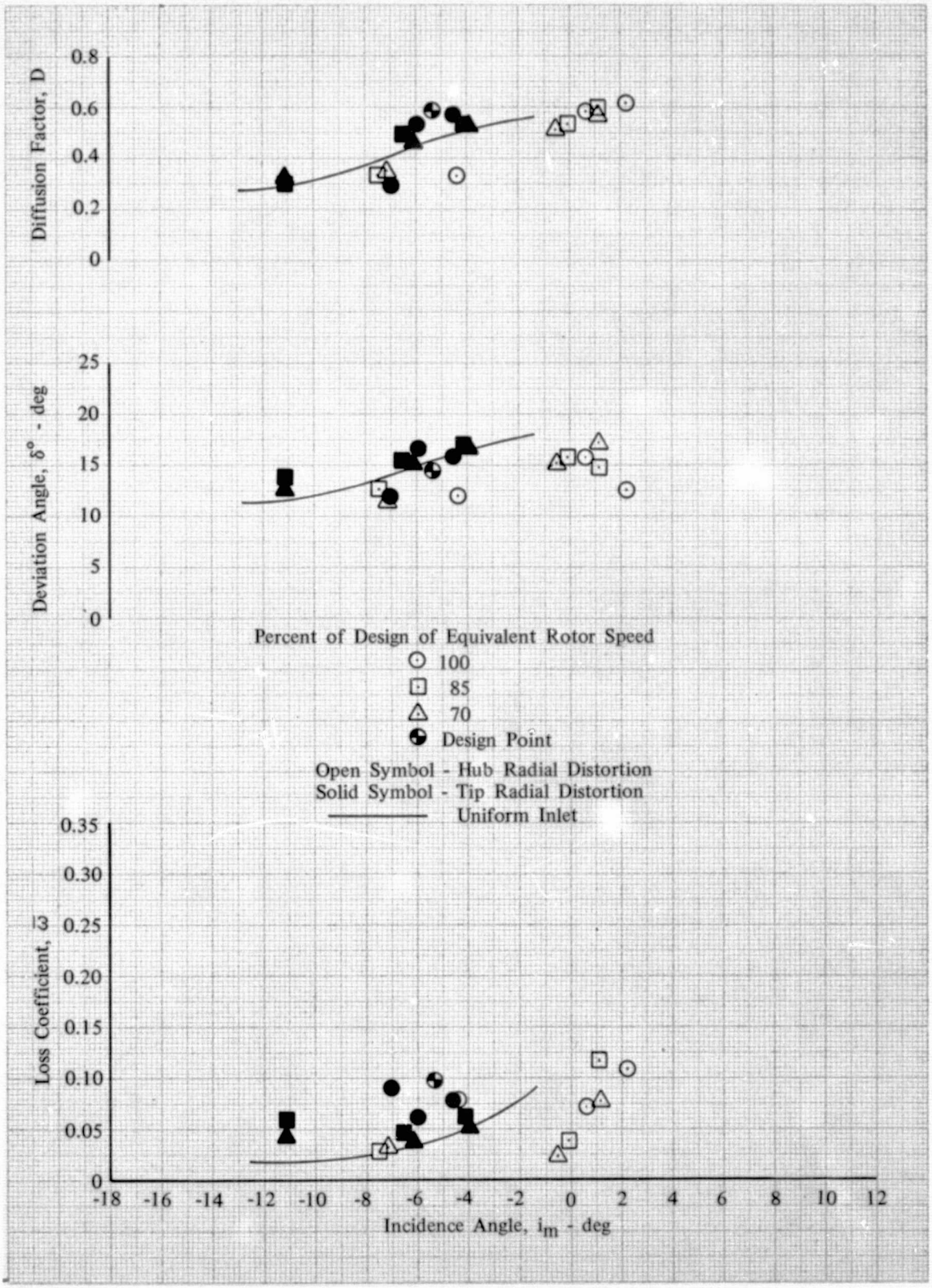


Figure 48f. Stator F Blade Element Performance; 70% Span from Tip; Hub and Tip Radial Distortion

DF 102164

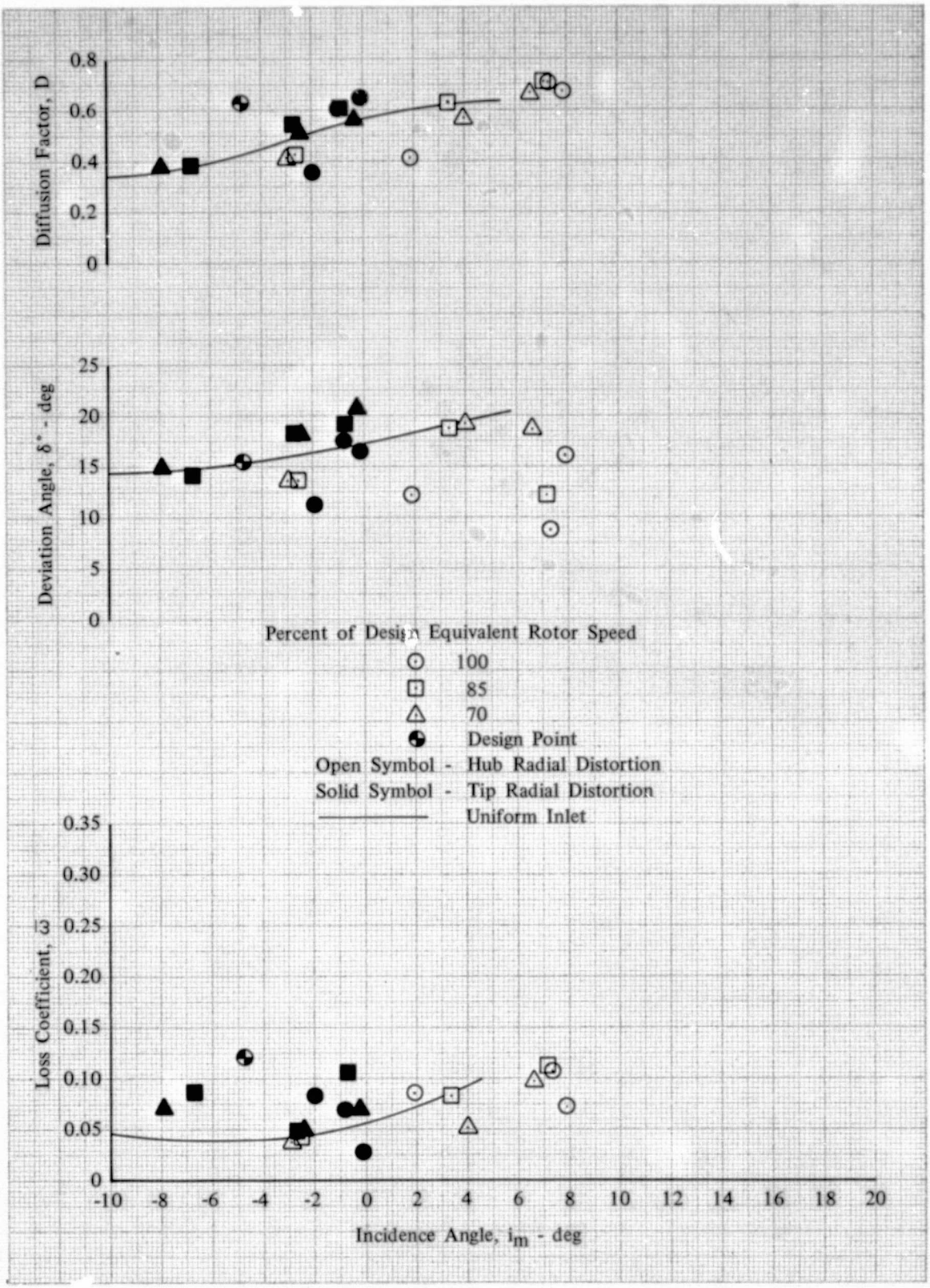


Figure 48g. Stator F Blade Element Performance; 85% Span from Tip; Hub and Tip Radial Distortion

DF 102165

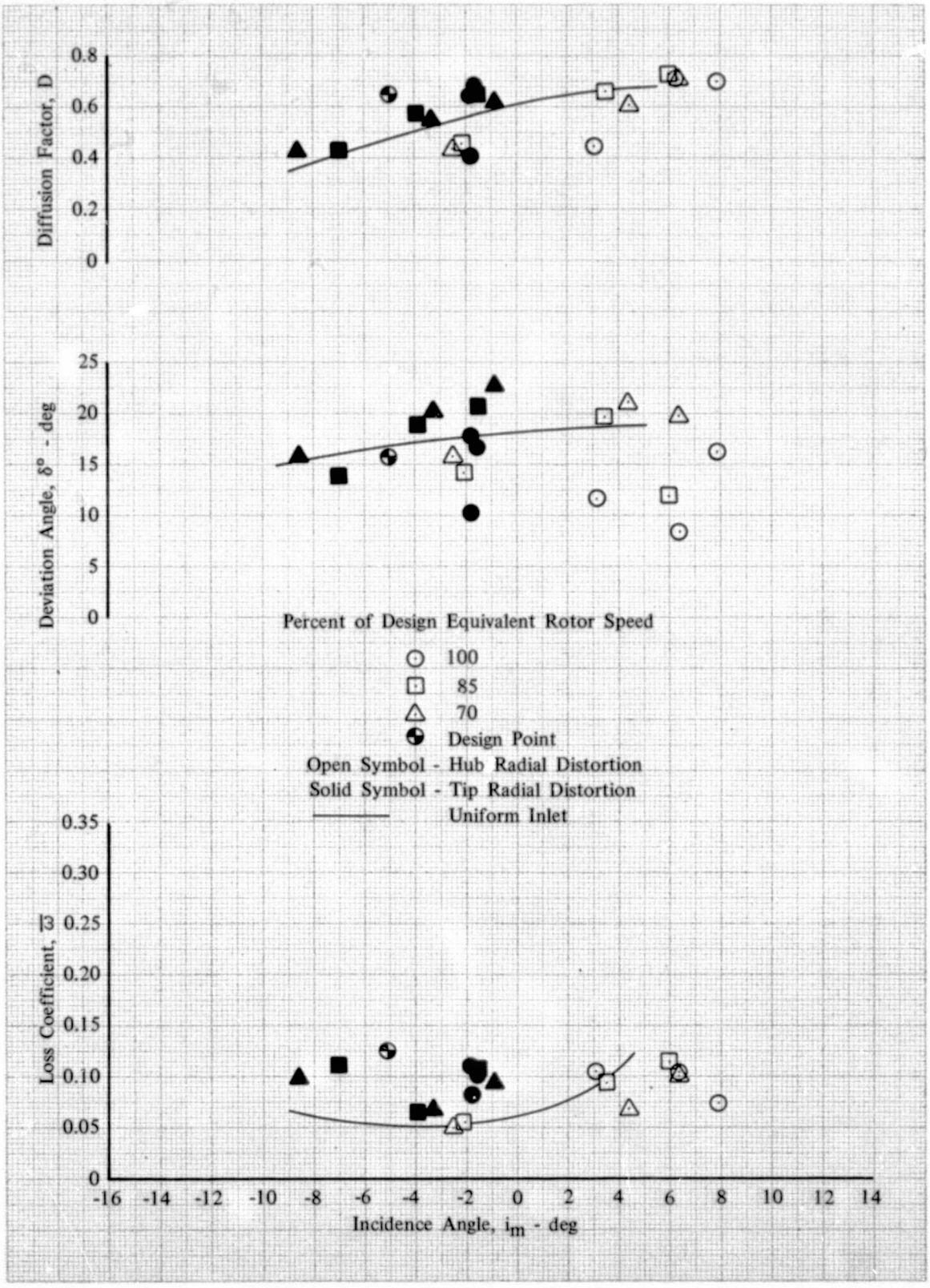


Figure 48h. Stator F Blade Element Performance; 90% Span from Tip; Hub and Tip Radial Distortion

DF 102166

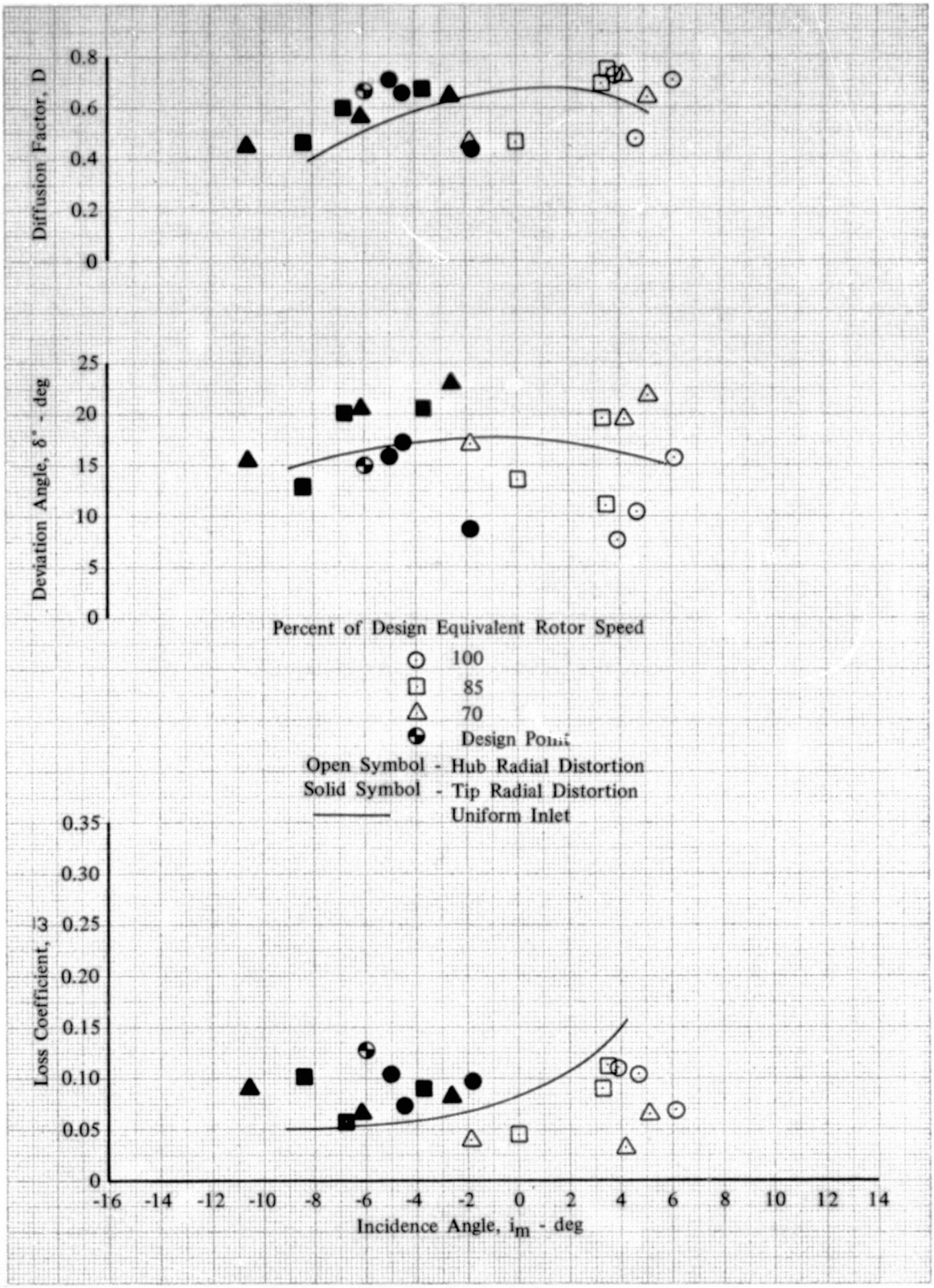


Figure 48i. Stator F Blade Element Performance; 95% Span from Tip; Hub and Tip Radial Distortion

DF 102167

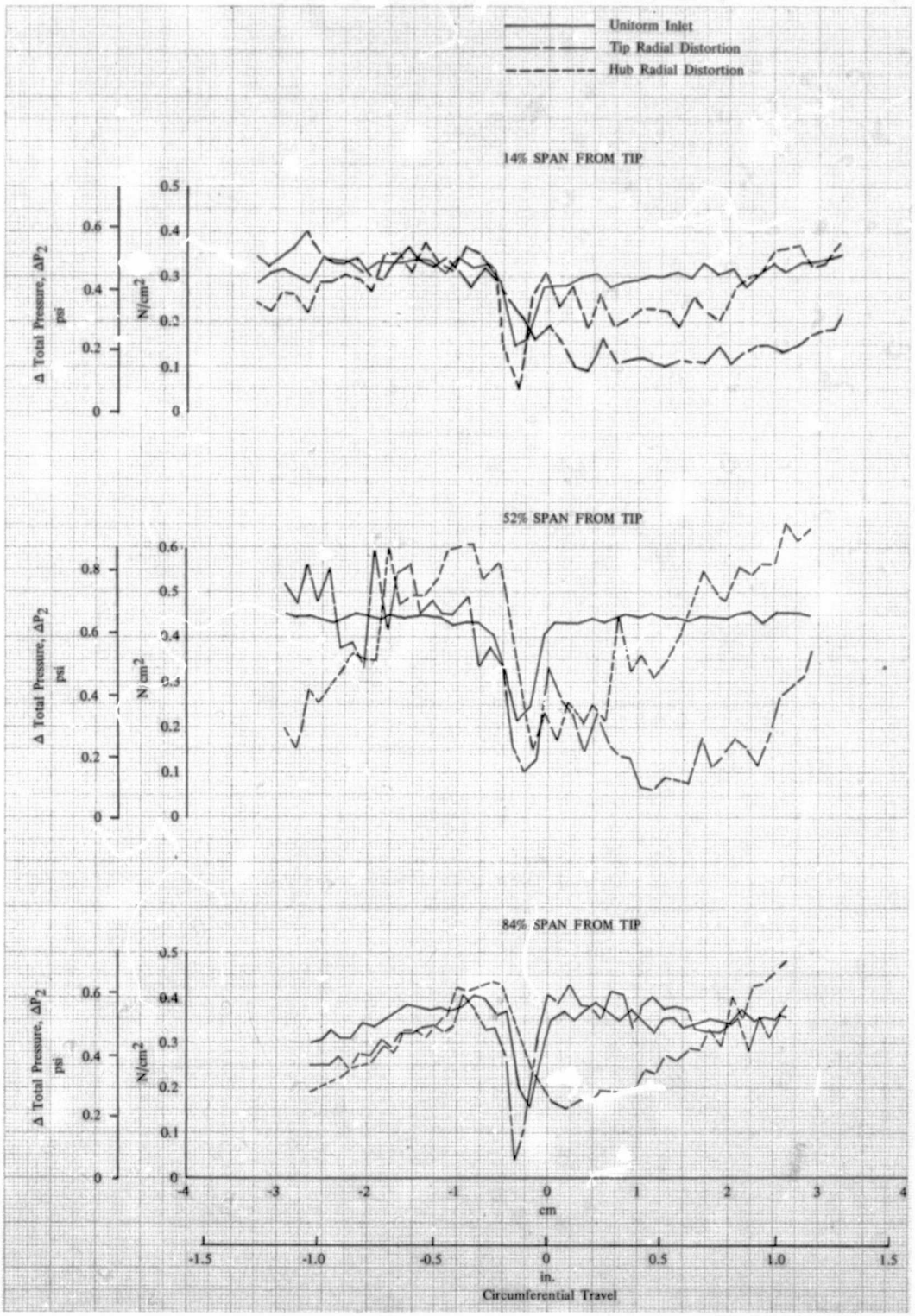


Figure 49. Comparison of Typical Inlet Guide Vane Exit Total Pressure Profiles at Hub, Mean and Tip for Uniform Inlet and Radial Inlet Distortion

DF 102168

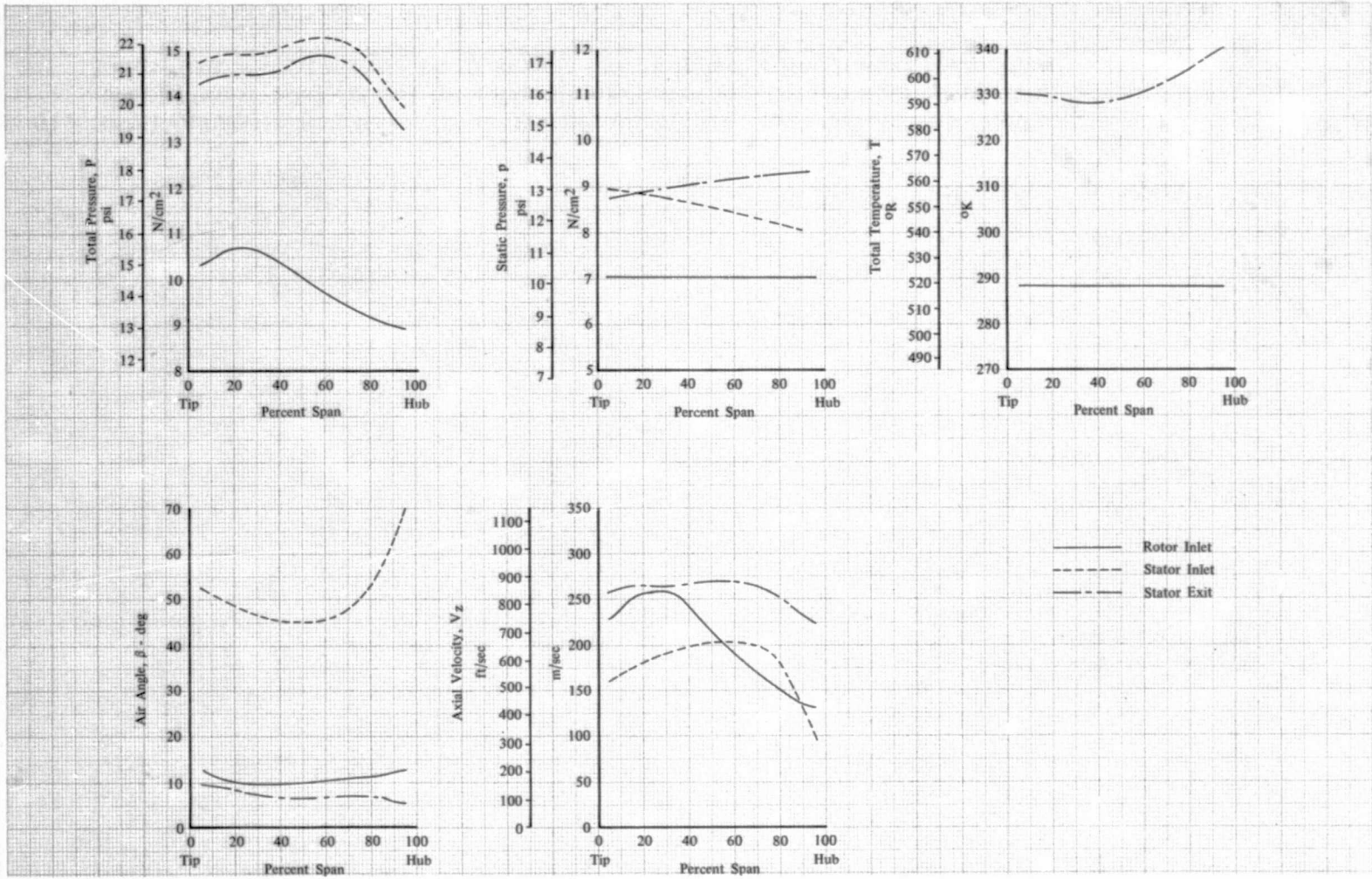


Figure 50. Total and Static Pressure, Total Temperature, Air Angle and Axial Velocity vs Span at Rotor Inlet, Stator Inlet and Stator Exit; 100% Design Equivalent Rotor Speed; Equivalent Weight Flow = 17.79 kg/sec (39.21 lb/sec); Hub Radial Distortion

DF 102169

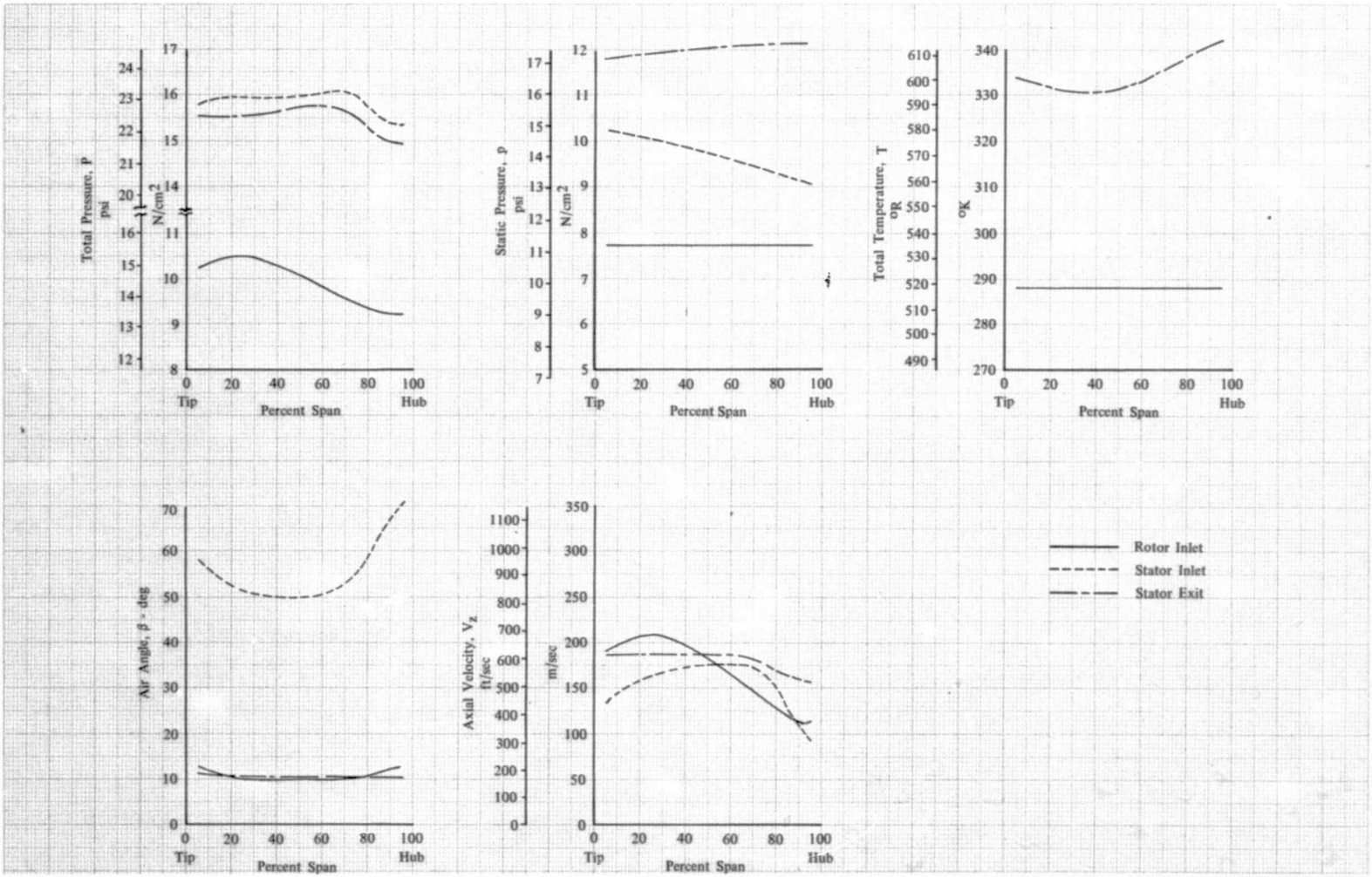


Figure 51. Total and Static Pressure, Total Temperature, Air Angle and Axial Velocity vs Span at Rotor Inlet, Stator Inlet and Stator Exit; 100% Design Equivalent Rotor Speed; Equivalent Weight Flow = 16.02 kg/sec (35.32 lb/sec); Hub Radial Distortion

DF 102170

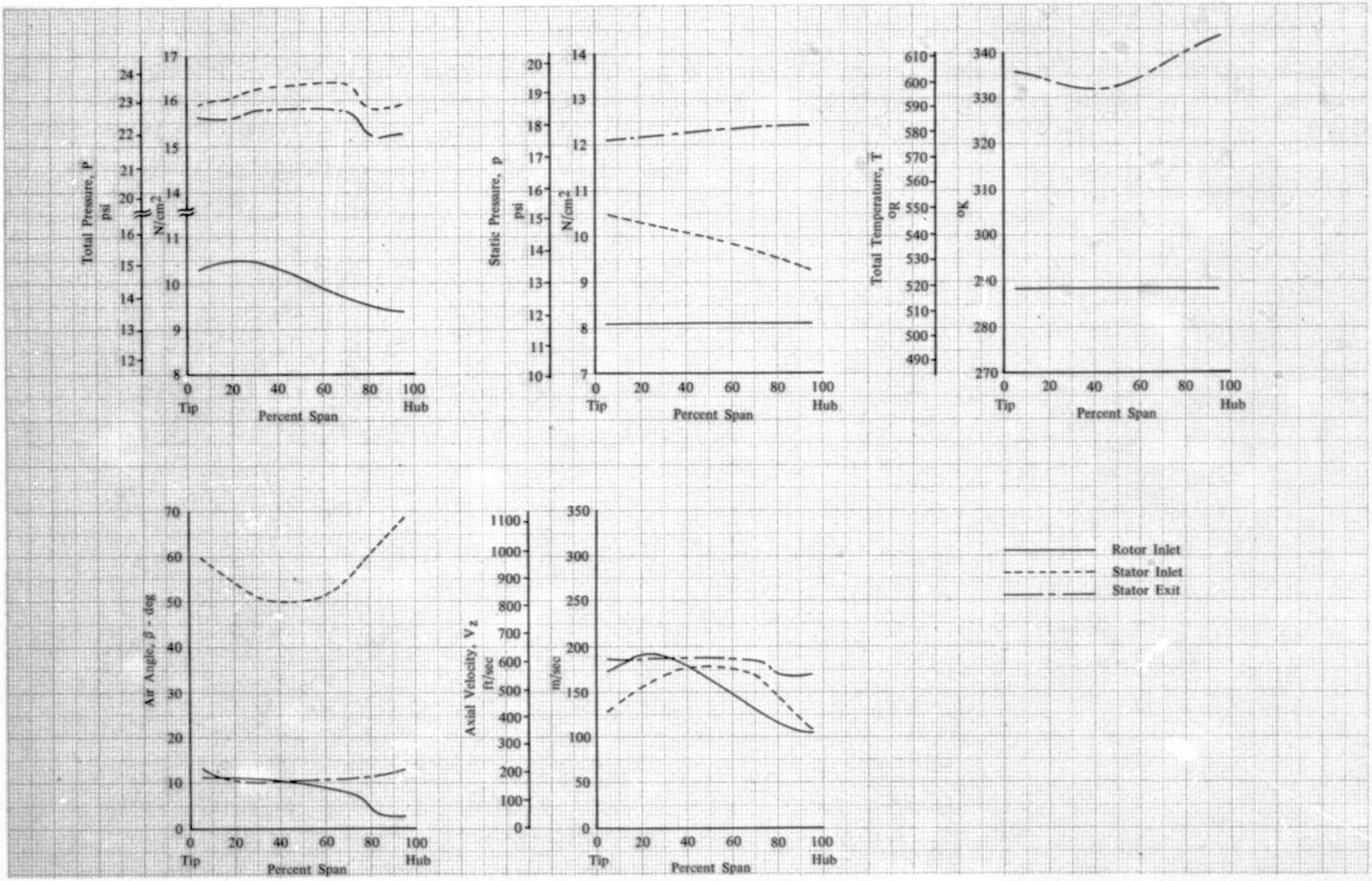


Figure 52. Total and Static Pressure, Total Temperature, Air Angle and Axial Velocity vs Span at Rotor Inlet, Stator Inlet and Stator Exit; 100% Design Equivalent Rotor Speed; Equivalent Weight Flow = 14.98 kg/sec (33.06 lb/sec); Hub Radial Distortion

DF 102171

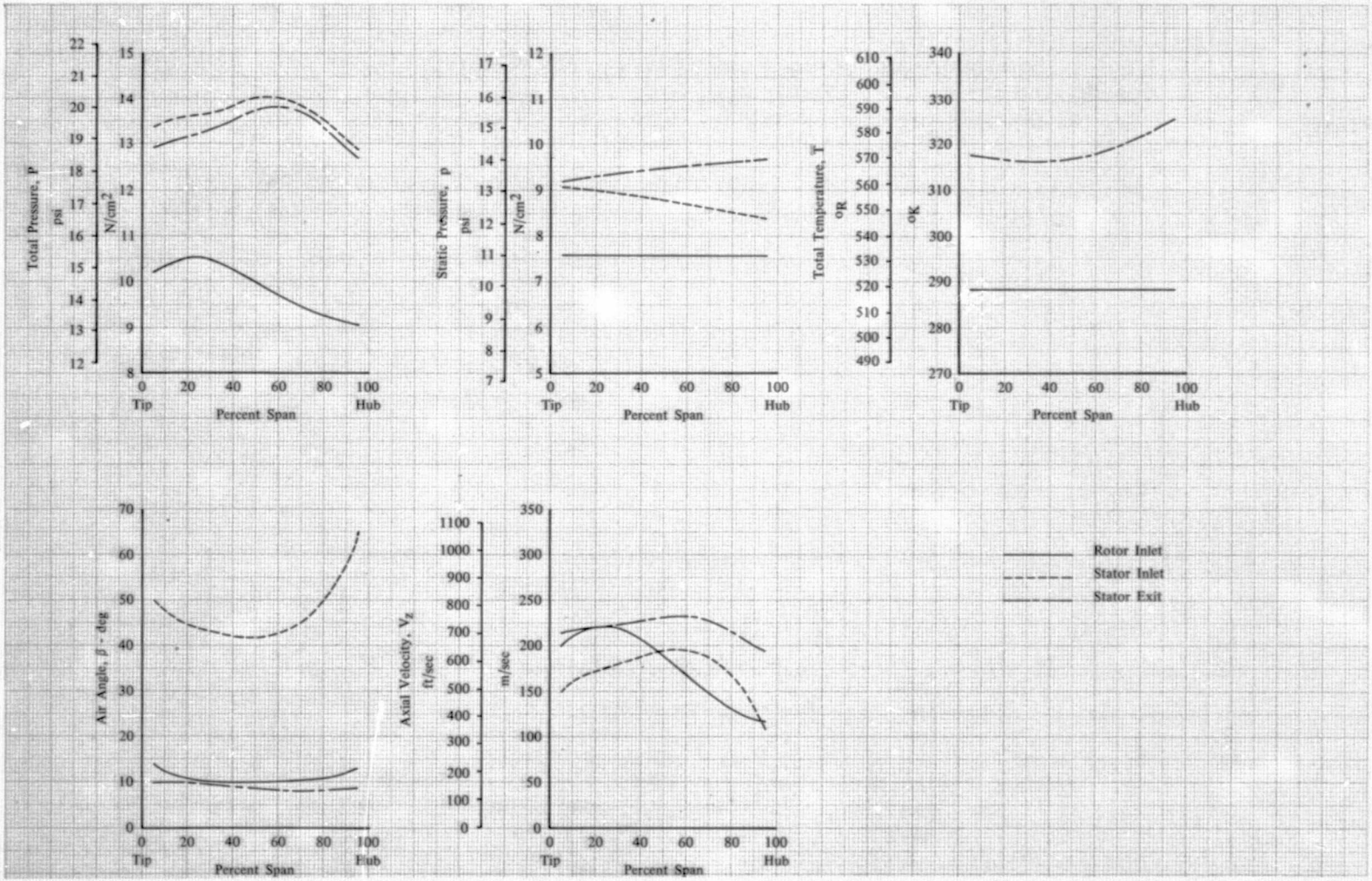


Figure 53. Total and Static Pressure, Total Temperature, Air Angle and Axial Velocity vs Span at Rotor Inlet, Stator Inlet and Stator Exit; 85% Design Equivalent Rotor Speed; Equivalent Weight Flow = 16.24 kg/sec (35.80 lb/sec); Hub Radial Distortion

DF 102172

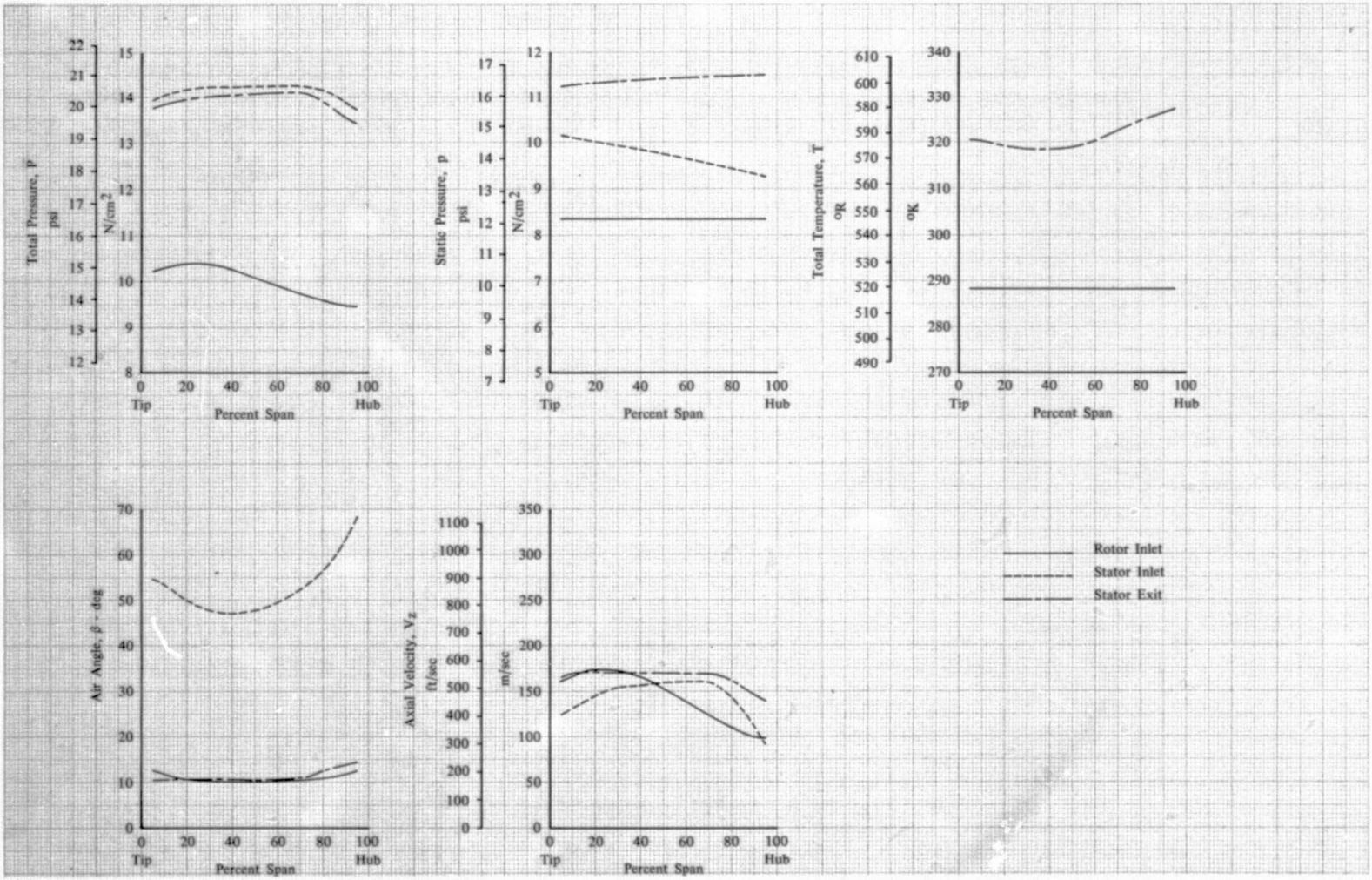


Figure 54. Total and Static Pressure, Total Temperature, Air Angle and Axial Velocity vs Span at Rotor Inlet, Stator Inlet and Stator Exit; 85% Design Equivalent Rotor Speed; Equivalent Weight Flow = 13.93 kg/sec (30.71 lb/sec); Hub Radial Distortion

DF 102173

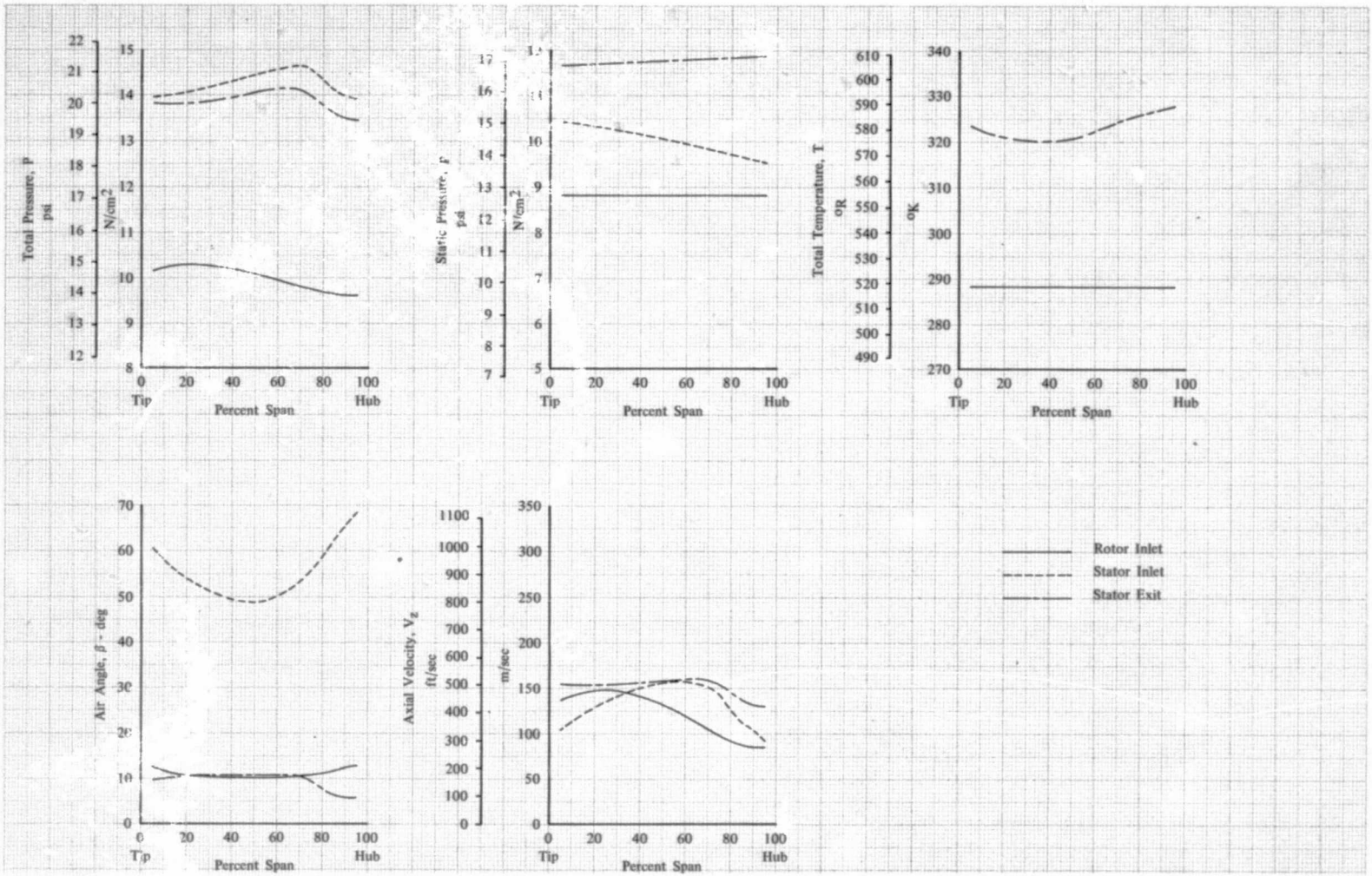


Figure 55. Total and Static Pressure, Total Temperature, Air Angle and Axial Velocity vs Span at Rotor Inlet, Stator Inlet and Stator Exit; 85% Design Equivalent Rotor Speed; Equivalent Weight Flow = 12.21 kg/sec (26.92 lb/sec); Hub Radial Distortion

DF 102174

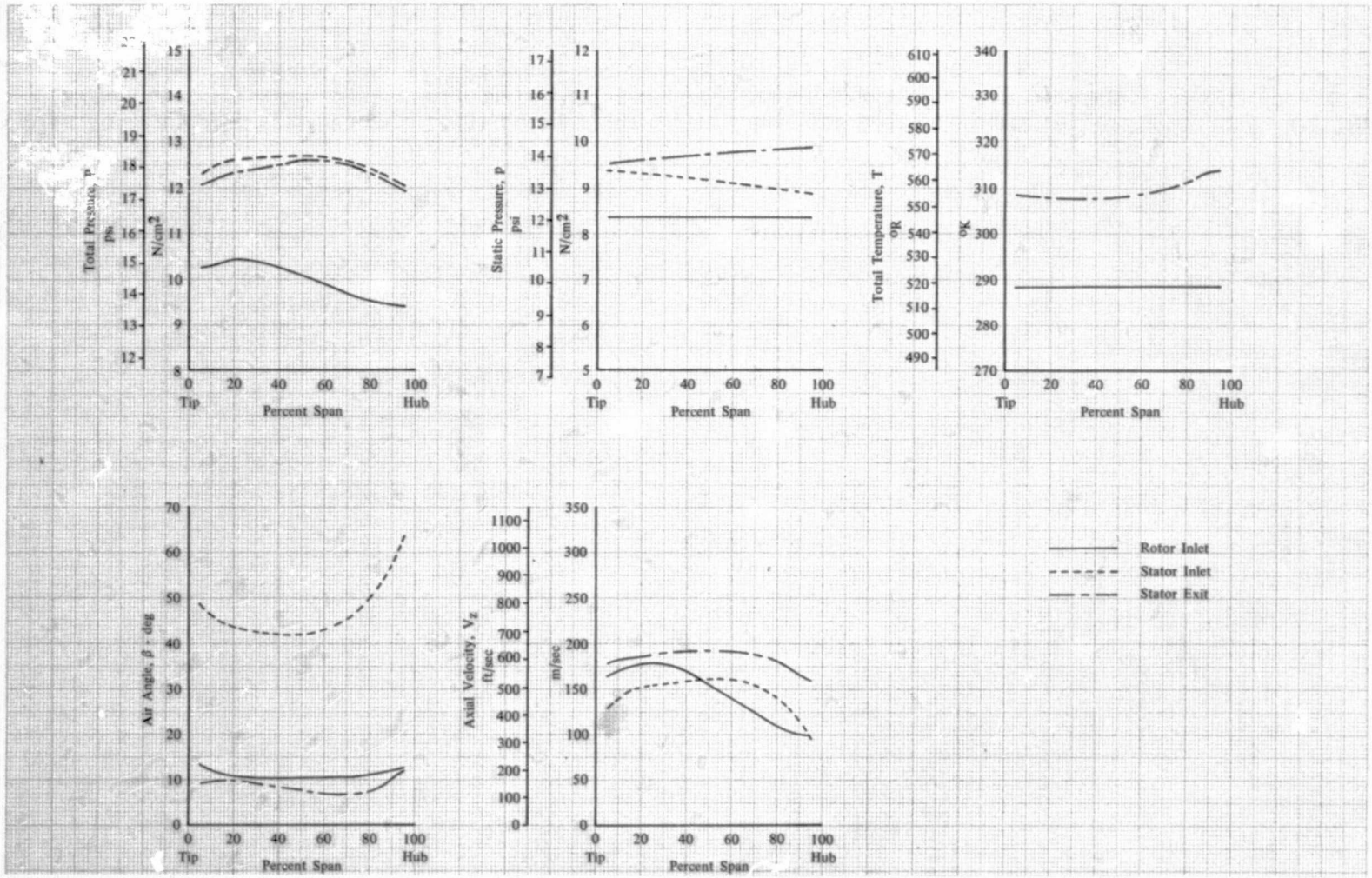


Figure 56. Total and Static Pressure, Total Temperature, Air Angle and Axial Velocity vs Span at Rotor Inlet, Stator Inlet and Stator Exit; 70% Design Equivalent Rotor Speed; Equivalent Weight Flow = 13.95 kg/sec (30.75 lb/sec); Hub Radial Distortion

DF 102175

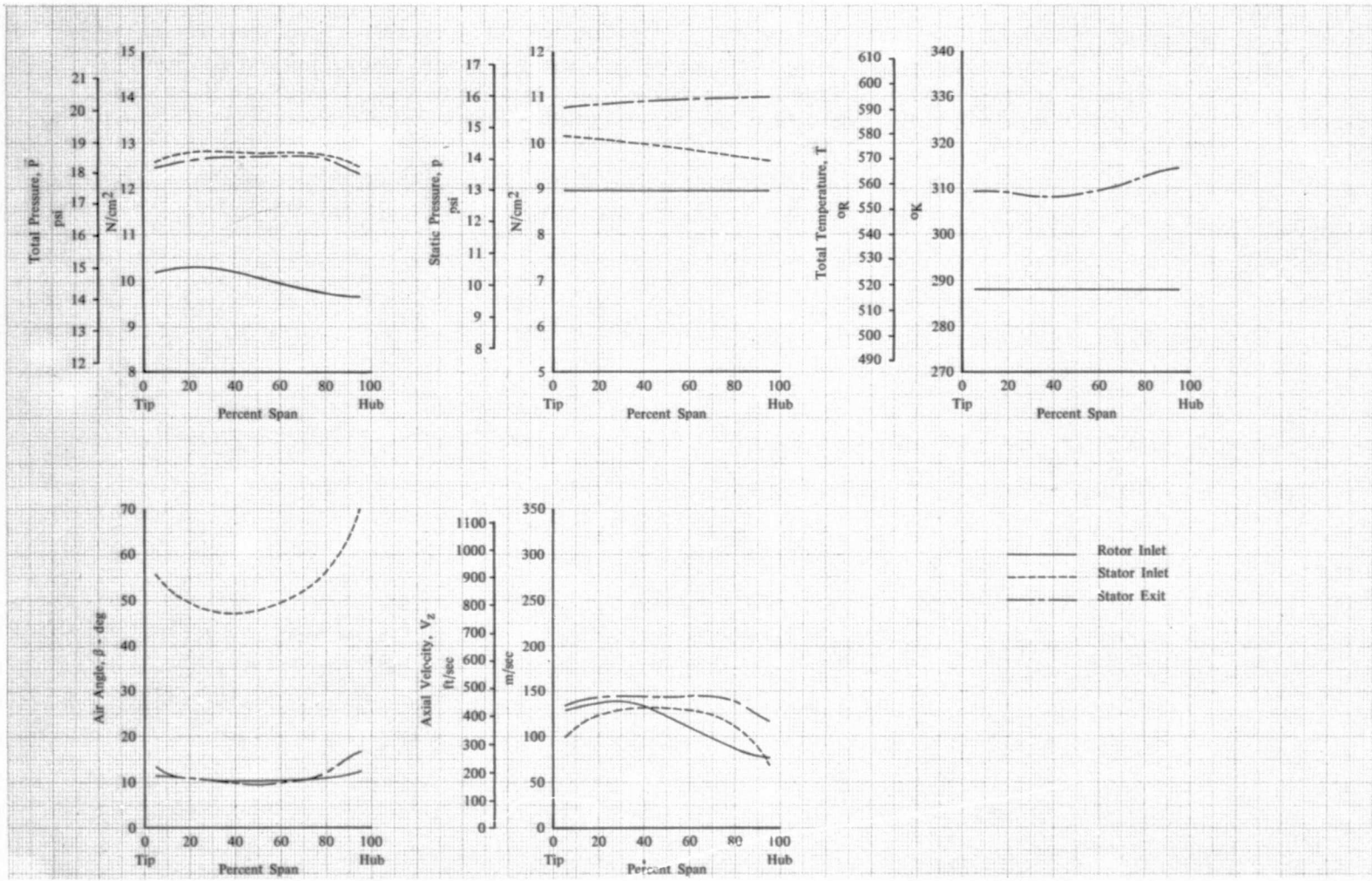


Figure 57. Total and Static Pressure, Total Temperature, Air Angle and Axial Velocity vs Span at Rotor Inlet, Stator Inlet and Stator Exit; 70% Design Equivalent Rotor Speed; Equivalent Weight Flow = 11.54 kg/sec (25.44 lb/sec); Hub Radial Distortion

DF 102176

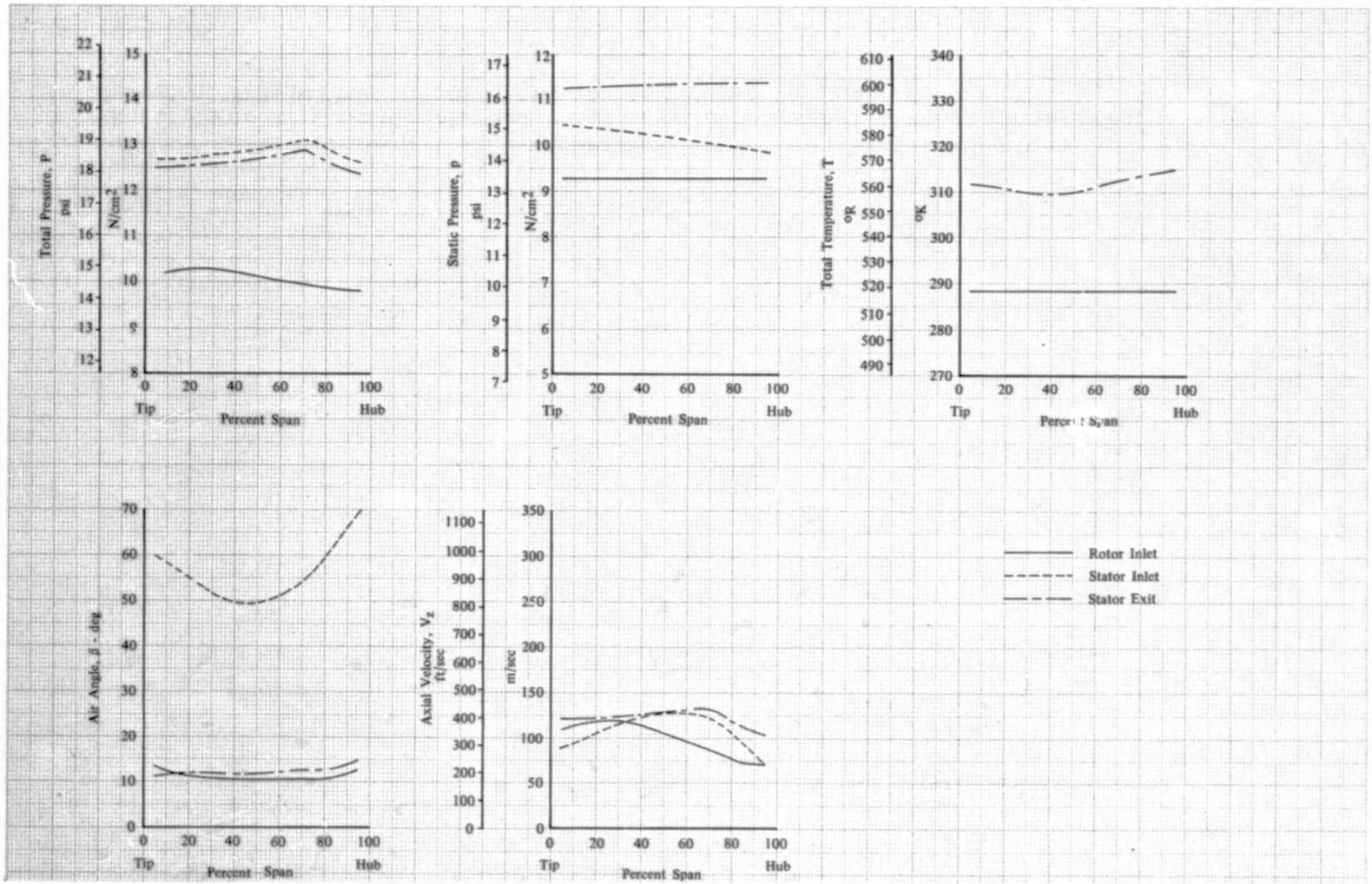


Figure 58. Total and Static Pressure, Total Temperature, Air Angle and Axial Velocity vs Span at Rotor Inlet, Stator Inlet and Stator Exit; 70% Design Equivalent Rotor Speed; Equivalent Weight Flow = 9.97 kg/sec (21.99 lb/sec); Hub Radial Distortion

DF 102177

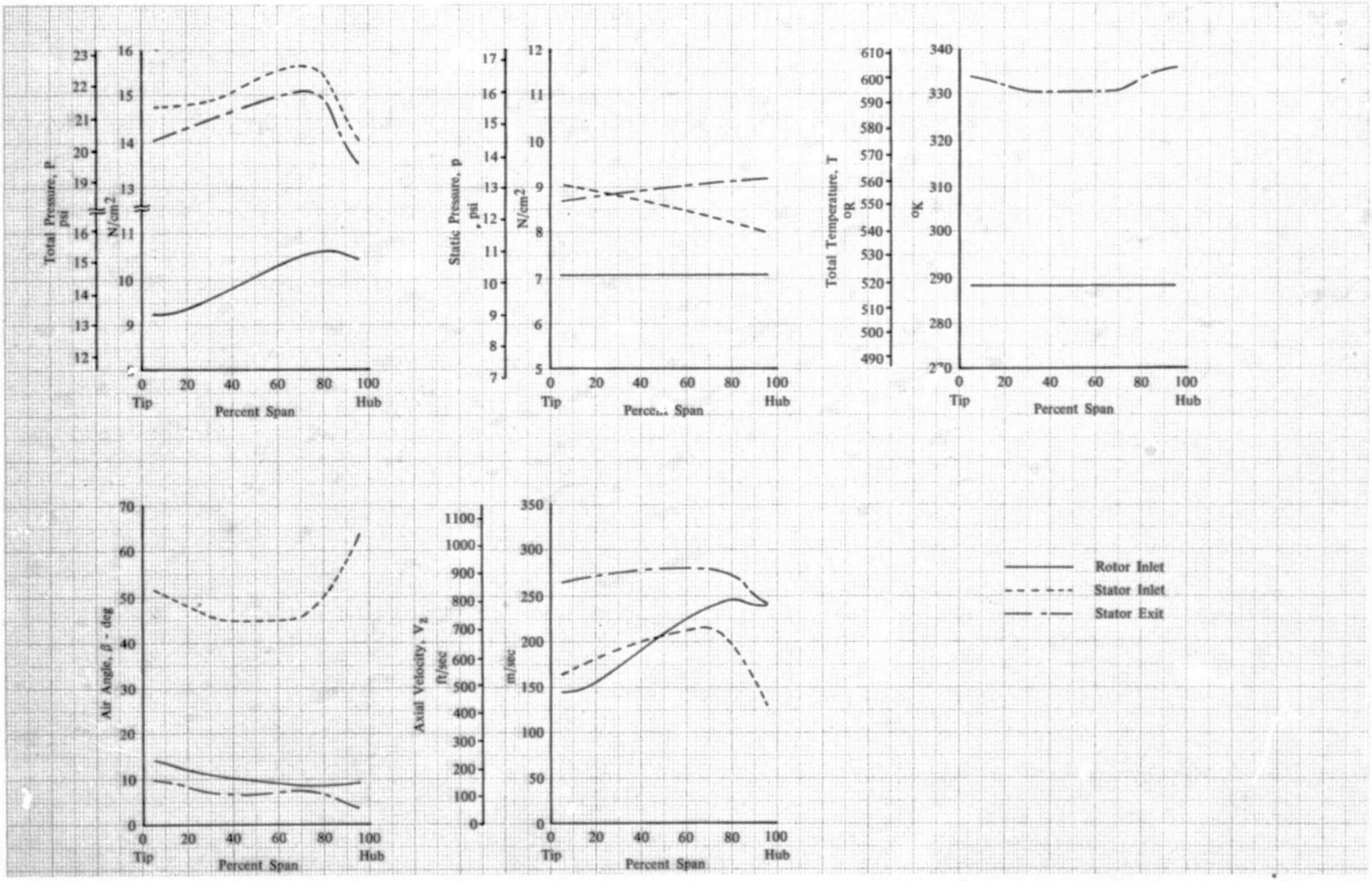


Figure 59. Total and Static Pressure, Total Temperature, Air Angle and Axial Velocity vs Span at Rotor Inlet, Stator Inlet and Stator Exit; 100% Design Equivalent Rotor Speed; Equivalent Weight Flow = 17.91 kg/sec (39.48 lb/sec); Tip Radial Distortion

DF 102178

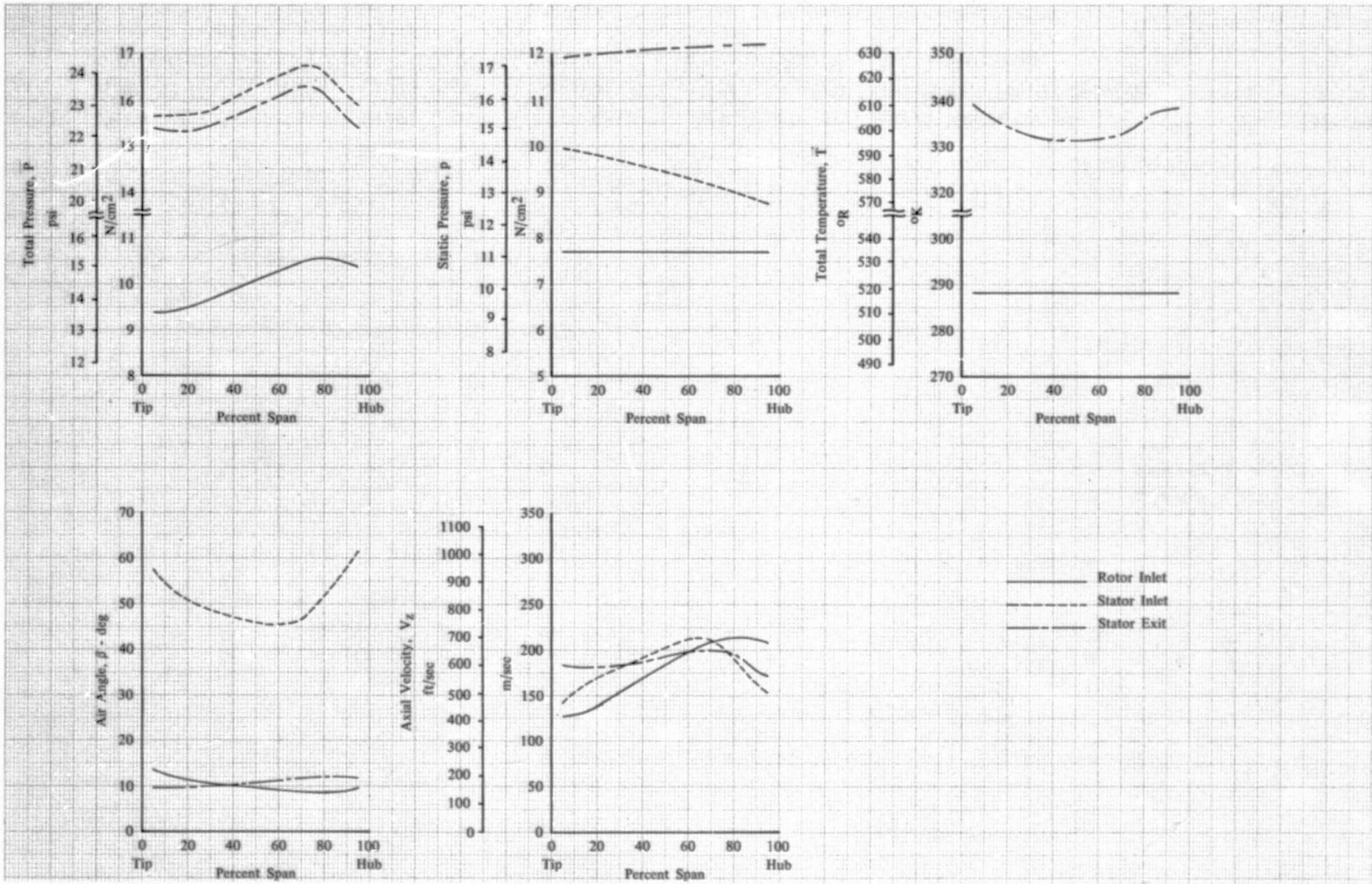


Figure 60. Total and Static Pressure, Total Temperature, Air Angle and Axial Velocity vs Span at Rotor Inlet, Stator Inlet and Stator Exit; 100% Design Equivalent Rotor Speed; Equivalent Weight Flow = 16.41 kg/sec (36.17 lb/sec); Tip Radial Distortion

DF 102179

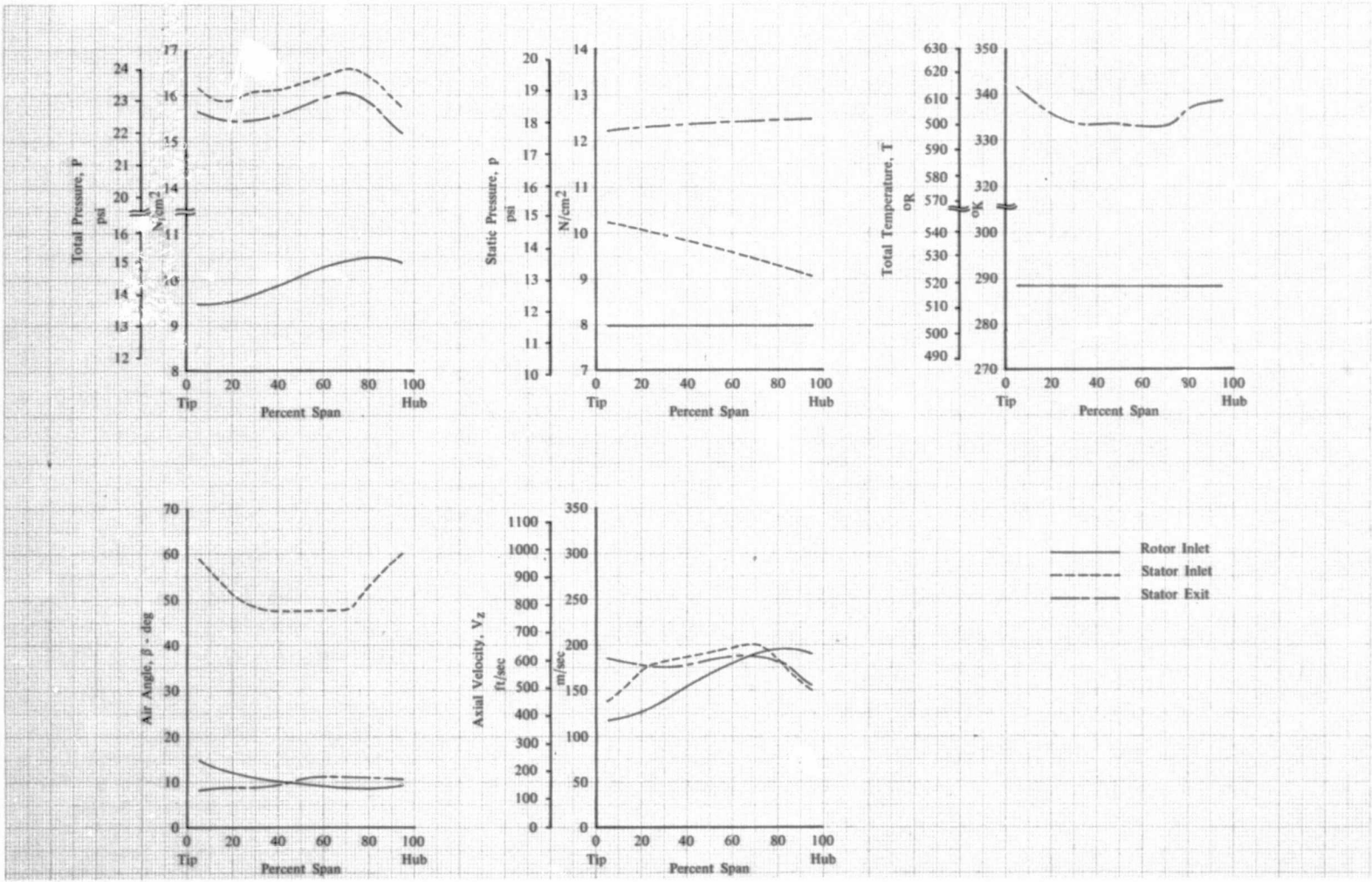


Figure 61. Total and Static Pressure, Total Temperature, Air Angle and Axial Velocity vs Span at Rotor Inlet, Stator Inlet and Stator Exit; 100% Design Equivalent Rotor Speed; Equivalent Weight Flow = 15.52 kg/sec (34.21 lb/sec); Tip Radial Distortion

DF 102180

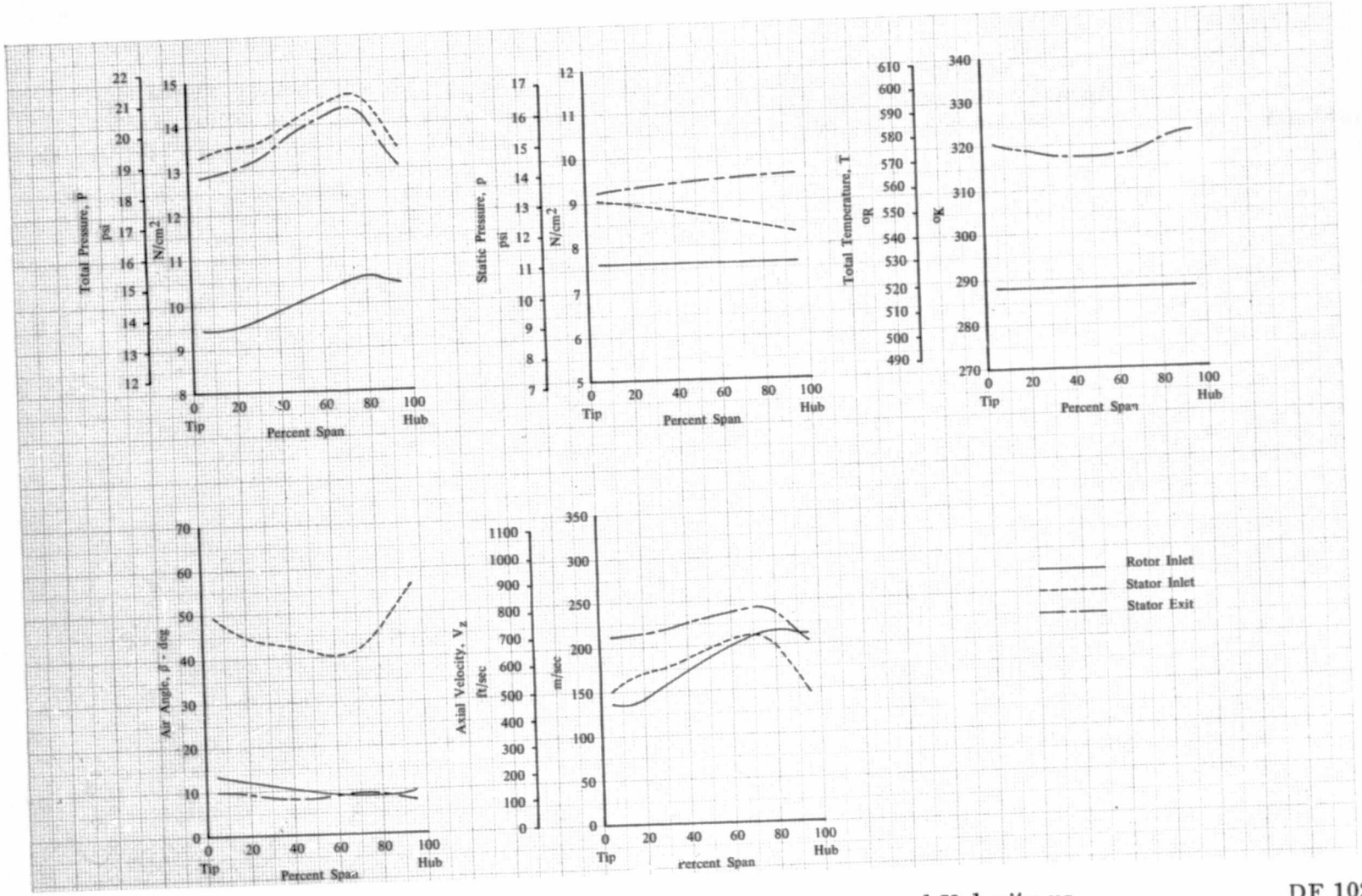


DF 102181

Figure 62. Total and Static Pressure, Total Temperature, Air Angle and Axial Velocity vs Span at Rotor Inlet, Stator Inlet and Stator Exit; 85% Design Equivalent Rotor Speed; Equivalent Weight Flow = 16.54 kg/sec (36.46 lb/sec); Tip Radial Distortion

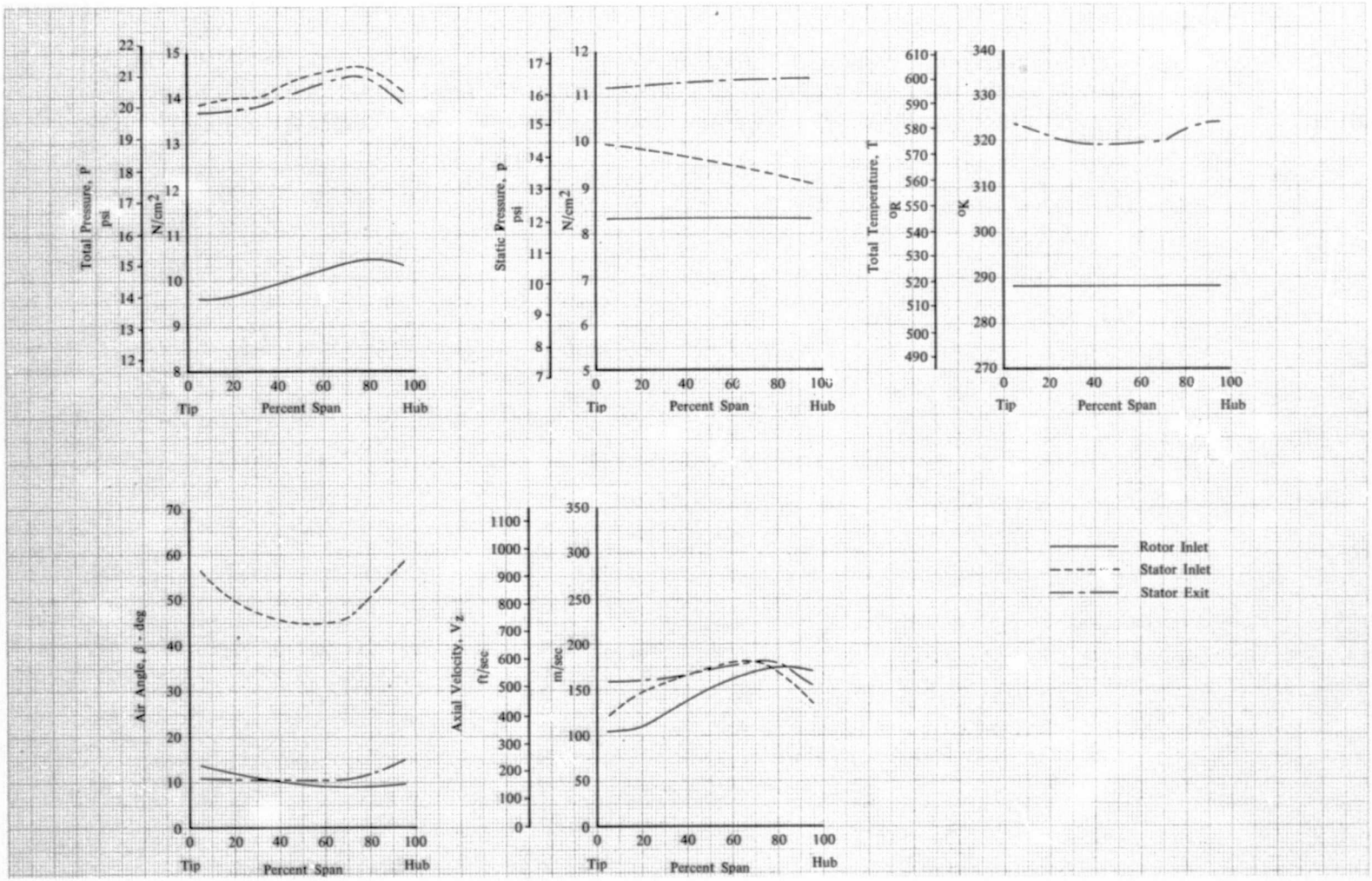


Figure 63. Total and Static Pressure, Total Temperature, Air Angle and Axial Velocity vs Span at Rotor Inlet, Stator Inlet and Stator Exit; 85% Design Equivalent Rotor Speed; Equivalent Weight Flow = 14.37 kg/sec (31.68 lb/sec); Tip Radial Distortion

DF 102182

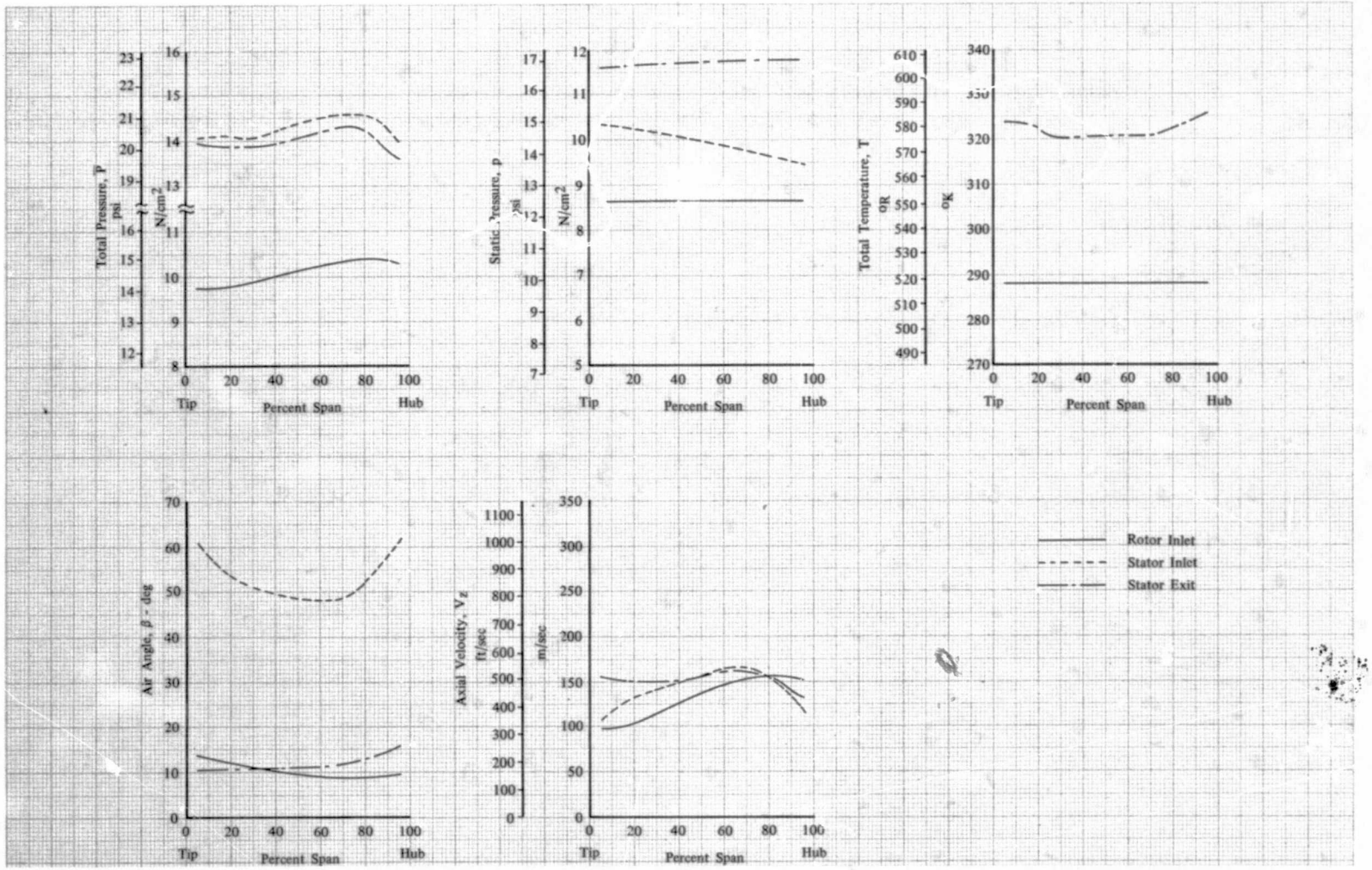


Figure 64. Total and Static Pressure, Total Temperature, Air Angle and Axial Velocity vs Span at Rotor Inlet, Stator Inlet and Stator Exit; 85% Design Equivalent Rotor Speed; Equivalent Weight Flow = 13.15 kg/sec (28.99 lb/sec); Tip Radial Distortion

DF 102183

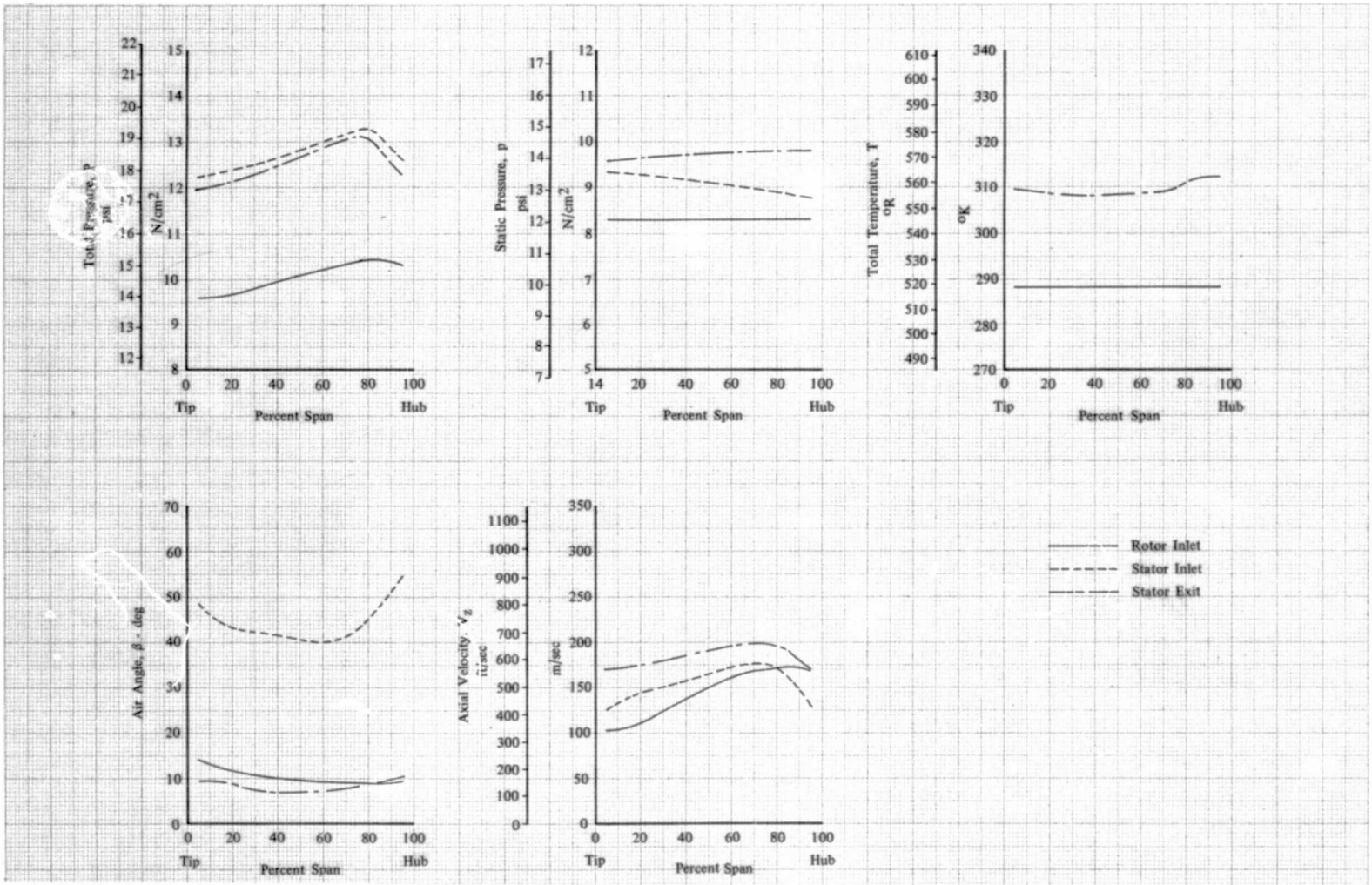


Figure 65. Total and Static Pressure, Total Temperature, Air Angle and Axial Velocity vs Span at Rotor Inlet, Stator Inlet and Stator Exit; 70% Design Equivalent Rotor Speed; Equivalent Weight Flow = 14.23 kg/sec (31.38 lb/sec); Tip Radial Distortion

DF 102184

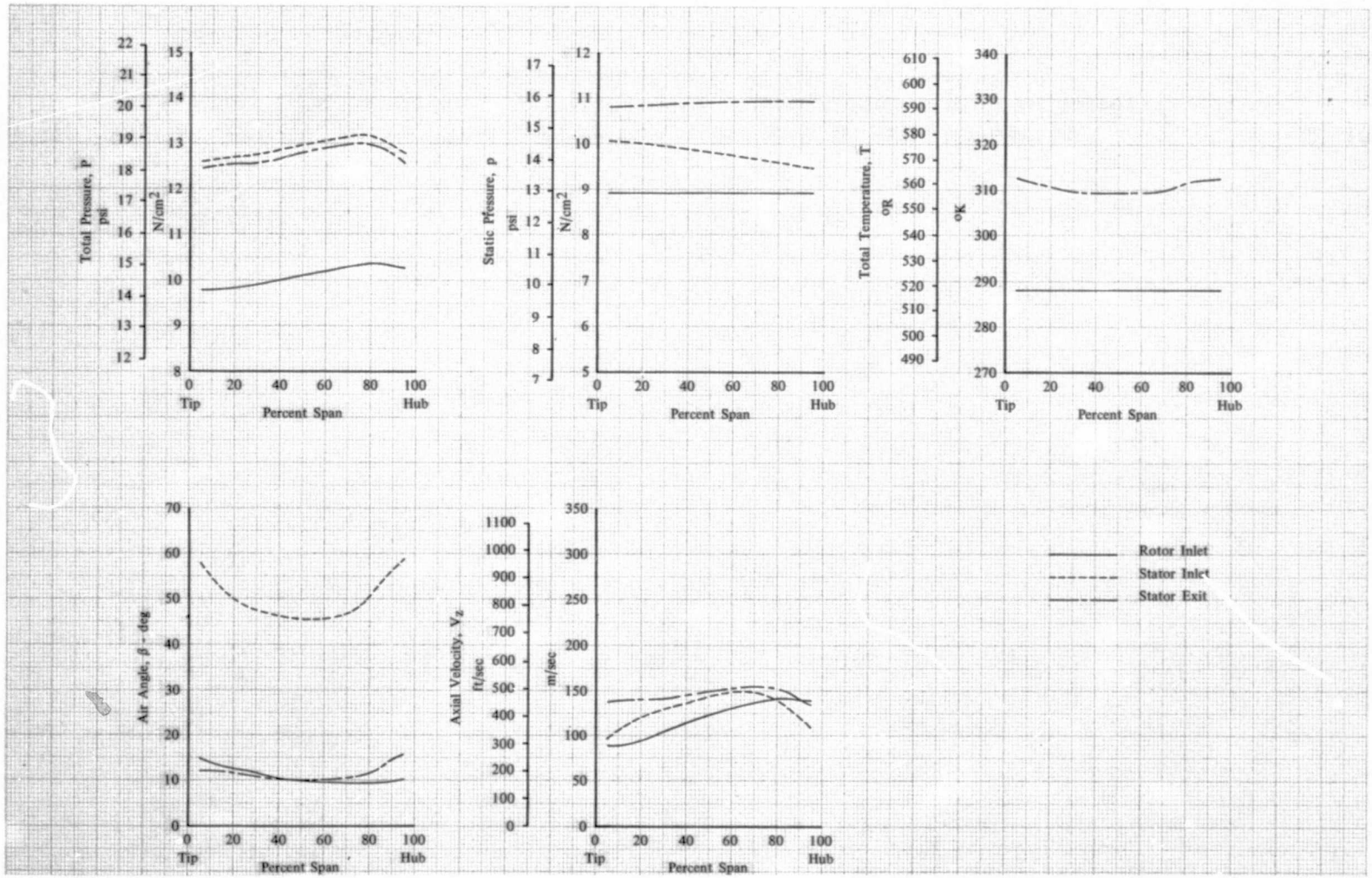


Figure 66. Total and Static Pressure, Total Temperature, Air Angle and Axial Velocity vs Span at Rotor Inlet; Stator Inlet and Stator Exit; 70% Design Equivalent Rotor Speed; Equivalent Weight Flow = 11.96 kg/sec (26.36 lb/sec); Tip Radial Distortion

DF 102185

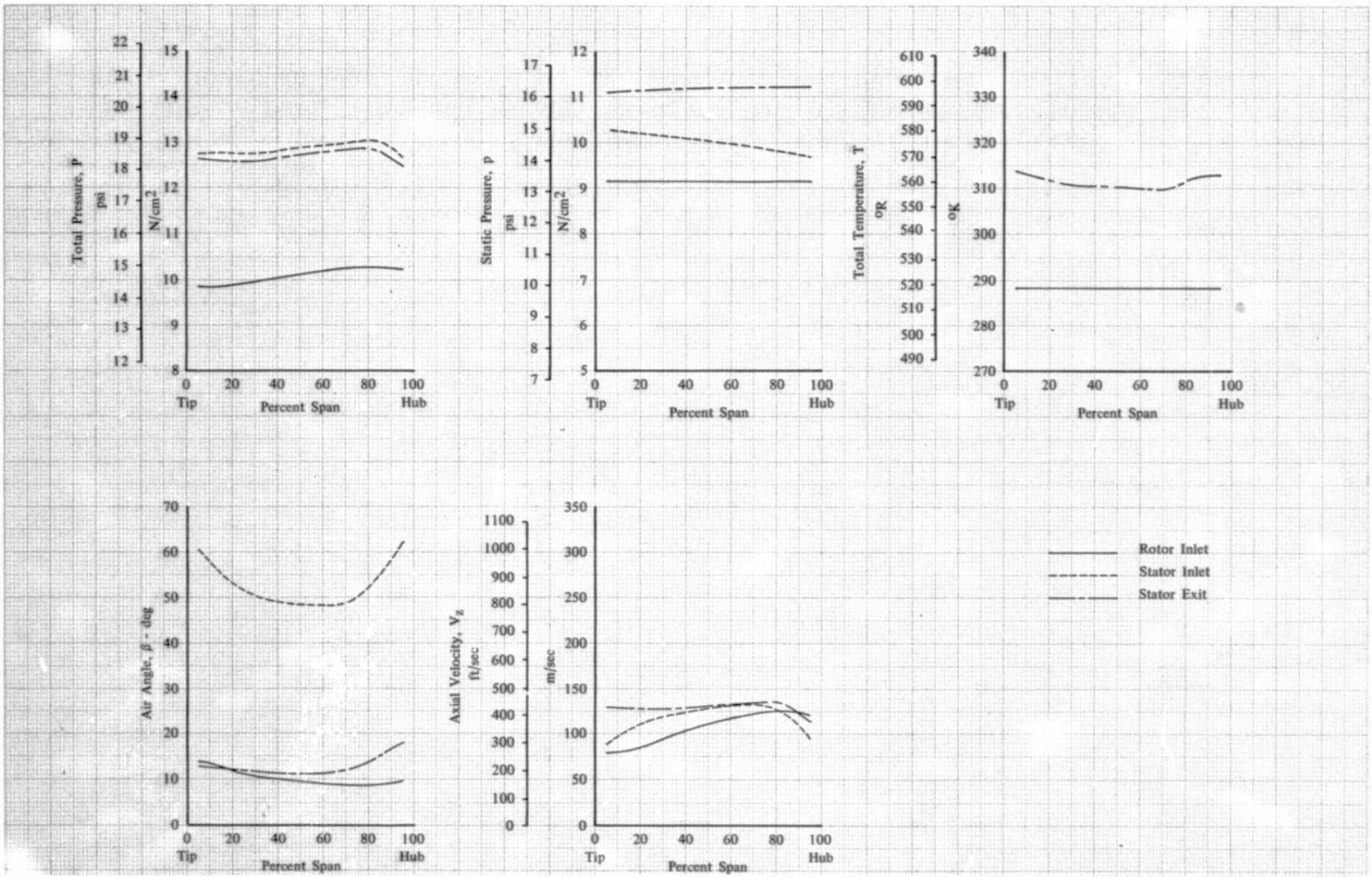


Figure 67. Total and Static Pressure, Total Temperature, Air Angle and Axial Velocity vs Span at Rotor Inlet, Stator Inlet and Stator Exit; 70% Design Equivalent Rotor Speed; Equivalent Weight Flow = 10.82 kg/sec (23.85 lb/sec); Tip Radial Distortion

DF 102186

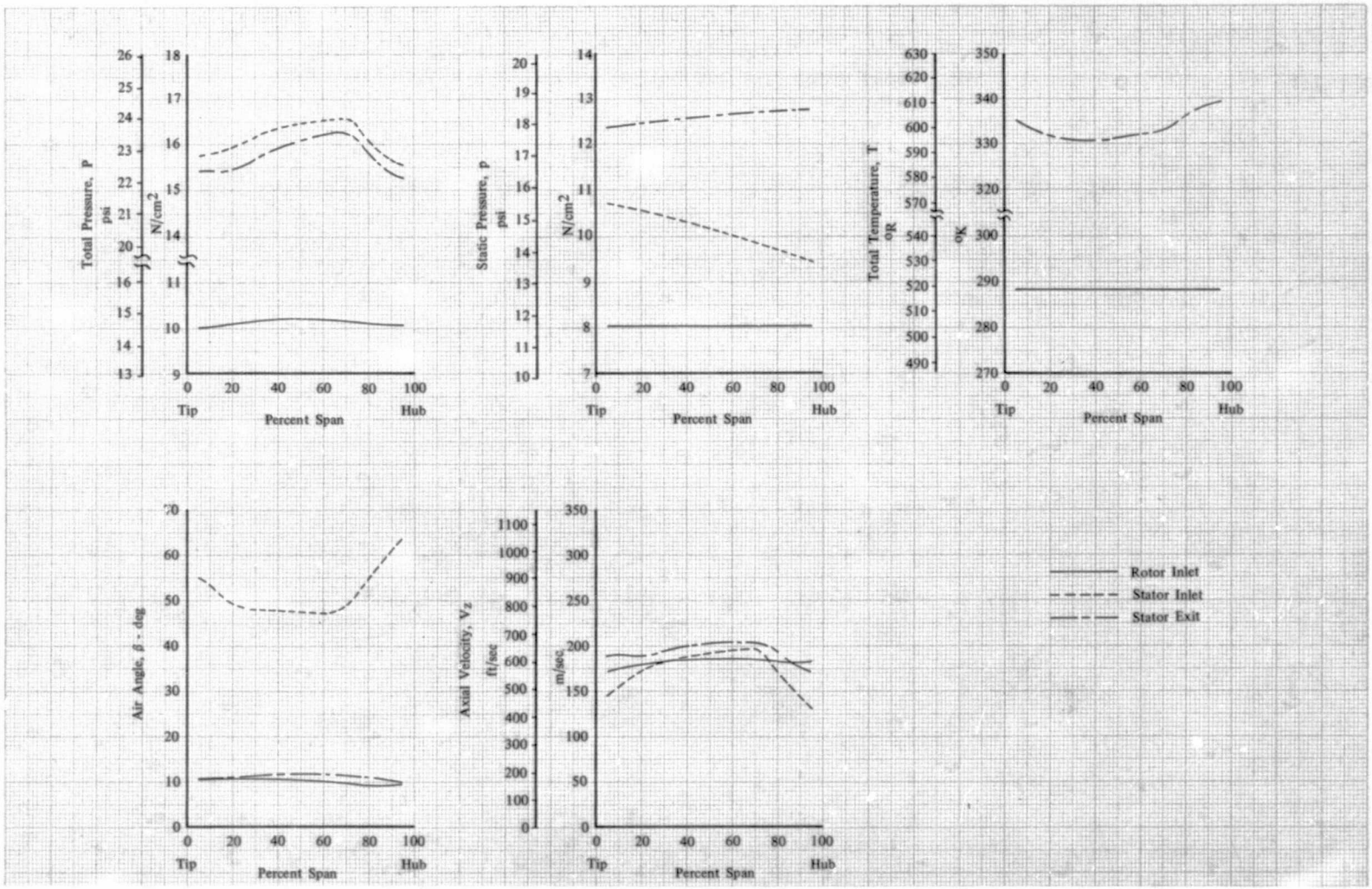


Figure 68. Total and Static Pressure, Total Temperature, Air Angle and Axial Velocity vs Span at Rotor Inlet, Stator Inlet and Stator Exit; 100% Design Equivalent Rotor Speed; Equivalent Weight Flow = 17.25 kg/sec (38.04 lb/sec); Uniform Inlet Flow

DF 102187

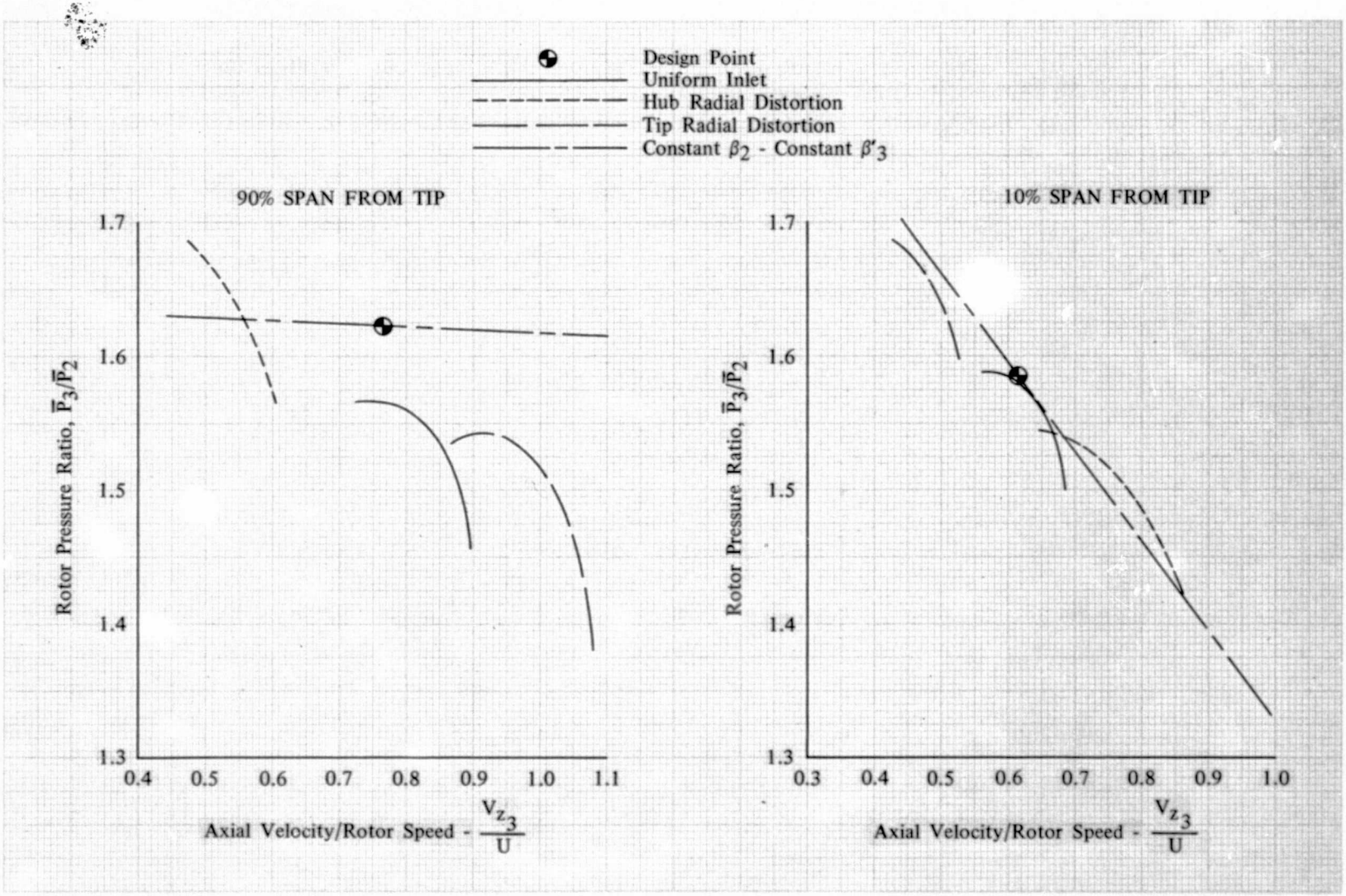


Figure 69. Rotor F Distortion Attenuation Capability at 10% and 90% Span from Tip

DF 102188

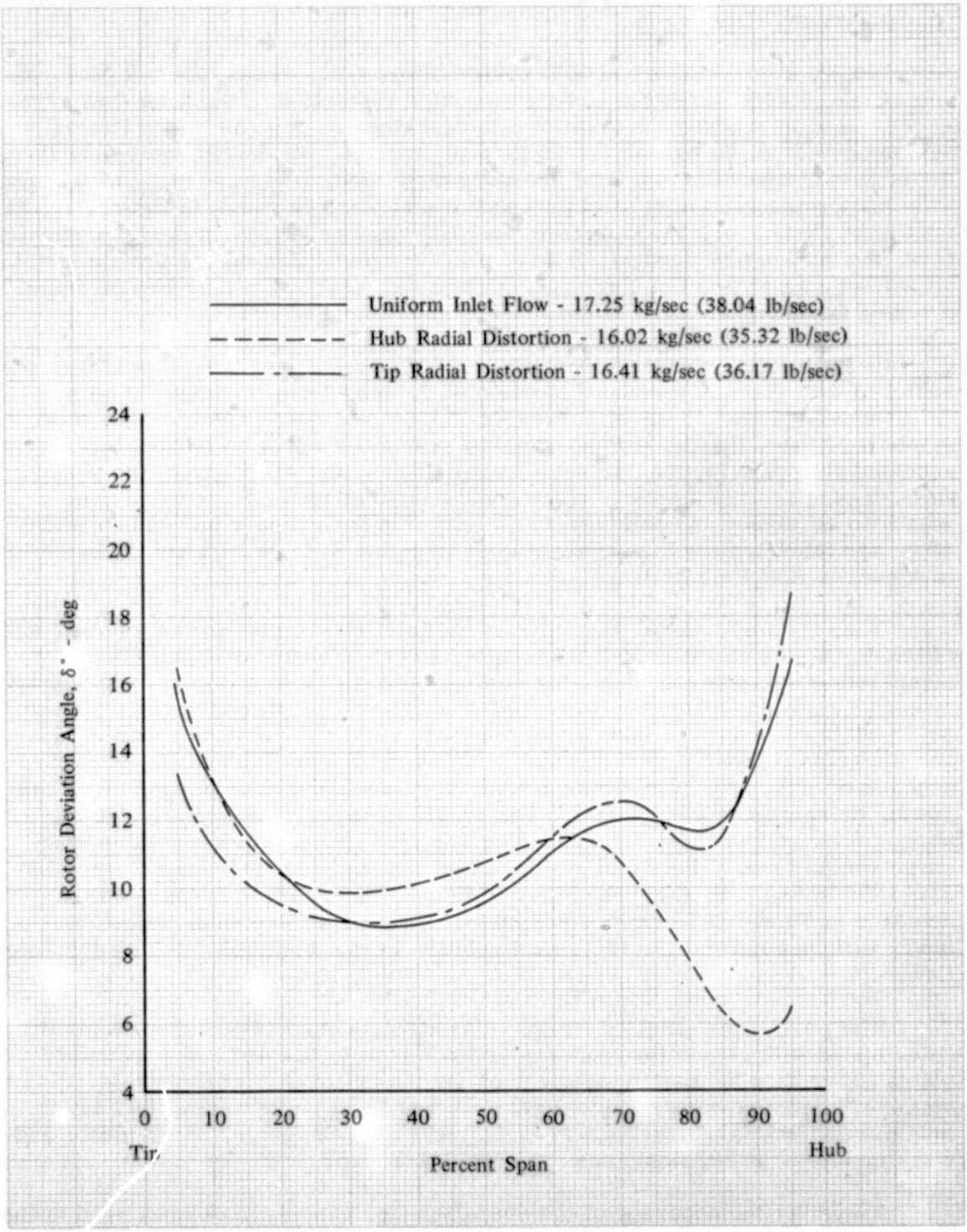


Figure 70. Rotor F Deviation vs Percent Span at Near Design Equivalent Flow with Uniform Inlet Flow and Hub and Tip Radial Distortion DF 102189

## Circumferential Distortion

Rotor, rotor-stator and IGV-rotor-stator, i.e., stage, overall performance was obtained with 180 deg arc circumferential distortion of the inlet flow. The screen used to produce the distortion is described on page 39. At a flow of approximately 16.74 kg/sec (36.90 lb/sec), i.e., 97.8% design equivalent flow, the screen produced 14.4% total pressure distortion, $(P1_{max} - P1_{min})/P1_{max}$. This inlet guide vane inlet total pressure distribution is shown in figure 71. At maximum flow, i.e., 17.93 kg/sec (39.53 lb/sec) or 104.8% of design equivalent flow, the screen produced 17.3% total pressure distortion. This profile is not shown because at that flow, pressure data were recorded at only two circumferential locations relative to the 180-deg arc distortion screen.

Overall Performance - The rotor, rotor-stator, and stage overall performance achieved with circumferential distortion of the inlet flow is compared with uniform inlet performance in figures 72, 73 and 74, respectively. The solid symbols of these figures indicate the data points for which both overall performance and flow distribution data were recorded; and the solid surge line passes through surge points determined from the transient data. Pressure ratio, adiabatic efficiency and polytropic efficiency for the rotor, rotor-stator and stage are tabulated for the steady-state data points in table XIII and repeated in Appendix B of Volume II.

With circumferential distortion of the inlet flow, rotor pressure ratio and efficiency at design equivalent rotor speed and flow were 1.586 and 89.3%, compared with 1.595 and 91.8% for uniform inlet flow. Similarly, rotor-stator pressure ratio and efficiency were 1.540 and 82.2% as compared to 1.561 and 86.7% with uniform inlet flow; stage pressure ratio and efficiency were 1.525 and 81.0% as compared to 1.560 and 86.3% with uniform inlet flow. With the addition of circumferential distortion at 70, 85 and 100% design equivalent rotor speed, there were +0.012, +0.010 and -0.015 changes, respectively, in stage surge pressure ratio and corresponding 4.4, 5.3 and 4.8% increases in stage surge weight flow. The effect of 4 to 5% increases in surge weight flow on the surge line more than offset the effect of increases in surge pressure ratio achieved at 70 and 85% design rotor speed. The surge line was, therefore, lower with circumferential distortion relative to that obtained with uniform inlet flow.

The peak rotor efficiency (figure 72) at 70, 85 and 100% design equivalent rotor speed with circumferential distortion was 1.2, 0.5 and 2.5 percentage points lower than the comparable values for the uniform inlet flow tests. Rotor-stator efficiencies (figure 73) were 3.3, 3.1 and 4.3 percentage points lower than the uniform inlet results. Peak efficiency for the rotor, rotor-stator and stage occurred at 70% design equivalent rotor speed.

To verify the accuracy of the overall performance values presented in figures 72 through 74, two calculation procedures were used. For all the test points shown, data were recorded at one screen position, but for the near-stall and mid-flow 100% design speed test points, data were recorded at five additional screen positions. The one screen position or open symbols of these figures represent an average of performance from one location within and one location outside the distorted area whereas the six-screen position or closed symbols represent an average of performance from 12 circumferential locations relative to the distortion screen. A comparison of these overall performance calculation results is presented in table XIV.

Table XIII. Overall Performance of Stage F
180 deg Arc Circumferential Distortion

| (IGV Inlet) Equivalent Weight Flow kg/sec | lb/sec | Rotor $\overline{P}_3/\overline{P}_2$ | Rotor $\eta_{ad}$ | Rotor $\eta_p$ | Rotor-Stator $\overline{P}_4/\overline{P}_2$ | Rotor-Stator $\eta_{ad}$ | Rotor-Stator $\eta_p$ | IGV-Rotor-Stator $\overline{P}_4/\overline{P}_1$ | IGV-Rotor-Stator $\eta_{ad}$ | IGV-Rotor-Stator $\eta_p$ |
|---|---|---|---|---|---|---|---|---|---|---|
| | | | | 100% Design Equivalent Rotor Speed | | | | | | |
| 17.93 | 39.53 | 1.527 | 0.855 | 0.863 | 1.450 | 0.744 | 0.757 | 1.443 | 0.734 | 0.747 |
| 17.40 | 38.36 | 1.570 | 0.884 | 0.891 | 1.522 | 0.814 | 0.825 | 1.515 | 0.805 | 0.816 |
| *16.74 | 36.90 | 1.592 | 0.890 | 0.897 | 1.540 | 0.821 | 0.832 | 1.531 | 0.809 | 0.820 |
| 16.27 | 35.88 | 1.597 | 0.875 | 0.883 | 1.545 | 0.809 | 0.820 | 1.538 | 0.800 | 0.812 |
| *15.81 | 34.85 | 1.585 | 0.868 | 0.876 | 1.532 | 0.799 | 0.811 | 1.526 | 0.792 | 0.804 |
| | | | | 85% Design Equivalent Rotor Speed | | | | | | |
| 16.25 | 35.81 | 1.401 | 0.933 | 0.936 | 1.353 | 0.831 | 0.838 | 1.348 | 0.820 | 0.827 |
| 14.38 | 31.70 | 1.420 | 0.919 | 0.923 | 1.383 | 0.847 | 0.854 | 1.380 | 0.839 | 0.846 |
| 13.57 | 29.91 | 1.415 | 0.884 | 0.889 | 1.384 | 0.826 | 0.833 | 1.380 | 0.818 | 0.826 |
| | | | | 70% Design Equivalent Rotor Speed | | | | | | |
| 13.84 | 30.51 | 1.264 | 0.944 | 0.946 | 1.240 | 0.864 | 0.868 | 1.237 | 0.852 | 0.856 |
| 11.70 | 25.80 | 1.265 | 0.907 | 0.910 | 1.246 | 0.853 | 0.857 | 1.244 | 0.846 | 0.850 |
| 10.82 | 23.86 | 1.269 | 0.877 | 0.881 | 1.251 | 0.823 | 0.828 | 1.250 | 0.819 | 0.825 |

*Data taken at multiple screen positions

Table XIV. Single vs Multiple Screen Position Performance Calculations at Design Rotor Speed

| Test Point Description | Parameter | Rotor | | Rotor-Stator | | Stage | |
|---|---|---|---|---|---|---|---|
| | | Single | Multiple | Single | Multiple | Single | Multiple |
| Near-Stall Flow | PR | 1.601 | 1.585 | 1.548 | 1.532 | 1.540 | 1.526 |
| 15.81 kg/sec | $\eta_{ad}$ % | 86.7 | 86.8 | 80.1 | 79.9 | 79.1 | 79.2 |
| (34.85 lb/sec) | $\eta_p$ % | 87.6 | 87.6 | 81.3 | 81.1 | 80.3 | 80.4 |
| Mid-Point Flow | PR | 1.594 | 1.592 | 1.540 | 1.540 | 1.532 | 1.531 |
| 16.74 kg/sec | $\eta_{ad}$ % | 90.2 | 89.0 | 82.9 | 82.1 | 81.9 | 80.9 |
| (36.90 lb/sec) | $\eta_p$ % | 90.8 | 89.7 | 84.0 | 83.2 | 82.9 | 82.0 |

As shown, the larger sample resulted in 0.016 and 0.002 losses in design speed rotor pressure ratio at near stall and mid-point flowrates. Corresponding efficiency changes were +0.1 and -1.2 percentage points. The values calculated for the rotor-stator at design speed using the larger data sample resulted in 0.01 and 0.0 losses in pressure ratio and 0.2 and 0.8% losses in efficiency for the near-stall and mid-point flowrates. No other multiple screen position data were recorded and consequently no part speed performance comparisons were made. This comparison of the two calculation procedures indicates fair agreement; however, additional data samples should be obtained if more accurate assessment of the performance with circumferential distortion is desired.

Flow Distribution Data - Tables B-11 and B-12 of Appendix B, Volume II presents flow distribution data at the instrumentation stations at 5, 10, 15, 30, 50, 70, 85, 90 and 95% span from the tip for circumferential increments of 30 deg around the compressor annulus. Circumferential distributions of total pressure, static pressure, total temperature, air angle and axial velocity at the rotor inlet and stator exit instrumentation stations at 10, 30, 50, 70 and 90% span from the tip are presented in figures 75 and 76 for the mid-flow and near-surge flow test points recorded at design rotor speed. A design streamline circumferential flow shift was assumed for the distorted area as it passed through the compressor and has been accounted for in the flow distribution data. The streamline position, noted at the top of each data sheet in tables B-11 and B-12 in Appendix B, Volume II, is the streamline location relative to the centerline of the local undistorted region at each instrumentation station. For the purpose of data presentation the center of the undistorted region corresponds to the 0/360 deg location on the circumferential plots of figures 75 and 76.

A comparison of the circumferential distribution of figures 75 and 76 design speed mid-flow and near-stall flow total pressure at the rotor inlet with the corresponding values at the stage exit, indicates fair attenuation of the inlet distortion by the hub and tip sections of the compressor, i.e., $(P_{max} - P_{min})/P_{max}$ decreased from approximately 0.14 to 0.04 and 0.07 at 10 and 90% span from the tip, whereas at mid-span, the decrease was from 0.14 to 0.11. A similar comparison indicates no attenuation of axial velocity at any span.

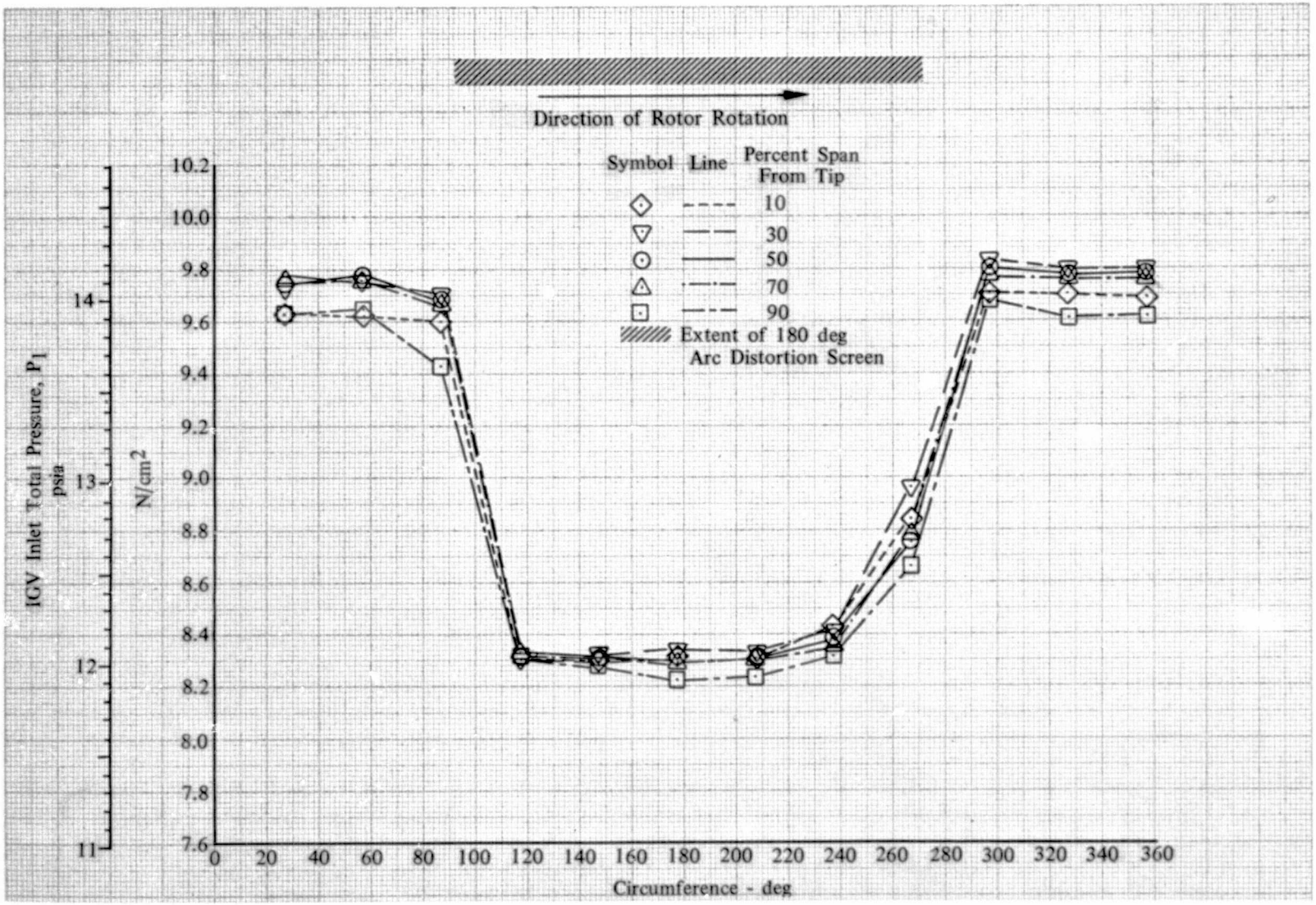


Figure 71. Inlet Guide Vane Inlet Total Pressure Distribution with 180 deg Arc Circumferential Distortion at Design Equivalent Rotor Speed; Equivalent Weight Flow = 16.74 kg/sec (36.90 lb/sec)

DF 102190

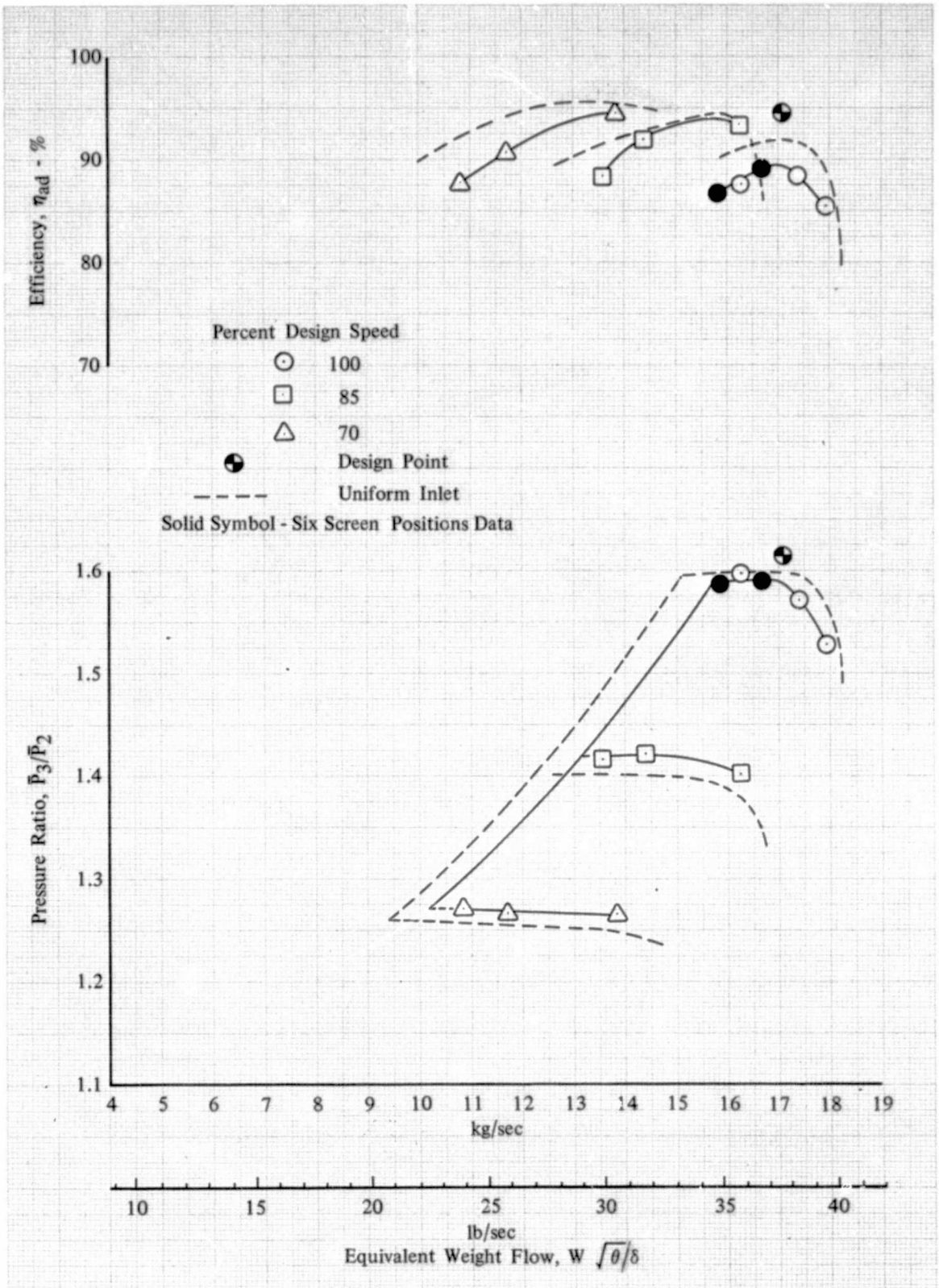


Figure 72. Overall Performance of Rotor F with Circumferential Distortion DF 102191

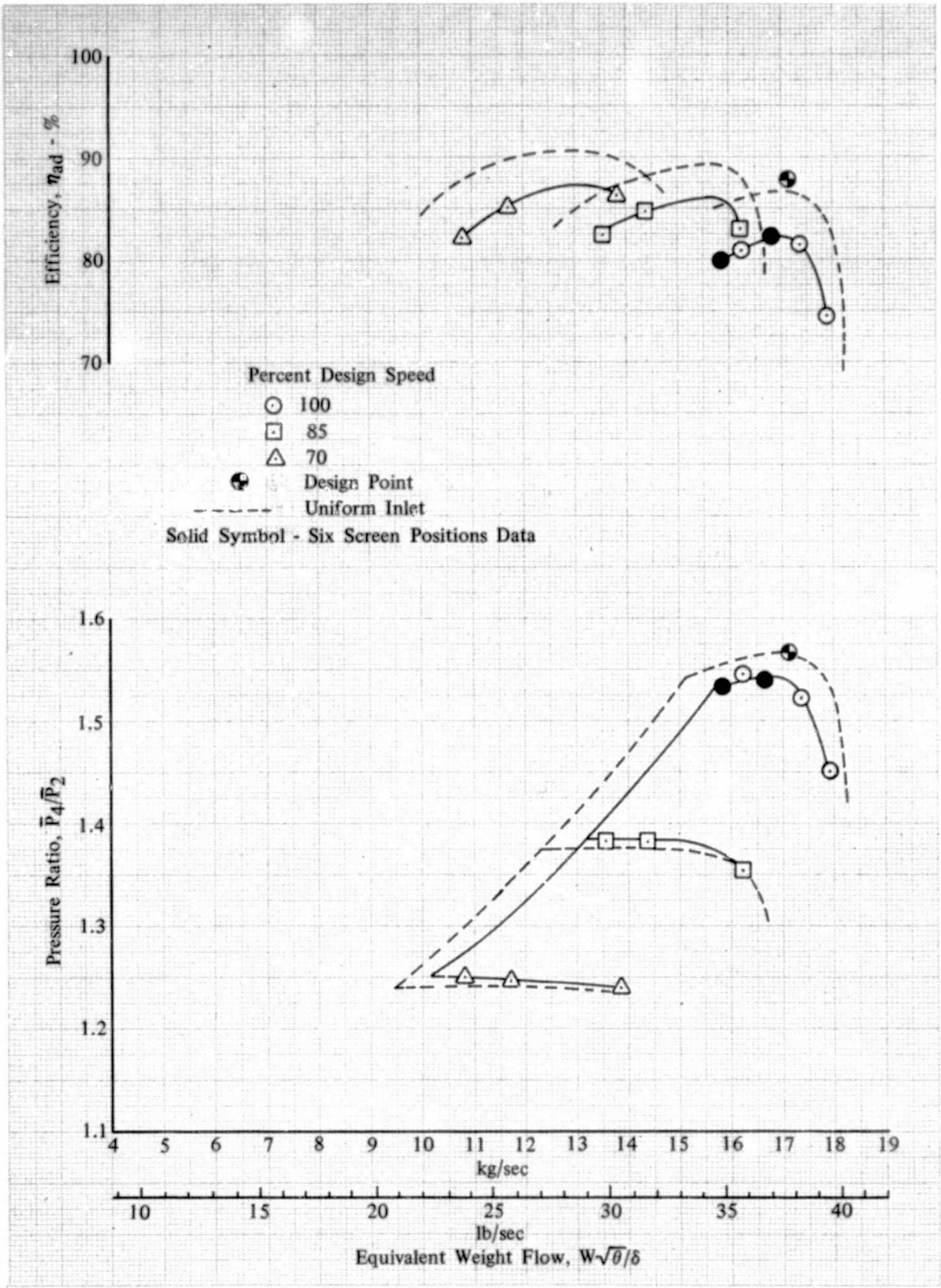


Figure 73. Overall Performance of Rotor F-Stator F with Circumferential Distortion DF 102192

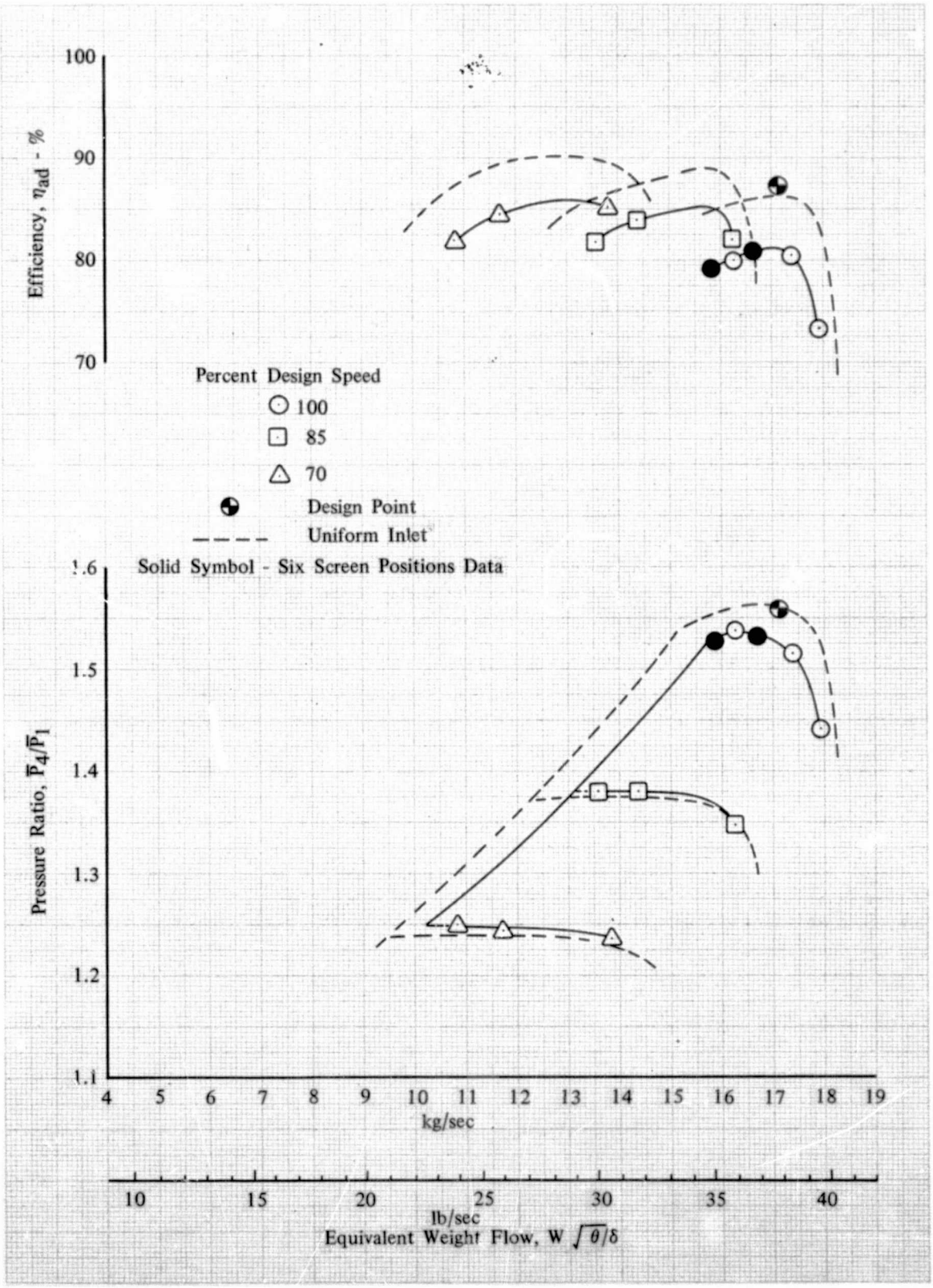


Figure 74. Overall Performance of Stage F with Circumferential Distortion DF 102193

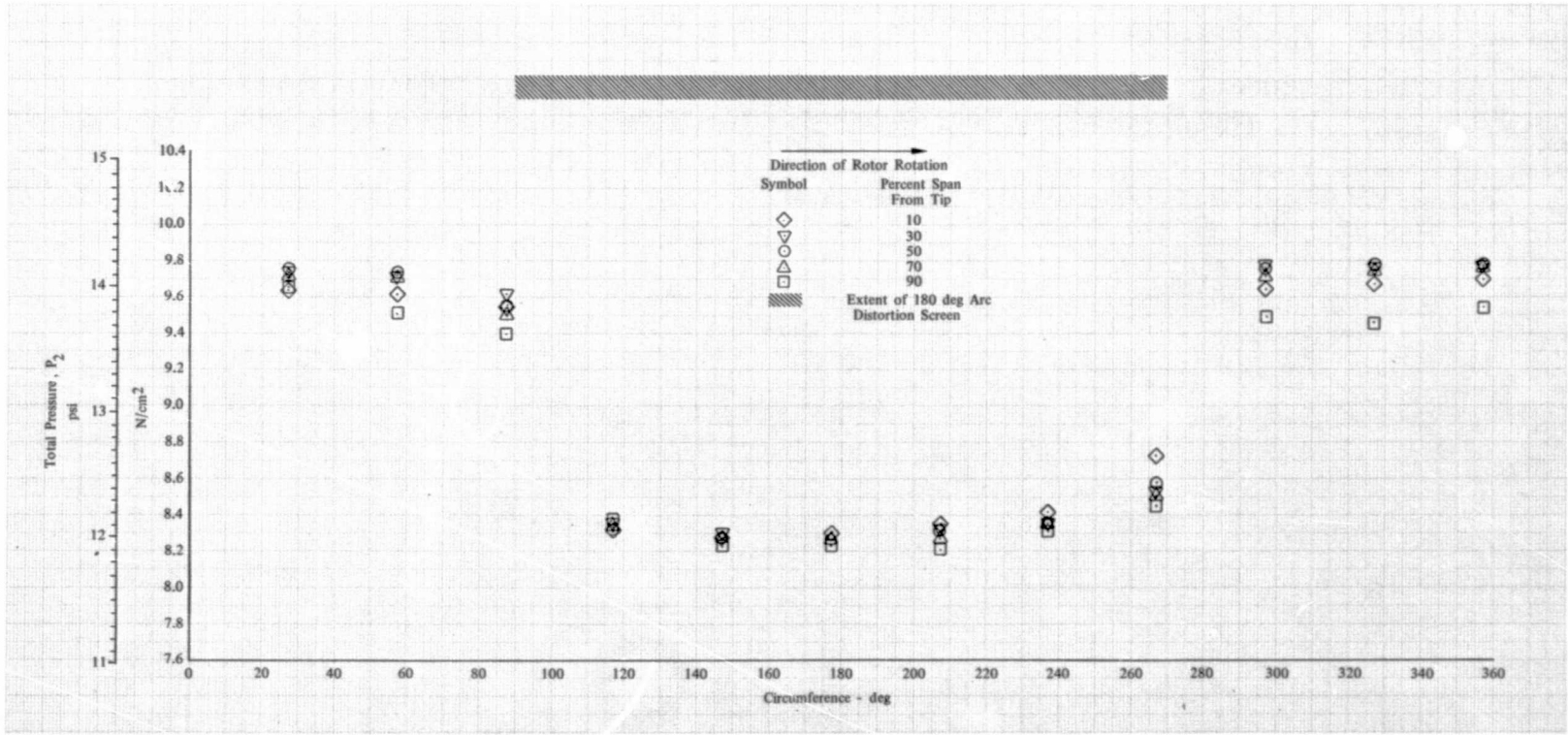


Figure 75a. Rotor Inlet Total Pressure vs Circumferential Location; 100% Design Equivalent Rotor Speed; Equivalent Weight Flow = 16.74 kg/sec (36.90 lb/sec); Circumferential Distortion

DF 102194

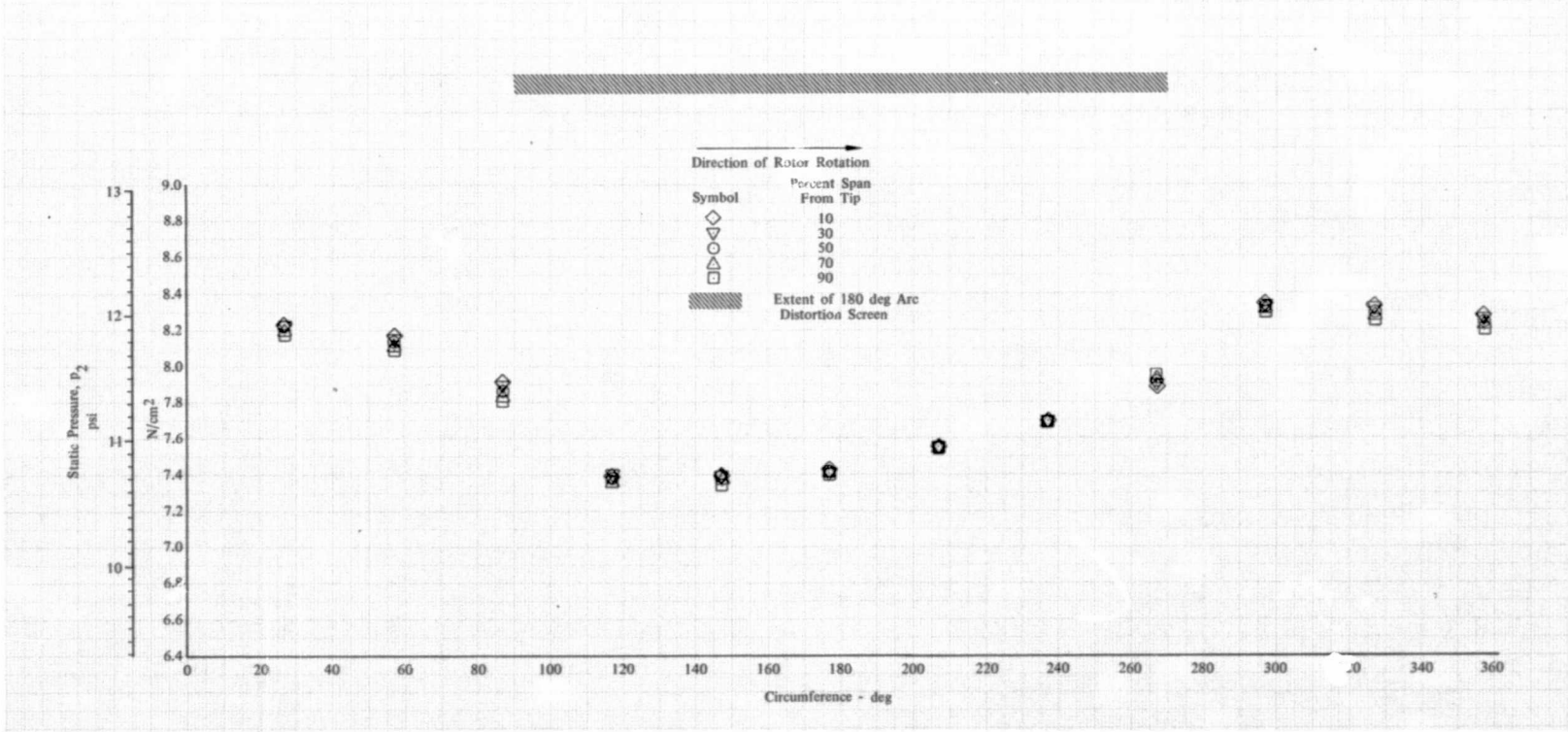


Figure 75b. Rotor Inlet Static Pressure vs Circumferential Location; 100% Design Equivalent Rotor Speed; Equivalent Weight Flow = 16.74 kg/sec (36.90 lb/sec); Circumferential Distortion

DF 102195

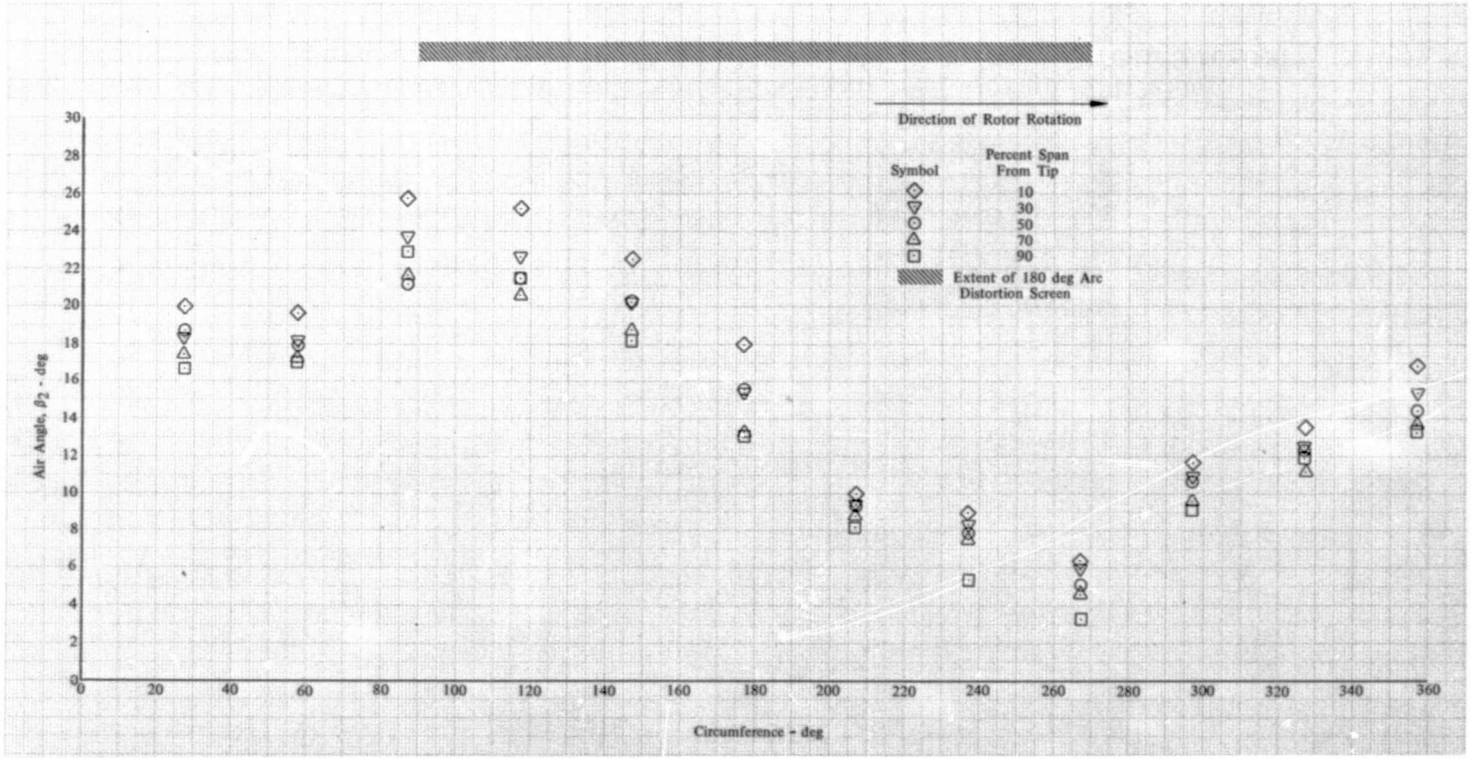


Figure 75c. Rotor Inlet Air Angle vs Circumferential Location; 100% Design Equivalent Rotor Speed; Equivalent Weight Flow = 16.74 kg/sec (36.90 lb/sec); Circumferential Distortion

DF 102196

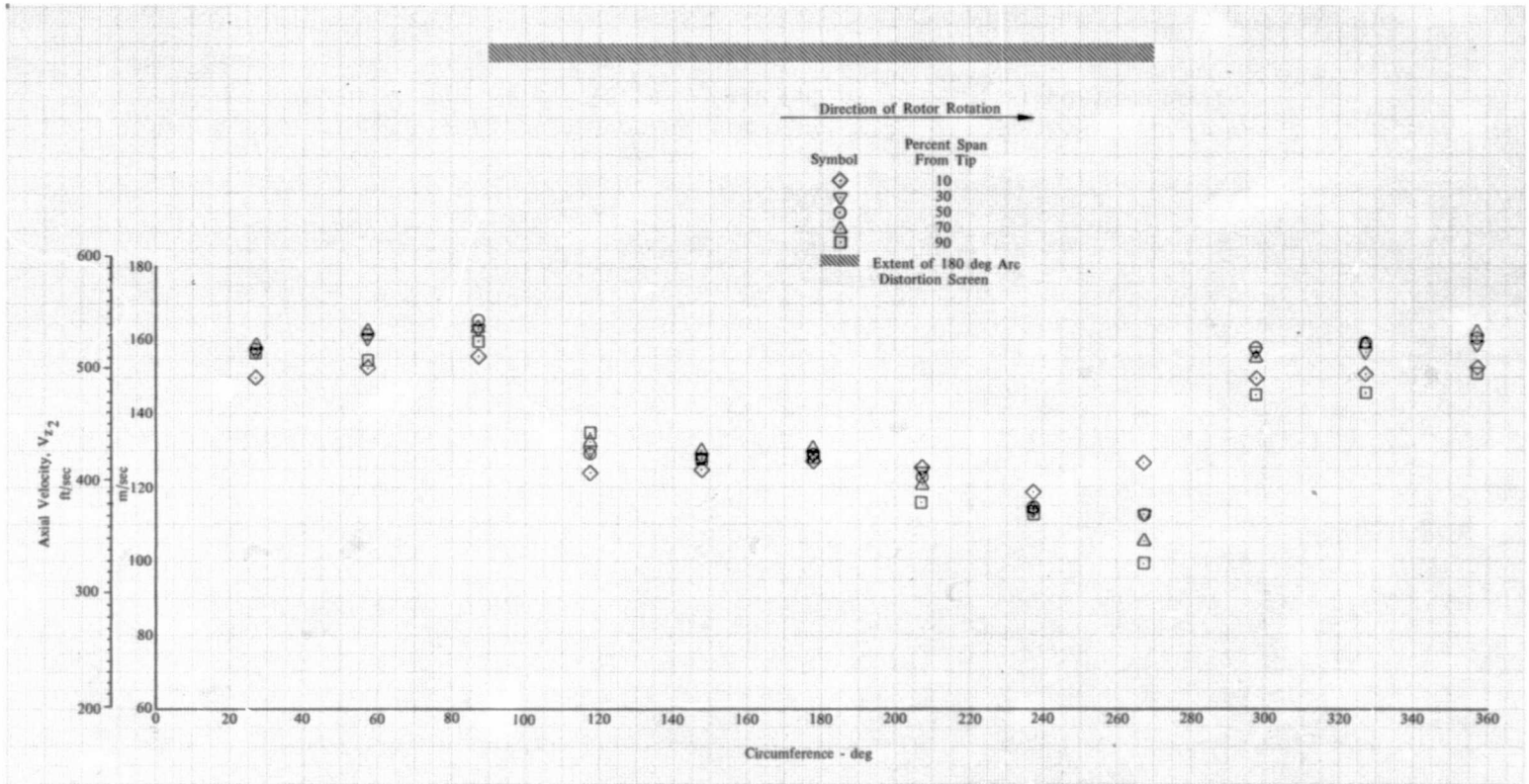


Figure 75d. Rotor Inlet Axial Velocity vs Circumferential Location; 100% Design Equivalent Rotor Speed; Equivalent Weight Flow = 16.74 kg/sec (36.90 lb/sec); Circumferential Distortion

DF 102197

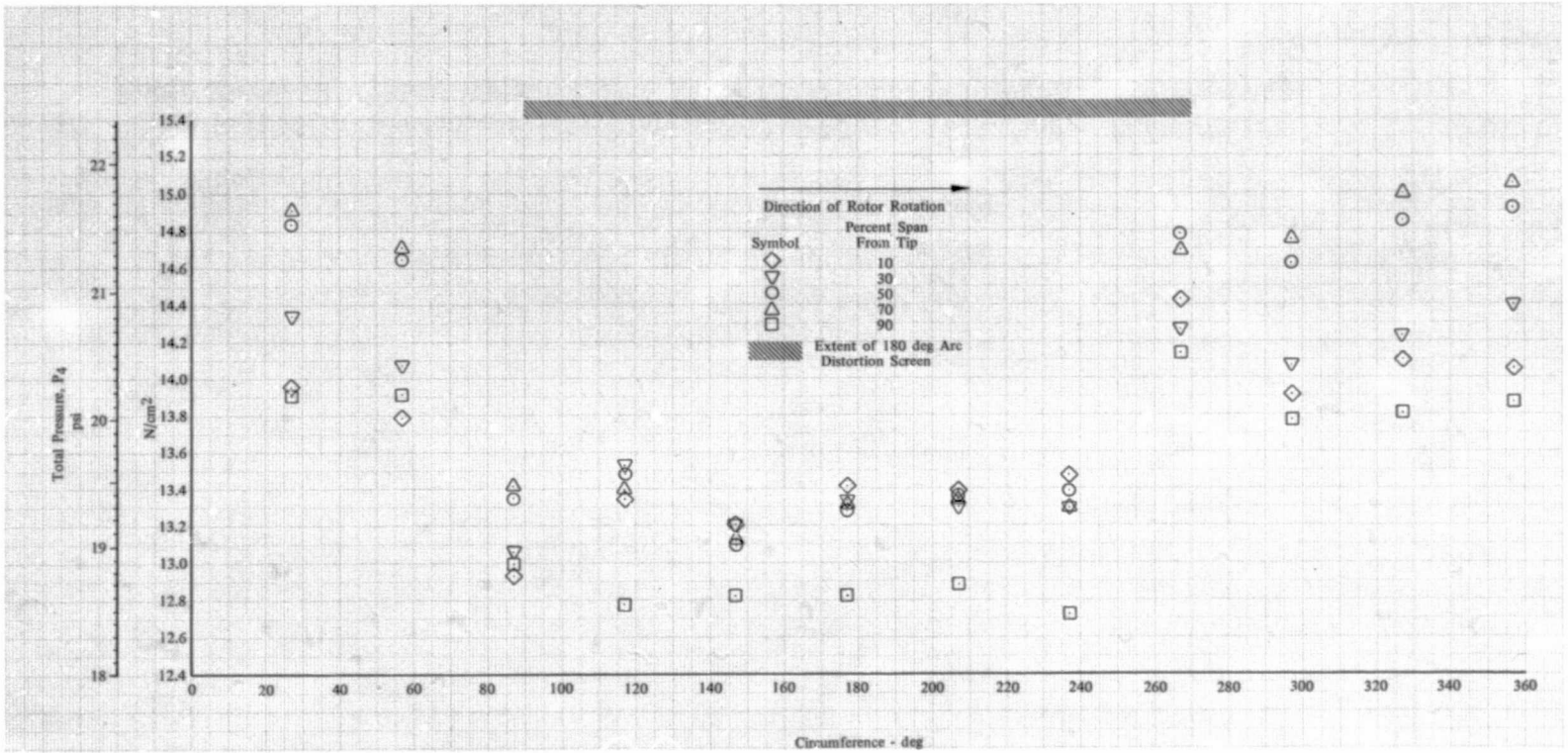


Figure 75e. Stator Exit Total Pressure vs Circumferential Location; 100% Design Equivalent Rotor Speed; Equivalent Weight Flow = 16.74 kg/sec (36.90 lb/sec); Circumferential Distortion

DF 102198

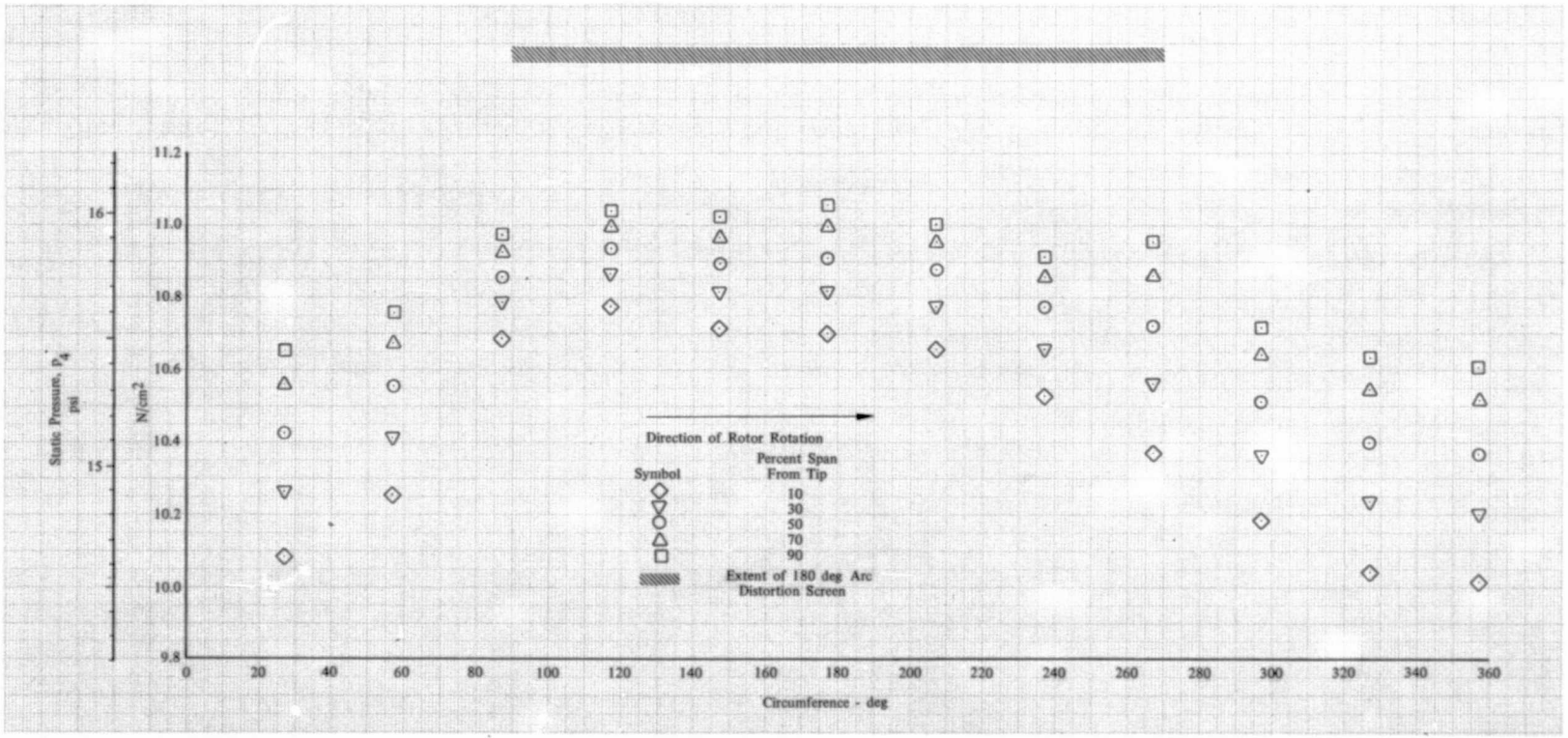


Figure 75f. Stator Exit Static Pressure vs Circumferential Location; 100% Design Equivalent Rotor Speed; Equivalent Weight Flow = 16.74 kg/sec (36.90 lb/sec); Circumferential Distortion

DF 102199

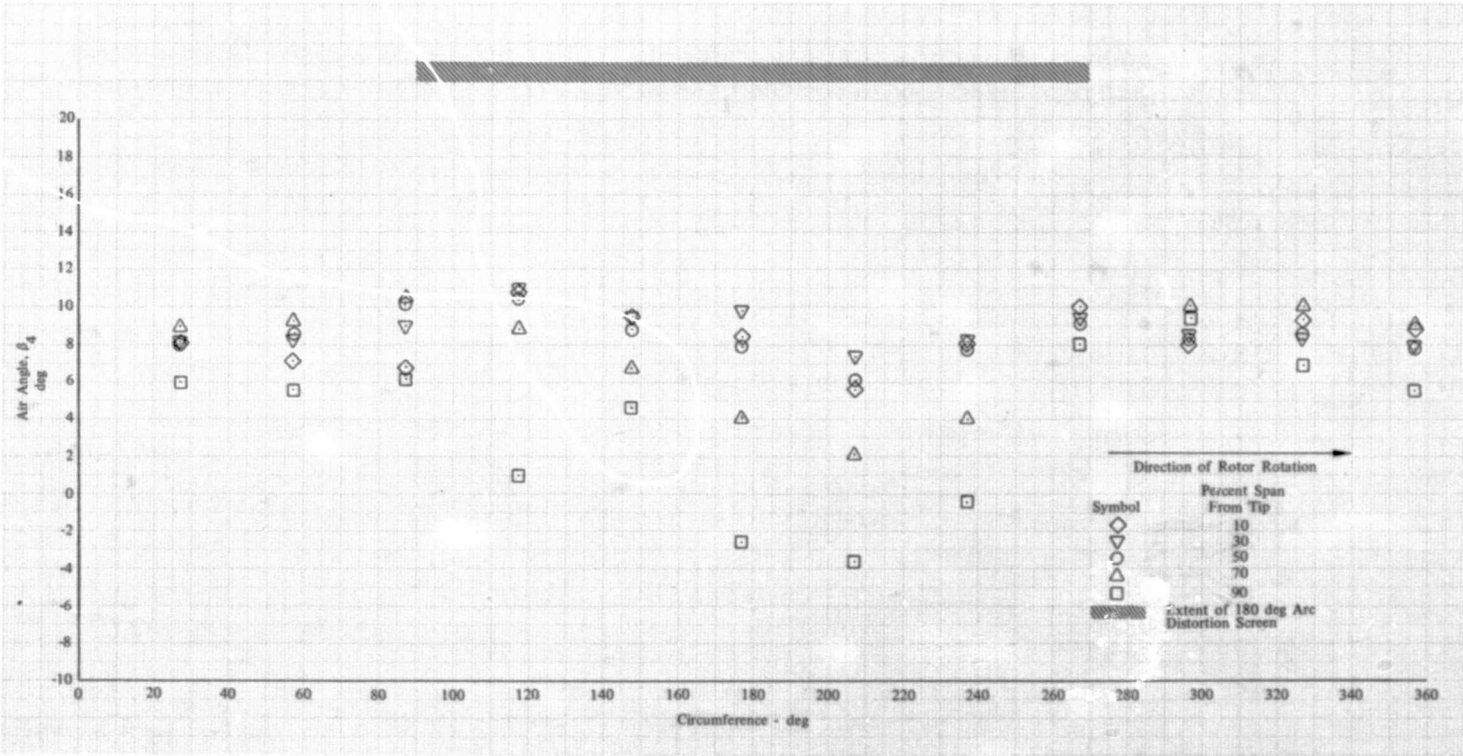


Figure 75g. Stator Exit Air Angle vs Circumferential Location; 100% Design Equivalent Rotor Speed; Equivalent Weight Flow = 16.74 kg/sec (36.90 lb/sec); Circumferential Distortion

DF 102200

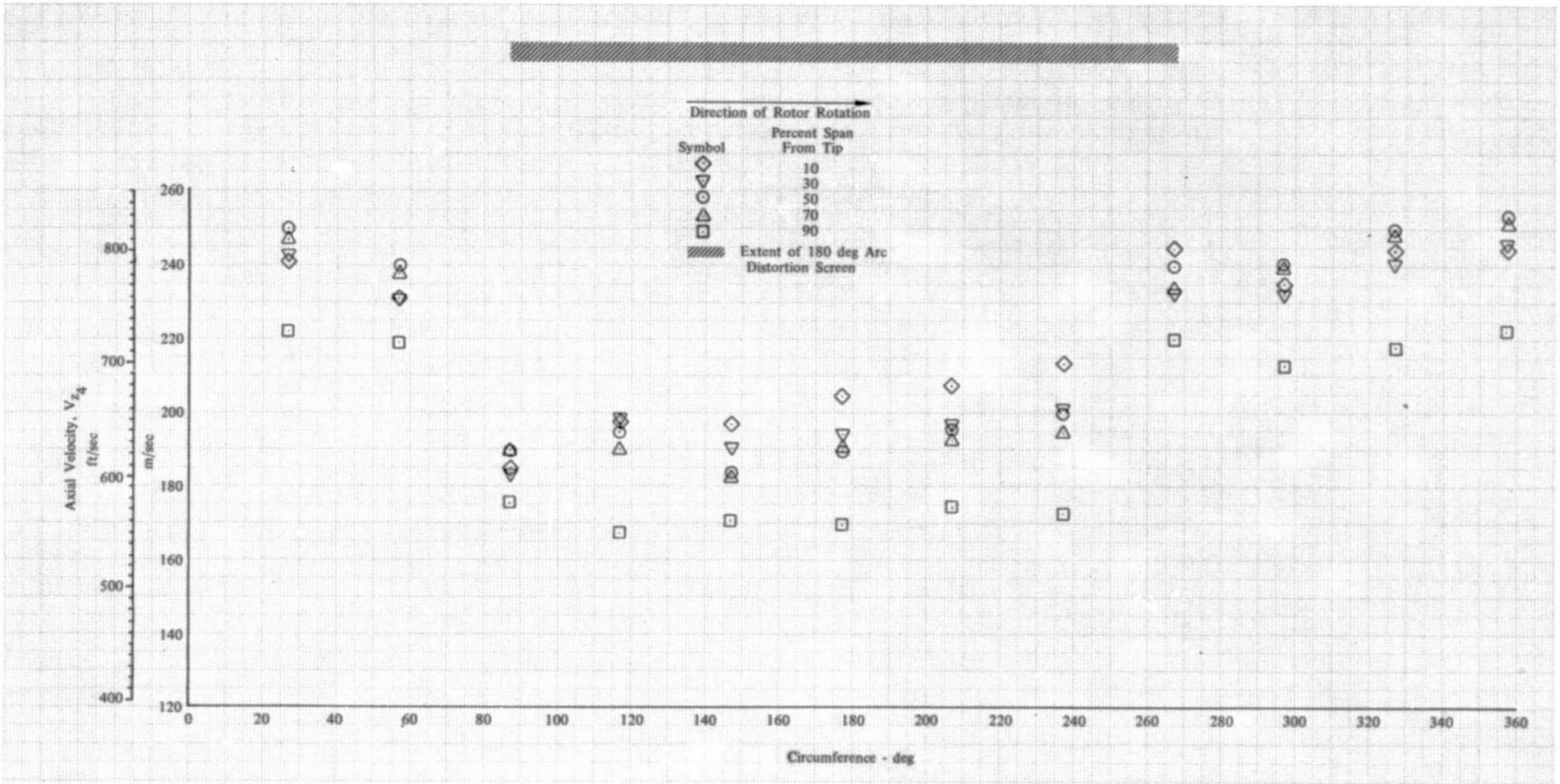


Figure 75h. Stator Exit Axial Velocity vs Circumferential Location; 100% Design Equivalent Rotor Speed; Equivalent Weight Flow = 16.74 kg/sec (36.90 lb/sec); Circumferential Distortion

DF 102201

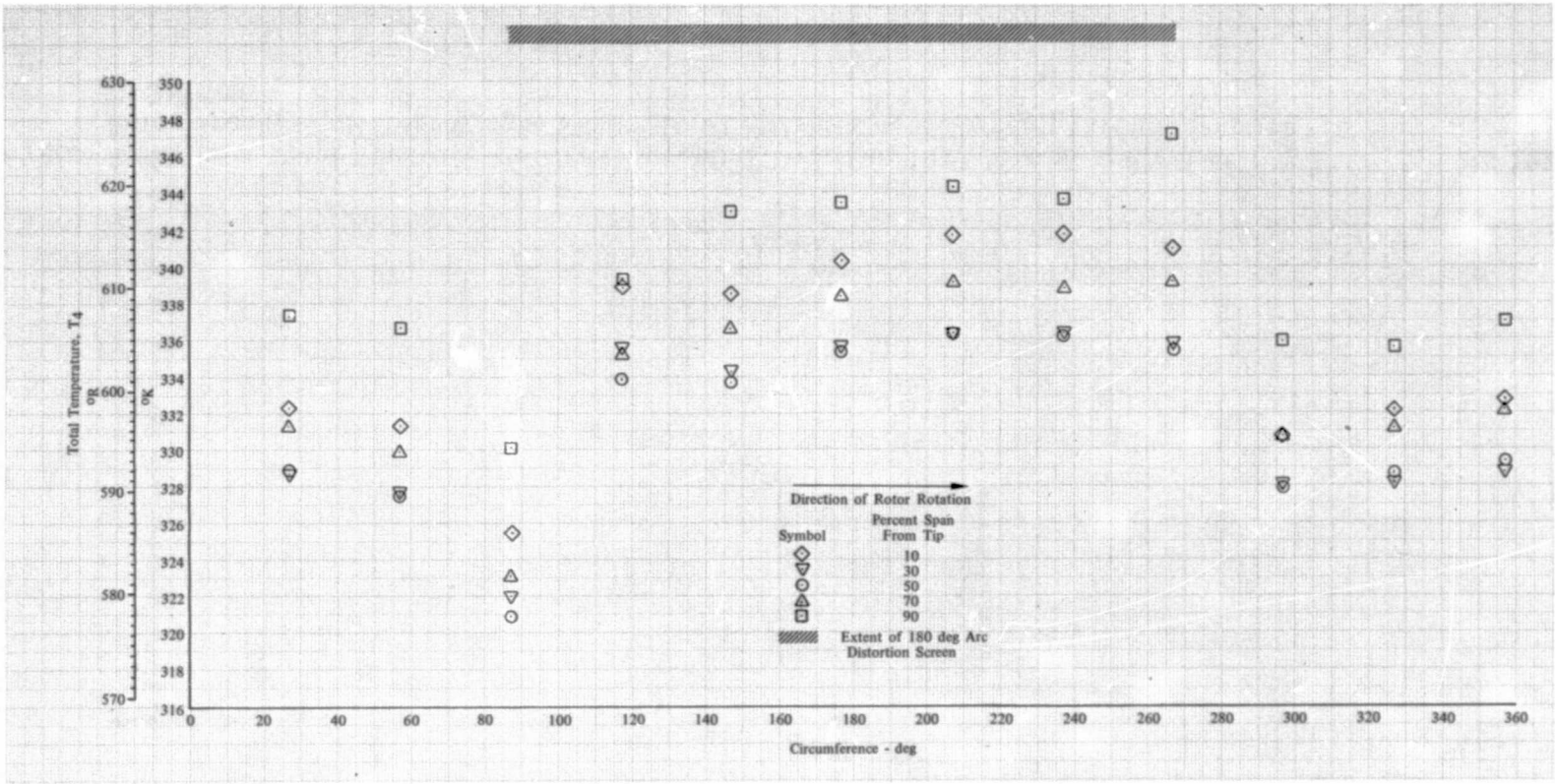


Figure 75i. Stator Exit Total Temperature vs Circumferential Location; 100% Design Equivalent Rotor Speed; Equivalent Weight Flow = 16.74 kg/sec (36.90 lb/sec); Circumferential Distortion

DF 102202

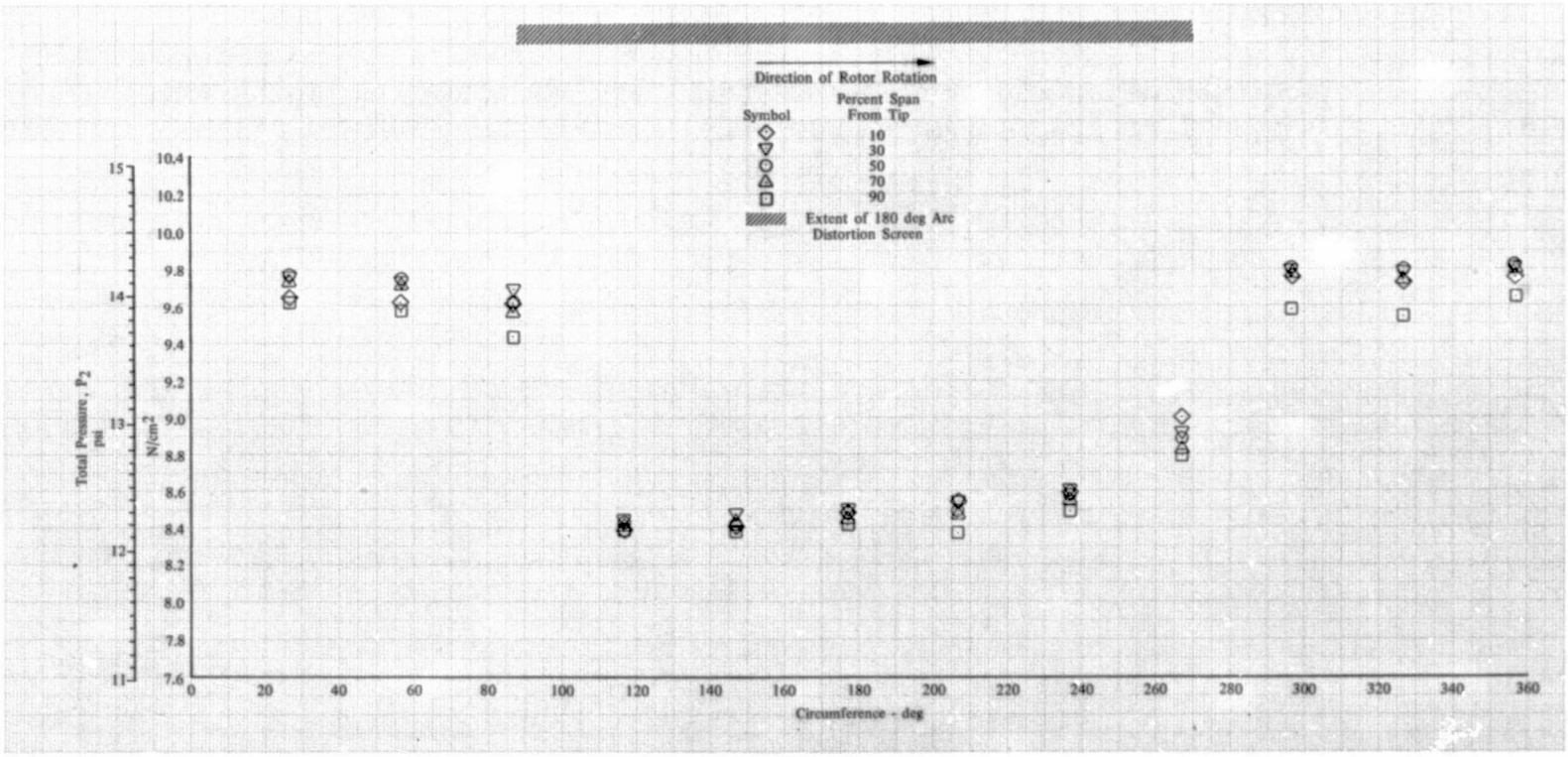


Figure 76a. Rotor Inlet Total Pressure vs Circumferential Location; 100% Design Equivalent Rotor Speed; Equivalent Weight Flow = 15.81 kg/sec (34.85 lb/sec); Circumferential Distortion

DF 102203

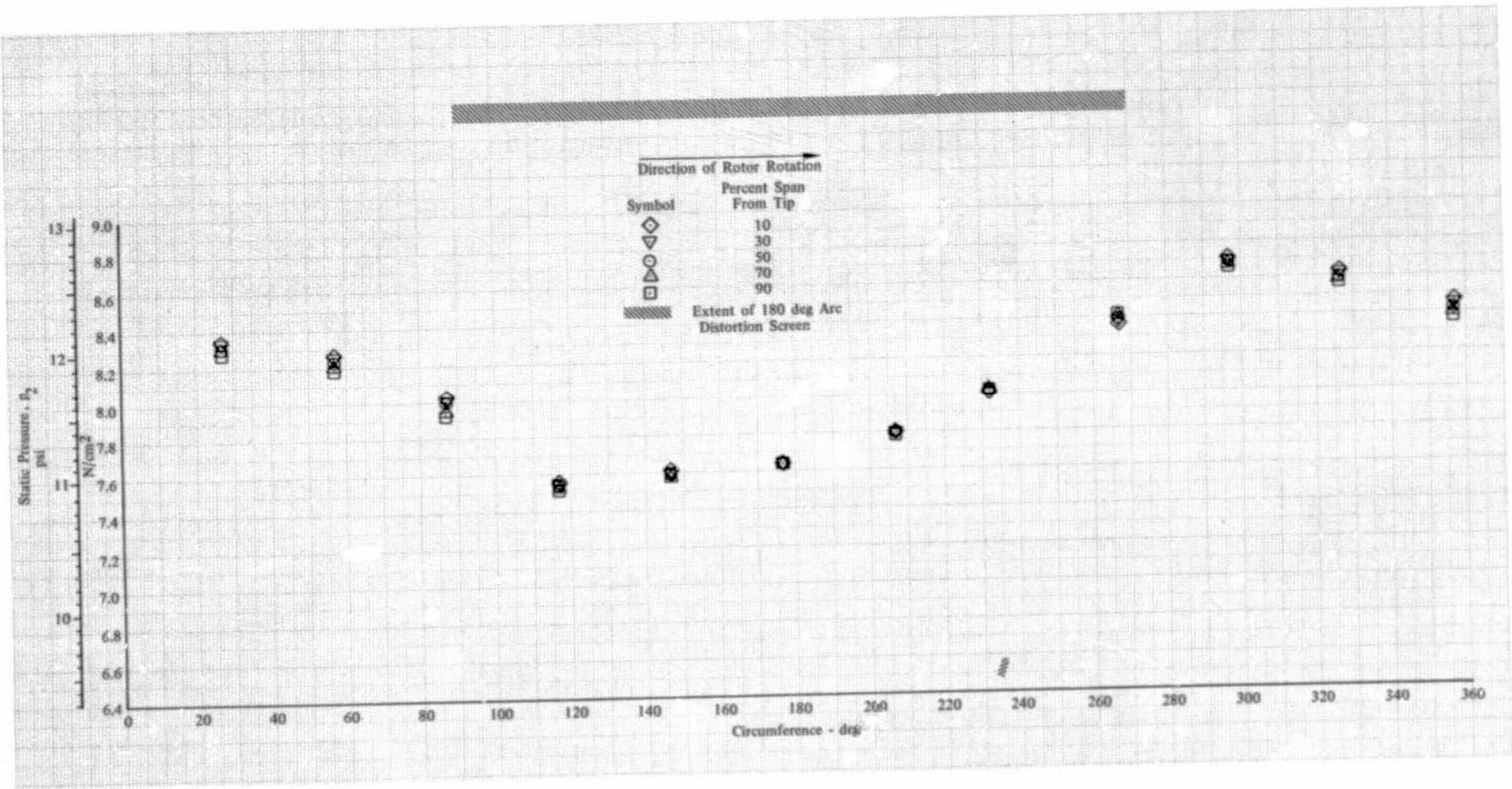


DF 102204

Figure 76b. Rotor Inlet Static Pressure vs Circumferential Location; 100% Design Equivalent Rotor Speed; Equivalent Weight Flow = 15.81 kg/sec (34.85 lb/sec); Circumferential Distortion

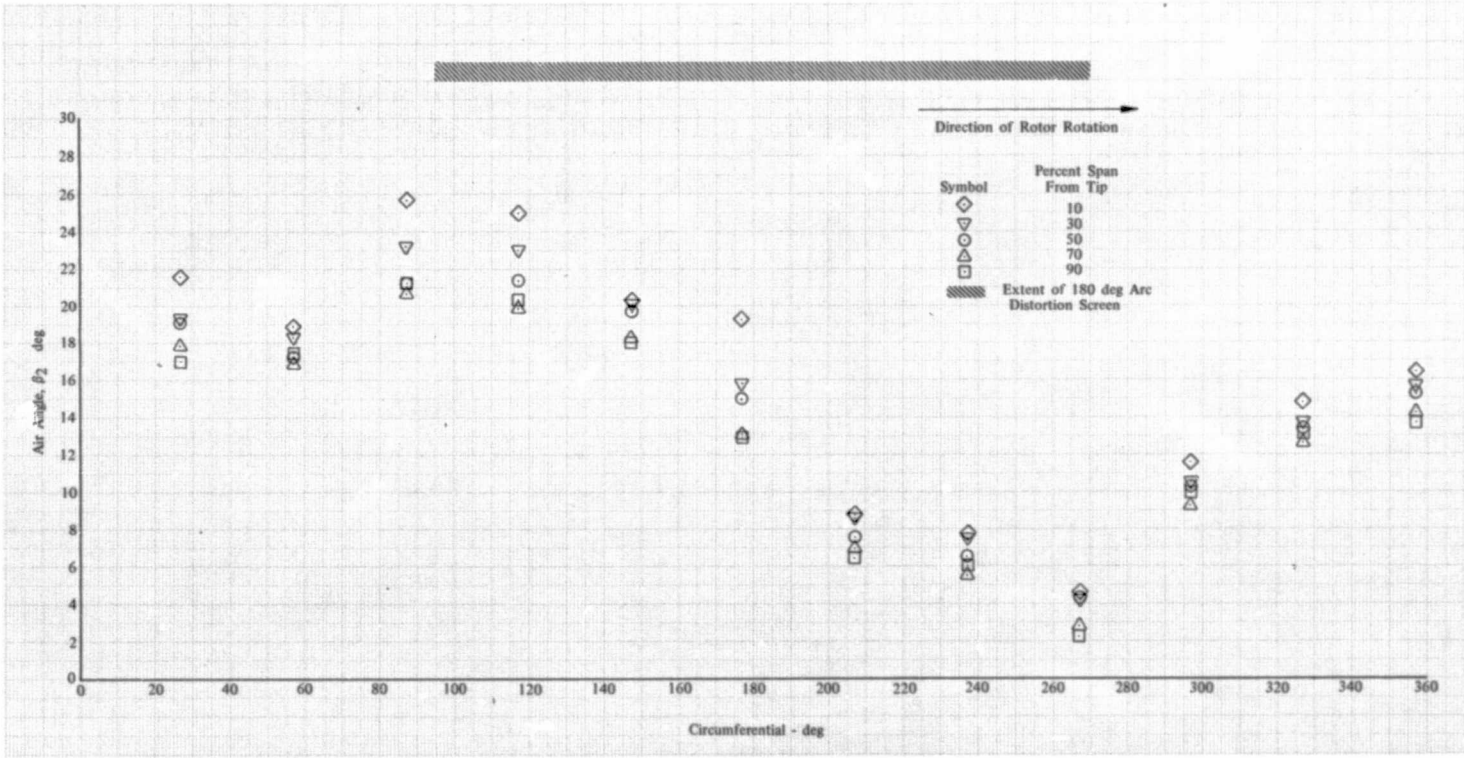


Figure 76c. Rotor Inlet Air Angle vs Circumferential Location; 100% Design Equivalent Rotor Speed; Equivalent Weight Flow = 15.81 kg/sec (34.85 lb/sec); Circumferential Distortion

DF 102205

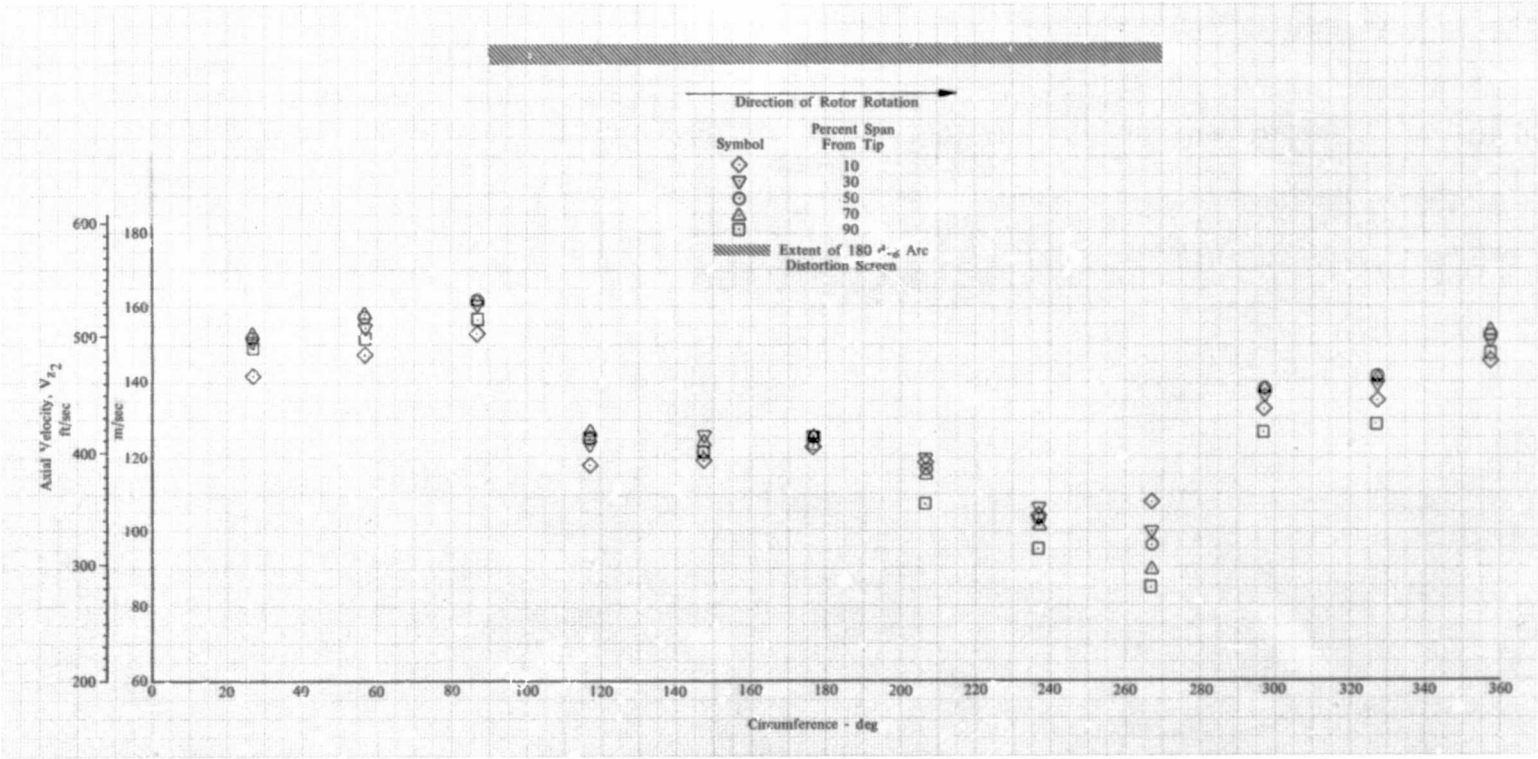


Figure 76d. Rotor Inlet Axial Velocity vs Circumferential Location; 100% Design Equivalent Rotor Speed; Equivalent Weight Flow = 15.81 kg/sec (34.85 lb/sec); Circumferential Distortion

DF 102206

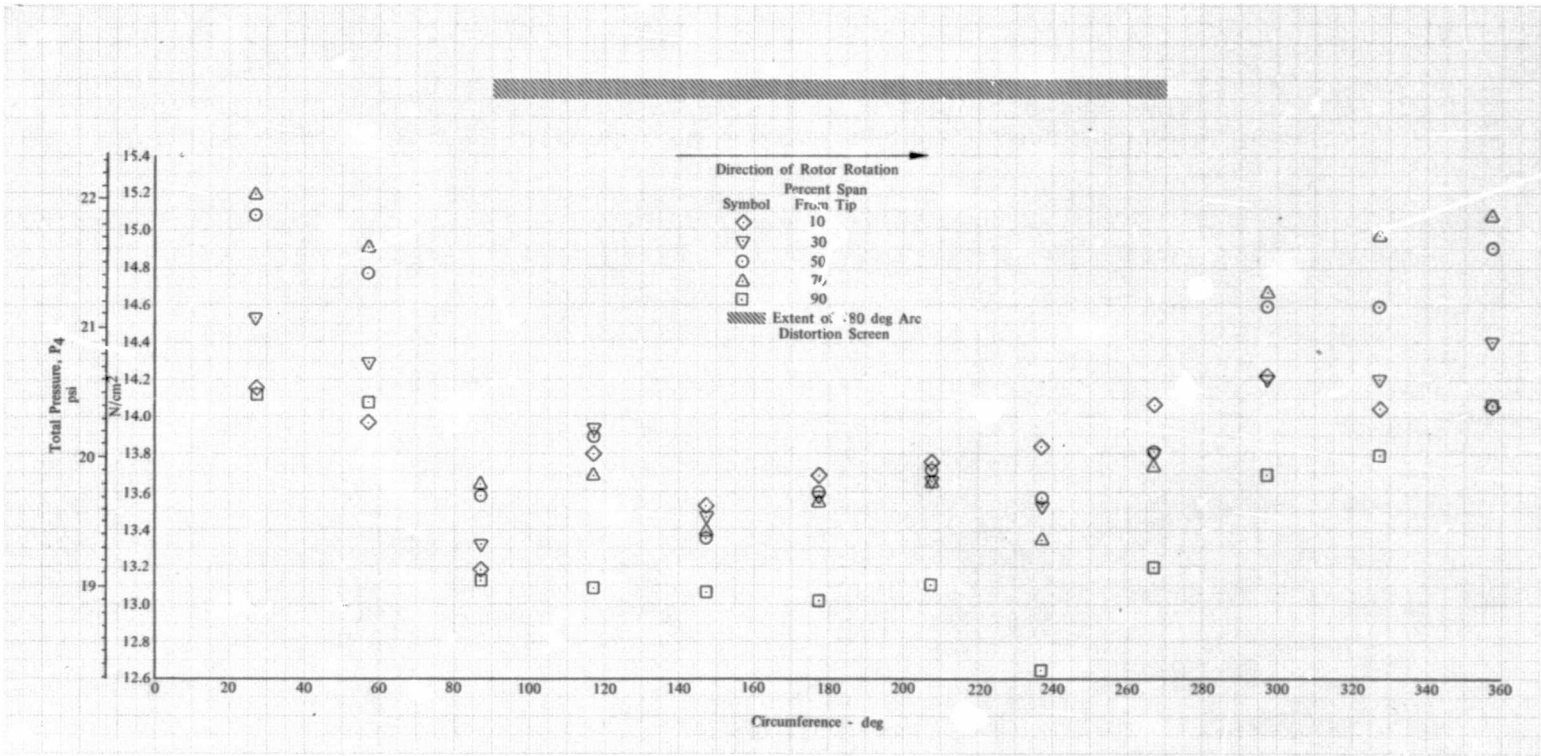


Figure 76e. Stator Exit Total Pressure vs Circumferential Location; 100% Design Equivalent Rotor Speed; Equivalent Weight Flow = 15.81 kg/sec (34.85 lb/sec); Circumferential Distortion

DF 102207

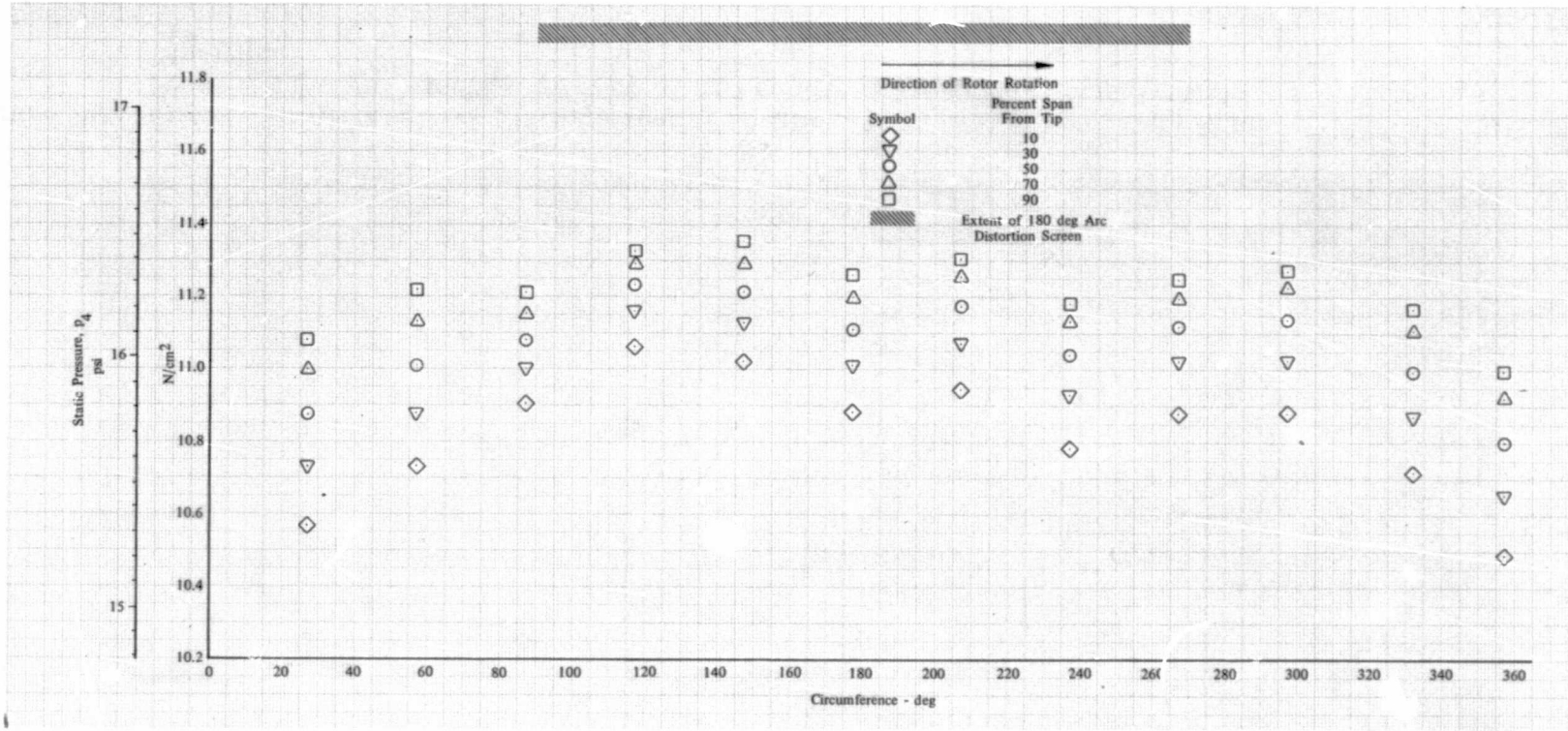


Figure 76f. Stator Exit Static Pressure vs Circumferential Location; 100% Design Equivalent Rotor Speed; Equivalent Weight Flow = 15.81 kg/sec (34.85 lb/sec); Circumferential Distortion

DF 102208

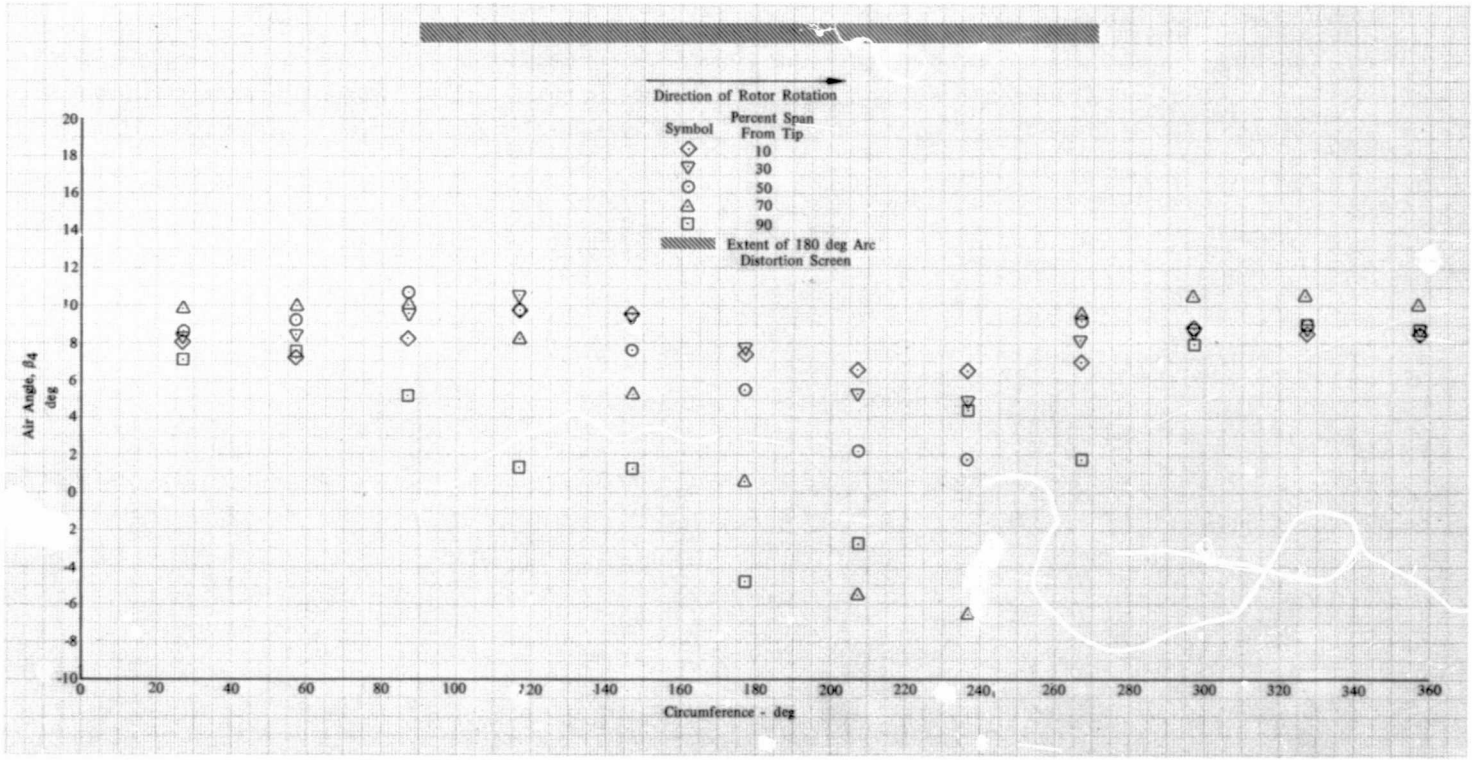


Figure 76g. Stator Exit Air Angle vs Circumferential Location; 100% Design Equivalent Rotor Speed; Equivalent Weight Flow = 15.81 kg/sec (34.85 lb/sec); Circumferential Distortion

DF 102209

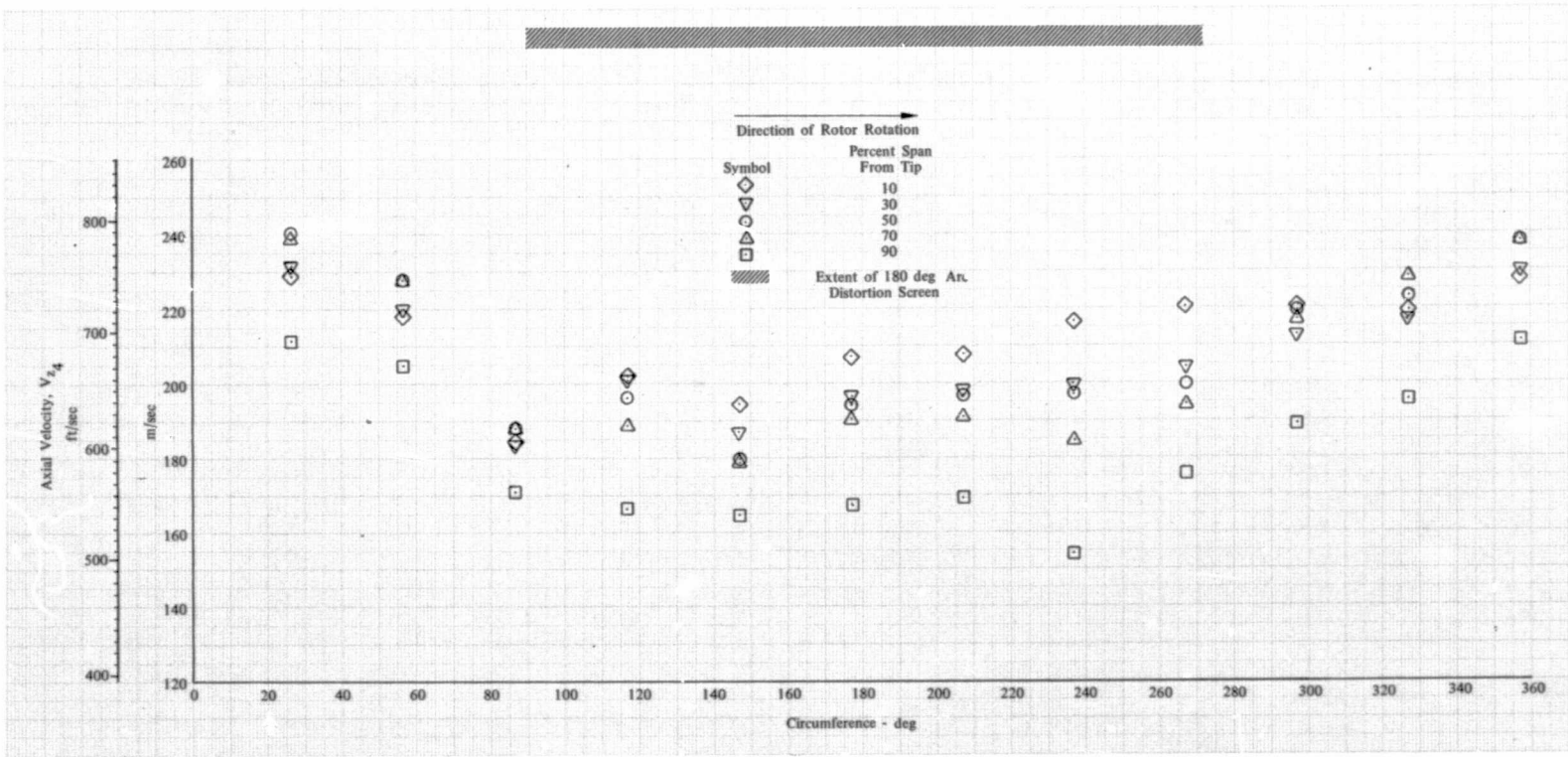


Figure 76h. Stator Exit Axial Velocity vs Circumferential Location; 100% Design Equivalent Rotor Speed; Equivalent Weight Flow = 15.81 kg/sec (34.85 lb/sec); Circumferential Distortion

DF 102210

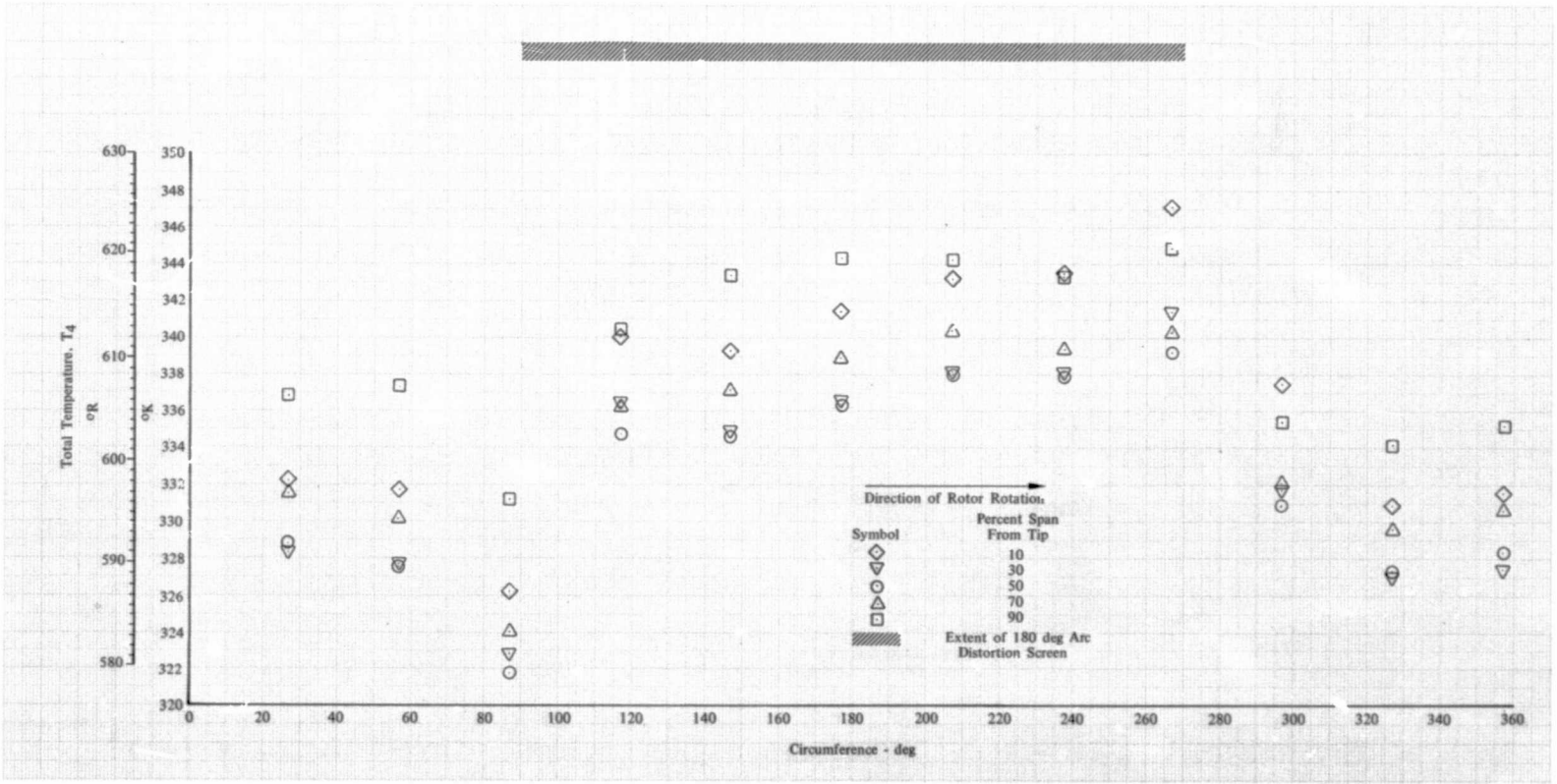


Figure 76i. Stator Exit Total Temperature vs Circumferential Location; 100% Design Equivalent Rotor Speed; Equivalent Weight Flow = 15.81 kg/sec (34.85 lb/sec); Circumferential Distortion

DF 102211

## Summary

Stage F, composed of an inlet guide vane, Rotor F and Stator F, was tested with uniform inlet flow, hub radial, tip radial and circumferential distortion of the inlet flow. With uniform inlet flow, the rotor and the rotor-stator combination essentially achieved their respective design pressure ratio goals, but did not achieve their respective design efficiency goals. With uniform inlet flow at design equivalent rotor speed and flow, the rotor achieved a pressure ratio of 1.595 with an adiabatic efficiency of 91.8% compared with respective design values of 1.614 and 94.5%. At the same flow and rotor speed, the rotor-stator achieved a pressure ratio of 1.561 and an adiabatic efficiency of 86.7% compared with design values of 1.565 and 87.8%. These efficiencies were achieved at average diffusion factors of 0.65 and 0.53 for the rotor and stator, respectively.

Imposition of hub radial, tip radial and circumferential inlet flow distortion had a varied effect on Stage F. With tip radial distortion, surge flow increased 1.4%; with hub radial distortion, surge flow decreased 4.2%; and with circumferential distortion, surge flow increased 3.8%. These values are relative to the uniform inlet results at design equivalent rotor speed. Rotor F-Stator F decreases in peak adiabatic efficiency at 70, 85 and 100% design equivalent rotor speed relative to uniform inlet flow results were 3.3, 2.3 and 3.2% with hub radial distortion; 1.6, 0.5 and 1.2% with tip radial distortion; and 3.3, 3.1 and 4.3% with circumferential inlet distortion. With radial inlet flow distortion, the compressor substantially attenuated the inlet total pressure and velocity distortion across the span. With circumferential inlet flow distortion, the compressor slightly attenuated the inlet total pressure distortion at the endwalls; it did not attenuate the velocity distortion.

## PART II

## TASK V - STAGE G AERODYNAMIC DESIGN AND OVERALL AND BLADE ELEMENT PERFORMANCE

Part II of this report summarizes the work performed under Task V of Contract NAS3-11158. Task V was a two-month program undertaken to obtain performance data on a single-stage compressor, designated as Stage G, which had similar aspect ratio, solidity, and loading level to that of Stage F, but utilized multiple circular arc (MCA) blading. This test program provided comparative data between MCA and double circular arc (DCA) blading.

The blading utilized for Stage G was not designed as part of this program, but rather was existing P&WA blades adapted for the program. The original design was based on a solidity of 1.0 but was changed to a solidity of 1.25 by adding spare blades and vanes to provide a closer match to the Stage F solidity.

The description of the design of these blades, which is presented in the following section, relates to the actual aerodynamic design at a solidity of 1.0. Six rotor blades and eight stator vanes were added to raise the solidity to 1.25 for the Stage G test. Performance at the higher solidity was re-estimated by altering the deviation angles in accordance with Carter's rule, and the resulting Stage G performance is presented in table XV.

Table XV. Performance Goals for Stage G

| Parameter | Performance Goal Stage G |
|---|---|
| Flow, $W\sqrt{\theta}/\delta$, kg/sec (lb/sec) | 16.72 (36.86) |
| Speed, $N/\sqrt{\theta}$, rpm | 11,529 |
| Inlet Hub/Tip Ratio | 0.772 |
| Pressure Ratio, Rotor | 1.657 |
| Pressure Ratio, Rotor-Stator | 1.604 |
| Efficiency, Adiabatic, Rotor | 90.6 |
| Efficiency, Adiabatic, Rotor-Stator | 84.14 |
| $U_{tip}/\sqrt{\theta}$, m/sec (ft/sec) | 327 (1074) |
| Rotor Inlet Tip Diameter, cm (in.) | 54.244 (21.356) |
| Aspect Ratio, Rotor | 1.00 |
| Aspect Ratio, Stator | 1.00 |
| Solidity, Rotor | 1.250 |
| Solidity, Stator | 1.248 |
| Diffusion Factor, Rotor | 0.68 |
| Diffusion Factor, Stator | 0.54 |
| Chord, Rotor, cm (in.) | 5.885 (2.317) |
| Chord, Stator, cm (in.) | 5.151 (2.028) |

## Aerodynamic Design

### Design Velocity Diagrams

Design velocity diagrams were selected to satisfy the criteria specified in table XVI.

Table XVI. Design Criteria for MCA Blading

| | |
|---|---|
| Equivalent Flow, $W\sqrt{\theta}/\delta$, kg/sec (lb/sec) Rotor Inlet | 16.72 (36.86) |
| Equivalent Rotor Speed, $N/\sqrt{\theta}$, rpm | 11,536 |
| Stage Pressure Ratio | 1.495 |
| Rotor Inlet Prewhirl, deg | 18.1 |
| Rotor Tip Speed, m/sec (ft/sec) | 329 (1080) |
| Rotor Inlet Hub/Tip Ratio | 0.772 |
| Stage Exit Absolute Air Angle, deg | 18.5 |

In addition to the criteria specified in table XVI, the rotor and stator aspect ratios and mean solidities were specified as 1.0.

The velocity diagrams were calculated using a streamline analysis computer program which solved the continuity, energy and radial equilibrium equations. The calculation required that the rotor relative inlet air angle, stage exit air angle, stage exit total pressure and blade row losses be input into the program. The blade row losses were synthesized from a P&WA empirical prediction system. The radial distributions of loss used in the design are shown in figure 77. The resulting velocity diagrams for the MCA low solidity, i.e., 1.0, stage are presented in tables XVII, XVIII, and XIX for the inlet guide vane, Rotor G and Stator G, respectively.

## Stage G Geometry

### Inlet Guide Vane

The existing Stage F inlet guide vane, NACA Series 63 ($C1_0A_4K_6$) 06 airfoil, was closed approximately seven deg to obtain the desired rotor relative inlet air angle distribution. The metal geometries for the airfoil sections on planes tangent to conic surfaces that approximate the design streamlines of revolution are presented in table XX.

### Rotor G and Stator G

Rotor and stator blading were composed of MCA airfoil sections designed on conical surfaces which approximated stream surfaces of revolution. In general, the MCA airfoil is a combination of two double circular arc sections of different turning rates, permitting some control of suction surface aerodynamics. A typical cross section of a MCA airfoil is shown in figure 78. The chord lengths and the number of blades and vanes were established by the selected flowpath dimensions, blade row aspect ratios and blade row solidities. Thickness-to-chord ratio distributions were selected to give minimum airfoil cross sections consistent with safe mechanical design practices.

Table XVII. Stage G Inlet Guide Vane Vector Diagram Calculation Results

SI (Metric) Units

Equivalent Rotor Speed = 11596 rpm

Equivalent Weight Flow = 16.72 kg/sec

| | Percent Span From Tip | | | | | | | | | | |
|---|---|---|---|---|---|---|---|---|---|---|---|
| | Leading Edge | Trailing Edge | $V_{le}$ (m/sec) | $V_{zle}$ (m/sec) | $V_{\theta le}$ (m/sec) | $\beta_{le}$ (deg) | $V_{te}$ (m/sec) | $V_{zte}$ (m/sec) | $V_{\theta te}$ (m/sec) | $\beta_{te}$ (deg) | $\alpha$ (deg) |
| Hub | 94.1 | 94.2 | 113.6 | 113.6 | 0.0 | 0.0 | 142.6 | 133.1 | 51.1 | 20.99 | -0.58 |
| | 88.3 | 88.4 | 113.6 | 113.6 | 0.0 | 0.0 | 142.5 | 132.9 | 51.5 | 21.17 | -1.14 |
| | 77.2 | 77.3 | 113.6 | 113.6 | 0.0 | 0.0 | 142.2 | 132.3 | 52.2 | 21.53 | -2.19 |
| | 61.2 | 61.3 | 113.6 | 113.6 | 0.0 | 0.0 | 141.5 | 131.2 | 53.1 | 22.04 | -3.61 |
| | 46.0 | 46.2 | 113.6 | 113.6 | 0.0 | 0.0 | 140.6 | 129.9 | 53.9 | 22.52 | -4.88 |
| | 31.5 | 31.7 | 113.6 | 113.6 | 0.0 | 0.0 | 139.7 | 128.6 | 54.6 | 22.99 | -6.03 |
| | 17.7 | 17.8 | 113.6 | 113.6 | 0.0 | 0.0 | 138.8 | 127.3 | 55.2 | 23.43 | -7.07 |
| | 8.7 | 8.8 | 113.6 | 113.6 | 0.0 | 0.0 | 138.1 | 126.5 | 55.6 | 23.72 | -7.70 |
| Tip | 4.3 | 4.4 | 113.6 | 113.6 | 0.0 | 0.0 | 137.7 | 126.0 | 55.7 | 23.86 | -8.01 |

| | Percent Span From Tip | | | | |
|---|---|---|---|---|---|
| | Leading Edge | Trailing Edge | $M_{le}$ | $\overline{\omega}$ | $P_{le}$ ($N/cm^2$) |
| Hub | 94.1 | 94.2 | 0.3375 | 0.066 | 10.132 |
| | 88.3 | 88.4 | 0.3375 | 0.060 | 10.132 |
| | 77.2 | 77.3 | 0.3375 | 0.050 | 10.132 |
| | 61.2 | 61.3 | 0.3375 | 0.043 | 10.132 |
| | 46.0 | 46.2 | 0.3375 | 0.041 | 10.132 |
| | 31.5 | 31.7 | 0.3375 | 0.041 | 10.132 |
| | 17.7 | 17.8 | 0.3375 | 0.043 | 10.132 |
| | 8.7 | 8.8 | 0.3375 | 0.046 | 10.132 |
| Tip | 4.3 | 4.4 | 0.3375 | 0.049 | 10.132 |

Table XVII. Stage G Inlet Guide Vane Vector Diagram Calculation Results

U.S. Customary Units

Equivalent Rotor Speed = 11596 rpm

Equivalent Weight Flow = 36.86 lb/sec

| | Percent Span From Tip | | | | | | | | | | |
|---|---|---|---|---|---|---|---|---|---|---|---|
| | Leading Edge | Trailing Edge | $V_{le}$ (ft/sec) | $V_{zle}$ (ft/sec) | $V_{\theta le}$ (ft/sec) | $\beta_{le}$ (deg) | $V_{te}$ (ft/sec) | $V_{zte}$ (ft/sec) | $V_{\theta te}$ (ft/sec) | $\beta_{te}$ (deg) | $\alpha$ (deg) |
| Hub | 94.1 | 94.2 | 372.6 | 372.6 | 0.0 | 0.0 | 467.9 | 436.8 | 167.6 | 20.99 | -0.58 |
| | 88.3 | 88.4 | 372.6 | 372.6 | 0.0 | 0.0 | 467.5 | 436.0 | 168.8 | 21.17 | -1.14 |
| | 77.2 | 77.3 | 372.6 | 372.6 | 0.0 | 0.0 | 466.6 | 434.0 | 171.2 | 21.53 | -2.19 |
| | 61.2 | 61.3 | 372.6 | 372.6 | 0.0 | 0.0 | 464.3 | 430.4 | 174.2 | 22.04 | -3.61 |
| | 46.0 | 46.2 | 372.6 | 372.6 | 0.0 | 0.0 | 461.4 | 426.2 | 176.7 | 22.52 | -4.88 |
| | 31.5 | 31.7 | 372.6 | 372.6 | 0.0 | 0.0 | 458.4 | 422.0 | 179.0 | 22.99 | -6.03 |
| | 17.7 | 17.8 | 372.6 | 372.6 | 0.0 | 0.0 | 455.4 | 417.8 | 181.0 | 23.43 | -7.07 |
| | 8.7 | 8.8 | 372.6 | 372.6 | 0.0 | 0.0 | 453.1 | 414.9 | 182.3 | 23.72 | -7.70 |
| Tip | 4.3 | 4.4 | 372.6 | 372.6 | 0.0 | 0.0 | 451.9 | 413.3 | 182.8 | 23.86 | -8.01 |

| | Percent Span From Tip | | | | |
|---|---|---|---|---|---|
| | Leading Edge | Trailing Edge | $M_{le}$ | $\overline{\omega}$ | $P_{le}$ (psia) |
| Hub | 94.1 | 94.2 | 0.3375 | 0.066 | 14.694 |
| | 88.3 | 88.4 | 0.3375 | 0.060 | 14.694 |
| | 77.2 | 77.3 | 0.3375 | 0.050 | 14.694 |
| | 61.2 | 61.3 | 0.3375 | 0.043 | 14.694 |
| | 46.0 | 46.2 | 0.3375 | 0.041 | 14.694 |
| | 31.5 | 31.7 | 0.3375 | 0.041 | 14.694 |
| | 17.7 | 17.8 | 0.3375 | 0.043 | 14.694 |
| | 8.7 | 8.8 | 0.3375 | 0.046 | 14.694 |
| Tip | 4.3 | 4.4 | 0.3375 | 0.049 | 14.694 |

# Table XVIII. Rotor G Vector Diagram Calculation Results

SI (Metric) Units

Equivalent Rotor Speed = 11596 rpm

Equivalent Weight Flow = 16.72 kg/sec

| | Percent Span From Tip | | | | | | | | | | | | | |
|---|---|---|---|---|---|---|---|---|---|---|---|---|---|---|
| | Leading Edge | Trailing Edge | $V'_{1e}$ (m/sec) | $V_{z1e}$ (m/sec) | $V'_{\theta 1e}$ (m/sec) | $\beta'_{1e}$ (deg) | $\beta_{1e}$ (deg) | $U_{1e}$ (m/sec) | $V'_{te}$ (m/sec) | $V_{zte}$ (m/sec) | $V'_{\theta te}$ (m/sec) | $\beta'_{te}$ (deg) | $U_{te}$ (m/sec) | $\alpha$ (deg) |
| Hub | 94.3 | 94.4 | 271.8 | 175.6 | 207.5 | 49.77 | 16.28 | 258.8 | 192.3 | 190.0 | 29.6 | 8.86 | 258.2 | -0.49 |
| | 88.7 | 88.9 | 274.5 | 175.4 | 211.2 | 50.30 | 16.47 | 263.1 | 195.6 | 192.0 | 37.2 | 10.96 | 261.9 | -0.97 |
| | 77.7 | 78.0 | 279.9 | 174.9 | 218.5 | 51.33 | 16.83 | 271.4 | 203.5 | 194.9 | 58.2 | 16.68 | 269.1 | -1.88 |
| | 61.9 | 62.3 | 287.7 | 174.0 | 229.2 | 52.79 | 17.32 | 283.4 | 210.5 | 192.7 | 84.7 | 23.75 | 279.6 | -3.16 |
| | 46.8 | 47.1 | 295.5 | 173.0 | 239.6 | 54.17 | 17.77 | 295.0 | 212.7 | 187.3 | 100.8 | 28.28 | 289.7 | -4.93 |
| | 32.2 | 32.5 | 303.1 | 172.0 | 249.6 | 55.44 | 18.18 | 306.1 | 213.2 | 179.7 | 114.6 | 32.52 | 299.4 | -5.45 |
| | 18.1 | 18.3 | 310.7 | 170.9 | 259.4 | 56.62 | 18.56 | 316.8 | 208.0 | 168.7 | 121.6 | 35.80 | 308.9 | -6.49 |
| | 8.9 | 9.0 | 215.7 | 170.2 | 265.8 | 57.37 | 18.80 | 323.8 | 201.2 | 156.0 | 127.1 | 39.18 | 315.0 | -7.14 |
| Tip | 4.4 | 4.5 | 318.1 | 169.8 | 269.0 | 57.73 | 18.91 | 327.2 | 198.3 | 148.7 | 131.2 | 41.42 | 318.0 | -7.45 |

| | Percent Span From Tip | | | | | | | | | | |
|---|---|---|---|---|---|---|---|---|---|---|---|
| | Leading Edge | Trailing Edge | $M'_{1e}$ | D | $\bar{\omega}'$ | Loss Parameter | Momentum Thickness Parameter | $P_{1e}$ ($N/cm^2$) | $T_{1e}$ (°K) | $P_{te}$ ($N/cm^2$) | $T_{te}$ (°K) |
| Hub | 94.3 | 94.4 | 0.823 | 0.525 | 0.132 | 0.057 | 0.133 | 10.081 | 288.1 | 16.024 | 333.6 |
| | 88.7 | 88.9 | 0.831 | 0.516 | 0.117 | 0.052 | 0.120 | 10.086 | 288.1 | 16.083 | 333.1 |
| | 77.7 | 78.0 | 0.847 | 0.486 | 0.068 | 0.031 | 0.070 | 10.094 | 288.1 | 15.923 | 330.2 |
| | 61.9 | 62.3 | 0.871 | 0.463 | 0.040 | 0.017 | 0.040 | 10.099 | 288.1 | 15.601 | 326.9 |
| | 46.8 | 47.1 | 0.894 | 0.469 | 0.049 | 0.021 | 0.048 | 10.100 | 288.1 | 15.459 | 326.2 |
| | 32.2 | 32.5 | 0.917 | 0.482 | 0.078 | 0.034 | 0.074 | 10.100 | 288.1 | 15.283 | 325.9 |
| | 18.1 | 18.3 | 0.940 | 0.521 | 0.144 | 0.062 | 0.134 | 10.099 | 288.1 | 15.182 | 327.5 |
| | 8.9 | 9.0 | 0.955 | 0.555 | 0.184 | 0.077 | 0.159 | 10.096 | 288.1 | 14.950 | 328.3 |
| Tip | 4.4 | 4.5 | 0.962 | 0.569 | 0.206 | 0.084 | 0.166 | 10.094 | 288.1 | 14.783 | 328.3 |

## Table XVIII. Rotor G Vector Diagram Calculation Results

U. S. Customary Units

Equivalent Rotor Speed = 11596 rpm

Equivalent Weight Flow = 36.86 lb/sec

| | Percent Span From Tip | | | | | | | | | | | | | |
|---|---|---|---|---|---|---|---|---|---|---|---|---|---|---|
| | Leading Edge | Trailing Edge | $V'_{1e}$ (ft/sec) | $V_{z1e}$ (ft/sec) | $V'_{\theta 1e}$ (ft/sec) | $\beta'_{1e}$ (deg) | $\beta_{1e}$ (deg) | $U_{1e}$ (ft/sec) | $V'_{te}$ (ft/sec) | $V_{zte}$ (ft/sec) | $V'_{\theta te}$ (ft/sec) | $\beta'_{te}$ (deg) | $U_{te}$ (ft/sec) | $\alpha$ (deg) |
| Hub | 94.3 | 94.4 | 891.8 | 576.0 | 680.9 | 49.77 | 16.28 | 849.1 | 630.8 | 623.2 | 97.0 | 8.86 | 847.1 | -0.49 |
| | 88.7 | 88.9 | 900.7 | 575.3 | 693.0 | 50.30 | 16.47 | 863.1 | 641.7 | 630.0 | 122.0 | 10.96 | 859.2 | -0.97 |
| | 77.7 | 78.0 | 918.2 | 573.8 | 716.9 | 51.33 | 16.83 | 890.4 | 667.5 | 639.5 | 191.0 | 16.68 | 882.9 | -1.88 |
| | 61.9 | 62.3 | 944.0 | 570.8 | 751.9 | 52.79 | 17.32 | 929.9 | 690.6 | 632.1 | 278.0 | 23.75 | 917.2 | -3.16 |
| | 46.8 | 47.1 | 969.4 | 567.5 | 786.0 | 54.17 | 17.77 | 967.8 | 697.8 | 614.8 | 339.6 | 28.28 | 950.3 | -4.93 |
| | 32.2 | 32.5 | 994.5 | 564.2 | 819.0 | 55.44 | 18.18 | 1004.3 | 699.4 | 589.7 | 376.0 | 32.52 | 982.3 | -5.45 |
| | 18.1 | 18.3 | 1019.3 | 560.8 | 851.1 | 56.62 | 18.56 | 1039.5 | 682.4 | 553.4 | 399.1 | 35.80 | 1013.3 | -6.49 |
| | 8.9 | 9.0 | 1035.6 | 558.5 | 872.1 | 57.37 | 18.80 | 1062.3 | 660.1 | 511.7 | 417.0 | 39.18 | 1033.5 | -7.14 |
| Tip | 4.4 | 4.5 | 1043.7 | 557.2 | 882.5 | 57.73 | 18.91 | 1073.5 | 650.5 | 487.9 | 430.3 | 41.42 | 1043.4 | -7.45 |

| | Percent Span From Tip | | | | | | | | | | |
|---|---|---|---|---|---|---|---|---|---|---|---|
| | Leading Edge | Trailing Edge | $M'_{1e}$ | D | $\bar{\omega}$ | Loss Parameter | Momentum Thickness Parameter | $P_{1e}$ (psia) | $T_{1e}$ (°R) | $P_{te}$ (psia) | $T_{te}$ (°R) |
| Hub | 94.3 | 94.4 | 0.823 | 0.525 | 0.132 | 0.057 | 0.133 | 14.621 | 518.6 | 23.240 | 600.4 |
| | 88.7 | 88.9 | 0.831 | 0.516 | 0.117 | 0.052 | 0.120 | 14.628 | 518.6 | 23.326 | 599.5 |
| | 77.7 | 78.0 | 0.847 | 0.486 | 0.068 | 0.031 | 0.070 | 14.639 | 518.6 | 23.094 | 594.3 |
| | 61.9 | 62.3 | 0.871 | 0.463 | 0.040 | 0.017 | 0.040 | 14.647 | 518.6 | 22.627 | 588.5 |
| | 46.8 | 47.1 | 0.894 | 0.469 | 0.049 | 0.021 | 0.048 | 14.649 | 518.6 | 22.420 | 587.2 |
| | 32.2 | 32.5 | 0.917 | 0.482 | 0.078 | 0.034 | 0.074 | 14.649 | 518.6 | 22.166 | 586.7 |
| | 18.1 | 18.3 | 0.940 | 0.521 | 0.144 | 0.062 | 0.134 | 14.647 | 518.6 | 22.019 | 589.5 |
| | 8.9 | 9.0 | 0.955 | 0.555 | 0.184 | 0.077 | 0.159 | 14.643 | 518.6 | 21.682 | 590.9 |
| Tip | 4.4 | 4.5 | 0.962 | 0.569 | 0.206 | 0.084 | 0.166 | 14.640 | 518.6 | 21.440 | 590.9 |

Table XIX. Stator G Vector Diagram Calculation Results

SI (Metric) Units

Equivalent Rotor Speed = 11596 rpm

Equivalent Weight Flow = 16.72 kg/sec

| | Percent Span From Tip | | | | | | | | | | |
|---|---|---|---|---|---|---|---|---|---|---|---|
| | Leading Edge | Trailing Edge | $V_{le}$ (m/sec) | $V_{zle}$ (m/sec) | $V_{\theta le}$ (m/sec) | $\beta_{le}$ (deg) | $V_{te}$ (m/sec) | $V_{zte}$ (m/sec) | $V_{\theta te}$ (m/sec) | $\beta_{te}$ (deg) | $\alpha$ (deg) |
| Hub | 94.4 | 94.5 | 297.2 | 190.0 | 228.6 | 50.27 | 184.6 | 175.3 | 57.9 | 18.26 | -0.47 |
| | 88.9 | 89.0 | 295.6 | 192.0 | 224.7 | 49.49 | 189.8 | 180.4 | 59.2 | 18.17 | -0.92 |
| | 78.0 | 78.2 | 287.0 | 194.9 | 210.7 | 47.23 | 192.0 | 182.8 | 58.9 | 17.88 | -1.80 |
| | 62.3 | 62.6 | 274.0 | 192.7 | 194.8 | 45.31 | 188.2 | 179.3 | 57.5 | 17.78 | -3.03 |
| | 47.1 | 47.4 | 266.0 | 187.3 | 188.9 | 45.24 | 185.7 | 176.9 | 56.7 | 17.76 | -4.19 |
| | 32.5 | 32.7 | 257.8 | 179.7 | 184.8 | 45.80 | 178.4 | 169.8 | 54.8 | 17.90 | -5.27 |
| | 18.3 | 18.4 | 252.0 | 168.7 | 187.2 | 47.98 | 171.3 | 162.2 | 55.2 | 18.80 | -6.29 |
| | 9.0 | 9.1 | 244.2 | 156.0 | 187.9 | 50.30 | 162.5 | 153.1 | 54.3 | 19.48 | -6.94 |
| Tip | 4.5 | 4.6 | 238.8 | 148.7 | 186.9 | 51.49 | 157.1 | 147.9 | 53.0 | 19.72 | -7.26 |

| | Percent Span From Tip | | | | | | | |
|---|---|---|---|---|---|---|---|---|
| | Leading Edge | Trailing Edge | $M_{le}$ | D | $\bar{\omega}$ | Loss Parameter | Momentum Thickness Parameter | $P_{te}$ ($N/cm^2$) |
| Hub | 94.4 | 94.5 | 0.871 | 0.587 | 0.152 | 0.066 | 0.145 | 15.11 |
| | 88.9 | 89.0 | 0.866 | 0.562 | 0.128 | 0.056 | 0.121 | 15.29 |
| | 78.0 | 78.2 | 0.842 | 0.529 | 0.089 | 0.040 | 0.079 | 15.40 |
| | 62.3 | 62.6 | 0.803 | 0.507 | 0.052 | 0.025 | 0.045 | 15.33 |
| | 47.1 | 47.4 | 0.778 | 0.501 | 0.039 | 0.019 | 0.035 | 15.27 |
| | 32.5 | 32.7 | 0.751 | 0.517 | 0.047 | 0.024 | 0.044 | 15.06 |
| | 18.3 | 18.4 | 0.731 | 0.544 | 0.073 | 0.038 | 0.077 | 14.85 |
| | 9.0 | 9.1 | 0.705 | 0.572 | 0.078 | 0.041 | 0.090 | 14.62 |
| Tip | 4.5 | 4.6 | 0.688 | 0.588 | 0.076 | 0.041 | 0.092 | 14.48 |

Table XIX. Stator G Vector Diagram Calculation Results

U.S. Customary Units

Equivalent Rotor Speed = 11596 rpm

Equivalent Weight Flow = 36.86 lb/sec

| | Percent Span From Tip | | | | | | | | | | |
|---|---|---|---|---|---|---|---|---|---|---|---|
| | Leading Edge | Trailing Edge | $V_{le}$ (ft/sec) | $V_{zle}$ (ft/sec) | $V_{\theta le}$ (ft/sec) | $\beta_{le}$ (deg) | $V_{te}$ (ft/sec) | $V_{zte}$ (ft/sec) | $V_{\theta te}$ (ft/sec) | $\beta_{te}$ (deg) | $\alpha$ (deg) |
| Hub | 94.4 | 94.5 | 975.1 | 623.2 | 750.0 | 50.27 | 605.7 | 575.2 | 189.8 | 18.26 | -0.47 |
| | 88.9 | 89.0 | 969.7 | 630.0 | 737.2 | 49.49 | 622.8 | 591.7 | 194.2 | 18.17 | -0.92 |
| | 78.0 | 78.2 | 941.7 | 639.5 | 691.3 | 47.23 | 630.0 | 599.6 | 193.4 | 17.88 | -1.80 |
| | 62.3 | 62.6 | 898.9 | 632.1 | 639.1 | 45.31 | 617.6 | 588.1 | 188.6 | 17.78 | -3.03 |
| | 47.1 | 47.4 | 872.7 | 614.5 | 619.7 | 45.24 | 609.3 | 580.3 | 185.9 | 17.76 | -4.19 |
| | 32.5 | 32.7 | 845.8 | 589.7 | 606.3 | 45.80 | 585.4 | 557.1 | 179.9 | 17.90 | -5.27 |
| | 18.3 | 18.4 | 826.8 | 553.4 | 614.2 | 47.98 | 561.9 | 532.0 | 181.1 | 18.80 | -6.29 |
| | 9.0 | 9.1 | 801.2 | 511.7 | 616.5 | 50.30 | 533.0 | 502.4 | 178.1 | 19.48 | -6.94 |
| Tip | 4.5 | 4.6 | 783.5 | 487.9 | 613.1 | 51.49 | 515.3 | 485.1 | 173.8 | 19.72 | -7.26 |

| | Percent Span From Tip | | | | | | | |
|---|---|---|---|---|---|---|---|---|
| | Leading Edge | Trailing Edge | $M_{le}$ | D | $\overline{\omega}$ | Loss Parameter | Momentum Thickness Parameter | $P_{te}$ (psia) |
| Hub | 94.4 | 94.5 | 0.871 | 0.587 | 0.152 | 0.066 | 0.145 | 21.92 |
| | 88.9 | 89.0 | 0.866 | 0.562 | 0.128 | 0.056 | 0.121 | 22.17 |
| | 78.0 | 78.2 | 0.842 | 0.529 | 0.089 | 0.040 | 0.079 | 22.33 |
| | 62.3 | 62.6 | 0.803 | 0.507 | 0.052 | 0.025 | 0.045 | 22.23 |
| | 47.1 | 47.4 | 0.778 | 0.501 | 0.039 | 0.019 | 0.035 | 22.14 |
| | 32.5 | 32.7 | 0.751 | 0.517 | 0.047 | 0.024 | 0.044 | 21.84 |
| | 18.3 | 18.4 | 0.731 | 0.544 | 0.073 | 0.038 | 0.077 | 21.54 |
| | 9.0 | 9.1 | 0.705 | 0.572 | 0.078 | 0.041 | 0.090 | 21.20 |
| Tip | 4.5 | 4.6 | 0.688 | 0.588 | 0.076 | 0.041 | 0.092 | 21.00 |

As for Stage F, the first step in selecting the actual airfoil shapes was to calculate the two-dimensional turning that combines with axial velocity ratio and secondary flow effects to produce the desired blade row exit conditions. This procedure is outlined in Reference 4. The two-dimensional turning was then used to calculate incidence and camber angles. Incidence angles were based on the data from References 5 through 11. Deviation angles were calculated using Carter's rule modified to account for the chordwise distance to the maximum camber point.

The transition point from one circular arc section to the other was selected to be 2% of chord downstream of the calculated suction surface shock location, and the maximum thickness point was positioned at 50% chord. The ratio of front-camber to total camber was chosen to minimize the shock strength and thereby losses without causing excessive turning, i.e., high losses, in the rear portion of the airfoil.

Knowing the front and total camber, transition point location, maximum thickness, location of maximum thickness, total chord, incidence angle, deviation angle and total turning, an existing computer program was used to complete the airfoil shapes for thirteen sections between the hub and tip. Each section was on a conic surface that approximated design streamlines of revolution. The resulting metal geometries for Rotor G and Stator G are summarized in tables XXI and XXII, respectively. The spanwise distributions of front and total camber, front and total chord, and maximum camber point are presented in figures 79 through 82 for both the rotor and stator.

For manufacturing purposes, the rotor and stator airfoil coordinates were redefined on planes tangent to cylindrical surfaces normal to a radial line, i.e., the stacking line, using the procedure presented in Reference 2. The airfoil sections were positioned such that the stacking line passed through the center of gravity of each section. Coordinates for the redefined sections are given in tables A-5 through A-8 of Appendix A, Volume II. Photographs of the airfoils are shown in figure 83.

Table XX. Stage G Inlet Guide Vane Geometry Data

Airfoil: NACA 63 ($C1_0A4K_6$) 06 No. of Vanes: 42 Average Chord Length: 3.886 cm (1.530 in.)

| | Percent Span from Tip | | | | | | | |
|---|---|---|---|---|---|---|---|---|
| | Leading Edge | Trailing Edge | $\kappa_{le}$ | $\kappa_{te}$ | $\phi$ | $\gamma°$ | $\sigma$ | t/c |
| Hub | 94.1 | 94.2 | -16.08 | 19.78 | -35.86 | 12.17 | 1.213 | 0.06 |
| | 88.3 | 88.4 | -16.38 | 20.08 | -36.46 | 12.33 | 1.188 | 0.06 |
| | 77.2 | 77.3 | -17.12 | 20.68 | -37.80 | 12.62 | 1.143 | 0.06 |
| | 61.2 | 61.3 | -18.11 | 21.54 | -39.65 | 13.06 | 1.084 | 0.06 |
| | 46.0 | 46.2 | -19.03 | 22.36 | -41.39 | 13.41 | 1.033 | 0.06 |
| | 31.5 | 31.7 | -19.88 | 23.14 | -43.02 | 13.85 | 0.989 | 0.06 |
| | 17.7 | 17.8 | -20.66 | 23.89 | -44.55 | 14.22 | 0.949 | 0.06 |
| | 8.7 | 8.8 | -21.14 | -24.36 | -45.50 | 14.46 | 0.926 | 0.06 |
| Tip | 4.3 | 4.4 | -21.38 | -24.60 | -45.98 | 14.57 | 0.915 | 0.06 |



C.3

Table XXI. Rotor G Geometry Data

Airfoil: Multiple Circular Arc  No. of Blades: 32  Average Chord Length: 5.885 cm (2.317 in.)

| | Percent Span From Tip | | | | | | | | | LER/TER | |
|---|---|---|---|---|---|---|---|---|---|---|---|
| | Leading Edge | Trailing Edge | $\kappa'_{le}$ | $\kappa'_{te}$ | $\phi$ | $\phi_f$ | $b_f/b$ | a/b | c/b | cm | in. |
| Hub | 94.3 | 94.4 | 47.90 | -11.21 | 59.11 | 10.00 | 0.344 | 0.531 | 0.500 | 0.0246 | (0.0097) |
| | 88.7 | 88.9 | 48.08 | - 7.60 | 55.68 | 9.51 | 0.358 | 0.536 | 0.500 | 0.0241 | (0.0095) |
| | 77.7 | 78.0 | 48.42 | 0.96 | 47.47 | 8.62 | 0.386 | 0.543 | 0.500 | 0.0231 | (0.0091) |
| | 61.9 | 62.3 | 48.99 | 10.69 | 38.30 | 7.55 | 0.419 | 0.555 | 0.500 | 0.0213 | (0.0084) |
| | 46.8 | 47.1 | 49.72 | 15.75 | 33.97 | 6.50 | 0.455 | 0.569 | 0.500 | 0.0198 | (0.0078) |
| | 32.2 | 32.5 | 50.52 | 19.77 | 30.75 | 5.95 | 0.490 | 0.588 | 0.500 | 0.0183 | (0.0072) |
| | 18.1 | 18.3 | 51.89 | 20.53 | 31.36 | 5.50 | 0.526 | 0.310 | 0.500 | 0.0170 | (0.0067) |
| | 8.9 | 9.0 | 53.35 | 20.66 | 32.69 | 5.65 | 0.552 | 0.624 | 0.500 | 0.0163 | (0.0064) |
| Tip | 4.4 | 4.5 | 54.16 | 21.23 | 32.93 | 5.88 | 0.559 | 0.629 | 0.500 | 0.0157 | (0.0062) |

| | Percent Span From Tip | | | | | | | |
|---|---|---|---|---|---|---|---|---|
| | Leading Edge | Trailing Edge | $\sigma$ | t/b | $\delta°$ | $i_m$ | $i_{ss}$ | $\gamma°$ |
| Hub | 94.3 | 94.4 | 1.408 | 0.0632 | 20.07 | 1.87 | -4.05 | 22.83 |
| | 88.7 | 88.9 | 1.387 | 0.0615 | 18.56 | 2.23 | -3.58 | 24.98 |
| | 77.7 | 78.0 | 1.346 | 0.0582 | 15.72 | 2.90 | -2.62 | 29.91 |
| | 61.9 | 62.3 | 1.293 | 0.0534 | 13.06 | 3.81 | -1.32 | 34.89 |
| | 46.8 | 47.1 | 1.246 | 0.0489 | 12.53 | 4.44 | -0.24 | 38.24 |
| | 32.2 | 32.5 | 1.203 | 0.0446 | 12.75 | 4.92 | 0.60 | 40.75 |
| | 18.1 | 18.3 | 1.164 | 0.0404 | 15.27 | 4.72 | 0.86 | 43.05 |
| | 8.9 | 9.0 | 1.140 | 0.0376 | 18.51 | 4.01 | 0.42 | 45.28 |
| Tip | 4.4 | 4.5 | 1.129 | 0.0363 | 20.19 | 3.58 | 0.09 | 47.06 |

Table XXII. Stator G Geometry Data

Airfoil: Multiple Circular Arc  No. of Stators: 36  Average Chord Length: 5.151 cm (2.028 in.)

| | Percent Span From Tip | | | | | | | | | LER/TER | |
|---|---|---|---|---|---|---|---|---|---|---|---|
| | Leading Edge | Trailing Edge | $\kappa_{le}$ | $\kappa_{te}$ | $\phi$ | $\phi_f$ | $b_f/b$ | a/b | c/b | cm | in. |
| Hub | 94.4 | 94.5 | 44.45 | -9.13 | 53.58 | 9.98 | 0.464 | 0.582 | 0.500 | 0.0157 | (0.0062) |
| | 88.9 | 89.0 | 44.31 | -7.68 | 51.99 | 9.51 | 0.448 | 0.575 | 0.500 | 0.0163 | (0.0064) |
| | 78.0 | 78.2 | 42.42 | -3.54 | 45.96 | 8.65 | 0.404 | 0.556 | 0.500 | 0.0170 | (0.0067) |
| | 62.3 | 62.6 | 40.75 | 0.73 | 40.03 | 7.54 | 0.347 | 0.534 | 0.500 | 0.0183 | (0.0072) |
| | 47.1 | 47.4 | 41.04 | 1.74 | 39.30 | 6.62 | 0.308 | 0.526 | 0.500 | 0.0198 | (0.0078) |
| | 32.5 | 32.7 | 42.04 | 1.40 | 40.64 | 5.95 | 0.274 | 0.516 | 0.500 | 0.0213 | (0.0084) |
| | 18.3 | 18.4 | 44.60 | 0.89 | 43.71 | 5.50 | 0.247 | 0.517 | 0.500 | 0.0231 | (0.0091) |
| | 9.0 | 9.1 | 46.45 | 1.43 | 45.02 | 5.67 | 0.217 | 0.512 | 0.500 | 0.0241 | (0.0095) |
| Tip | 4.5 | 4.6 | 47.02 | 2.27 | 44.76 | 5.92 | 0.202 | 0.510 | 0.500 | 0.0246 | (0.0097) |

| | Percent Span From Tip | | | | | | | |
|---|---|---|---|---|---|---|---|---|
| | Leading Edge | Trailing Edge | $\sigma$ | t/b | $\delta°$ | $i_m$ | $i_{ss}$ | $\gamma°$ |
| Hub | 94.4 | 94.5 | 1.389 | 0.0511 | 27.39 | 5.82 | 0.50 | 25.95 |
| | 88.9 | 89.0 | 1.371 | 0.0523 | 25.85 | 5.18 | 0.16 | 25.79 |
| | 78.0 | 78.2 | 1.337 | 0.0543 | 21.42 | 4.81 | -0.32 | 24.79 |
| | 62.3 | 62.6 | 1.290 | 0.0575 | 17.06 | 4.56 | -0.91 | 24.06 |
| | 47.1 | 47.4 | 1.247 | 0.0605 | 16.03 | 4.20 | -1.46 | 23.85 |
| | 32.5 | 32.7 | 1.223 | 0.0635 | 16.50 | 3.76 | -2.18 | 24.04 |
| | 18.3 | 18.4 | 1.173 | 0.0663 | 17.91 | 3.38 | -2.80 | 25.76 |
| | 9.0 | 9.1 | 1.151 | 0.0682 | 18.09 | 3.86 | -2.49 | 26.77 |
| Tip | 4.5 | 4.6 | 1.141 | 0.0691 | 17.45 | 4.46 | -2.01 | 27.27 |

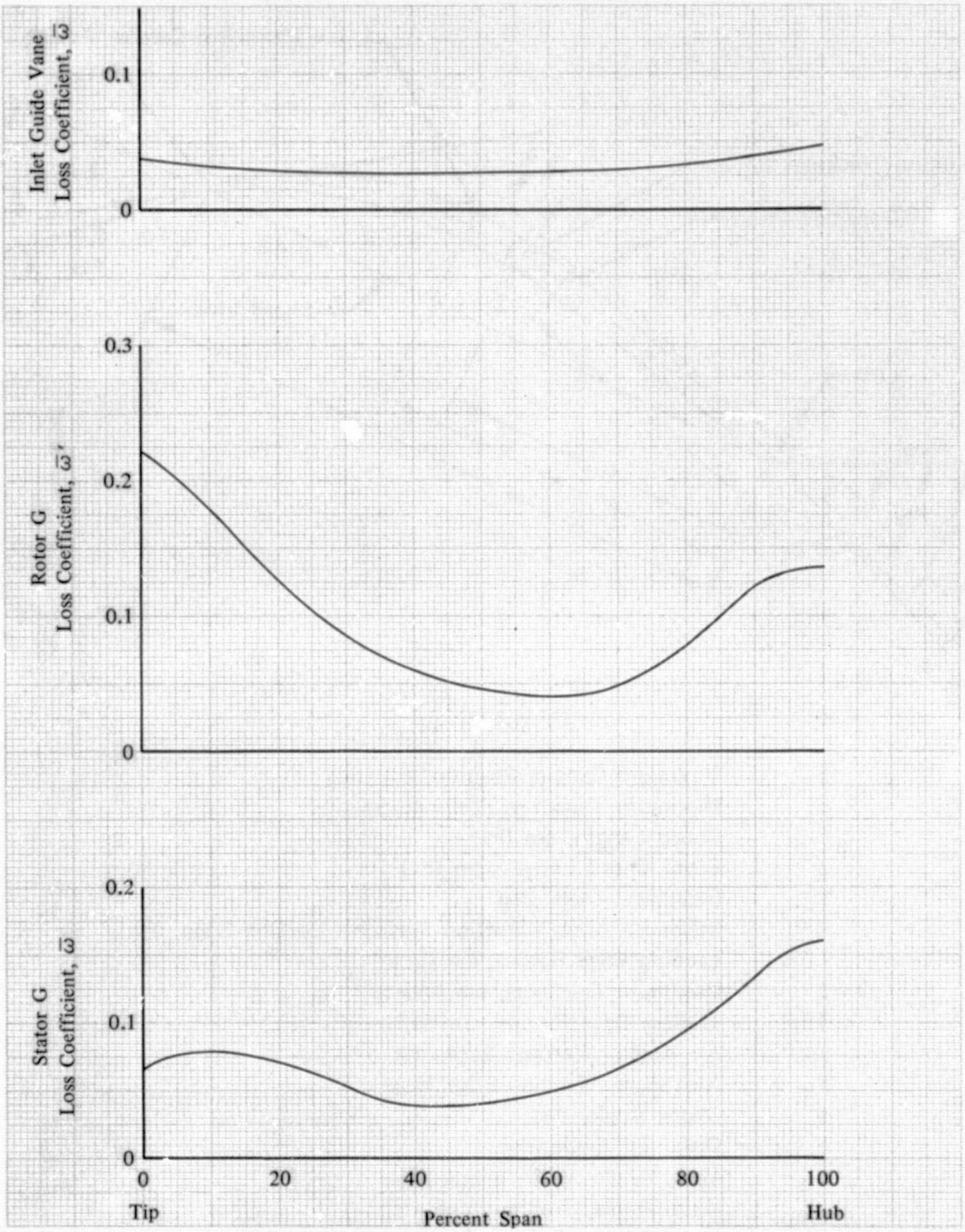


Figure 77. Design Loss Profiles for Stage G Inlet Guide Vane, Rotor and Stator DF 102213

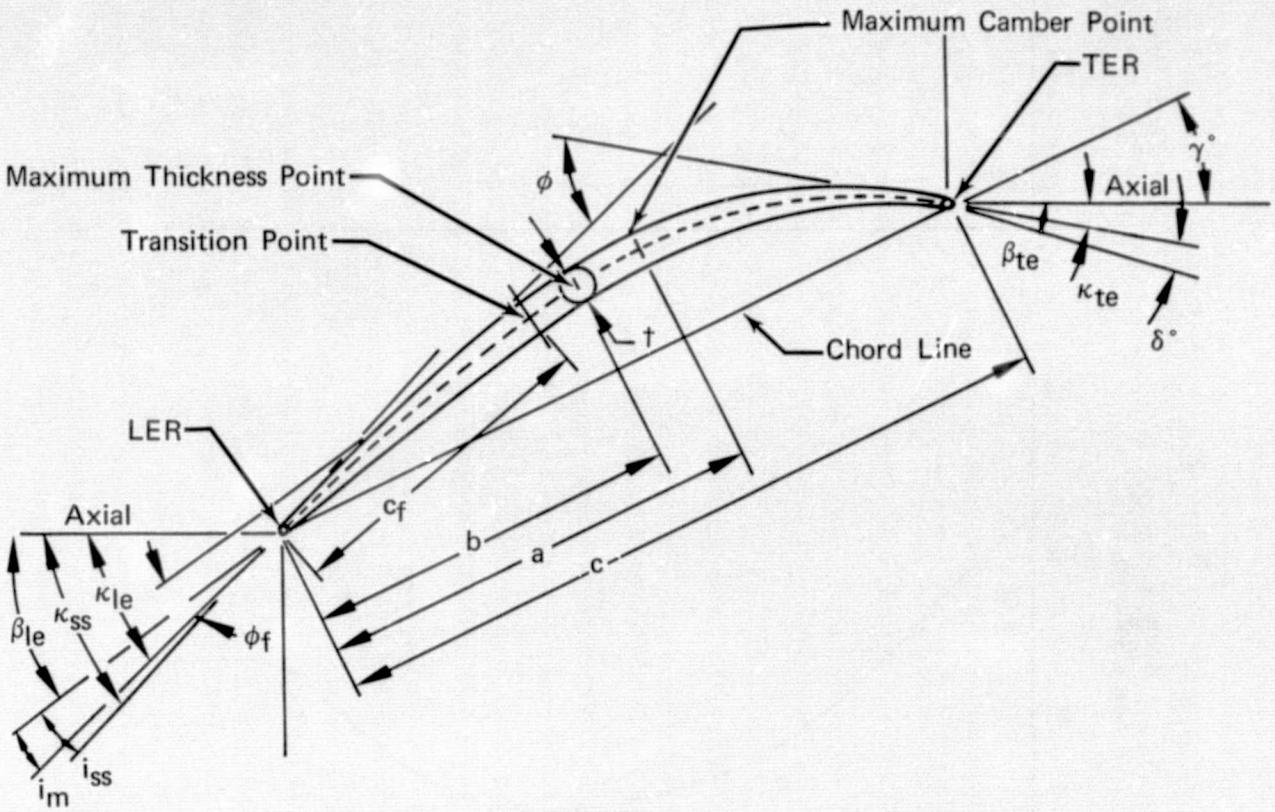


Definitions

| | |
|---|---|
| a | Maximum Camber Position, cm (in.) |
| b | Maximum Thickness Position, cm (in.) |
| c | Chord Length, cm (in.) |
| $c_f$ | Front Chord Length, cm (in.) |
| $i_m$ | Incidence Angle, deg |
| $i_{ss}$ | Incidence Angle - Suction Surface - Leading Edge, deg |
| LER | Leading Edge Radius, cm (in.) |
| t | Maximum Thickness, cm (in.) |
| TER | Trailing Edge Radius, cm (in.) |
| $\beta_{le}$ | Air Angle - Leading Edge, deg |
| $\beta_{te}$ | Air Angle - Trailing Edge, deg |
| $\gamma^\circ$ | Chord Angle, deg |
| $\delta^\circ$ | Deviation Angle, deg |
| $\kappa_{le}$ | Metal Angle, Leading Edge, deg |
| $\kappa_{te}$ | Metal Angle, Trailing Edge, deg |
| $\kappa_{ss}$ | Metal Angle - Suction Surface - Leading Edge, deg |
| $\phi$ | Camber, deg |
| $\phi_f$ | Front Camber, deg |

Figure 78. Multiple Circular-Arc Airfoil Definitions FD 97770

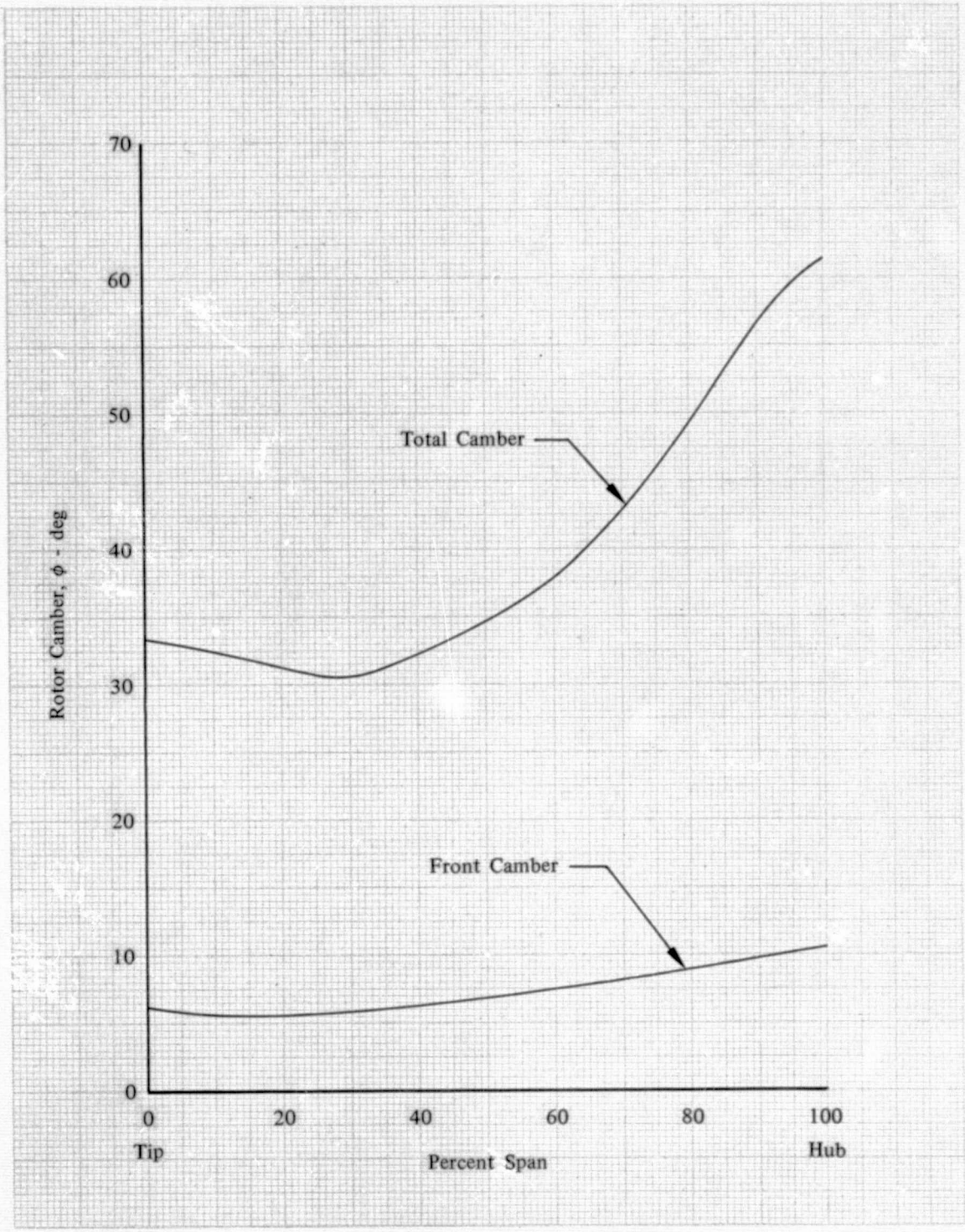


Figure 79. Rotor G Front and Total Camber Distribution DF 102265

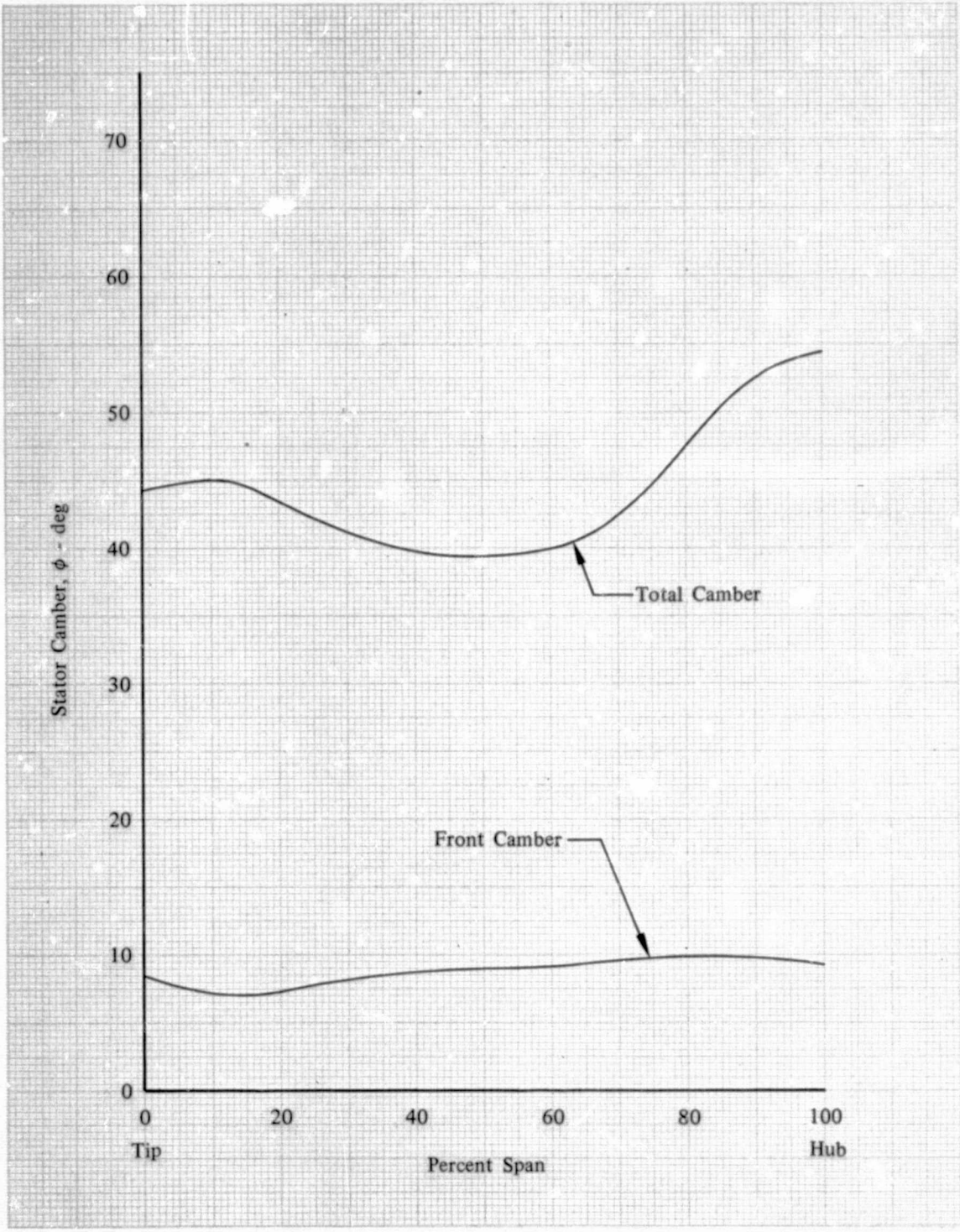


**Figure 80.** Stator G Front and Total Camber Distribution DF 102266

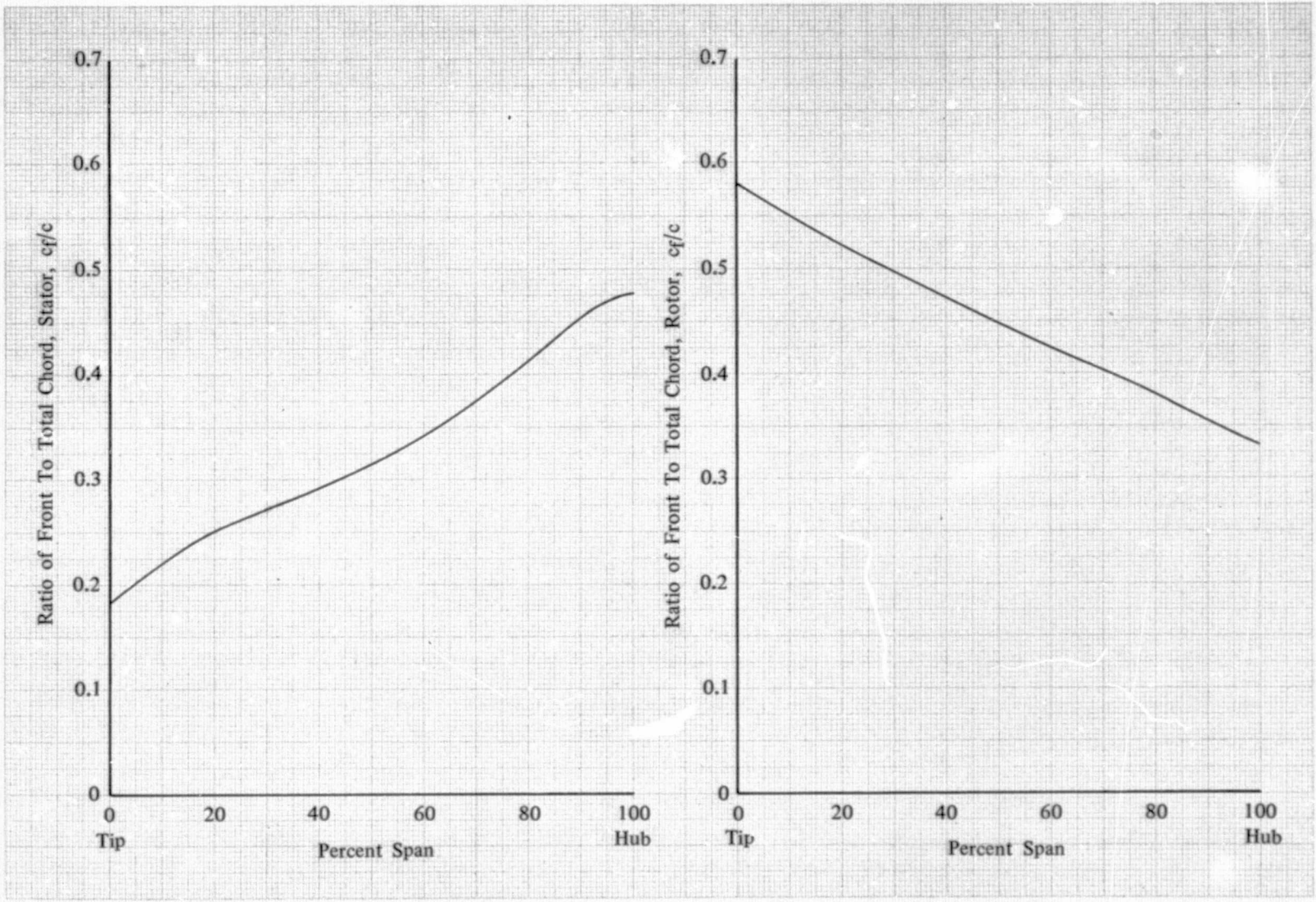


Figure 81. Distribution of Front-to-Total Chord for Rotor G and Stator G

DF 102267

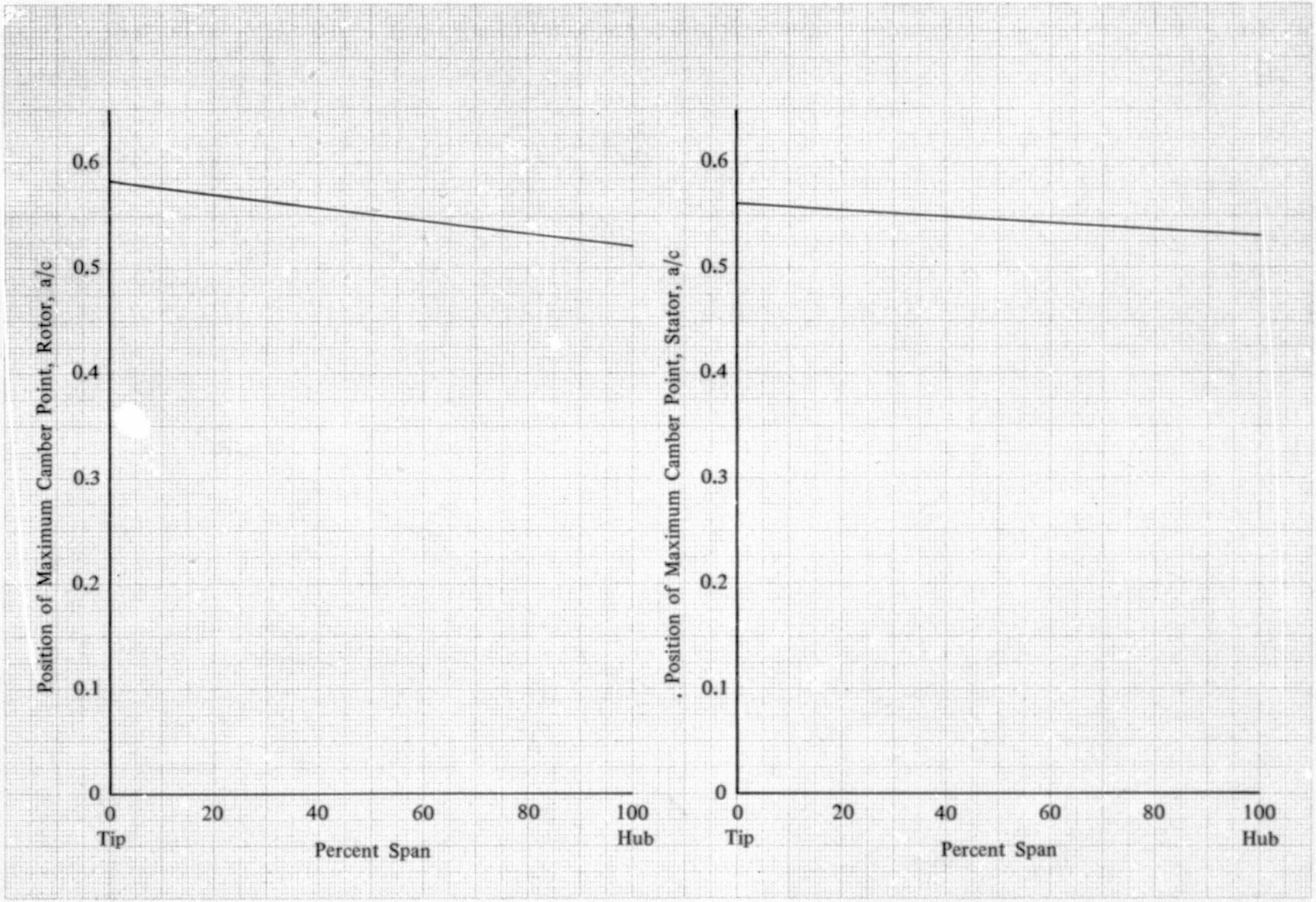


Figure 82. Distribution of Maximum Camber Point for Rotor G and Stator G

DF 102268

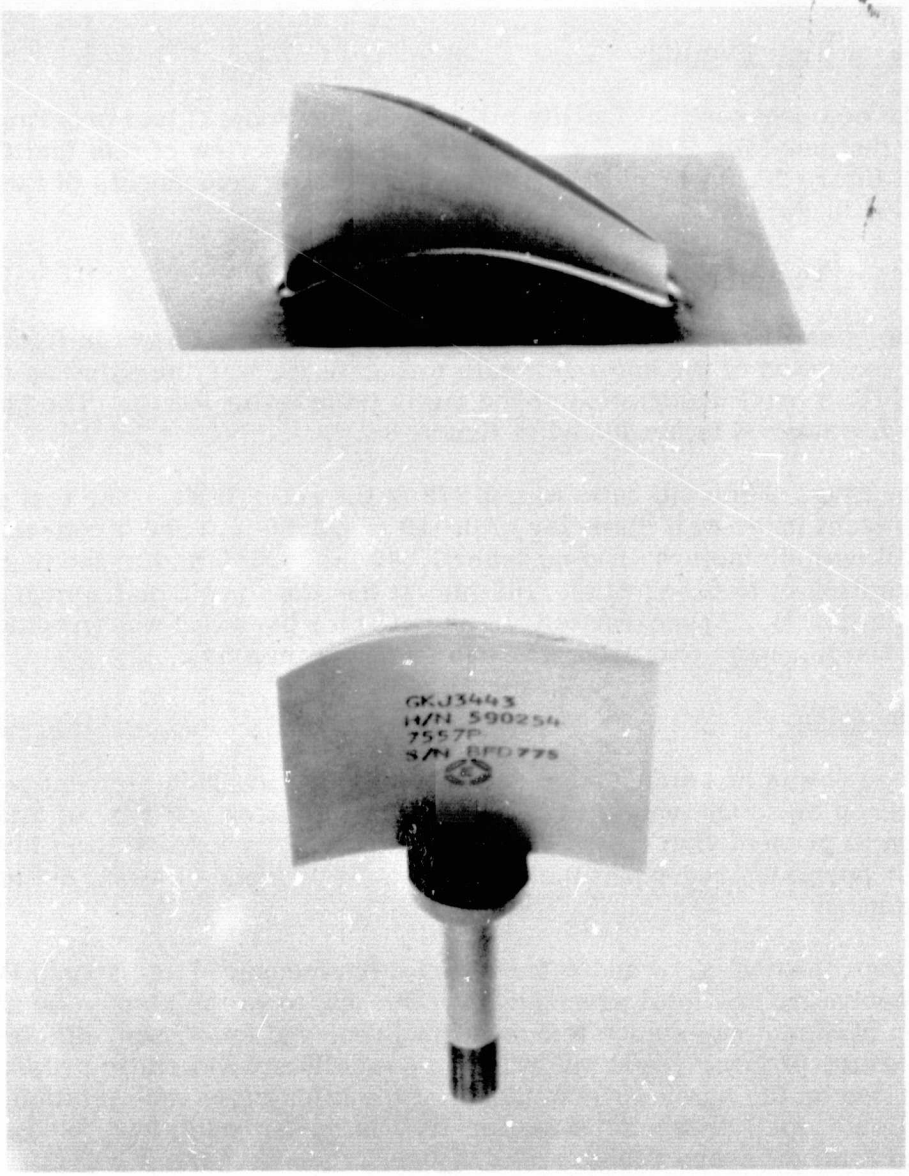


Figure 83. Rotor G and Stator G - Tip Section View FD 84734

## Test Equipment

### Compressor Test Facility

The compressor test facility utilized for the Stage G test program was the same as that used for Stage F (Task IV); an elevation view of this facility is shown in figure 20. A brief description of the major components of the facility is included in Part I.

### Compressor Test Rig

The general configuration of the Stage G test rig is shown in figure 84. With the exception of the outer flowpath wall, the rig was the same as that used for Task IV; a brief description of the rig is included in Part I. The specific flowpath for Stage G is presented in figure 85.

The Stage G hub/tip ratio was 0.772 at the rotor inlet. The test section has a constant inner wall diameter of 0.419 m (16.50 in.) and a convergent outer wall with diameters ranging from 0.649 m (25.560 in.) at the base grate screen (Station 0) to 0.512 m (20.163 in.) at the stator exit instrumentation station (Station 4). Approximately 18 deg of rotor preswirl was provided by the IGV; similarly, stage exit air angle was 18 deg from axial.

### Instrumentation

Stage G was instrumented to provide overall and blade element performance data for each blade and vane row. The specific location and type of all instrumentation is presented in figure 86 and summarized by axial station in table XXIII. Wherever possible, redundant measurements were made by using duplicate instrumentation.

Compressor airflow and rotor speed were measured as in Task IV. Inlet total temperature and total pressure were measured in the plenum by a Rosemount precision platinum resistance temperature probe and four fixed, single Kiel head total pressure probes, respectively. Four equally spaced static pressure orifices were located on the inner wall upstream of the inlet guide vane (Station 1B). Radial distribution of total pressure at Station 1A was measured by two fixed, four-sensor Kiel head total pressure rakes.

Radial distributions of total pressure and air angle were measured downstream of the inlet guide vane (Station 2) with two, five-sensor Kiel head total pressure circumferential traverse rakes (at centers of equal areas) and two 30-deg radial traverse wedge probes, respectively. Four equally spaced outer wall and two equally spaced inner wall static pressure orifices were located at Station 2; two of the outer and inner wall orifices were at mid-channel with the other two outer wall orifices downstream of the inlet guide vane trailing edge.

Radial distributions of total pressure/temperature and static pressure/air angle were measured at the rotor exit (Station 3) by means of a single Kiel head and 30-deg wedge traverse probes, respectively. Five outer wall static pressure orifices were located at Station 3 (two at 11% gap and one each at 7, 25, and 57% gap).

Radial distributions of total pressure/temperature and air angle were measured downstream of the stator (Station 4) by four, five-sensor Kiel head circumferential traverse rakes and two 30 deg wedge traverse probes, respectively. Six outer wall static pressure orifices were located at Station 4 (four at mid-gap and one each at 5 and 95% gap). Two of the five-sensor rakes were positioned 1.532 cm (0.603 in.) downstream of stator trailing edge (Station 4A), while the other two were 2.771 cm (1.091 in.) downstream (Station 4B).

Table XXIII. Instrumentation Summary for Stage G

| Axial Location | Type of Instrumentation | No. of Probes | Total Pressure | Air Angle | Static Pressure | Total Temperature | Radial Travel |
|---|---|---|---|---|---|---|---|
| Inlet Duct ASME Orifice | Wall Static | 2 | | | 2 | | |
| | Wall Static | 2 | | | Δ2 | | |
| Plenum | Rosemount Temperature Probe | 1 | | | | 1 | |
| | *Kiel Probe | 4 | 4 | | | | |
| IGV Inlet - Upstream (Instrumentation Station 1A) | *4 Sensor Radial Rake | 2 | 8 | | | | |
| IGV Inlet - Downstream (Instrumentation Station 1B) | *ID Wall Static | 4 | | | 4 | | |
| IGV Exit - Rotor Inlet (Instrumentation Station 2) | 30-deg Wedge (Traverse) | 2 | | 2 | | | 2 |
| | 5 Sensor Radial Rake | 2 | 2 | | | | |
| | *OD Wall Static | 4 | | | 4 | | |
| | *ID Wall Static | 2 | | | 2 | | |
| Rotor Exit - Stator Inlet (Instrumentation Station 3) | Single Kiel Probe (Traverse) | 1 | 1 | | | 1 | 1 |
| | 30-deg Wedge (Traverse) | 1 | | 1 | 1 | | 1 |
| | *OD Wall Static | 5 | | | 5 | | |
| Stator-Stage Exit (Upstream) (Instrumentation Station 4A) | 5 Sensor Radial Rake | 2 | 2 | | | 2 | |
| Stator-Stage Exit (Downstream) (Instrumentation Station 4B) | 5 Sensor Radial Rake | 4 | 20 | | | 20 | |
| | 30-deg Wedge (Traverse) | 2 | | 2 | | | |
| | *OD Wall Static | 6 | | | 6 | | |

*Indicates instrumentation connected to Scanivalve Transducer

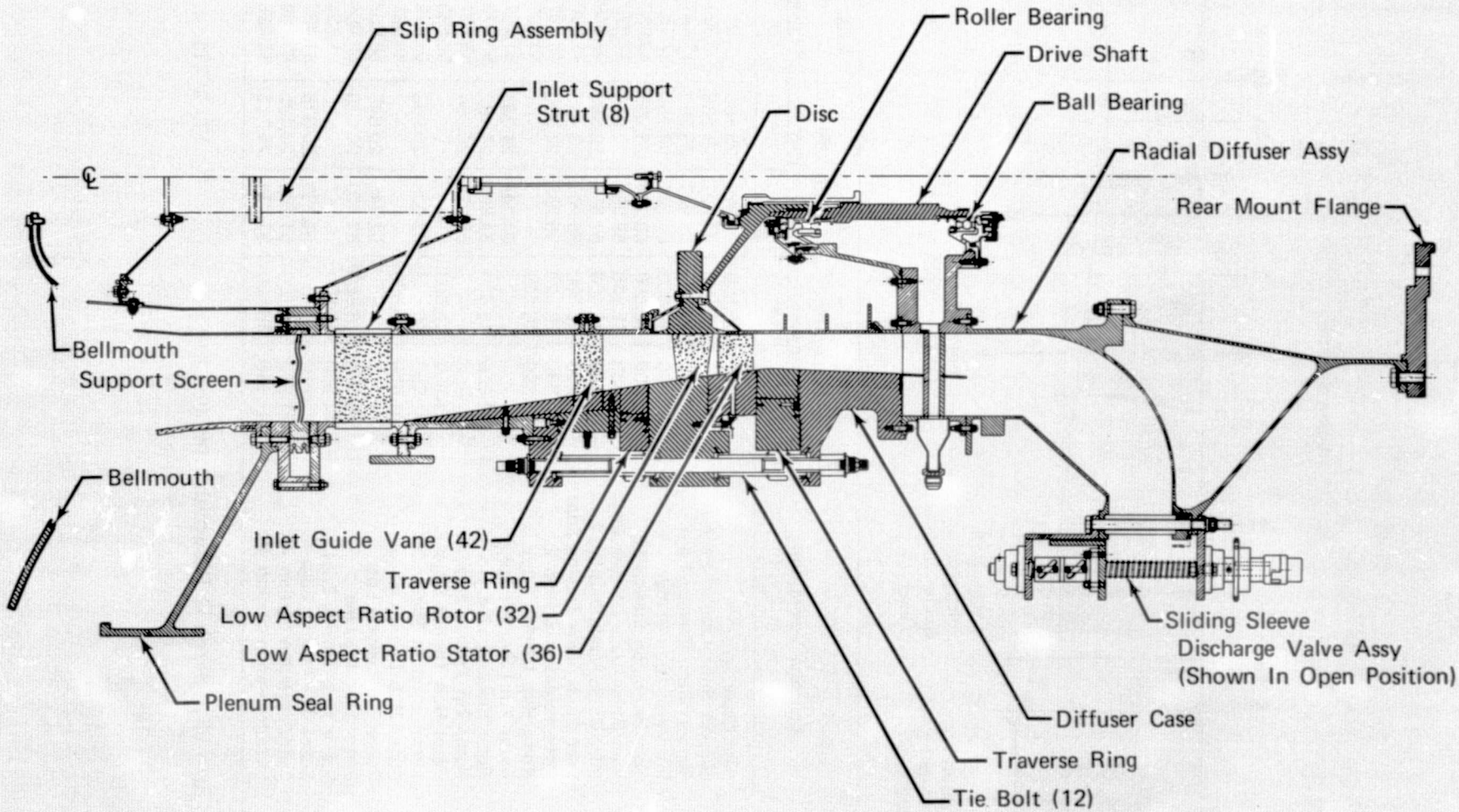


Figure 84. Single Stage Drum Rotor Cantilevered Stator Compressor Rig - Stage G Configuration FD 78416

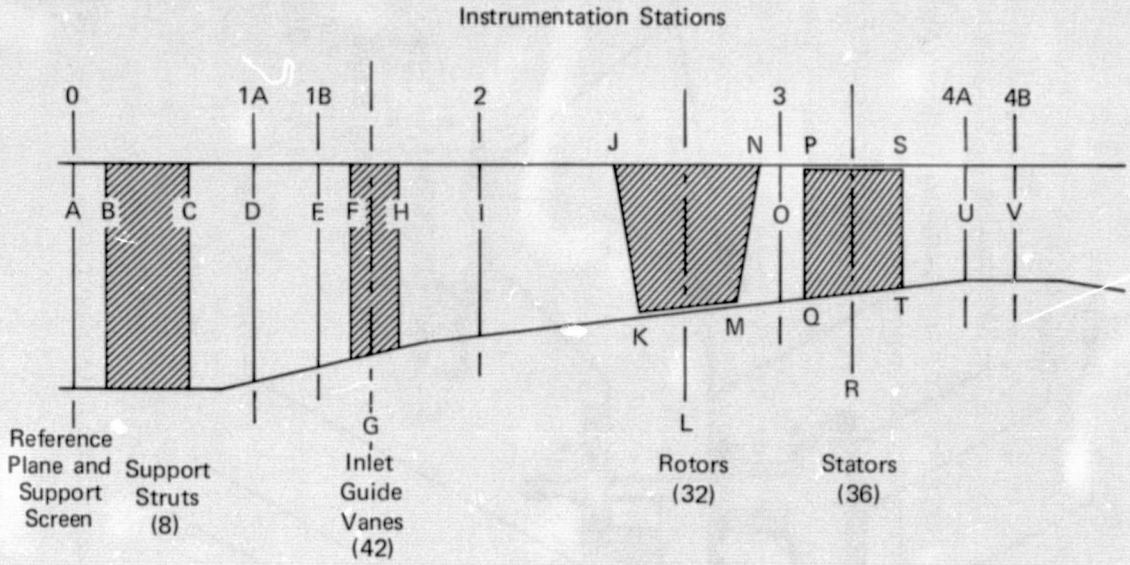


| Flowpath Location | Location Description | Inner Wall Diameter | | Outer Wall Diameter | | Axial Distance from Reference Plane | |
|---|---|---|---|---|---|---|---|
| | | cm | in. | cm | in. | cm | in. |
| A | Base Grate Screen | 41.950 | 16.500 | 64.922 | 25.560 | 0 | 0 |
| B | Support Strut Leading Edge | 41.950 | 16.500 | 64.922 | 25.560 | 5.821 | 2.292 |
| C | Support Strut Trailing Edge | 41.950 | 16.500 | 64.922 | 25.560 | 13.441 | 5.292 |
| D | Instrumentation Station 1A | 41.950 | 16.500 | 61.341 | 24.150 | 27.152 | 10.690 |
| E | Instrumentation Station 1B | 41.950 | 16.500 | 59.324 | 23.356 | 33.830 | 13.319 |
| F | Inlet Guide Vane Leading Edge | 41.950 | 16.500 | 58.090 | 22.870 | 37.922 | 14.930 |
| G | Inlet Guide Vane Stacking Line | 41.950 | 16.500 | 57.556 | 22.660 | 39.649 | 15.610 |
| H | Inlet Guide Vane Trailing Edge | 41.950 | 16.500 | 56.947 | 22.420 | 41.630 | 16.390 |
| I | Instrumentation Station 2 | 41.950 | 16.500 | 55.753 | 21.950 | 45.997 | 18.109 |
| J | Rotor Hub Leading Edge | 41.950 | 16.500 | — | — | 51.069 | 20.106 |
| K | Rotor Tip Leading Edge | — | — | 54.244 | 21.356 | 51.727 | 20.365 |
| L | Rotor Stacking Line | 41.950 | 16.500 | 53.802 | 21.182 | 53.573 | 21.092 |
| M | Rotor Tip Trailing Edge | — | — | 53.223 | 20.954 | 55.821 | 21.977 |
| N | Rotor Hub Trailing Edge | 41.950 | 16.500 | — | — | 56.553 | 22.265 |
| O | Instrumentation Station 3 | 41.950 | 16.500 | 53.005 | 20.868 | 56.672 | 22.312 |
| P | Stator Hub Leading Edge | 41.950 | 16.500 | — | — | 56.883 | 22.395 |
| Q | Stator Tip Leading Edge | — | — | 52.946 | 20.845 | 56.883 | 22.395 |
| R | Stator Stacking Line | 41.950 | 16.500 | 52.400 | 20.630 | 59.004 | 23.230 |
| S | Stator Hub Trailing Edge | 41.950 | 16.500 | — | — | 61.521 | 24.221 |
| T | Stator Tip Trailing Edge | — | — | 51.753 | 20.375 | 61.483 | 24.202 |
| U | Instrumentation Station 4A | 41.950 | 16.500 | 51.284 | 20.192 | 63.789 | 25.114 |
| V | Instrumentation Station 4B | 41.950 | 16.500 | 51.214 | 20.163 | 65.029 | 25.602 |

Figure 85. Stage G Flowpath Dimensions FD 97771

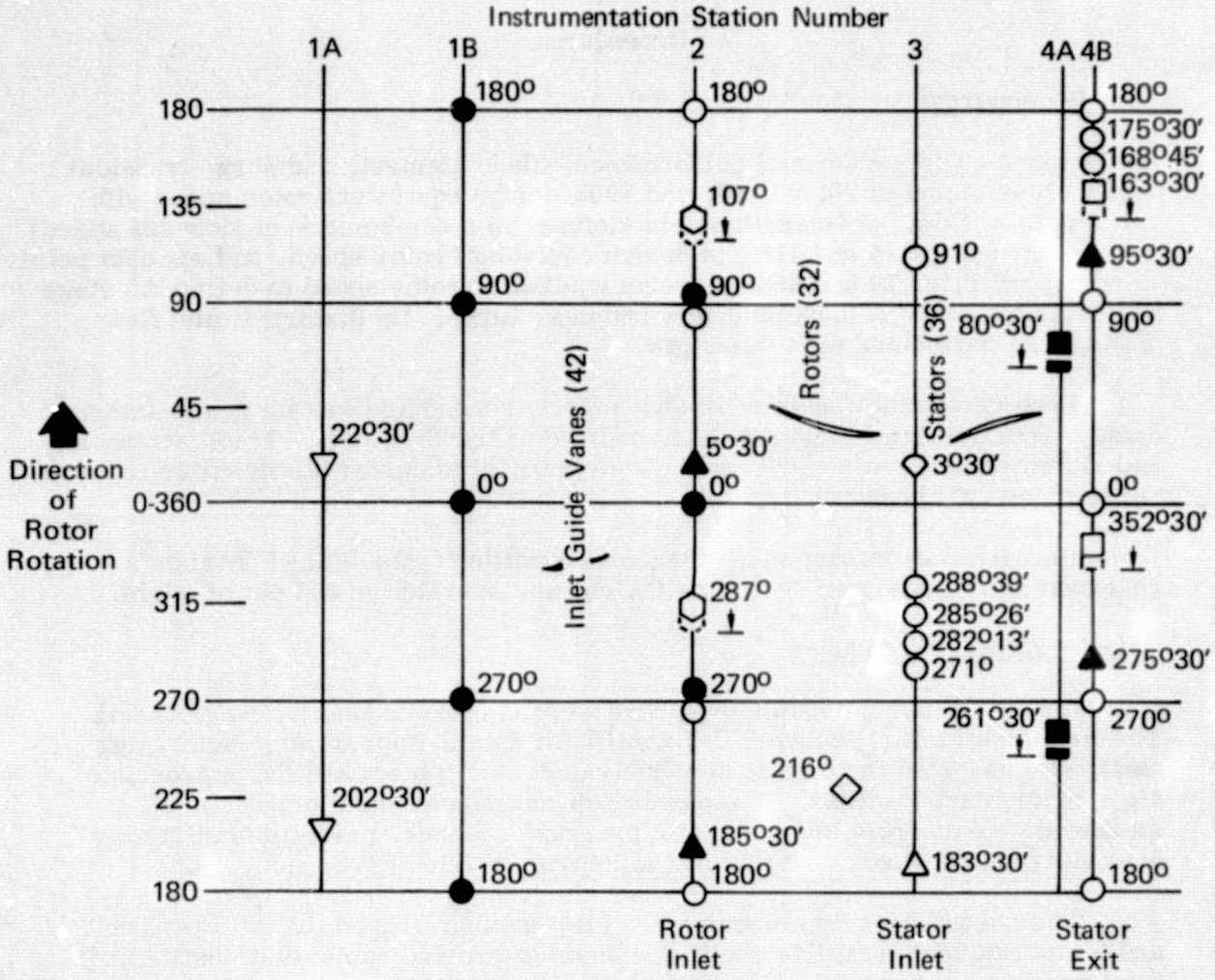


| Symbols | Description |
|---|---|
| ○ | OD Wall Static Pressure Orifice |
| ● | ID Wall Static Pressure Orifice |
| △ | 30 deg Wedge Air Angle/Static Pressure Traverse Probe |
| ▲ | 30 deg Wedge Air Angle Traverse Probe |
| ▽ | Total Pressure Probe (18.9, 42.1, 65.2, and 88.4% Spans) |
| ⬡ | Total Pressure Probe, Circumferentially Traversed Through 22 deg Arc (8.8, 27.2, 46.4, 66.8, and 88.5% Spans) |
| □ | Total Pressure/Temperature Probe Circumferentially Traversed Through 16 deg Arc (9.1, 28.0, 47.5, 67.8 and 89.0% Spans) |
| ■ | Total Pressure/Temperature Probe Circumferentially Traversed Through 16 deg Arc (9.0, 27.4, 46.5, 66.1, and 86.7% Spans) |
| ◇ | Total Pressure/Temperature Traverse Probe - Single Sensor |
| ◇ | Speed Sensor |

Figure 86. Instrumentation Layout for Stage G FD 97772

## Procedures

### Test Procedures

Performance Tests - Overall performance, blade element, and surge transient data were obtained at 70, 85, 95, and 100% design equivalent rotor speed with uniform inlet flow. Seven data points (defined as a combination of flow and speed) were recorded for 95 and 100% of design equivalent rotor speed, and six data points were recorded for 70 and 85% of design equivalent rotor speed to define the stage performance between maximum flow and near surge. No distorted inlet flow testing was performed with this stage.

Each data point consisted of sequentially recording fixed instrumentation data, circumferential traverse data, and radial traverse data. Blade stresses and rig vibration levels were continuously monitored during steady-state and surge transient operating conditions.

Performance during surge transient conditions was defined from data recorded at 10 times per second as the rig was operated in and out of surge.

### Data Reduction Procedures

A total of four computer programs were used to reduce the Stage G data. The first program: (1) converted the millivolt data to appropriate engineering units; (2) converted the data to absolute values; and (3) applied the appropriate Mach number corrections. A separate subroutine was used to process all steady-state data from the pneumatic pressure scanner, perform preliminary averaging calculations, and provide an instrumentation error analysis.

The second program circumferentially mass averaged the total pressure and temperature data at five radial locations to provide radial distributions of total pressure at the guide vane exit and total pressure, total temperature at the stator exit.

The third program used continuity, energy, and radial equilibrium equations to calculate rotor and stator exit static pressure and rotor exit air angle distributions. The required program input was compressor geometry, airflow, speed, IGV and rotor inlet total pressure and air angle, rotor exit total pressure and temperature, and stator exit total pressure and air angle. Rotor exit total pressure profiles were obtained in the same manner as for Stage F, (see page 49). The measured rotor exit total pressure was not used because the rotor had been locally back pressured by its proximity to the instrumentation. An axial, one-dimensional blockage distribution was used to achieve agreement between the measured outer wall static and calculated pressures at the rotor and stator exits. This calculation provided the input for the fourth and final data reduction step.

The fourth program calculated blade element performance variables for the inlet guide vane, rotor, and stator. Radial distributions of total and static pressures, total temperatures, and air angles as determined in the previous steps were input at each axial station.

## Overall Performance

Total pressure ratios and adiabatic efficiencies were calculated for the rotor, rotor-stator, and inlet guide vane-rotor-stator, i.e., stage. The inlet guide vane, rotor and stator exit total pressures and total temperatures were weighted according to local mass flow to obtain average values. This calculation procedure was described in Part I. The mass-averaged stator exit total temperatures were used for rotor, rotor-stator, and stage efficiency calculations.

## Blade Element Performance and Flow Distribution Data

Blade element performance calculations were made along design streamlines that pass through 10, 30, 50, 70 and 90% span at the rotor exit station. The calculations were performed at the instrumentation stations and at the inlet guide vane, rotor and stator leading and trailing edges. The pressures, temperatures, and air angles at the blade row leading and trailing edges were obtained by translating the measured values from the instrumentation stations assuming conservation of angular momentum, conservation of energy, continuity, and flow along design streamlines. A description of the translation method is presented in Reference 3.

## Surge Transient Data

The point of incipient surge was determined from examination of the orifice pressure drop, plenum pressure, bellmouth pressure and rotor exit pressure data that were recorded at 10 scans per second. Orifice pressure drop was determined at the incipient surge point, and the corresponding weight flow was determined from the correlation of orifice pressure drop and orifice weight flow shown in figure 87. The steady-state pressure ratio data were extrapolated to the stall flow using the shape of the steady-state data curve as a guideline. Incipient stall points were determined in this manner for each rotor speed.

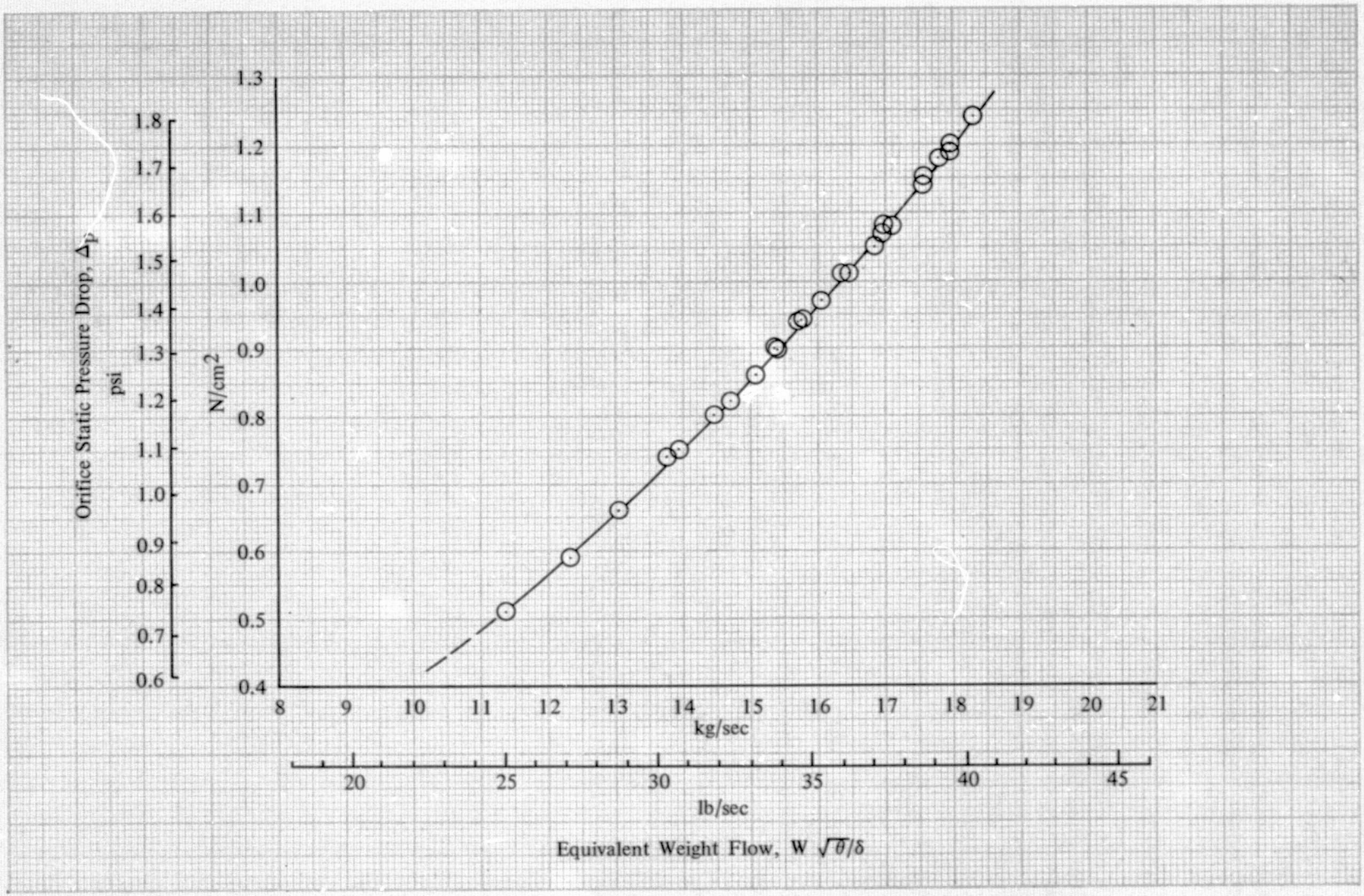


Figure 87. Orifice Static Pressure Drop vs Equivalent Weight Flow for Stage G Flowpath With Support Screen

DF 102269

## Presentation of Data

### Overall Performance

Overall performance data are presented in terms of total pressure ratio and adiabatic efficiency as functions of equivalent weight flow for 70, 85, 95 and 100% design equivalent rotor speed for the rotor, rotor-stator, and inlet guide vane-rotor-stator, i.e., stage, in figures 88, 89, and 90, respectively. The dashed stall line in each of these figures passes through surge points determined from the transient data. Pressure ratio, adiabatic efficiency, and polytropic efficiency for the rotor, rotor-stator, and stage are also tabulated for the steady-state data points in table XXIV and repeated in Appendix C, Volume II.

Based on a curve faired through the data points, the rotor achieved an adiabatic efficiency of 89.9% and a total pressure ratio of 1.640 at design equivalent rotor speed and flow. At the same flow and rotor speed, the rotor-stator achieved an adiabatic efficiency of 83.5% and a total pressure ratio of 1.585, and the stage achieved an adiabatic efficiency of 83.0% and a total pressure ratio of 1.580. At design equivalent rotor speed, rotor, rotor-stator, and stage peak adiabatic efficiencies of 90.0, 84.7, and 84.1%, respectively, were reached at approximately 101.4, 105.8, and 105.3% design equivalent flow. Corresponding surge margins were 11.9, 16.1, and 16.5%.

### Blade Element Performance and Flow Distribution Data

As discussed on page 50, the blade element performance data were calculated for the instrumentation stations and for the IGV, rotor and stator leading and trailing edges. Table C-2 of Appendix C, Volume II presents instrumentation station data for the near design point and is included only to illustrate the difference at the near design point between values calculated from the data at these locations and those that have been translated to the blade row leading and trailing edges. The differences are small except for the values translated to the IGV trailing edge and the rotor leading edge. These differences are caused by the convergence of the OD wall between the IGV and rotor (reduction of approximately 18% in annulus area). Only the translated values are given in tables C-3 and C-4 of Appendix C, Volume II for the remaining compressor test points. The plotted results discussed for the rotor and stator in the following paragraphs are based on the translated data.

Inlet Guide Vane Blade Element Performance - The inlet guide vane exit air angle distribution is presented in figure 91 for the data point closest to design speed and flow. Air angle data obtained with the two 30-deg wedge probes are compared to the predicted exit air angle profile. In general, the air angles measured with the two probes agree closely with a maximum difference of approximately one deg. The average of the measured air angles agrees within 1.5 deg of the predicted air angle across the span except at the tip where the difference increases to approximately 2 deg.

Rotor Blade Element Performance - Rotor diffusion factor, deviation angle, and loss coefficient are shown as functions of incidence angle in figures 92a through 92e. At the design incidence angle and rotor speed, the loss coefficient was approximately equal to the predicted value across the span, except at the hub (90% span) where losses were above the predicted level. Except at 30% span, the deviation angles were greater than the predicted level, especially at the tip (approximately 11 deg). The diffusion factors were approximately the same as the predicted values across the span.

Loss parameter versus diffusion factor is presented in figures 93a through 93e for 10, 30, 50, 70, and 90% span, respectively. The predicted value and the data point corresponding to the minimum loss coefficient at design equivalent rotor speed are shown in each figure. The minimum loss data point was selected as that data point closest to the center of the low loss region of the loss versus incidence profile. A comparison of the minimum loss data with the predicted values indicates that Rotor G operated at a lower diffusion factor, lower loss than predicted from 10 through 30% span, at a slightly higher diffusion factor, lower loss from 50 through 70% span, and at a higher diffusion factor, higher loss at 90% span.

Stator Blade Element Performance - Stator diffusion factor, deviation angle, and loss coefficient are presented as functions of incidence angle in figures 94a through 94e. At design incidence angle and rotor speed, the loss coefficient was approximately the same as the predicted value from 10 through 30% span, slightly above from 50 through 70% span, and slightly less at 90% span. Deviation angles, at design incidence, were one to two degrees less than the predicted value from 10 through 50% span, approximately equal at 70% span, and approximately three to four degrees more at 90% span. Diffusion factors were slightly less than the predicted values across the span.

Loss parameter versus diffusion factor is shown in figures 95a through 95e for 10, 30, 50, 70, and 90% spans, respectively. The predicted value and the data point corresponding to the minimum loss coefficient at design equivalent rotor speed are shown on each figure. A comparison of the minimum loss data with the predicted values indicates that Stator G operated at a lower diffusion factor than predicted. The loss was lower than predicted at both the hub and tip, but higher across the mid-span region of the vane.

Wall Static Pressure - The wall static pressure data at instrumentation stations 3 and 4 were examined to determine if circumferential gradients with respect to the stator vanes were significant. As with Stage F, the variations in static pressure at different circumferential locations, at approximately the same location relative to the stator vane, were small compared to the variations that existed within one stator vane gap. It was concluded that no significant circumferential variation existed but that there was substantial gap-wise variation in the data. This gap-wise variation was present at all speeds as was the case with Stage F. As an example, this variation is illustrated in figure 96 for the design equivalent flow and speed data point.

## Summary

At design equivalent rotor speed and flow, the rotor achieved an adiabatic efficiency of 89.9% at a pressure ratio of 1.640. Similarly, the rotor-stator achieved an adiabatic efficiency of 83.5% at a pressure ratio of 1.585 as compared to a design efficiency and pressure ratio of 84.14% and 1.604, respectively. At design equivalent rotor speed, the rotor and rotor-stator peak adiabatic efficiencies were 90.0 and 84.7%, respectively, occurring at 101.4 and 105.8% design equivalent flow.

Table XXIV. Overall Performance of Stage G
Uniform Inlet

| (IGV Inlet) Equivalent Weight Flow kg/sec | lb/sec | Rotor $\overline{P}_3/\overline{P}_2$ | Rotor $\eta_{ad}$ | Rotor $\eta_p$ | Rotor - Stator $\overline{P}_4/\overline{P}_2$ | Rotor - Stator $\eta_{ad}$ | Rotor - Stator $\eta_p$ | IGV - Rotor - Stator $\overline{P}_4/\overline{P}_1$ | IGV - Rotor - Stator $\eta_{ad}$ | IGV - Rotor - Stator $\eta_p$ |
|---|---|---|---|---|---|---|---|---|---|---|
| | | | | 100% Design Equivalent Rotor Speed | | | | | | |
| 18.27 | 40.29 | 1.413 | 0.774 | 0.785 | 1.360 | 0.685 | 0.698 | 1.353 | 0.674 | 0.686 |
| 17.96 | 39.59 | 1.575 | 0.888 | 0.896 | 1.542 | 0.843 | 0.853 | 1.533 | 0.833 | 0.842 |
| 17.56 | 38.72 | 1.606 | 0.891 | 0.900 | 1.571 | 0.847 | 0.858 | 1.564 | 0.840 | 0.850 |
| 16.98 | 37.43 | 1.629 | 0.894 | 0.902 | 1.587 | 0.842 | 0.853 | 1.580 | 0.835 | 0.845 |
| 16.43 | 36.23 | 1.648 | 0.902 | 0.910 | 1.585 | 0.828 | 0.839 | 1.579 | 0.821 | 0.832 |
| 15.70 | 34.62 | 1.666 | 0.889 | 0.899 | 1.585 | 0.797 | 0.811 | 1.578 | 0.790 | 0.803 |
| 15.38 | 33.92 | 1.676 | 0.884 | 0.893 | 1.584 | 0.782 | 0.796 | 1.579 | 0.776 | 0.790 |
| | | | | 95% Design Equivalent Rotor Speed | | | | | | |
| 17.95 | 39.58 | 1.382 | 0.799 | 0.809 | 1.338 | 0.717 | 0.728 | 1.332 | 0.705 | 0.717 |
| 17.79 | 39.23 | 1.475 | 0.870 | 0.879 | 1.449 | 0.829 | 0.839 | 1.441 | 0.817 | 0.826 |
| 17.53 | 38.64 | 1.511 | 0.900 | 0.906 | 1.484 | 0.858 | 0.866 | 1.477 | 0.848 | 0.856 |
| 16.91 | 37.27 | 1.550 | 0.909 | 0.915 | 1.511 | 0.853 | 0.862 | 1.503 | 0.842 | 0.850 |
| 16.35 | 36.04 | 1.575 | 0.904 | 0.911 | 1.529 | 0.841 | 0.852 | 1.522 | 0.833 | 0.842 |
| 15.77 | 34.76 | 1.585 | 0.902 | 0.909 | 1.530 | 0.828 | 0.839 | 1.524 | 0.821 | 0.831 |
| 15.38 | 33.90 | 1.597 | 0.902 | 0.911 | 1.527 | 0.811 | 0.823 | 1.522 | 0.806 | 0.817 |
| | | | | 85% Design Equivalent Rotor Speed | | | | | | |
| 17.09 | 37.68 | 1.308 | 0.816 | 0.823 | 1.289 | 0.769 | 0.778 | 1.282 | 0.752 | 0.761 |
| 16.83 | 37.11 | 1.364 | 0.899 | 0.905 | 1.344 | 0.854 | 0.861 | 1.338 | 0.843 | 0.848 |
| 16.07 | 35.44 | 1.386 | 0.915 | 0.921 | 1.366 | 0.873 | 0.880 | 1.358 | 0.857 | 0.863 |
| 15.40 | 33.96 | 1.405 | 0.912 | 0.915 | 1.383 | 0.867 | 0.873 | 1.378 | 0.858 | 0.863 |
| 14.69 | 32.38 | 1.426 | 0.907 | 0.911 | 1.400 | 0.857 | 0.864 | 1.396 | 0.849 | 0.857 |
| 13.92 | 30.70 | 1.441 | 0.893 | 0.899 | 1.408 | 0.833 | 0.842 | 1.403 | 0.825 | 0.833 |
| | | | | 70% Design Equivalent Rotor Speed | | | | | | |
| 15.08 | 33.24 | 1.223 | 0.887 | 0.890 | 1.213 | 0.849 | 0.853 | 1.208 | 0.831 | 0.835 |
| 14.42 | 31.78 | 1.239 | 0.917 | 0.920 | 1.225 | 0.866 | 0.872 | 1.220 | 0.848 | 0.854 |
| 13.74 | 30.29 | 1.245 | 0.909 | 0.913 | 1.235 | 0.877 | 0.879 | 1.231 | 0.863 | 0.866 |
| 13.01 | 28.68 | 1.261 | 0.900 | 0.905 | 1.250 | 0.867 | 0.871 | 1.246 | 0.855 | 0.858 |
| 12.30 | 27.12 | 1.275 | 0.900 | 0.904 | 1.262 | 0.861 | 0.866 | 1.258 | 0.849 | 0.854 |
| 11.38 | 25.10 | 1.292 | 0.896 | 0.899 | 1.270 | 0.832 | 0.839 | 1.266 | 0.820 | 0.828 |

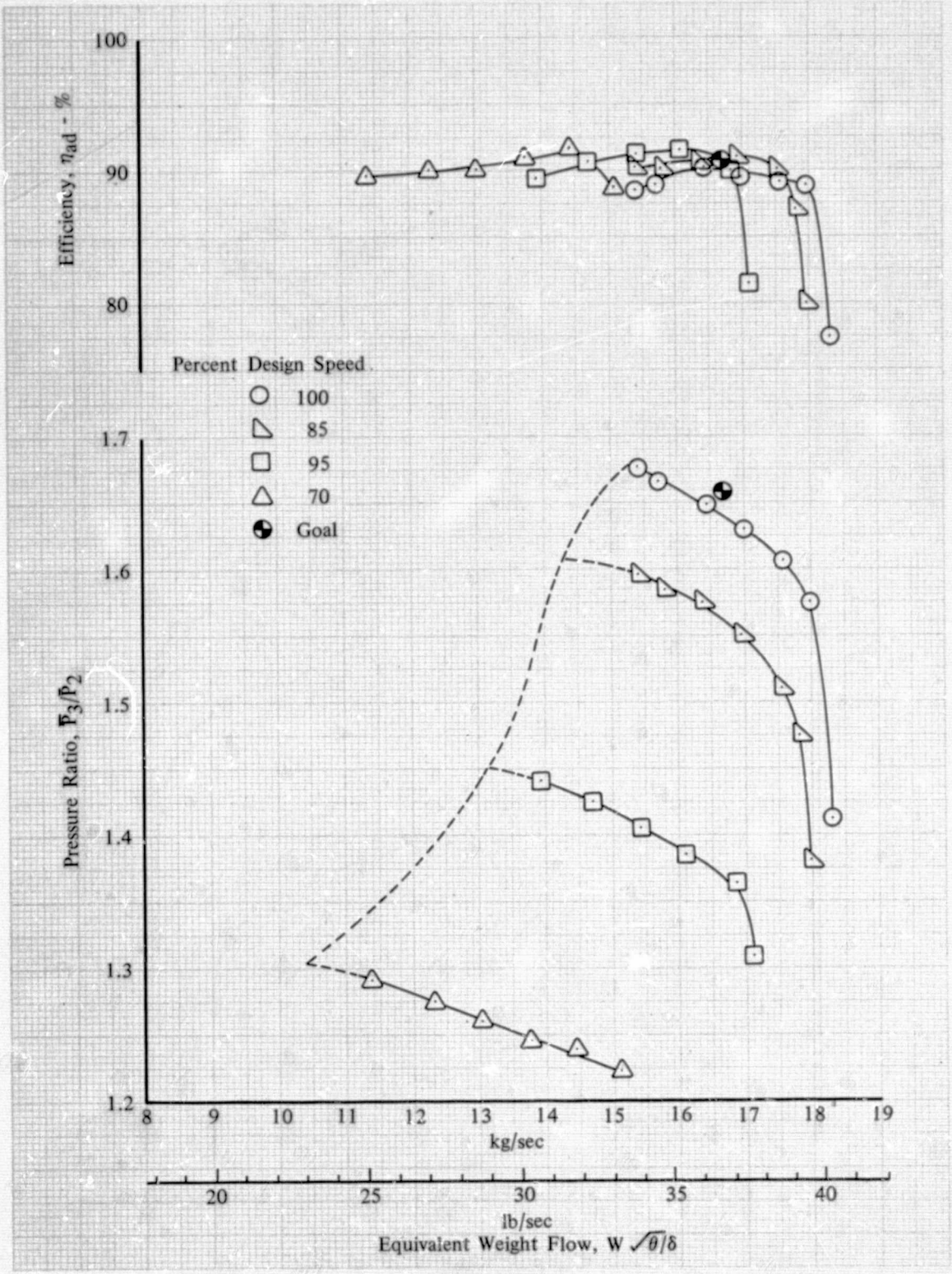


Figure 88. Overall Performance of Rotor G with Uniform Inlet Flow DF 102270

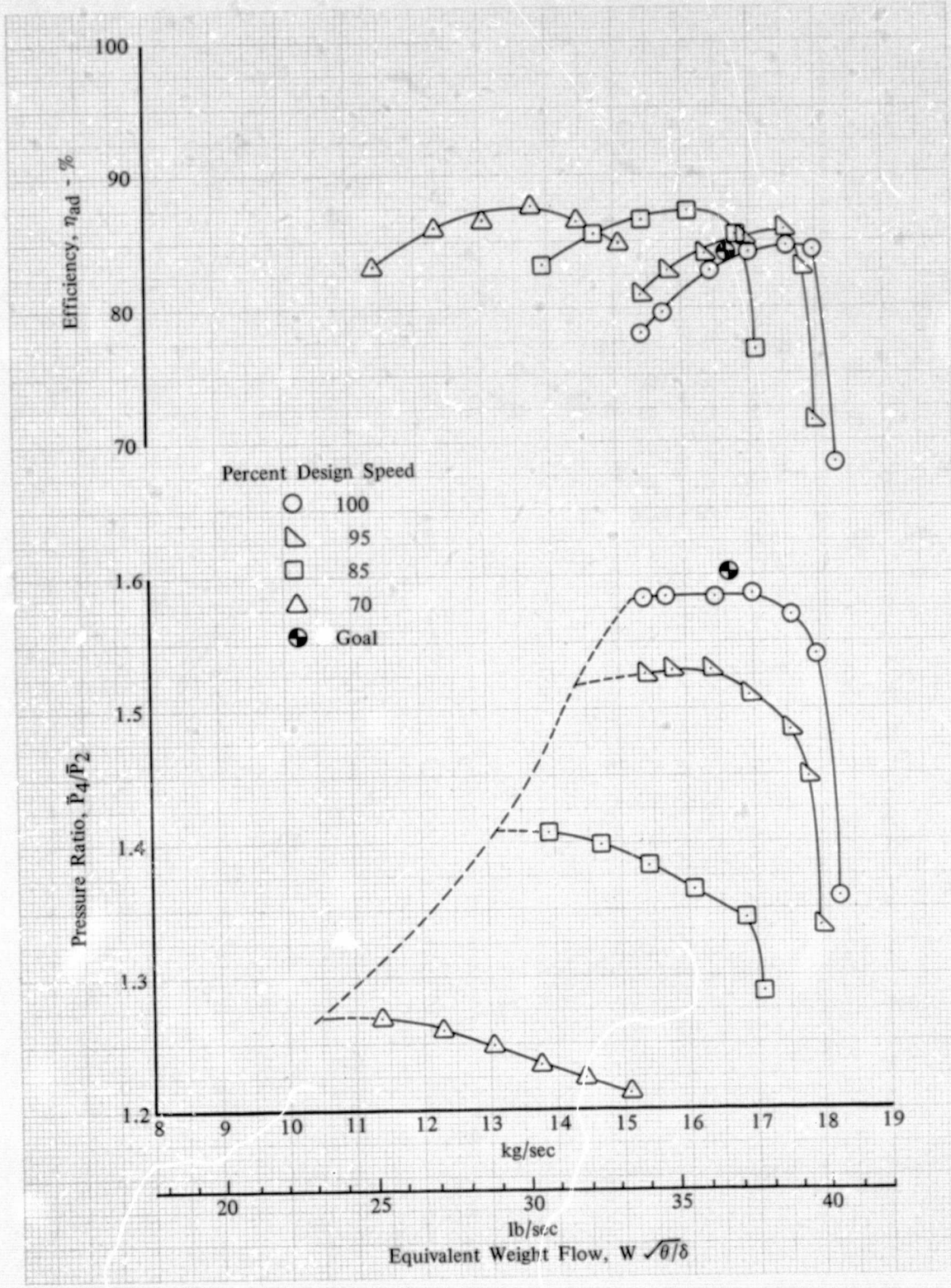


Figure 89. Overall Performance of Rotor G-Stator G with Uniform Inlet Flow DF 102271

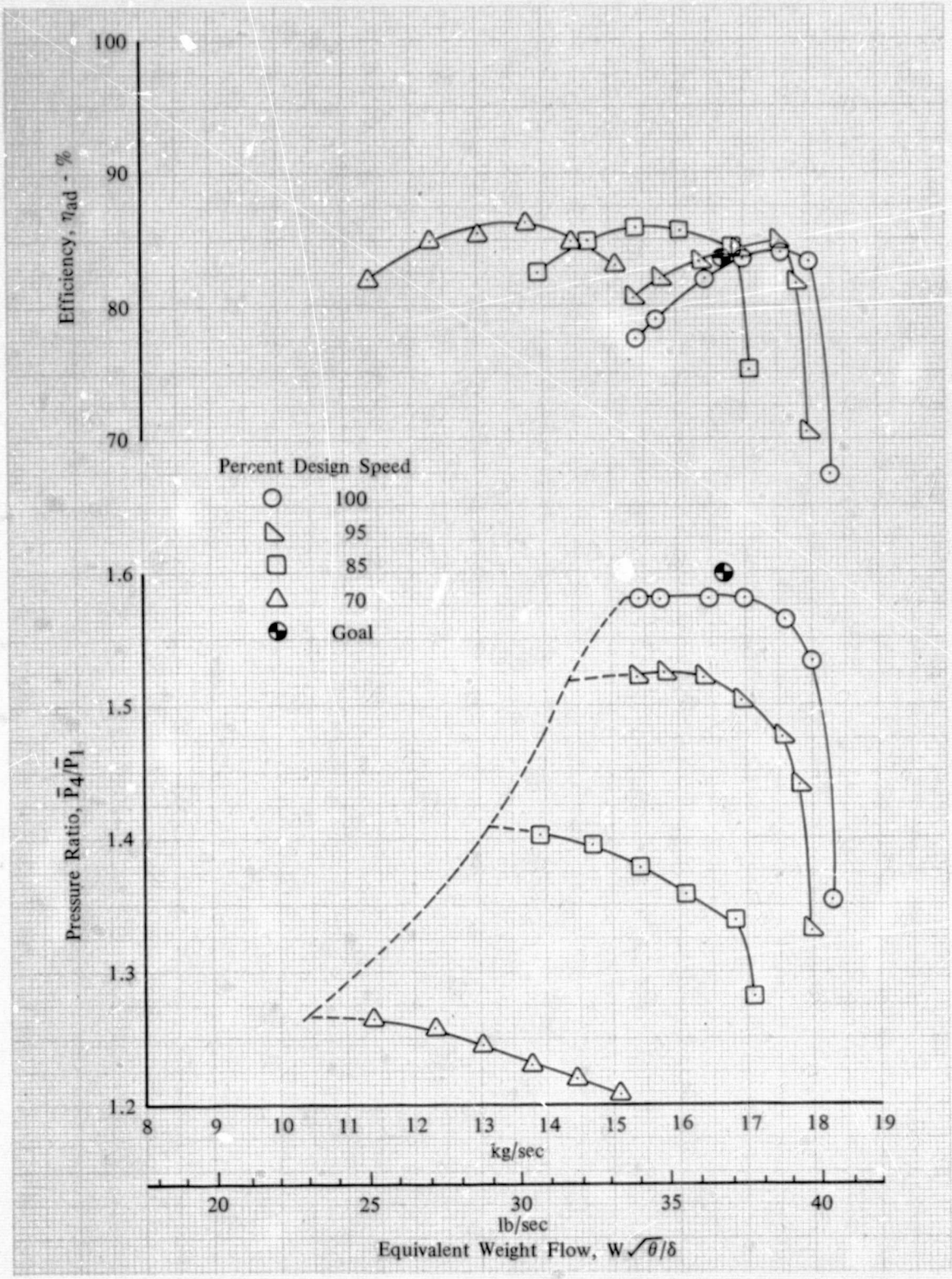


Figure 90. Overall Performance of Stage G with Uniform Inlet Flow DF 102272

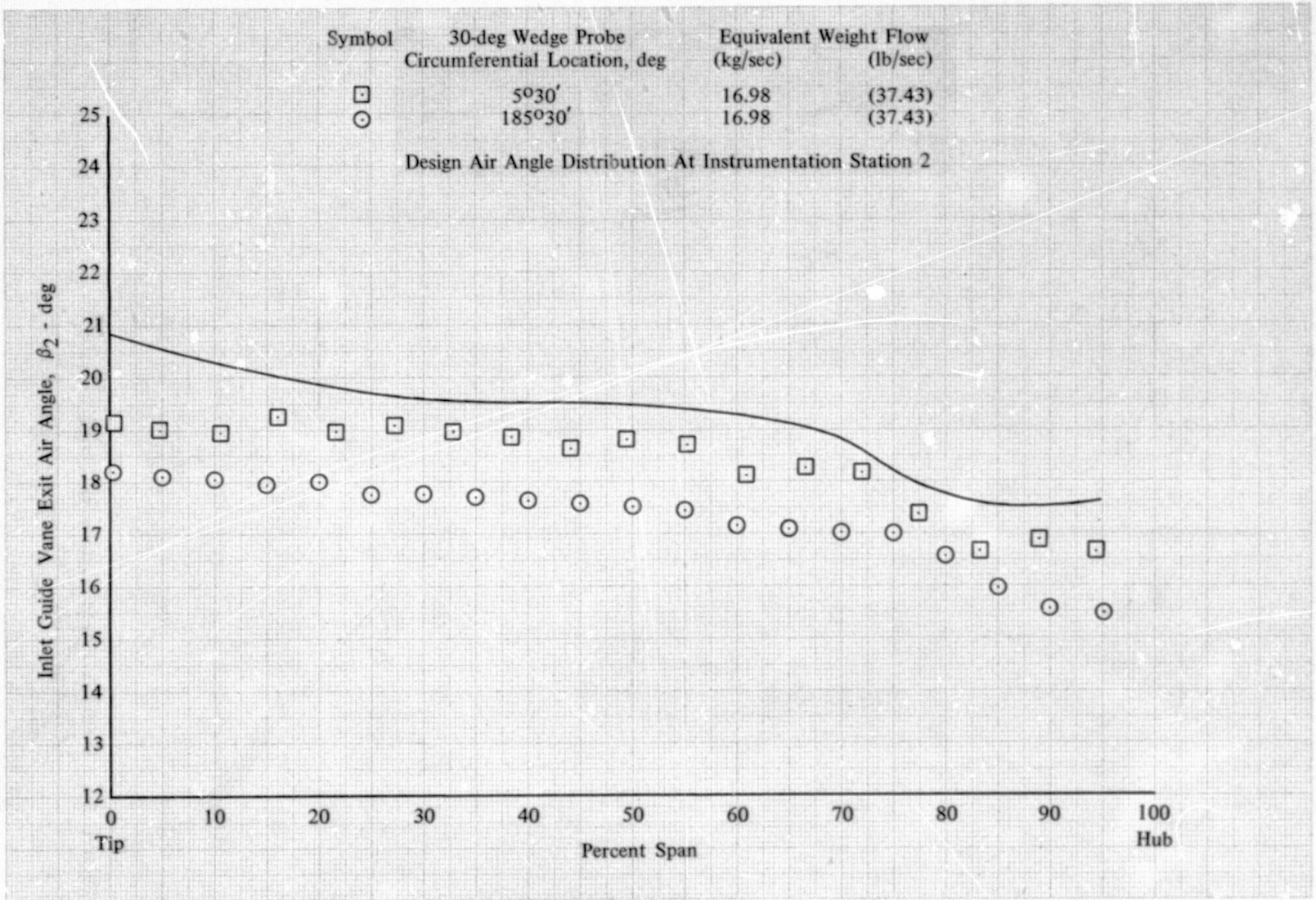


Figure 91. Stage G Inlet Guide Vane Exit Air Angle Distribution

DF 102273

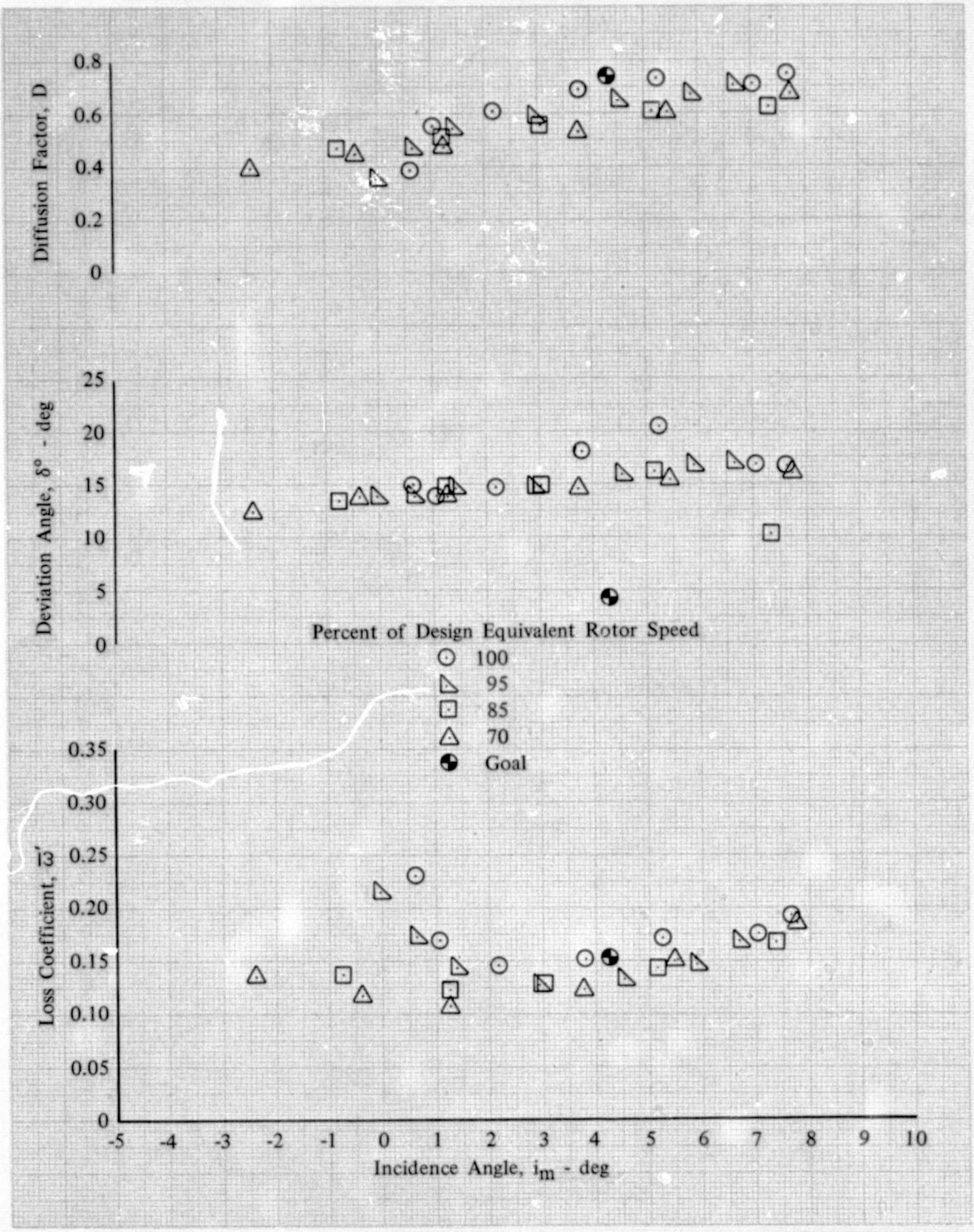


Figure 92a. Rotor G Blade Element Performance, 10% Span from Tip; Uniform Inlet Flow DF 102274

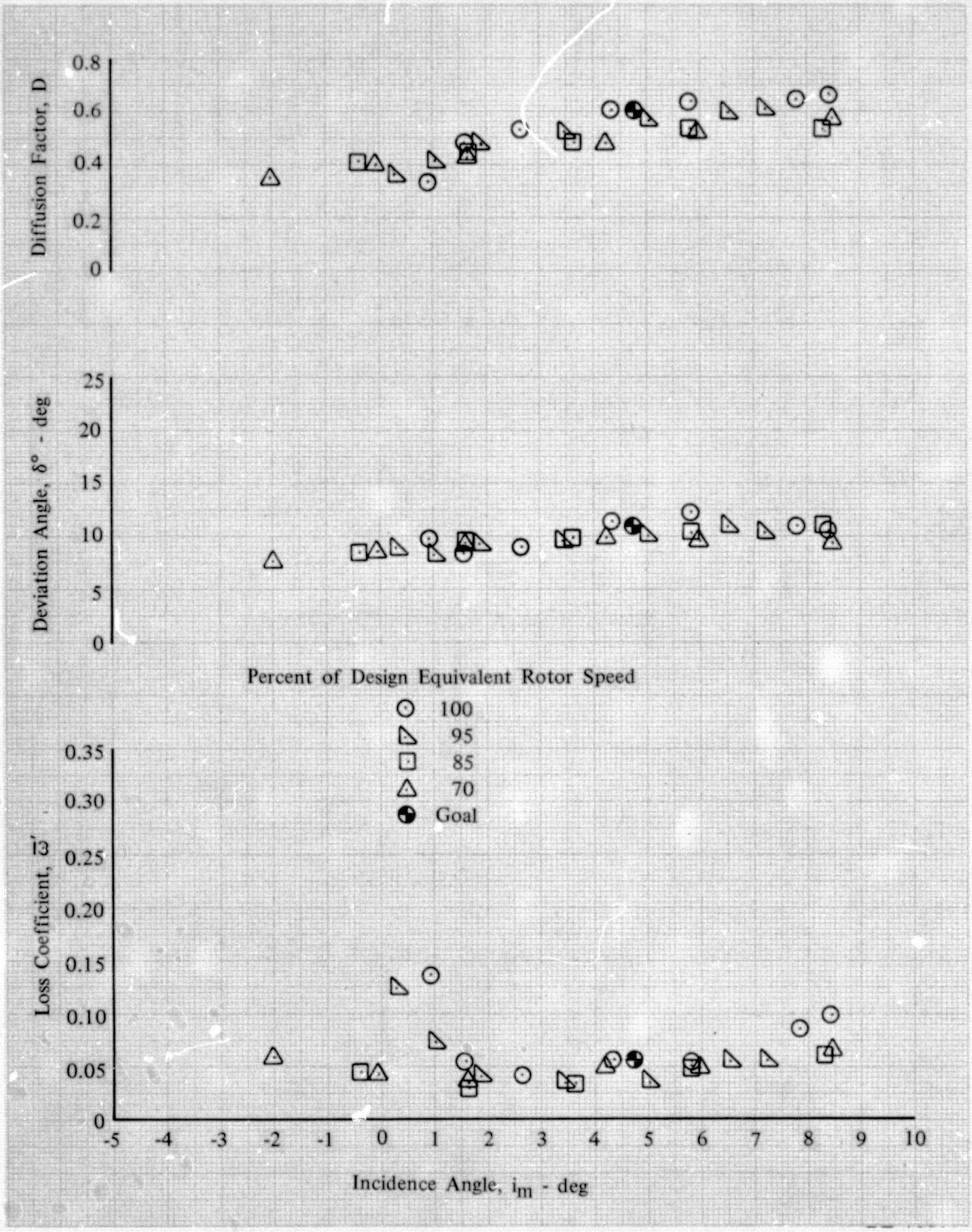


Figure 92b. Rotor G Blade Element Performance, 30% Span from Tip; Uniform Inlet Flow DF 102275

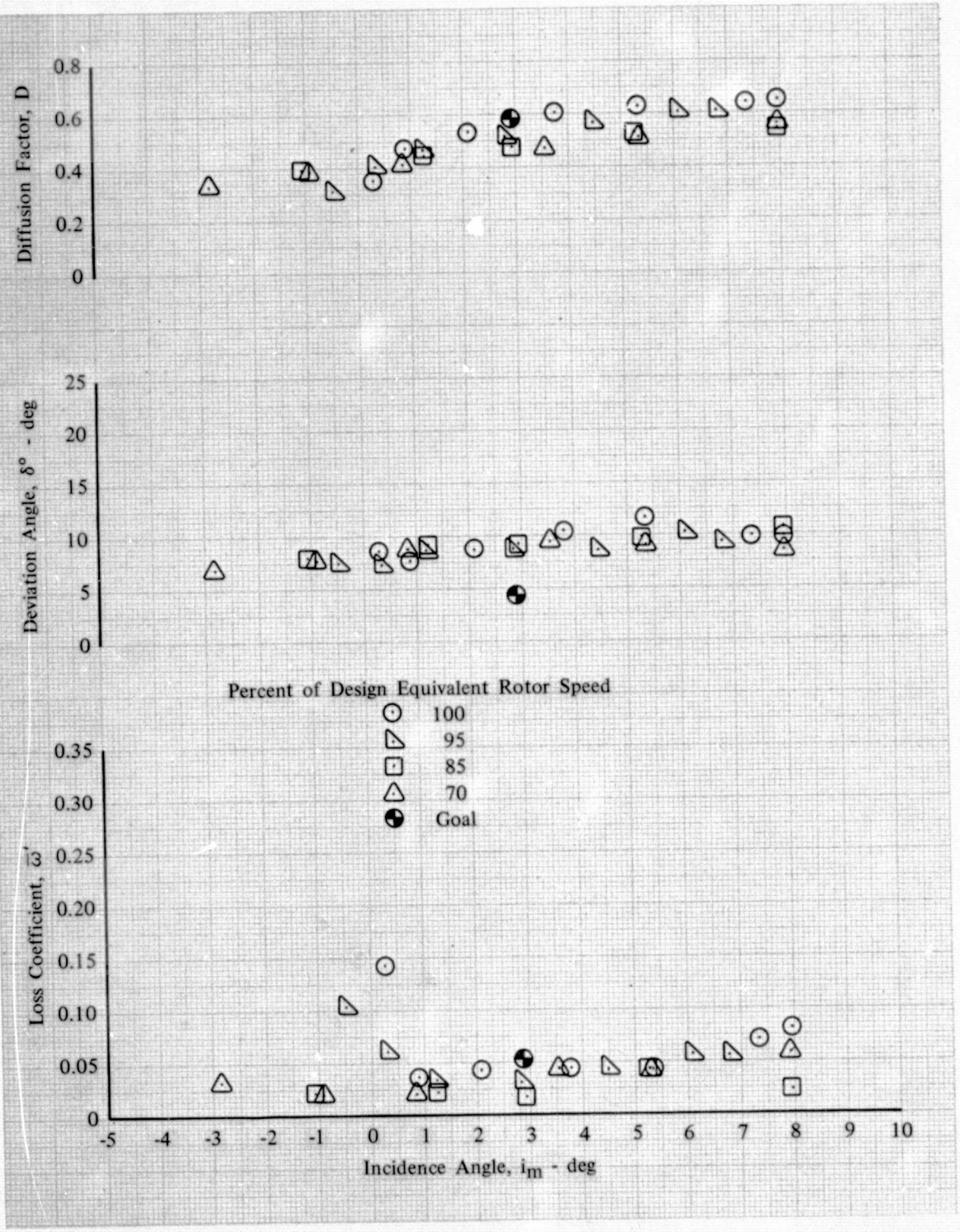


Figure 92c. Rotor G Blade Element Performance, 50% Span; Uniform Inlet Flow

DF 102276

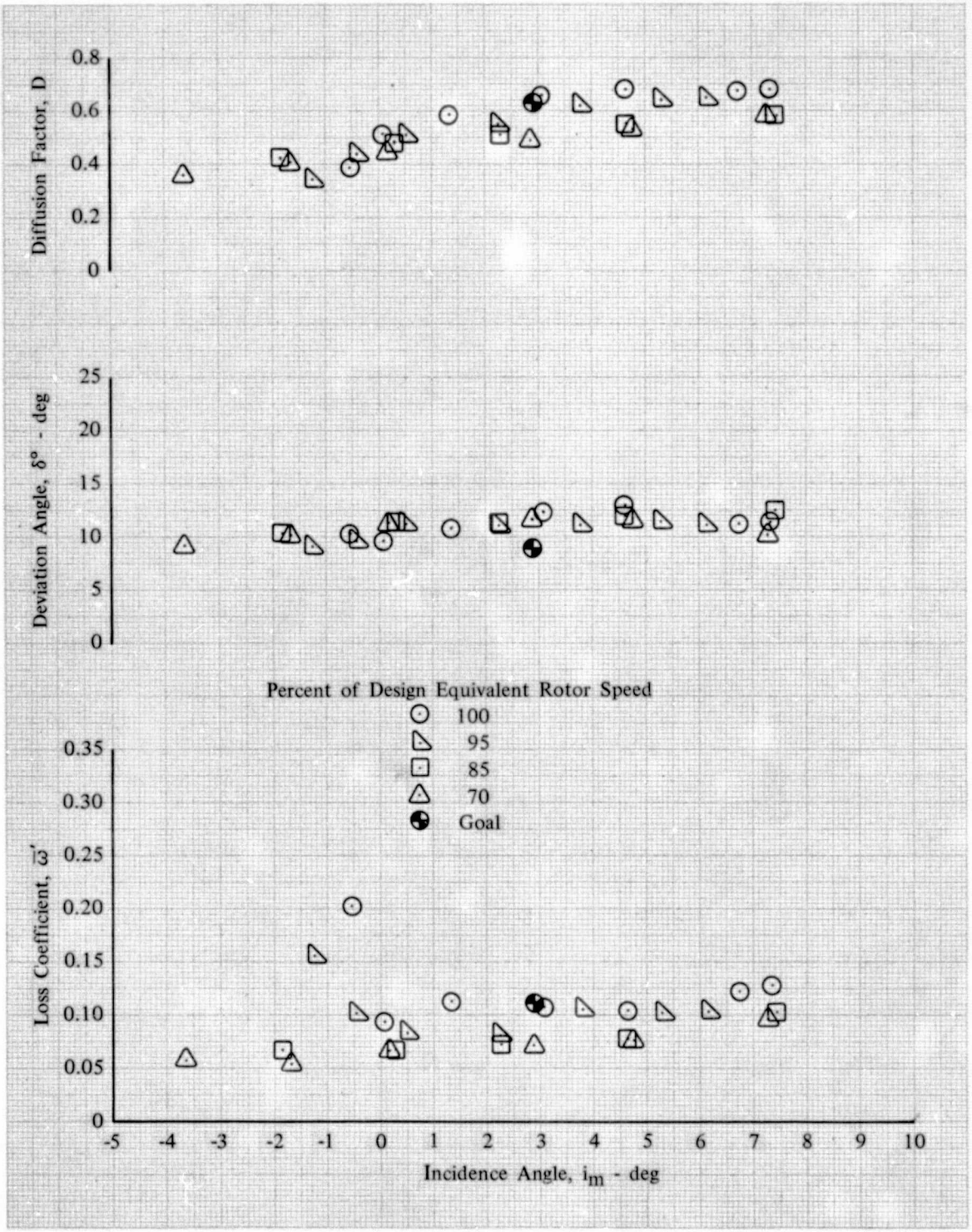


Figure 92d. Rotor G Blade Element Performance, 70% Span from Tip; Uniform Inlet Flow DF 102277

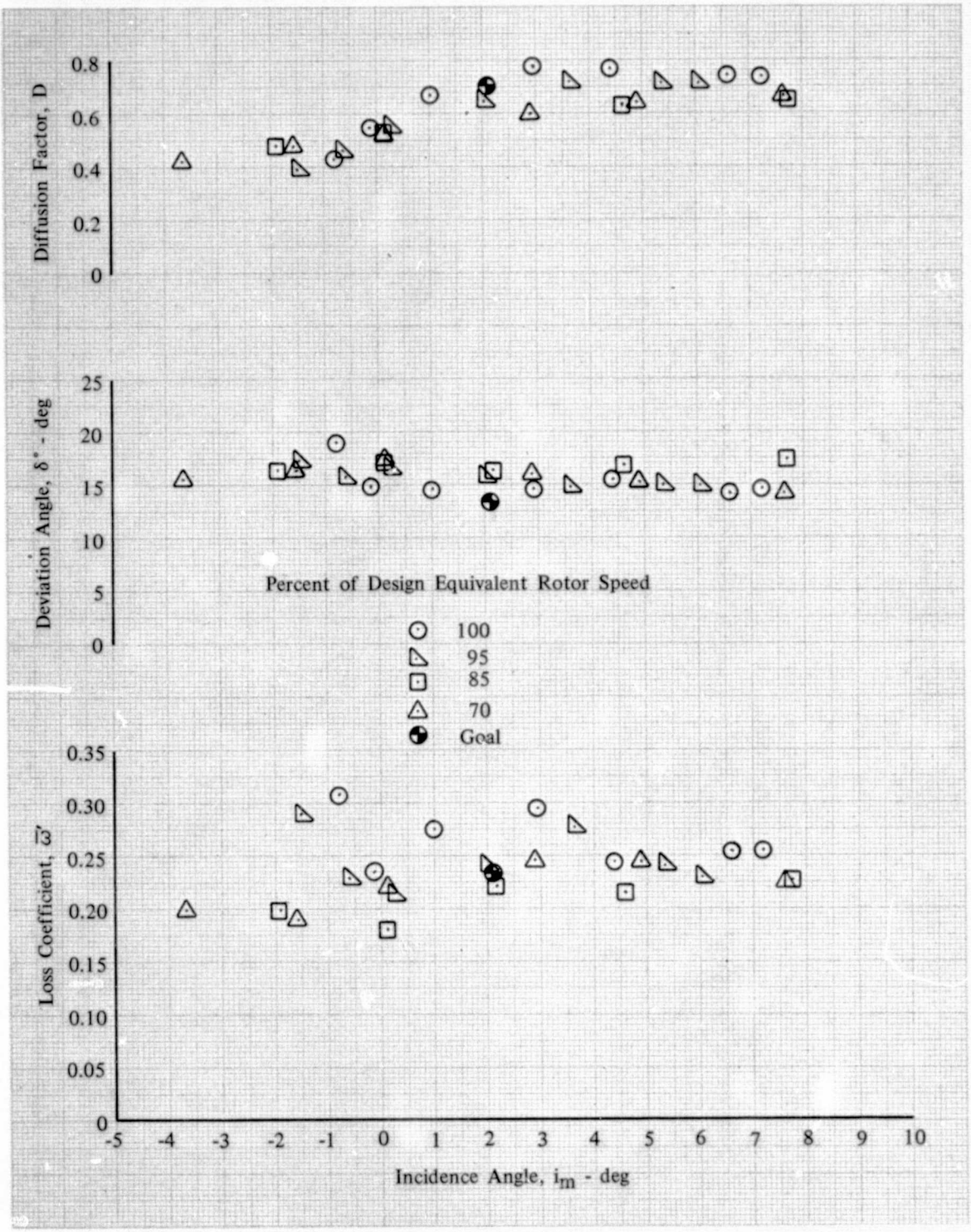


Figure 92e. Rotor G Blade Element Performance, 90% Span from Tip; Uniform Inlet Flow DF 102278

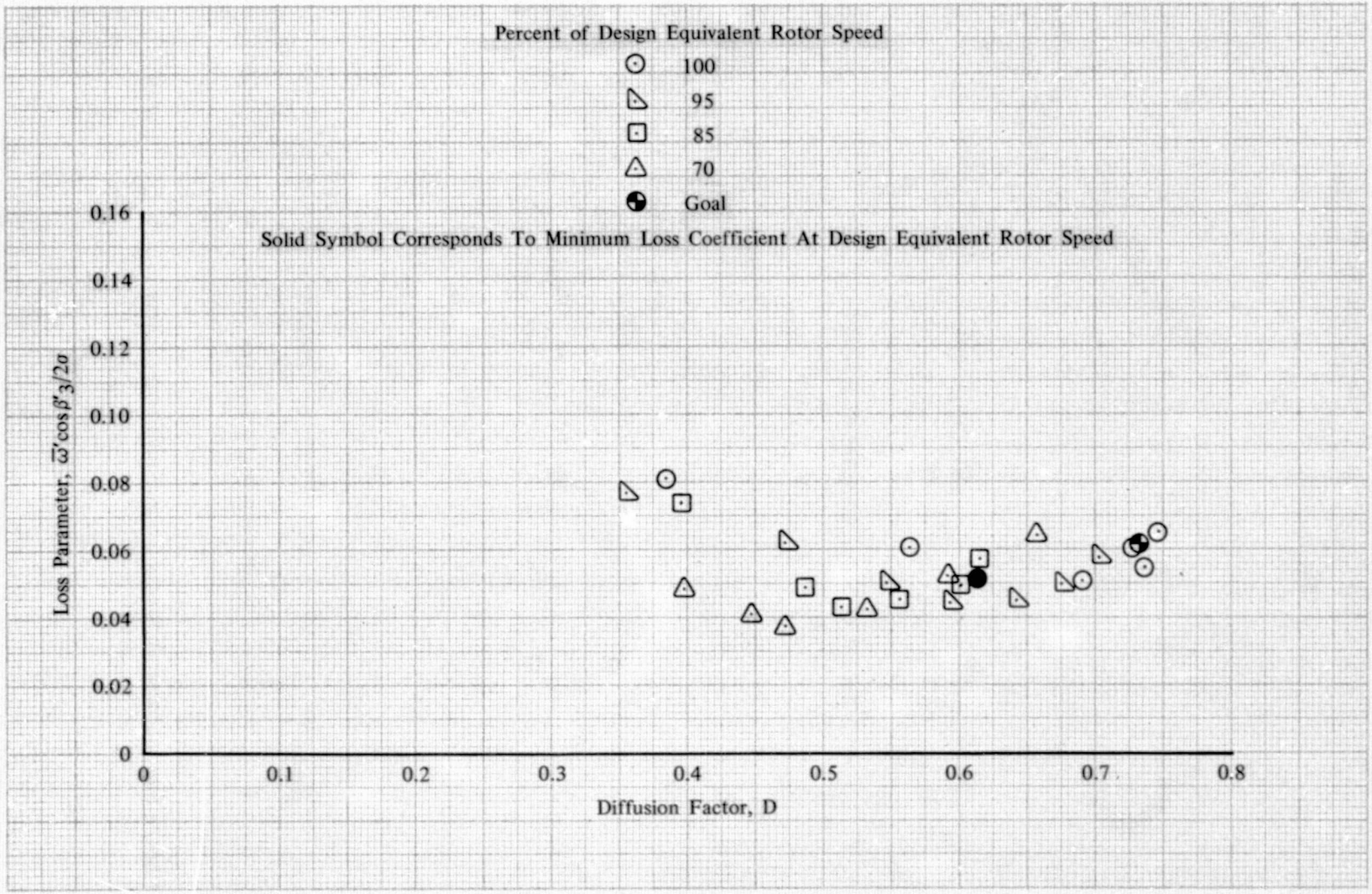


Figure 93a. Rotor G Loss Parameter vs Diffusion Factor, 10% Span from Tip; Uniform Inlet Flow DF 102279

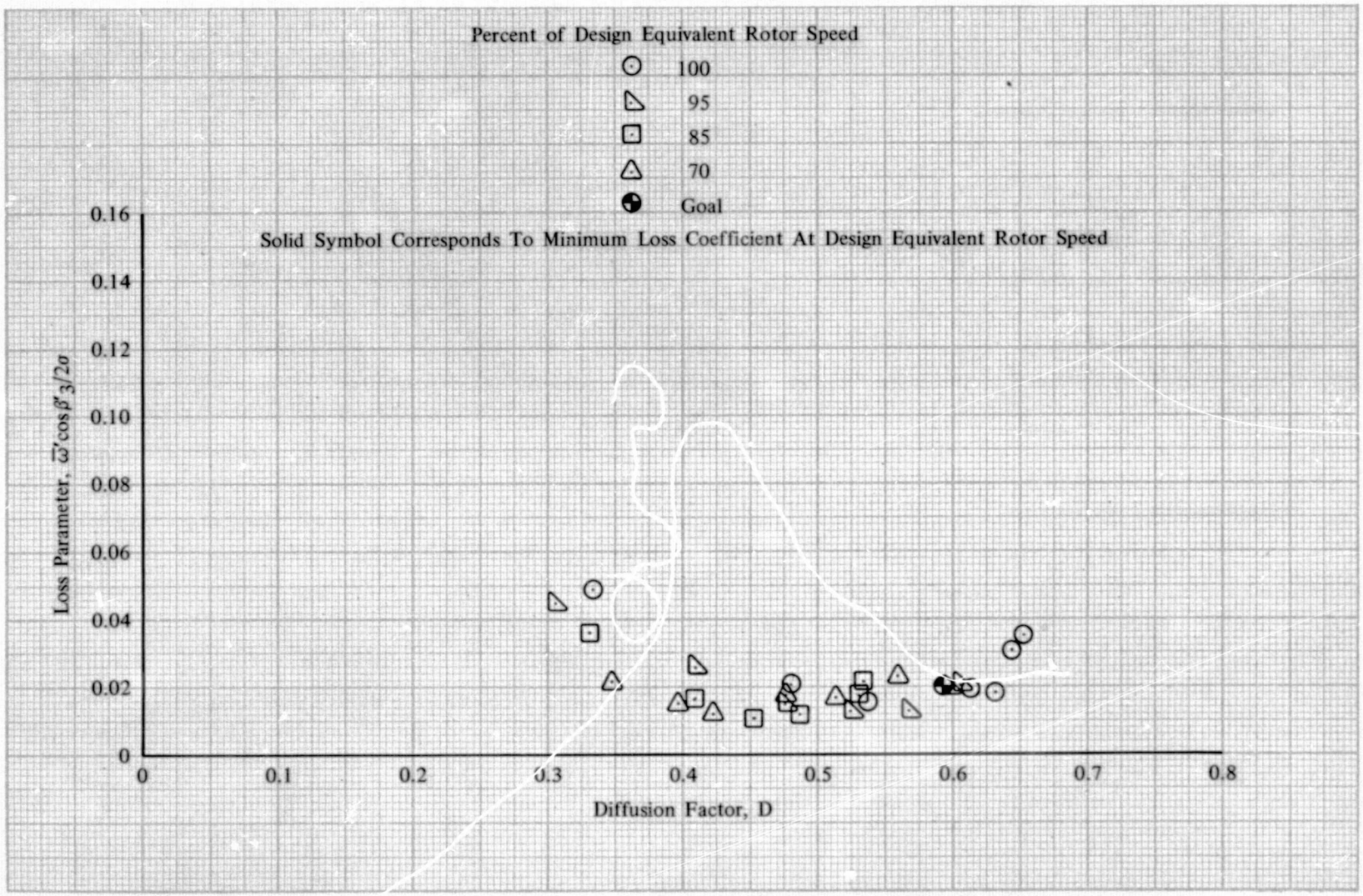


Figure 93b. Rotor G Loss Parameter vs Diffusion Factor, 30% Span from Tip; Uniform Inlet Flow DF 102280

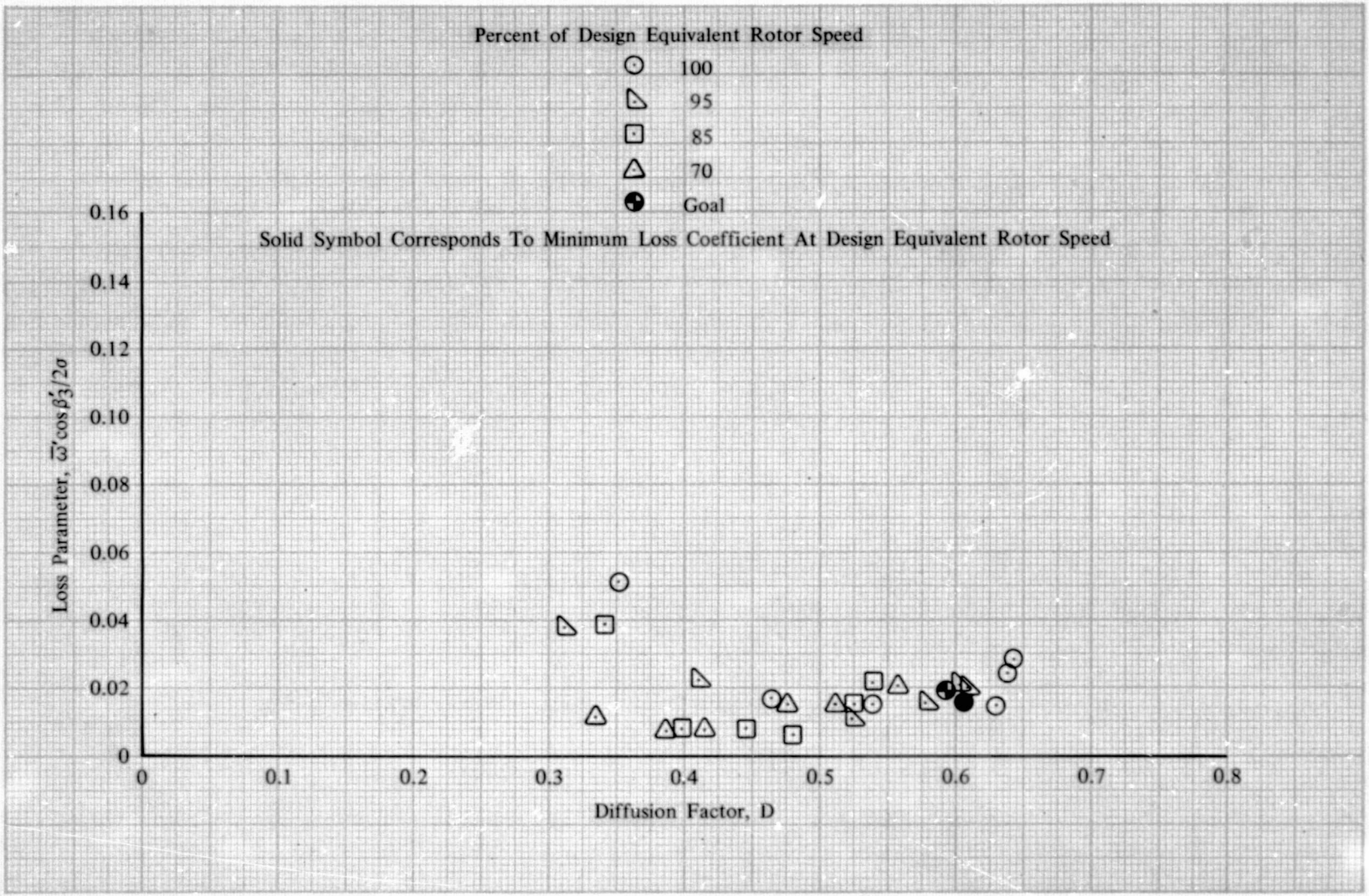


Figure 93c. Rotor G Loss Parameter vs Diffusion Factor, 50% Span; Uniform Inlet Flow

DF 102281

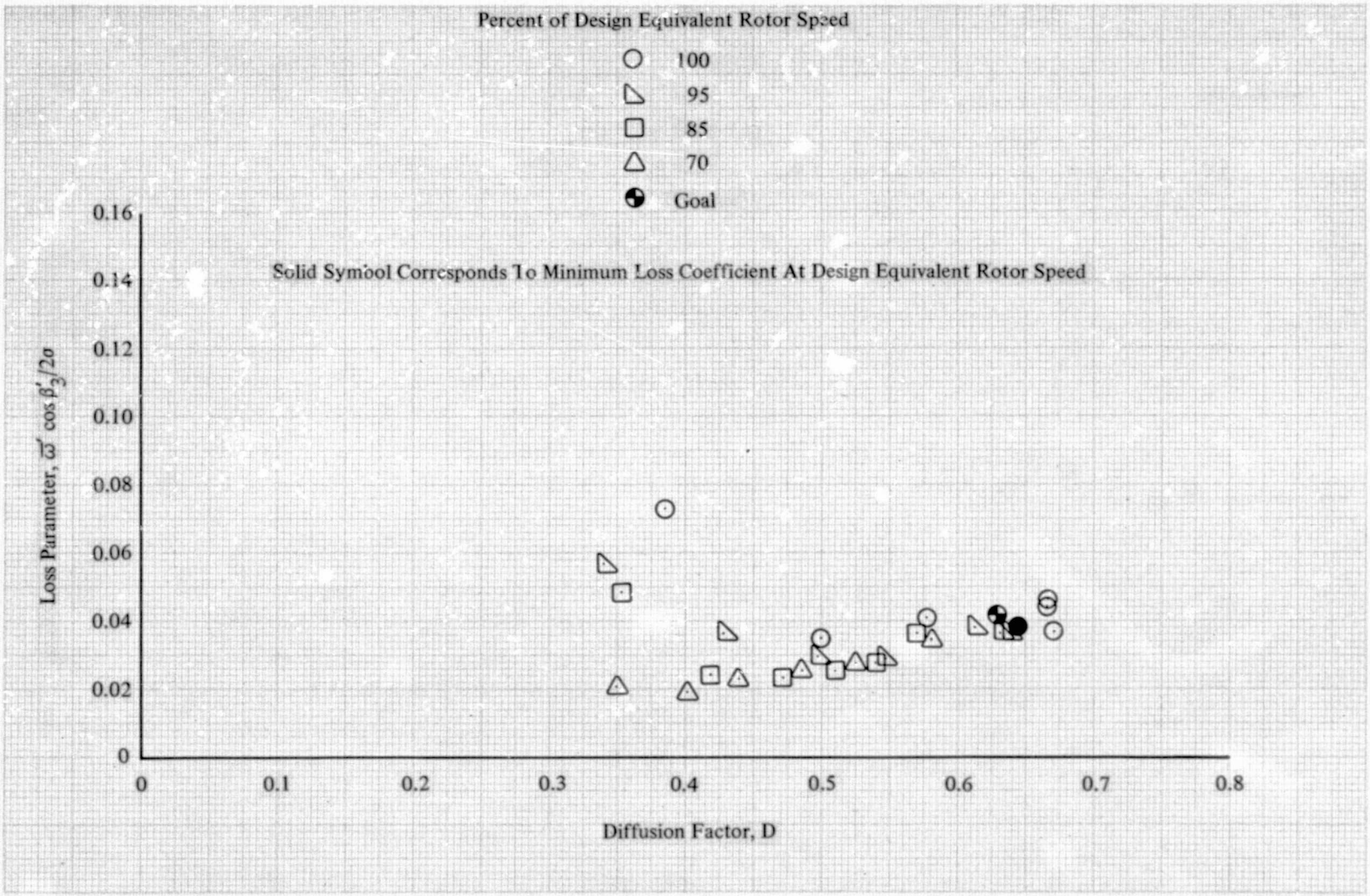


Figure 93d. Rotor G Loss Parameter vs Diffusion Factor, 70% Span from Tip; Uniform Inlet Flow DF 102282

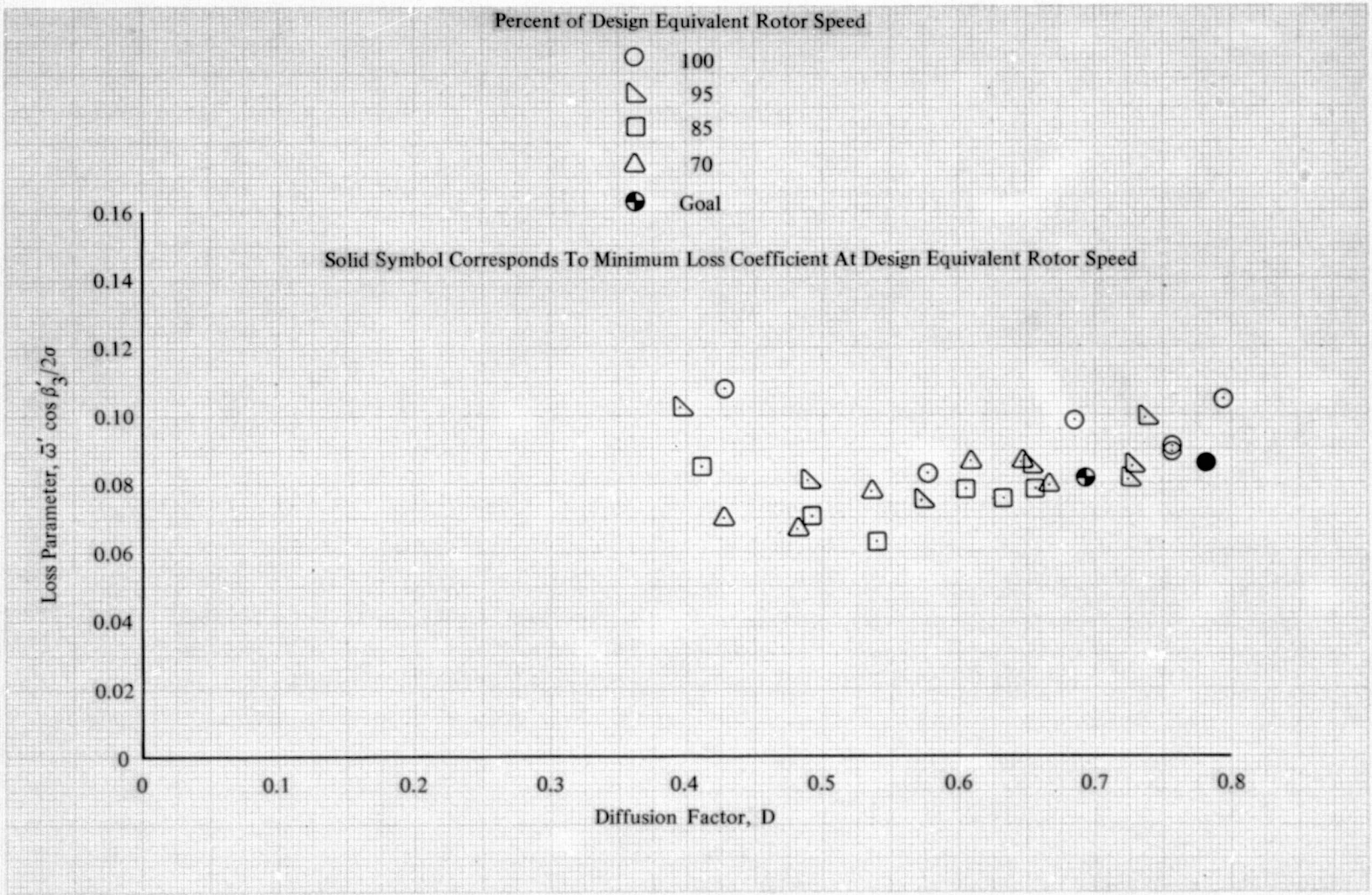


Figure 93e. Rotor G Loss Parameter vs Diffusion Factor, 90% Span from Tip; Uniform Inlet Flow DF 102283

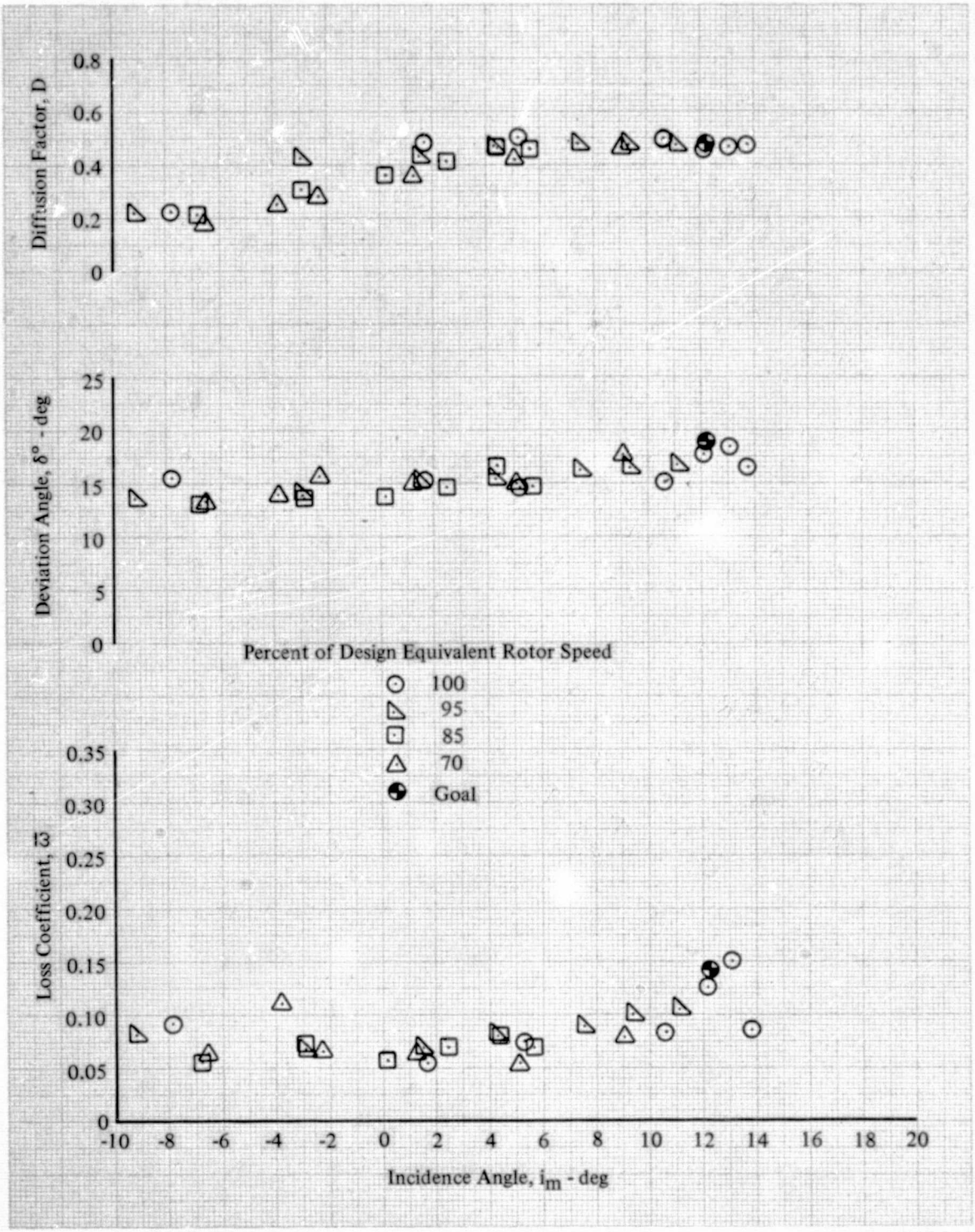


Figure 94a. Stator G Blade Element Performance, 10% Span from Tip; Uniform Inlet Flow DF 102284

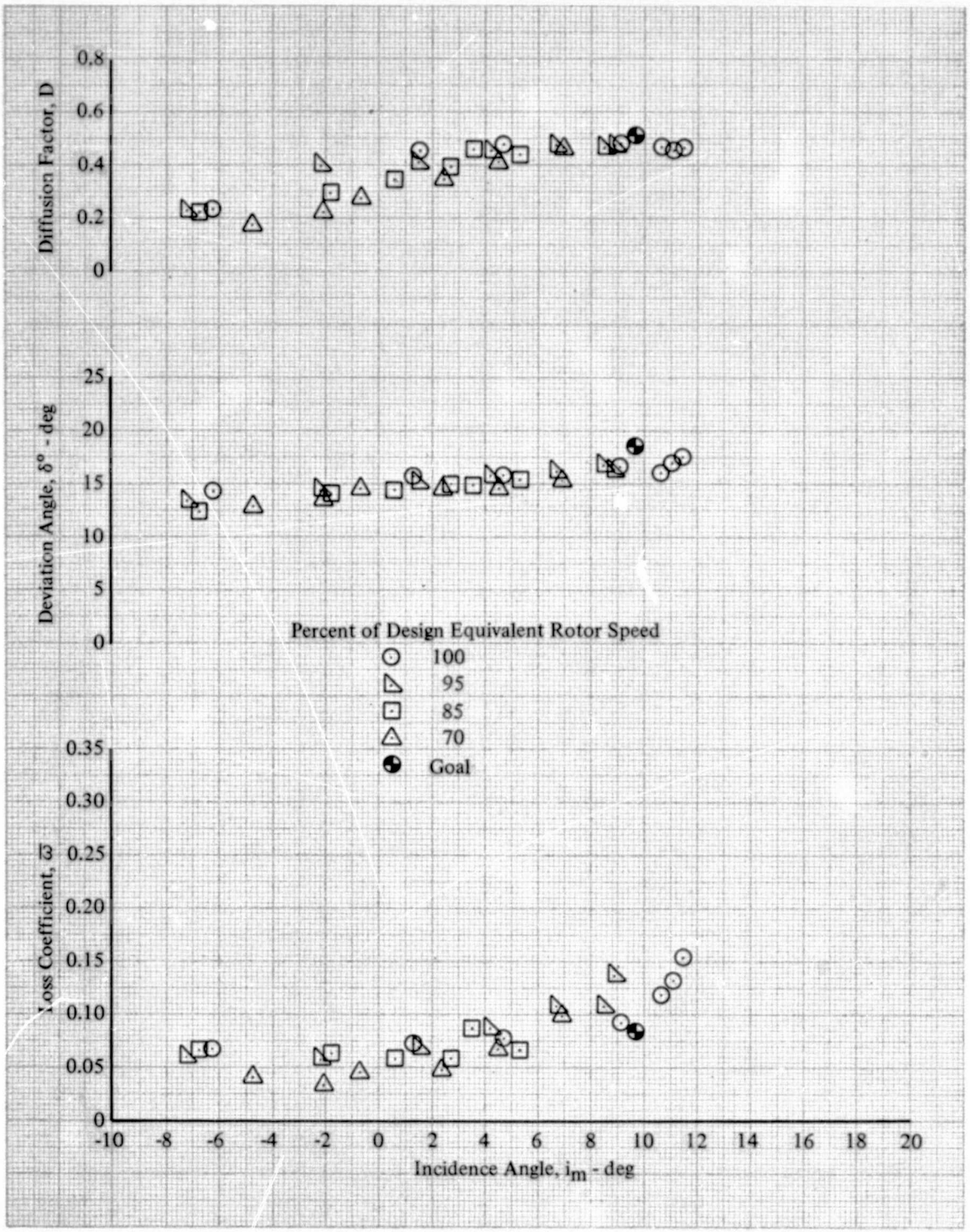


Figure 94b. Stator G Blade Element Performance, 30% Span from Tip; Uniform Inlet Flow DF 102285

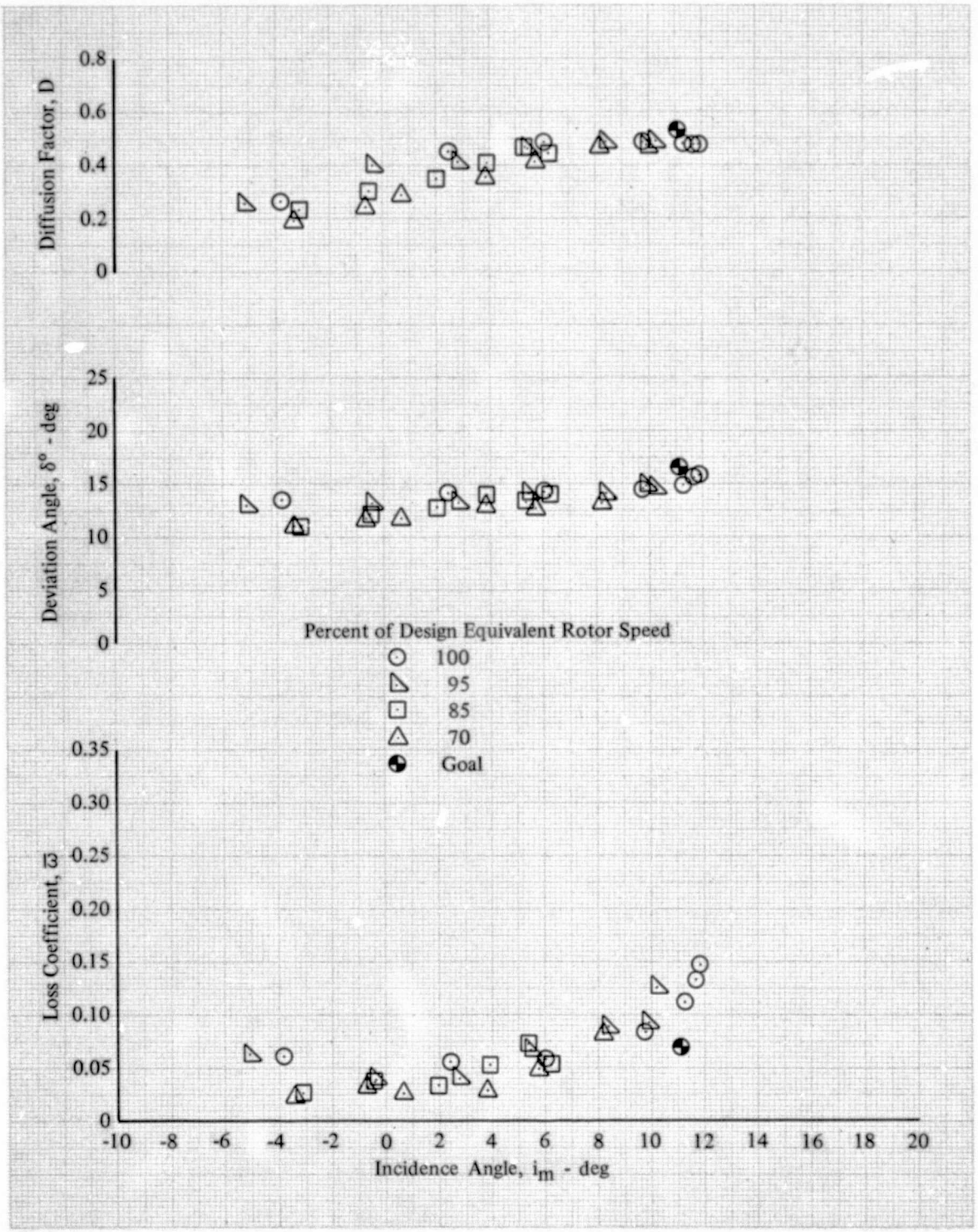


Figure 94c. Stator G Blade Element Performance, 50% Span; Uniform Inlet Flow DF 102286

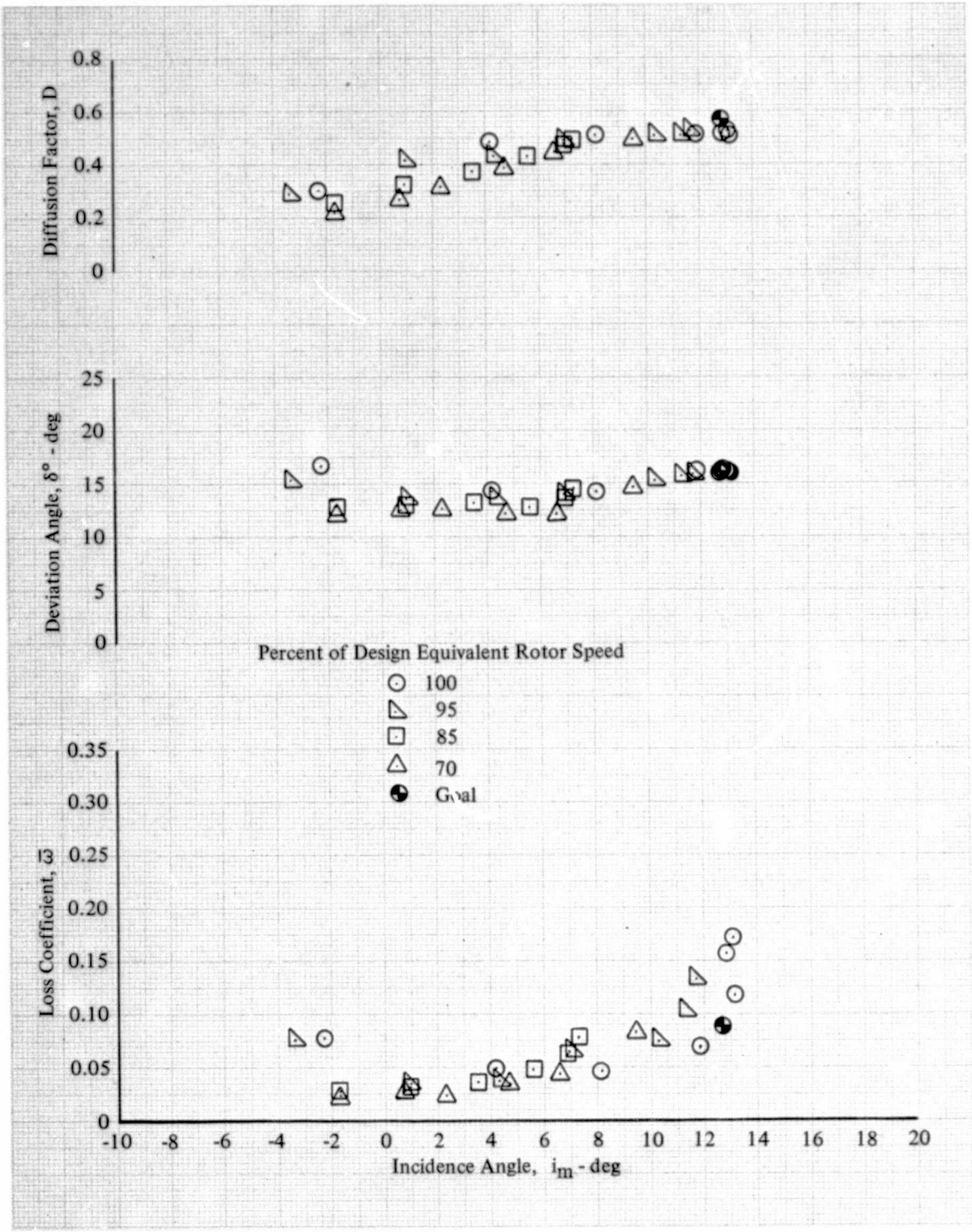


Figure 94d. Stator G Blade Element Performance, 70% Span from Tip; Uniform Inlet Flow

DF 102287

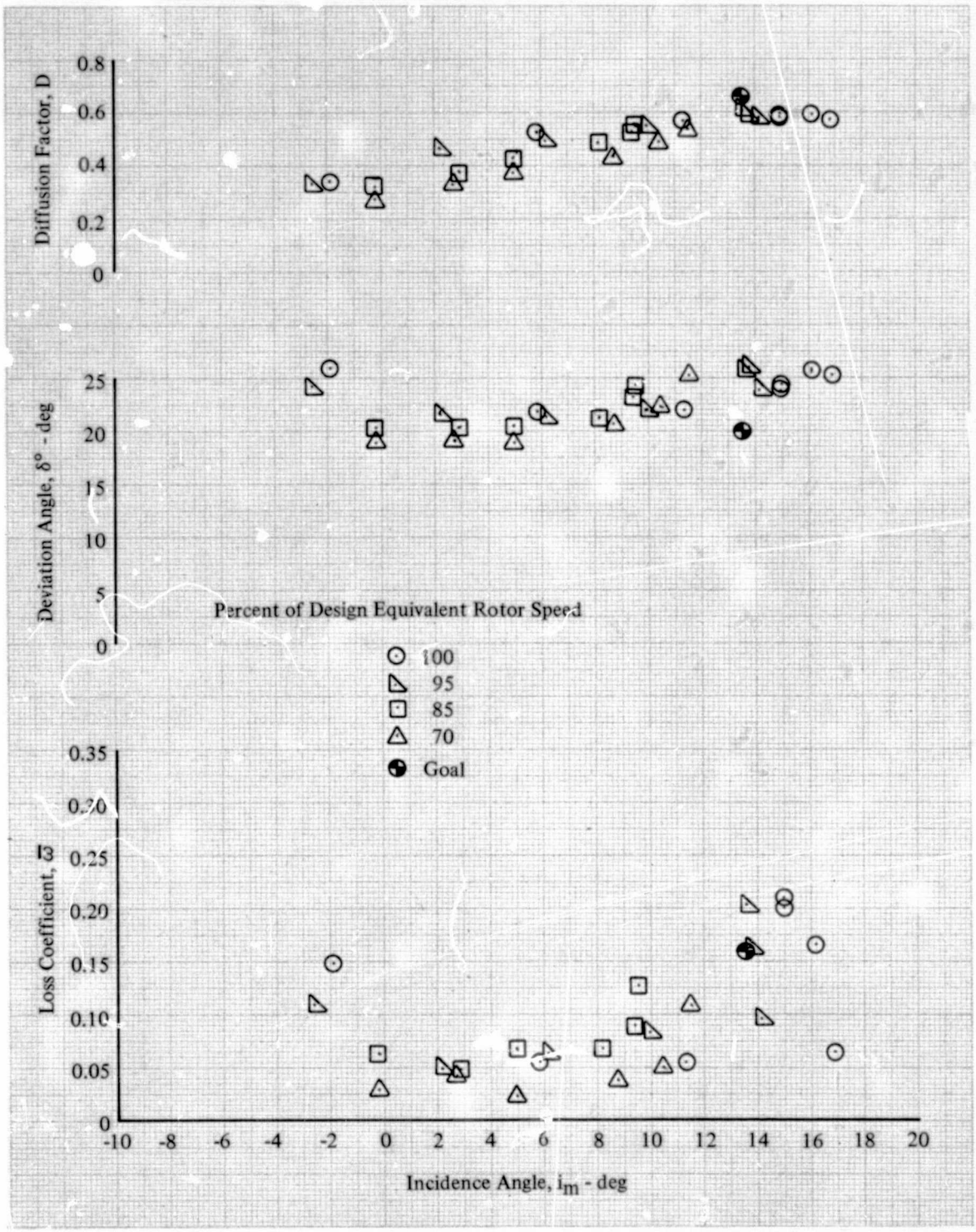


Figure 94e. Stator G Blade Element Performance, 90% Span from Tip; Uniform Inlet Flow DF 102288

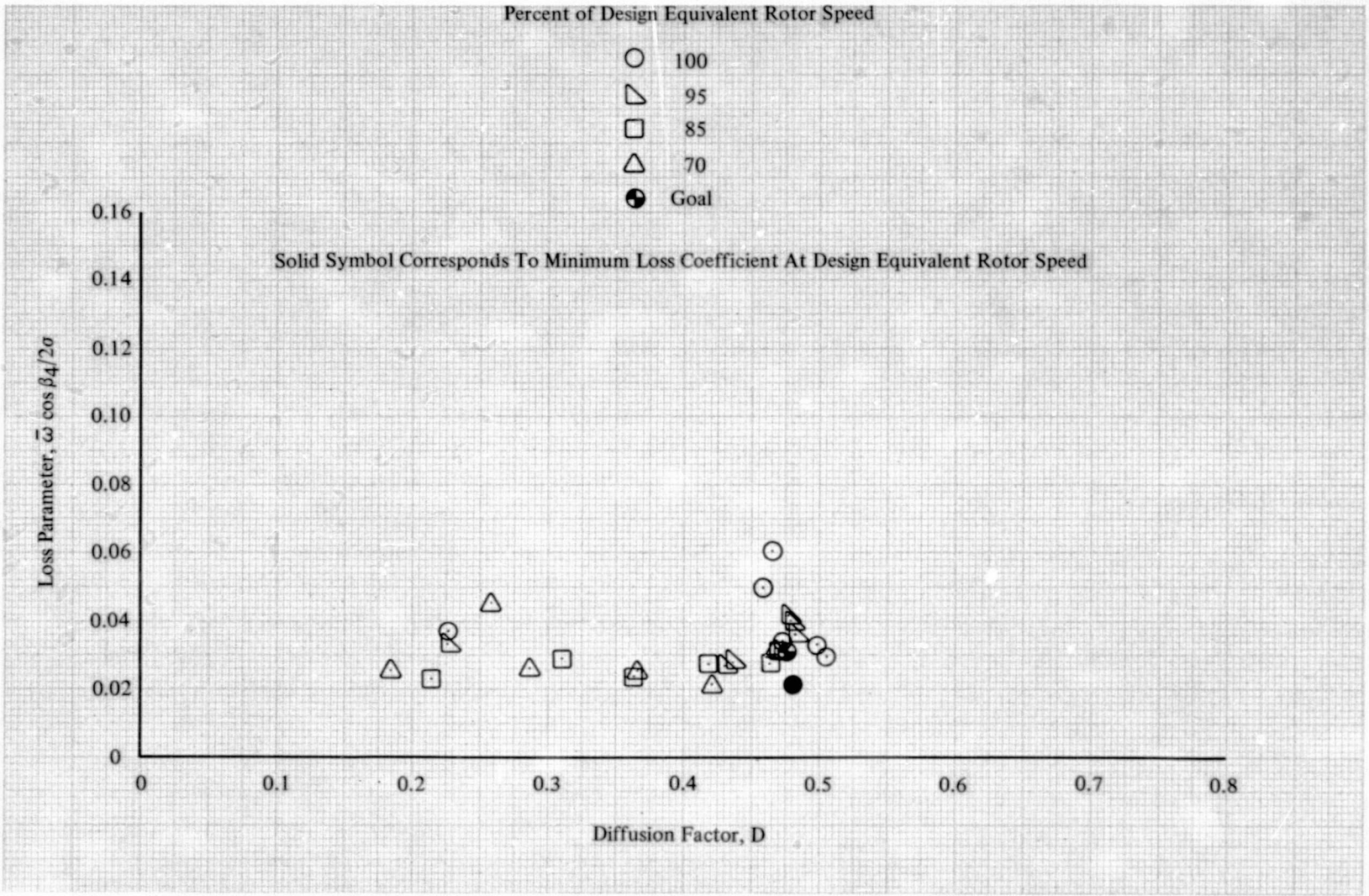


Figure 95a. Stator G Loss Parameter vs Diffusion Factor, 10% Span from Tip; Uniform Inlet Flow DF 102289

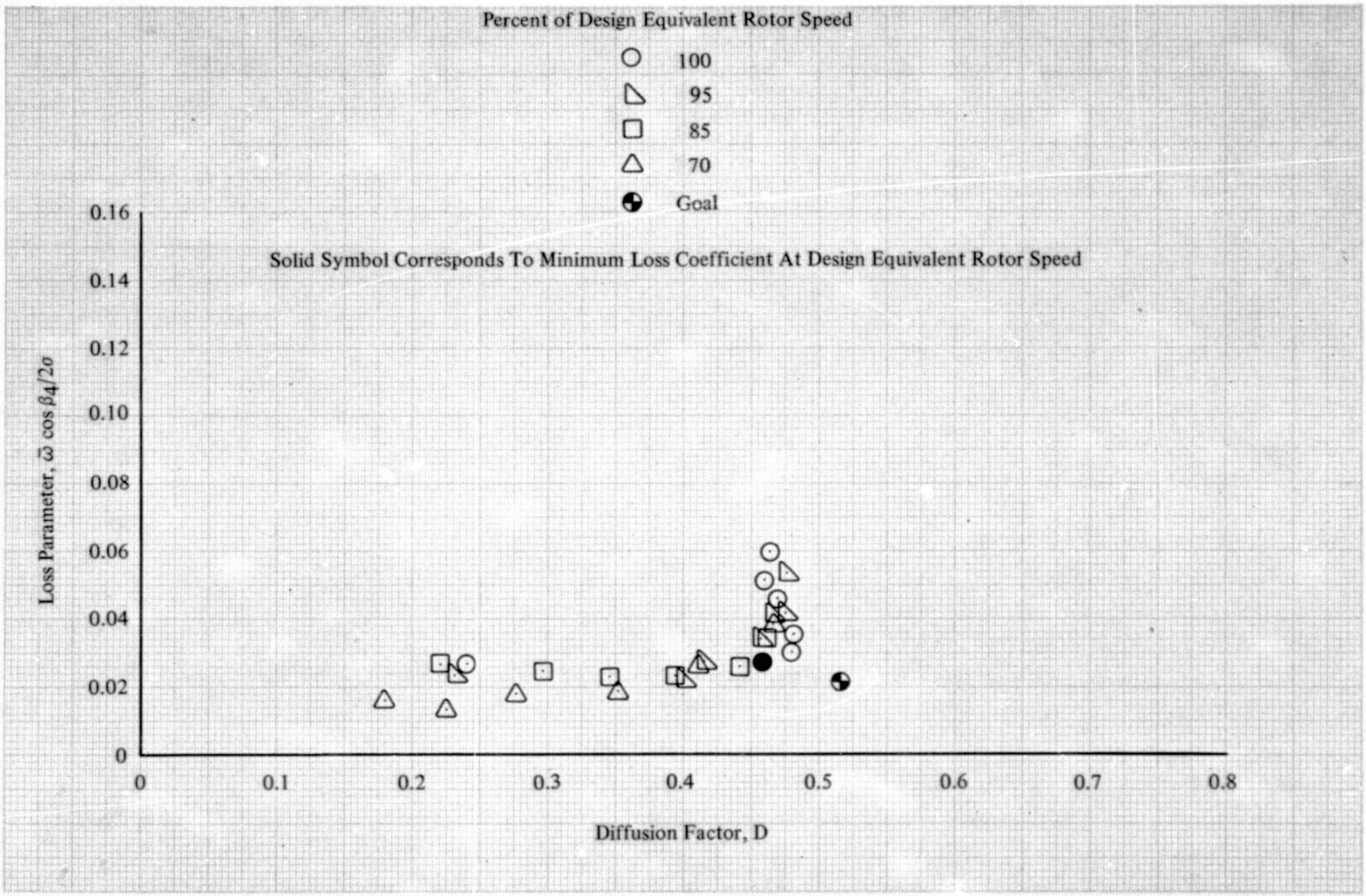


Figure 95b. Stator G Loss Parameter vs Diffusion Factor, 30% Span from Tip; Uniform Inlet Flow DF 102290

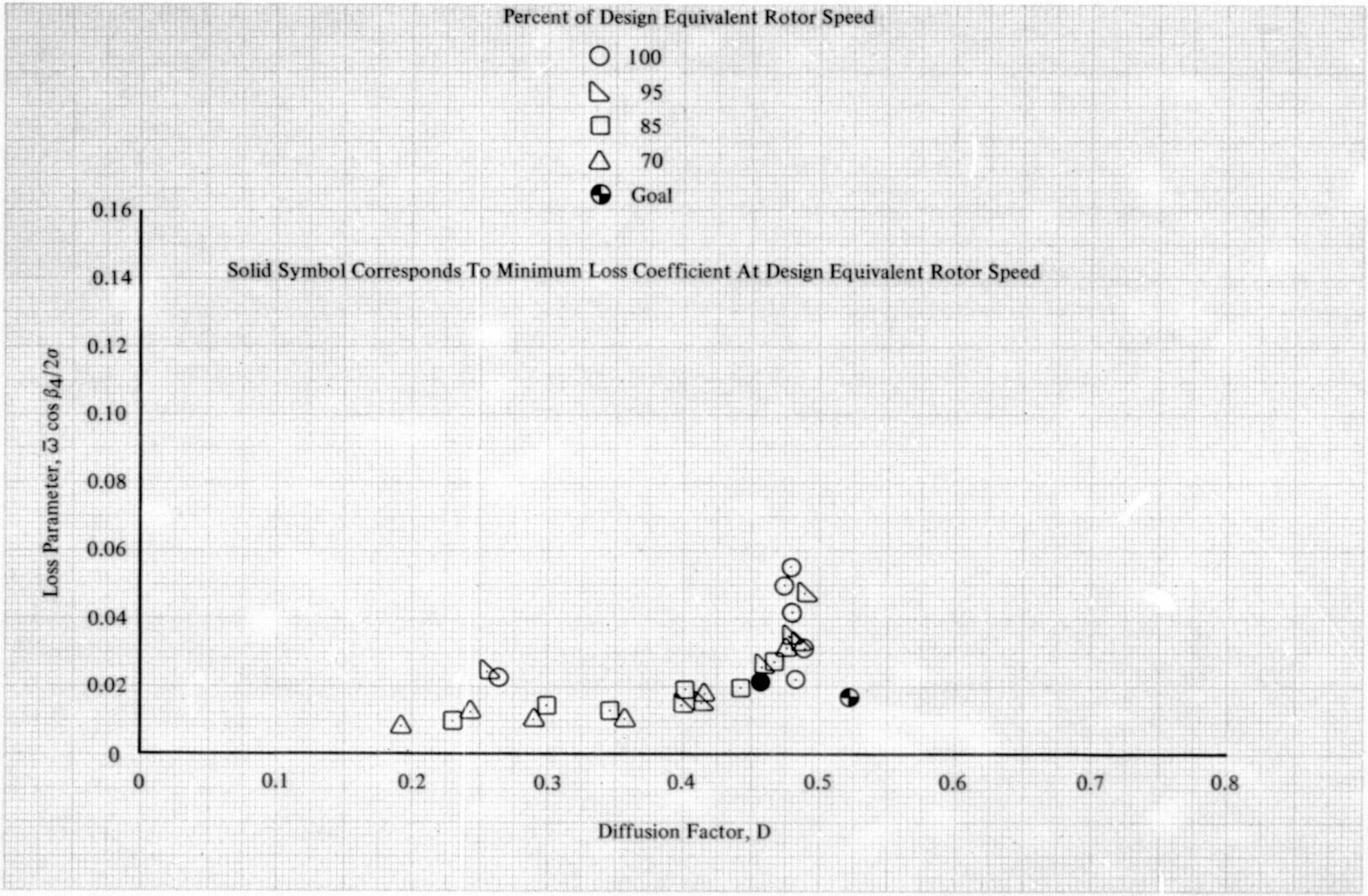


Figure 95c. Stator G Loss Parameter vs Diffusion Factor, 50% Span; Uniform Inlet Flow DF 102291

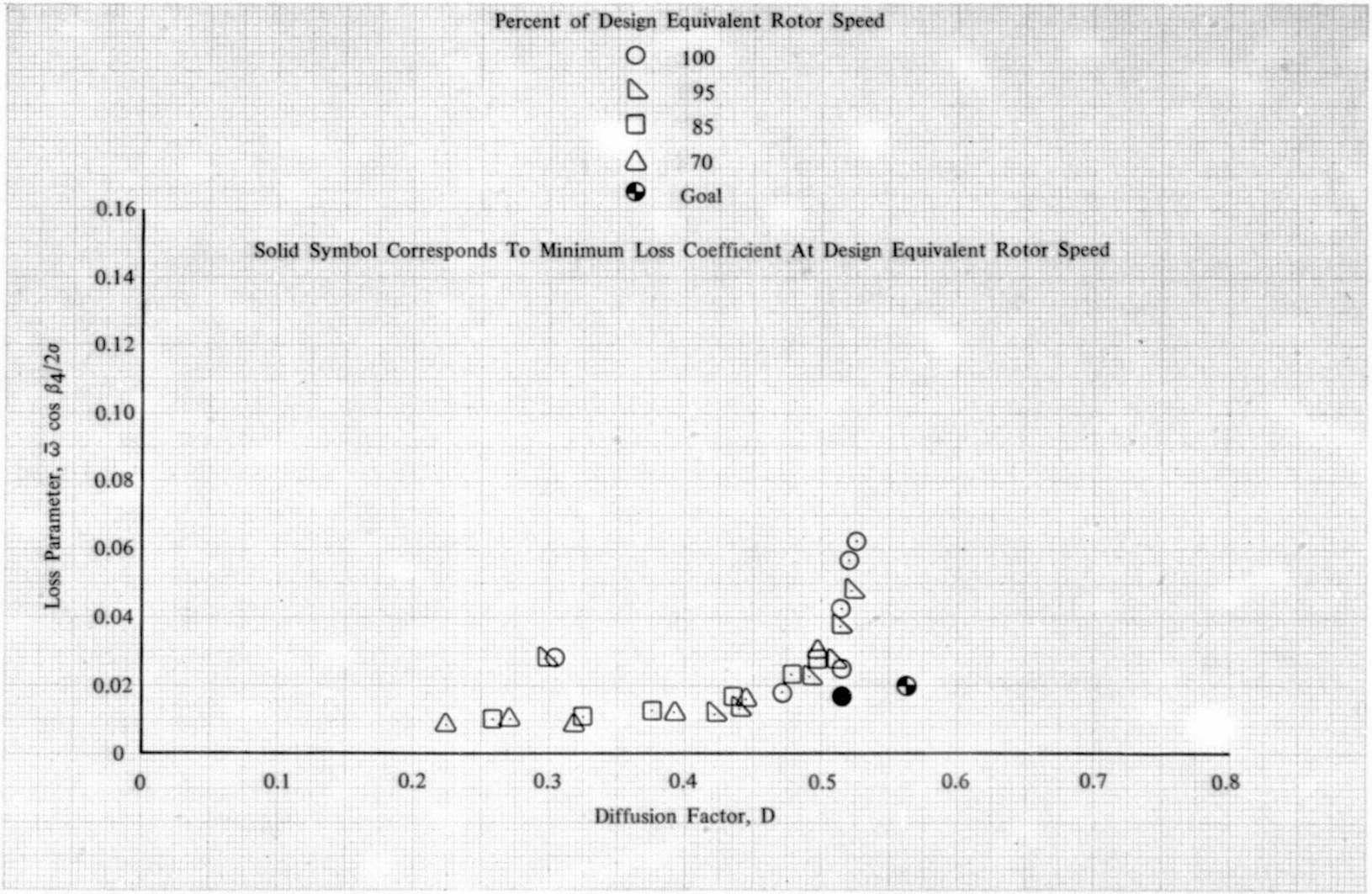


Figure 95d. Stator G Loss Parameter vs Diffusion Factor, 70% Span from Tip; Uniform Inlet Flow DF 102292

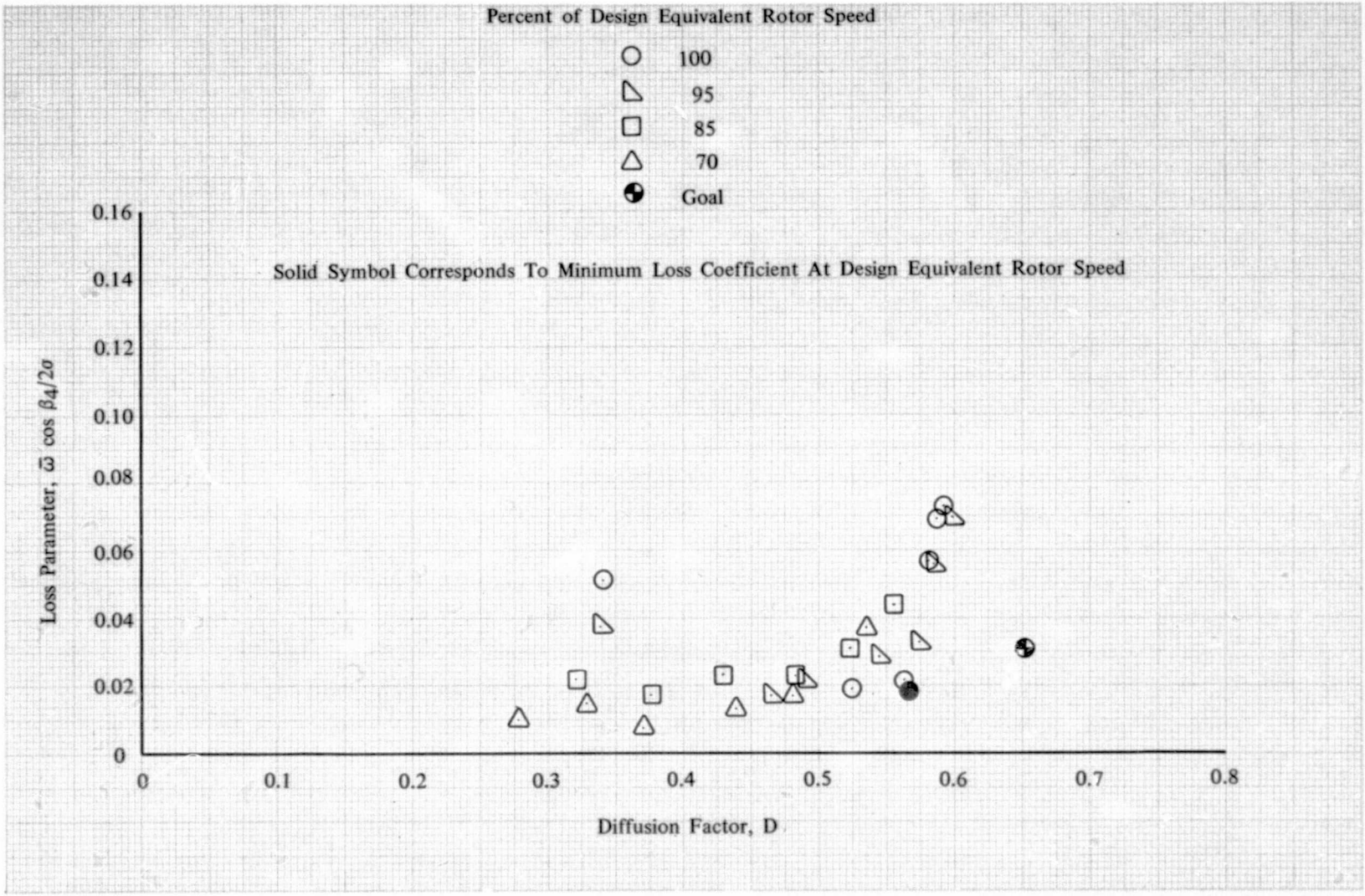


Figure 95e. Stator G Loss Parameter vs Diffusion Factor, 90% Span from Tip; Uniform Inlet Flow DF 102293

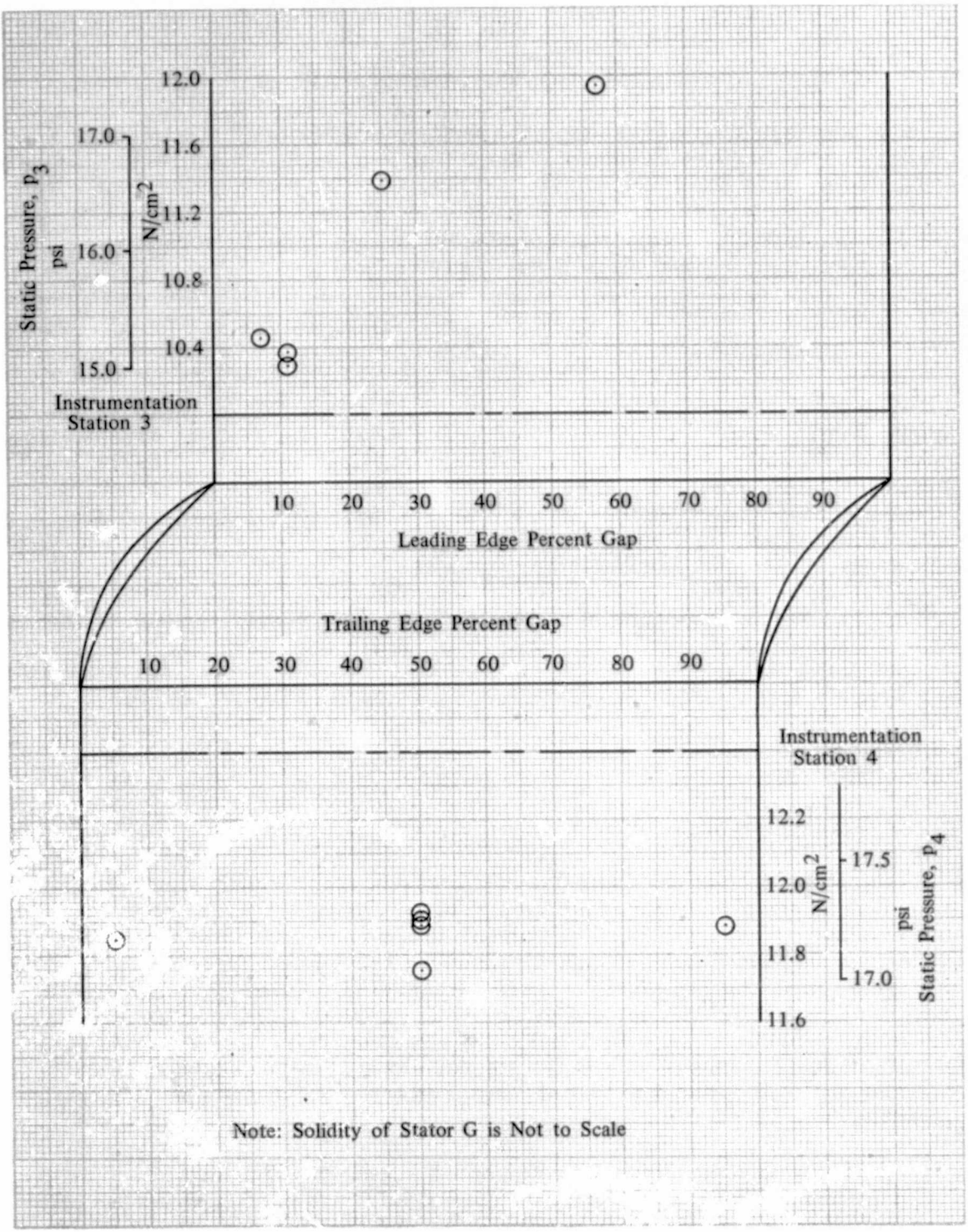


Figure 96. Rotor Exit and Stator Exit Wall Static Pressure Distributions; 100% Design Equivalent Rotor Speed; Equivalent Weight Flow = 16.43 kg/sec (36.37 lb/sec); Uniform Inlet Flow

DF 102294

## PART III

## COMPARISON OF STAGES F AND G

A comparison of the design point performance for Stage F with circular-arc blading and the performance goal of Stage G with multiple circular-arc blading is presented in table XXV.

Table XXV. Comparison of Stage F Design Point Performance and Stage G Performance Goal

| Parameter | Design Point Stage F | Performance Goal Stage G |
|---|---|---|
| Flow, $W\sqrt{\theta}/\delta$, kg/sec (lb/sec) | 17.11 (37.73) | 16.72 (36.86) |
| Speed, $N/\sqrt{\theta}$, rpm | 9,936 | 11,529 |
| Inlet Hub/Tip Ratio | 0.766 | 0.772 |
| Pressure Ratio, Rotor | 1.614 | 1.657 |
| Pressure Ratio, Rotor-Stator | 1.565 | 1.604 |
| Efficiency, Adiabatic, Rotor | 94.5 | 90.6 |
| Efficiency, Adiabatic, Rotor-Stator | 87.8 | 84.14 |
| $U_{tip}/\sqrt{\theta}$, m/sec (ft/sec) | 285 (934) | 327 (1074) |
| Rotor Tip Leading Edge Diameter, cm (in.) | 54.480 (21.449) | 54.244 (21.356) |
| Aspect Ratio, Rotor | 0.90 | 1.00 |
| Aspect Ratio, Stator | 0.90 | 1.00 |
| Solidity, Rotor | 1.36 | 1.250 |
| Solidity, Stator | 1.39 | 1.248 |
| Diffusion Factor, Rotor | 0.60 | 0.68 |
| Diffusion Factor, Stator | 0.58 | 0.54 |
| Chord, Rotor, cm (in.) | 6.632 (2.611) | 5.885 (2.317) |
| Chord, Stator, cm (in.) | 5.738 (2.259) | 5.151 (2.028) |

A comparison of the overall performance of Stage F and Stage G is given in figures 97 through 99 for rotor, rotor-stator and inlet guide vane-rotor-stator (stage), respectively. The comparison is made for uniform inlet flow conditions only since Stage G was not tested with distorted inlet flow. Figures 97 through 99 show that both compressors have good flow range, i.e., the surge margin at peak efficiency for design equivalent rotor speed for Rotor F. Stator F and Rotor G-Stator G were 13.1 and 16.1%, respectively. The superior surge margin of Stage G may be due to the steeper slope of its pressure ratio-flow characteristic as opposed to that of Stage F which was flat and thus inherently unstable.

In order to account for the rotor speed effects on efficiency and pressure rise, the peak efficiencies of the two rotor-stators are presented versus rotor tip relative inlet Mach number in figure 100, and the pressure rise at design rotor speed has been normalized into a pressure coefficient versus flow coefficient and is presented in figure 101. The corresponding values for the rotors are shown in figures 102 and 103.

Three observations can be made from the data shown in figures 100 through 103: First, the circular-arc blading had higher efficiency at Mach numbers up to the transonic regime. Second, both airfoil shapes exhibit a substantial degradation in performance for Mach numbers in the transonic regime, i.e., the efficiencies for Stages F and G are essentially the same at the higher Mach numbers. Third, the pressure rise coefficients for Rotor F-Stator F were substantially higher than those of Rotor G-Stator G; this appears inconsistent when considering the higher diffusion factors for Stage G but is the result of the higher Stage G wheel speed.

Figure 104 compares the spanwise loss distribution of Rotor F to Rotor G and Stator F to Stator G for peak efficiency at design rotor speed. At first glance the similarity of the losses seems inconsistent with the 2.0 percentage point difference in efficiency between Rotor F-Stator F and Rotor G-Stator G at design rotor speed. However, this is not the case since Stage G was operating at higher inlet Mach numbers and thus would experience a higher loss in total pressure for the same loss coefficient. Spanwise distributions of diffusion factor for Rotor F and Rotor G, Stator F and Stator G are compared in figure 105 for the peak efficiency points. These distributions show that Rotor F and Stator F achieved higher diffusion factors than Rotor G and Stator G at all spanwise positions except at 70% span where the diffusion factors were the same. The average of the diffusion factors at 10, 30, 50, 70 and 90% spans for each blade row at peak efficiency is given below; these values further illustrate the higher loading levels achieved by the circular-arc blading.

| Blade Row | Average Diffusion Factor |
|---|---|
| Rotor F | 0.646 |
| Rotor G | 0.590 |
| Stator F | 0.533 |
| Stator G | 0.510 |

## Conclusion

Two single-stage, axial-flow compressors were tested to evaluate the effectiveness of long chord, low aspect ratio blading as a means of obtaining higher stage loadings. One compressor was comprised of circular-arc blading, designated Stage F, with an aspect ratio of 0.9 for both the rotor and stator. This compressor was tested with uniform inlet, hub radial, tip radial, and circumferential inlet flow distortion. The second compressor was comprised of multiple circular-arc blading, designated Stage G, with an aspect ratio of 1.0 for both the rotor and stator. The major results of this evaluation are summarized below:

- Both stages operated at high loading levels with good efficiency and operating range. The peak efficiencies and corresponding average stage diffusion factors for Stages F and G were 86.4% and 84.1% and 0.59 and 0.55, respectively. The surge margins at peak efficiency were 12.6% and 16.5% for Stages F and G, respectively.

- Stage F, comprised of circular-arc blading, achieved significantly higher efficiencies than Stage G, which was comprised of multiple circular-arc blading at inlet Mach numbers up to the transonic regime.

- Both the circular-arc and multiple circular-arc rotors exhibited substantial degradation in efficiency at design rotor speed.

- The multiple circular-arc rotor delayed the onset of the rapid loss in efficiency with increasing Mach number to higher Mach numbers.

- The peak pressure rise coefficient for Stage F was approximately 30% higher than that of Stage G.

- At peak efficiency, the Stage F diffusion factors were higher than those of Stage G.

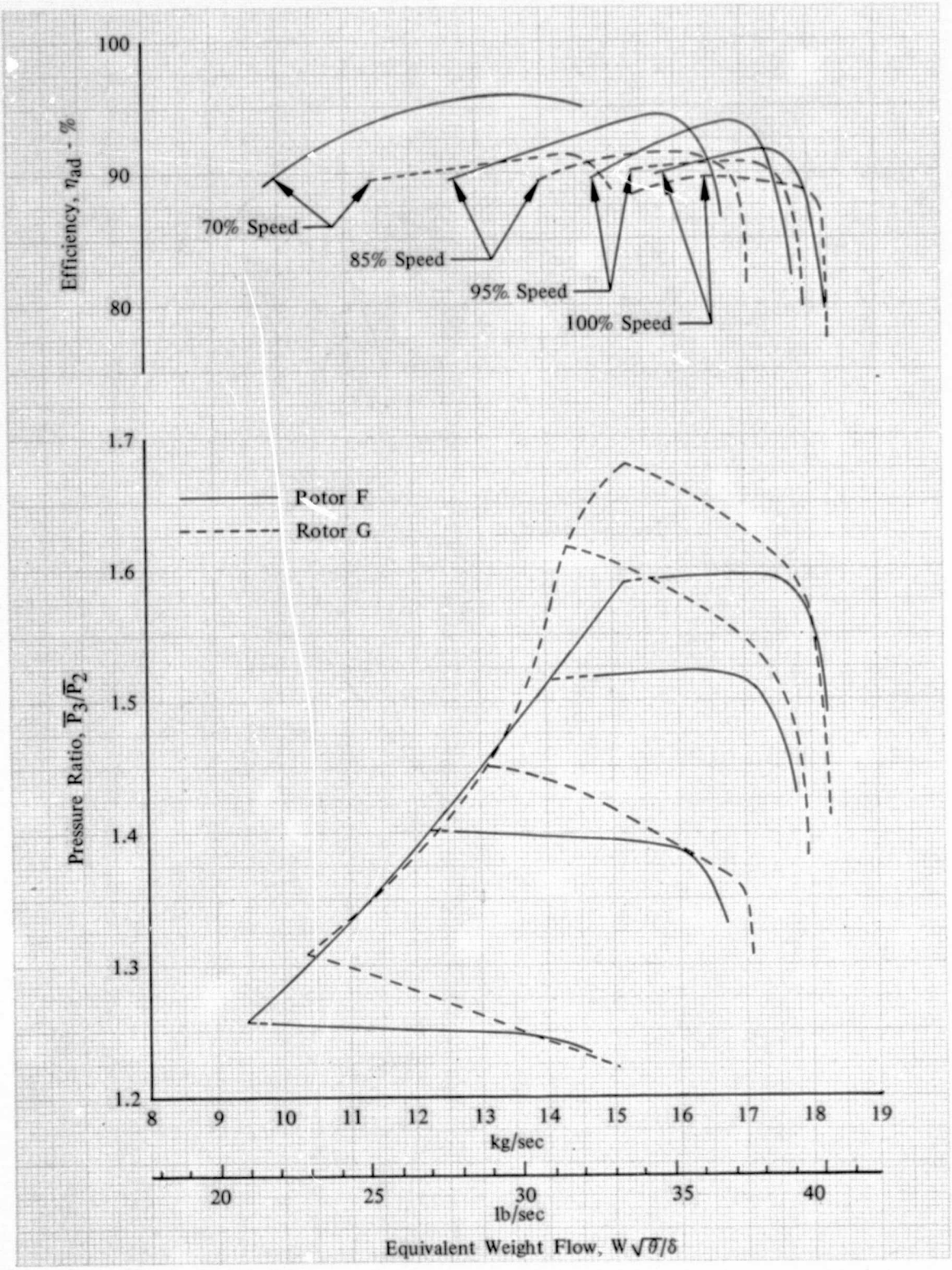


Figure 97. Overall Performance of Rotor F and Rotor G DF 102295

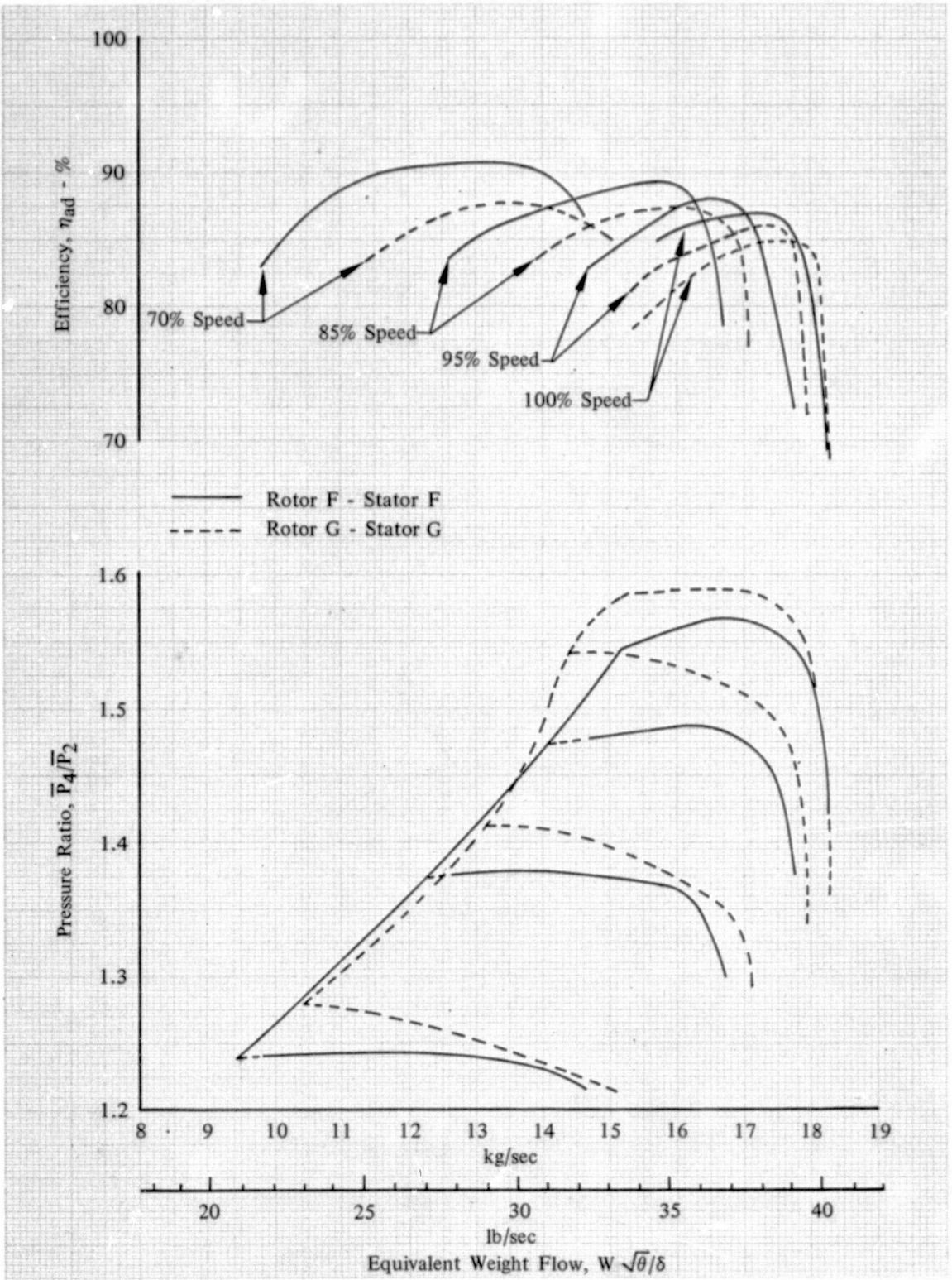


Figure 98. Overall Performance of Rotor F-Stator F and Rotor G-Stator G DF 102296

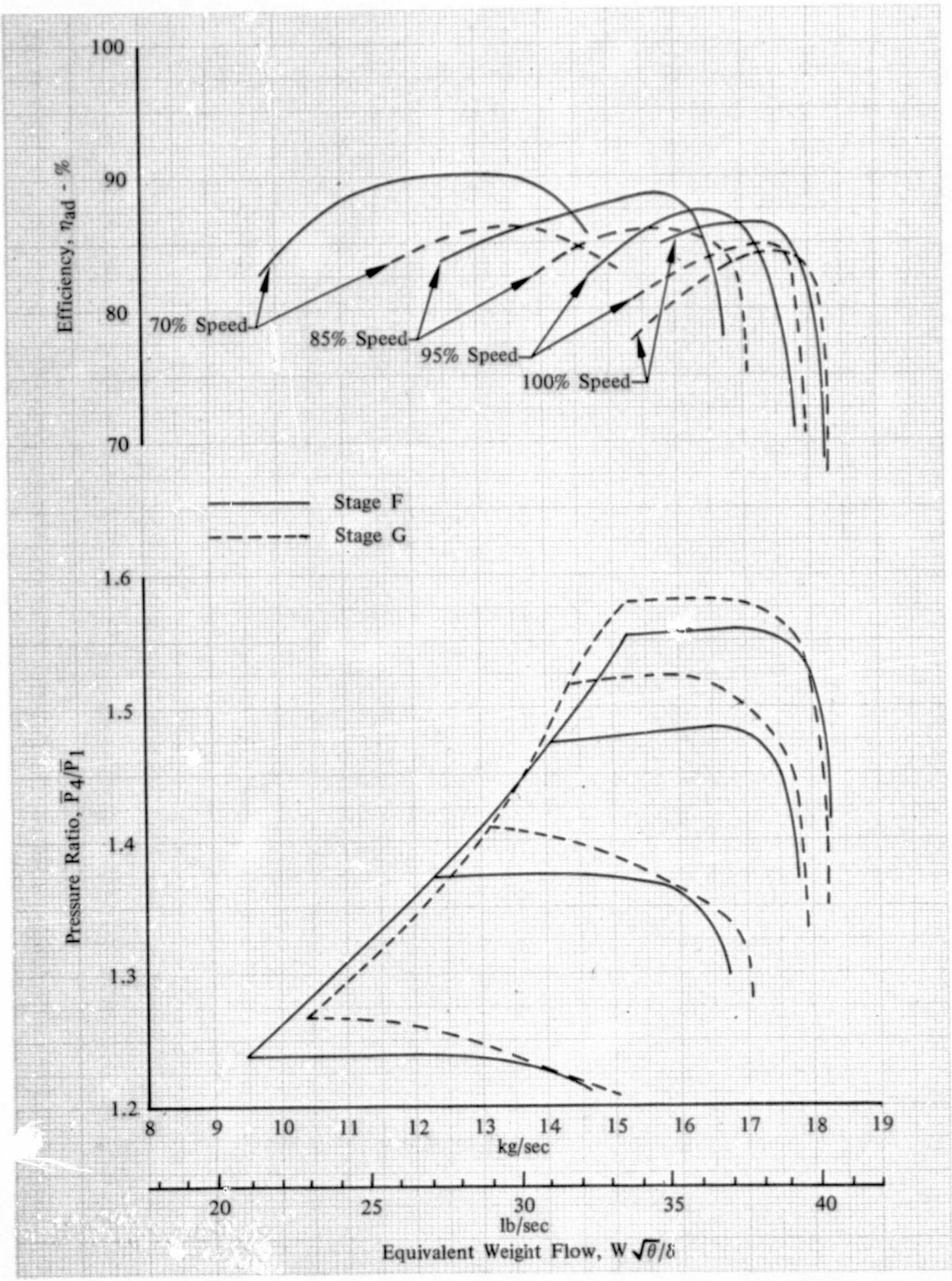


Figure 99. Overall Performance of Stage F and Stage G

DF 102297

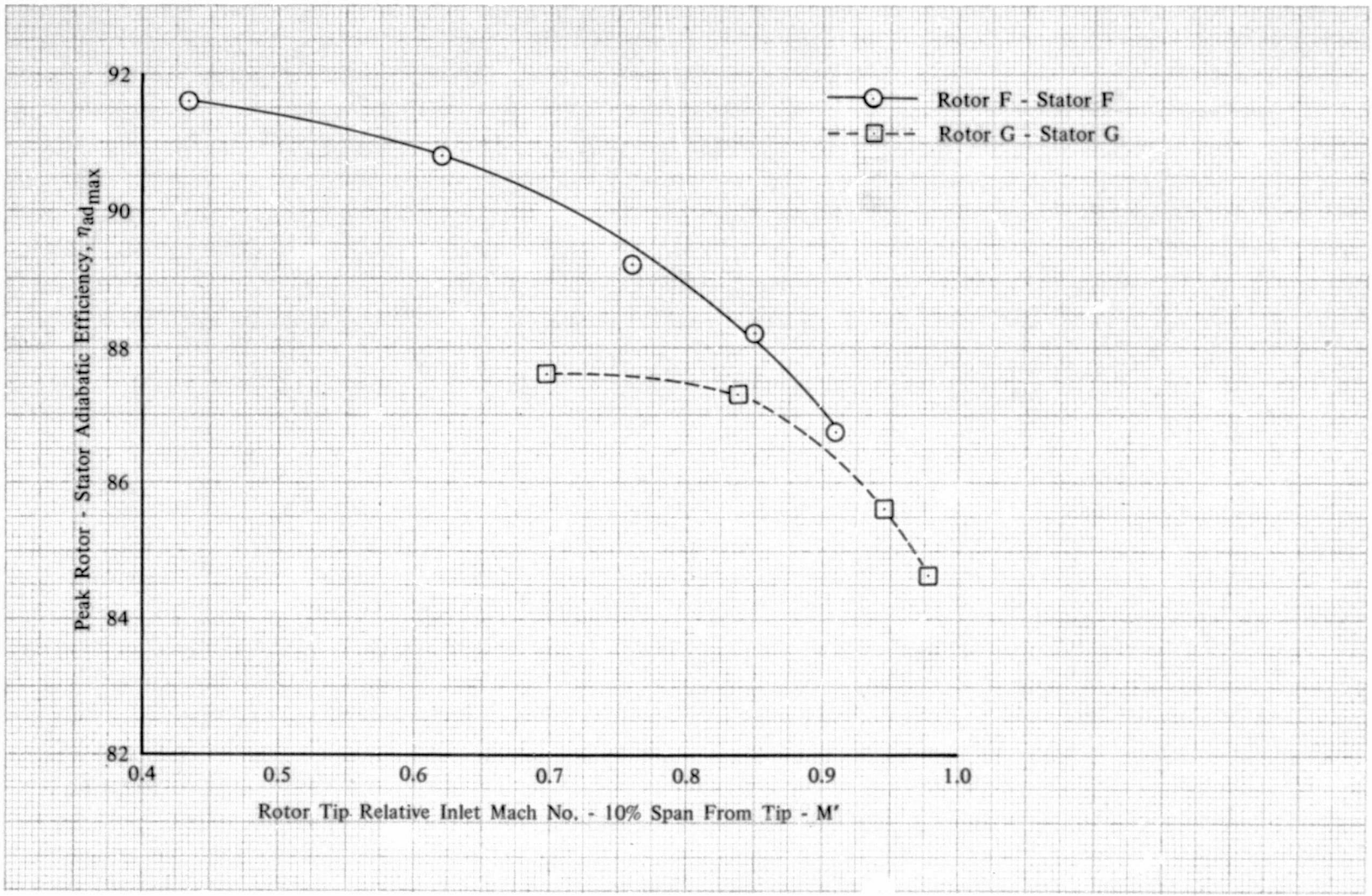


Figure 100. Comparison of Peak Efficiency vs Rotor Tip Relative Inlet Mach Number for Rotor F-Stator F and Rotor G-Stator G

DF 102298

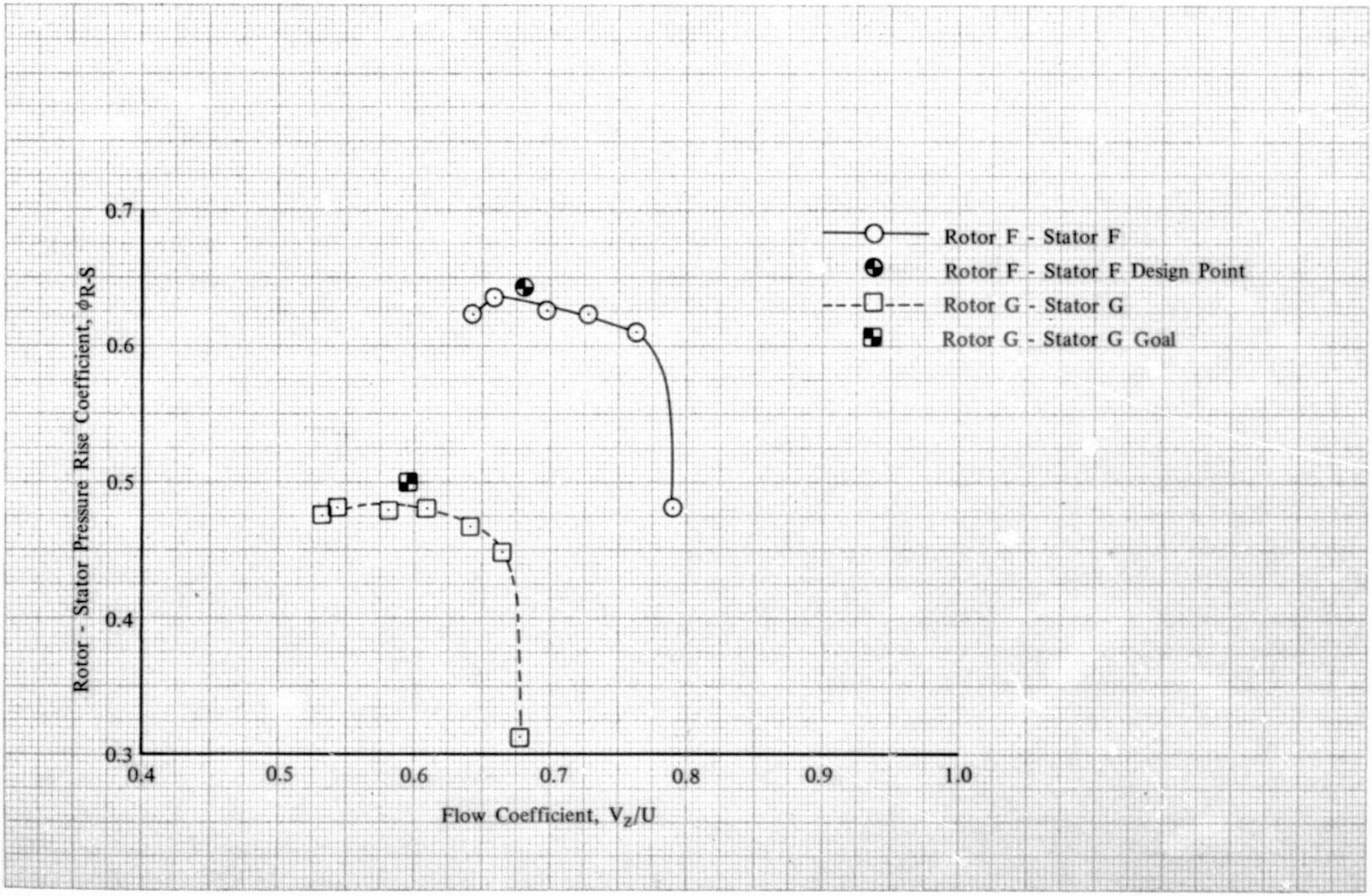


Figure 101. Comparison of Pressure Rise Coefficient vs Flow Coefficient at Design Equivalent Rotor Speed for Rotor F-Stator F and Rotor G-Stator G

DF 102299

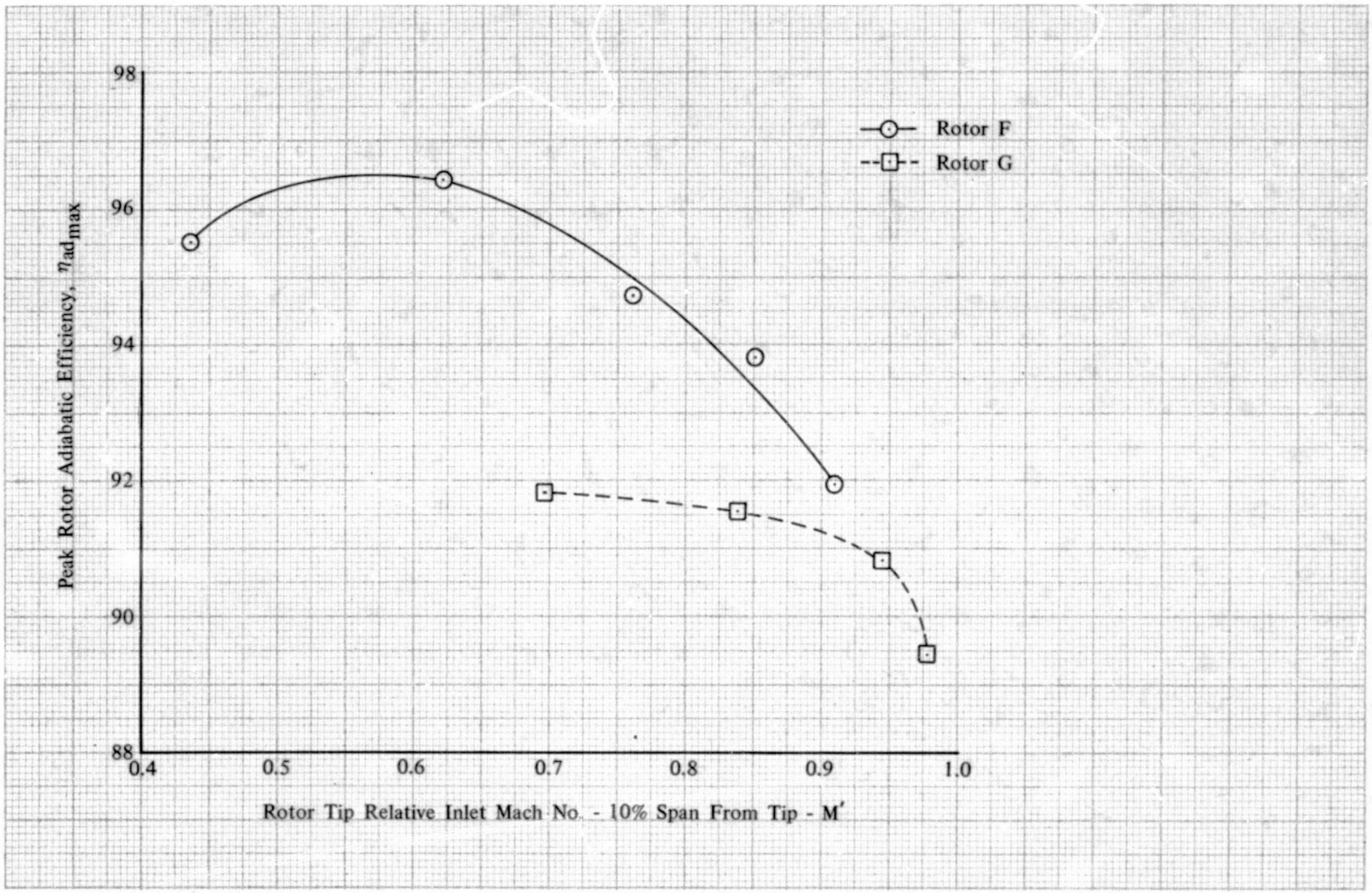


Figure 102. Comparison of Peak Efficiency vs Rotor Tip Relative Inlet Mach Number for Rotor F and Rotor G

DF 102300

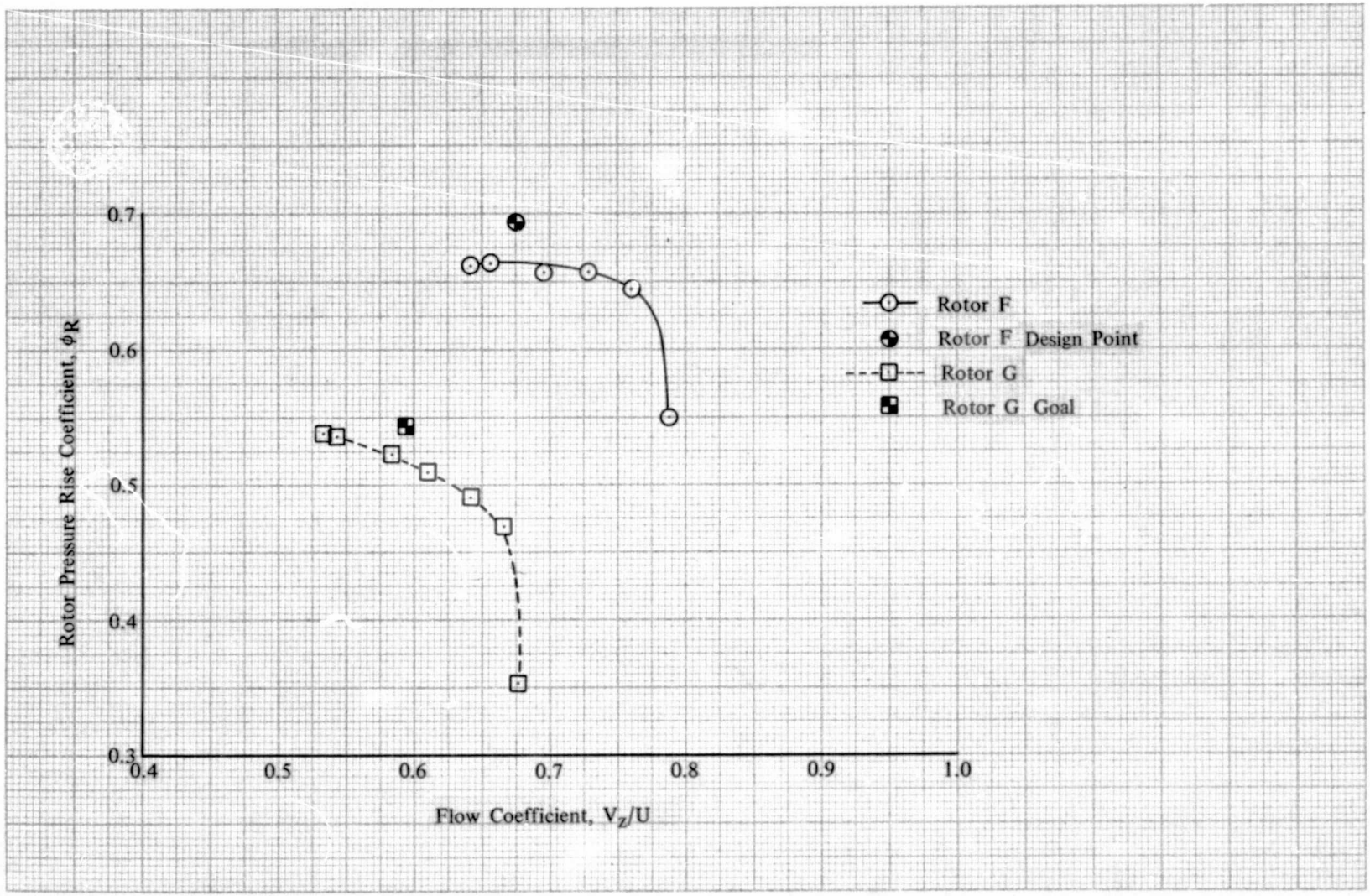


Figure 103. Comparison of Pressure Rise Coefficient vs Flow Coefficient at Design Equivalent Rotor Speed for Rotor F and Rotor G

DF 102301

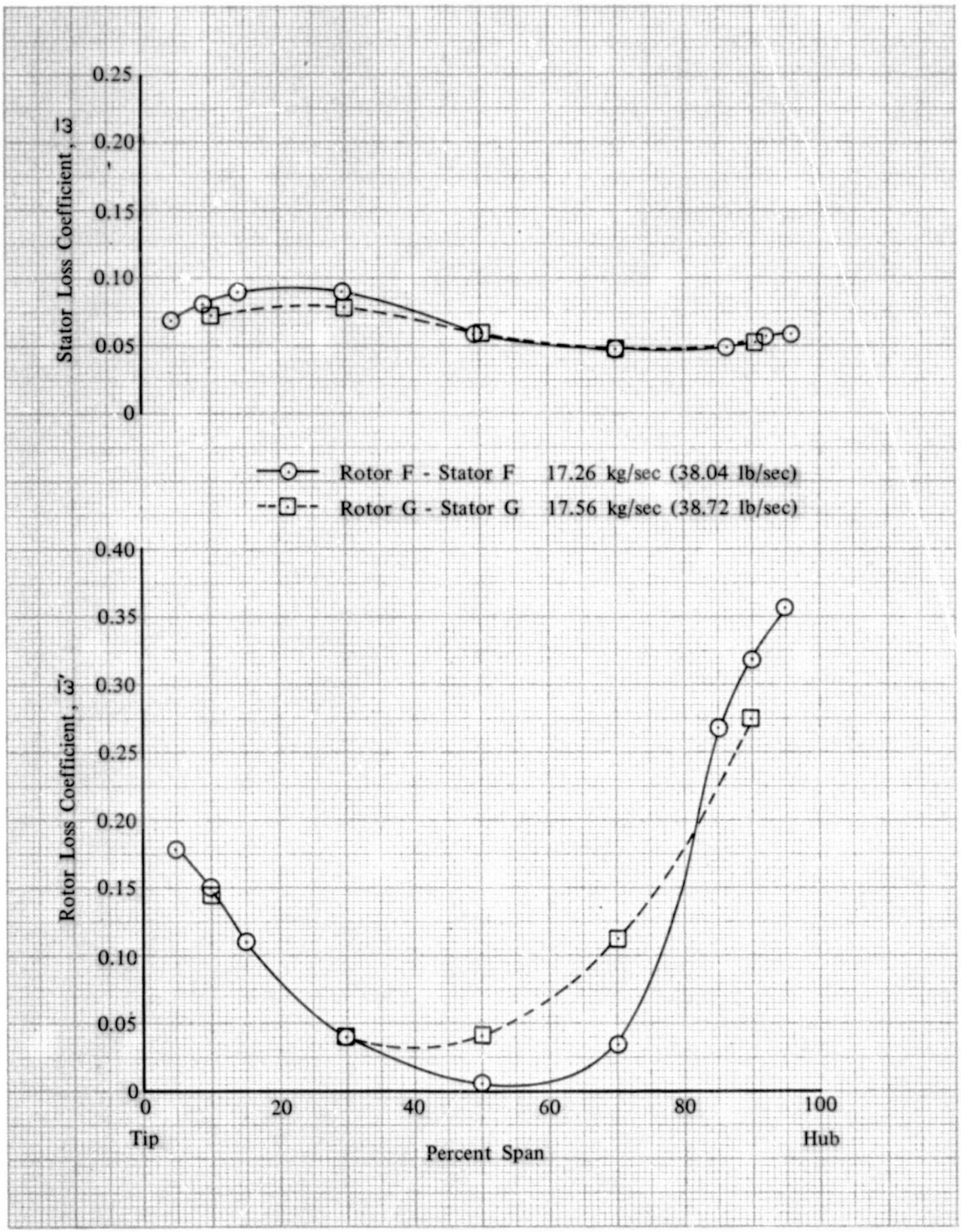


Figure 104. Spanwise Loss Distributions for Rotor F-Rotor G and Stator F-Stator G DF 102302

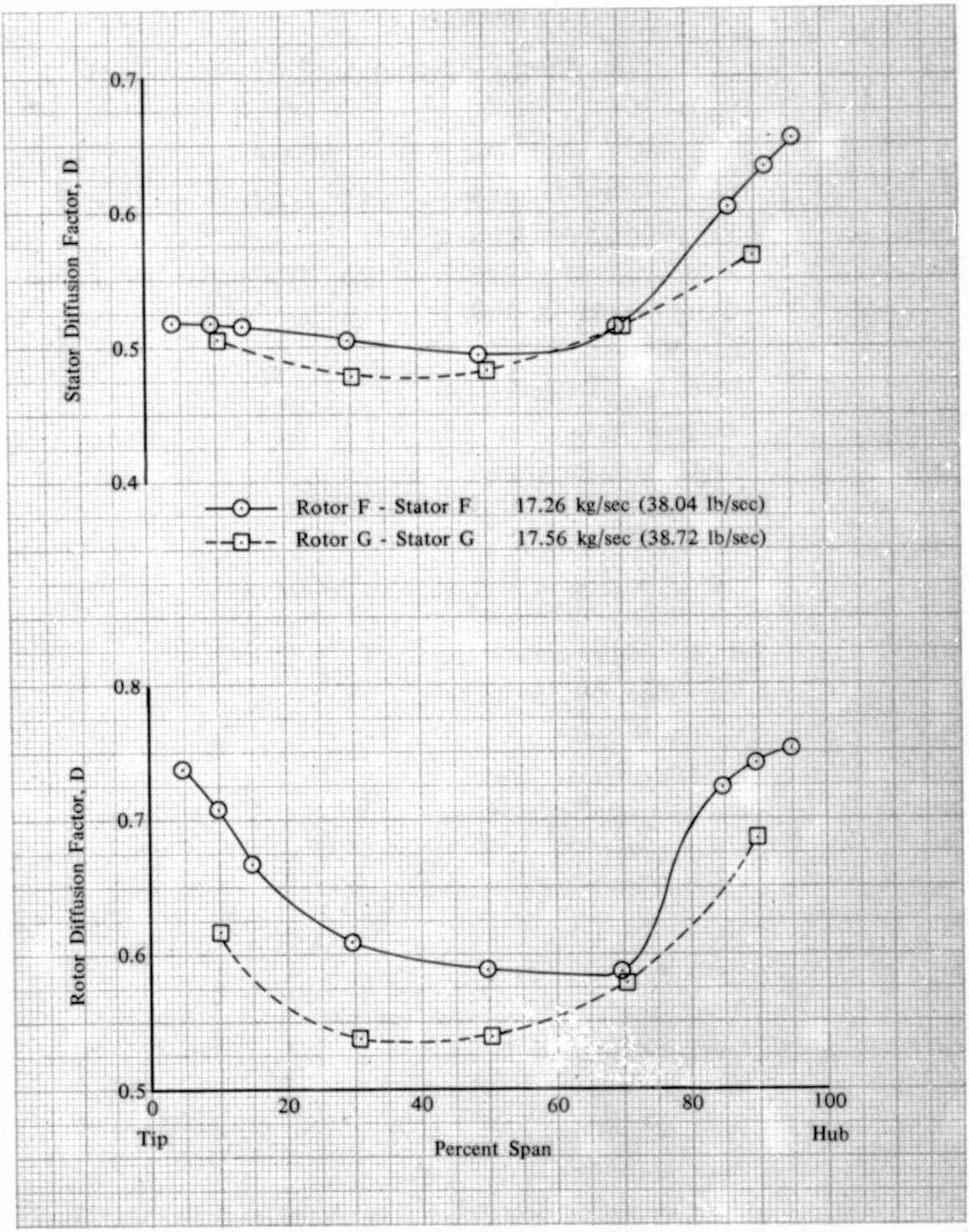


Figure 105. Spanwise Diffusion Factor Distributions for Rotor F-Rotor G and Stator F-Stator G DF 102303

## APPENDIX A

## DEFINITION OF SYMBOLS

| | |
|---|---|
| a | Maximum camber point position, MCA airfoil, cm (inches) |
| $a_o$ | Inlet relative stagnation velocity of sound, m/sec (ft/sec) |
| A | Flowpath annular area, $m^2$ ($ft^2$) |
| b | Maximum thickness point position, MCA airfoil, cm (inches) |
| c | Chord Length, cm (inches) |
| $c_p$ | Specific heat |
| d | Diameter, m (inches) |
| D | Diffusion factor |
| DCA | Double circular arc |
| E | Multiple of rotor frequency |
| $f(i_m)$ | Incidence parameter |
| $g_c$ | Gravitational acceleration, 1.00 kg-m/N-$sec^2$ (32.175 $lb_m$-ft/$lb_f$-$sec^2$) |
| HPC | High pressure compressor |
| ID | Inner diameter, m (inches) |
| IGV | Inlet guide vane |
| $i_m$ | Incidence angle, degree |
| K | Reduced velocity parameter |
| $K_T$ | Notch factor |
| LER | Leading edge radius, cm (inches) |
| M | Mach number |
| MCA | Multiple circular arc |
| N | Rotor speed, rpm |
| OD | Outer diameter, m(inches) |
| P | Total pressure, N/$cm^2$ (psi) |
| PR | Pressure ratio |
| p | Static pressure, N/$cm^2$ (psi) |
| R | Gas constant for air, 287.0 J/kg-°K (53.34 ft-$lb_f$/$lb_m$-°R) |
| r | Radius, m (inches) |
| SL | Stacking line |
| t | Blade maximum thickness, cm (inches) |
| T | Total temperature, °K (°R) |
| $T_s$ | Static temperature, °K (°R) |

| | |
|---|---|
| TER | Trailing edge radius, cm (inches) |
| U | Rotor speed, m/sec (ft/sec) |
| V | Velocity, m/sec (ft/sec) |
| W | Actual flowrate, Kg/sec ($lb_m$/sec) |
| $\alpha$ | Cone angle (angle of plane tangent to conic surface that approximates the design streamline of revolution), deg. |
| $\beta$ | Air angle, degrees from axial direction |
| $\gamma$ | Ratio of specific heats |
| $\gamma°$ | Blade-chord angle, degree from axial direction |
| $\delta$ | Ratio of total pressure to NASA standard sea level pressure of 10.1315 N/cm$^2$ (14.694 psia) |
| $\delta°$ | Deviation angle, degree |
| $\eta$ | Efficiency |
| $\theta$ | Ratio of total temperature to NASA standard sea level temperature of 288.17°K (518.7°R) |
| $\kappa$ | Blade metal angle, degree from axial direction |
| $\rho$ | Density, N/sec$^2$/m$^4$ ($lb_f$/sec$^2$/ft$^4$) |
| $\sigma$ | Solidity, chord divided by blade spacing (c/S) |
| $\phi$ | Blade camber angle, $\kappa_1 - \kappa_2$, degree or pressure rise coefficient |
| $\omega$ | Frequency, Hertz |
| $\bar{\omega}$ | Loss coefficient |
| $\bar{\omega}\cos\beta/2\sigma$ | Loss parameter |

Subscripts

| | |
|---|---|
| 0 | Compressor inlet (bellmouth) |
| 1 | Inlet guide vane inlet - Stage F |
| 1A | Inlet guide vane inlet, Upstream - Stage G |
| 1B | Inlet guide vane inlet, Downstream - Stage G |
| 2 | Inlet guide vane exit/rotor inlet - Stage F and Stage G |
| 3 | Rotor exit/stator inlet - Stage F and Stage G |
| 4 | Stator exit - Stage F |
| 4A | Stator exit, upstream - Stage G |
| 4B | Stator exit, downstream - Stage G |
| ad | Adiabatic |
| b | Bending |
| f | Front |

| | |
|---|---|
| id | Isentropic condition |
| m | Mean or mass |
| max | Maximum |
| min | Minimum |
| le | Leading edge |
| p | Polytropic |
| ref | Minimum loss |
| R | Rotor |
| s | Static condition |
| ss | Suction surface, leading edge |
| S | Stator |
| t | Torsional |
| te | Trailing edge |
| tip | Blade tip |
| z | Axial component |
| $\theta$ | Tangential component |

Superscripts:

| | |
|---|---|
| ' | Related to rotor blade |
| – | Mass average value |

## APPENDIX B

## DEFINITION OF VARIABLES

Incidence Angle:

Rotor: $i_m = \beta'_2 - \kappa_2$ Stator: $i_m = \beta_3 - \kappa_3$

Diffusion Factor:

$$\text{Rotor:} \quad D = 1 - \frac{V'_3}{V'_2} + \frac{d_3 V_{\theta 3} - d_2 V_{\theta 2}}{(d_2 + d_3)\sigma V'_2}$$

$$\text{Stator:} \quad D = 1 - \frac{V_4}{V_3} - \frac{d_4 V_{\theta 4} - d_3 V_{\theta 3}}{(d_3 + d_4)\sigma V_3}$$

Deviation Angle:

Rotor: $\delta^\circ = \beta'_3 - \kappa_3$ Stator: $\delta^\circ = \beta_4 - \kappa_4$

Loss Coefficient:

$$\text{Rotor:} \quad \overline{\omega}' = \frac{(P'_3)_{id} - P'_3}{\overline{P}'_2 - p_2}$$

where:

$$(P'_3)_{id} = P'_2 \left\{ 1 + \frac{\gamma - 1}{2} \left( \frac{U^2_3}{a'^2_{o_2}} \right) \left[ 1 - \left( \frac{d_2}{d_3} \right)^2 \right] \right\}^{\frac{\gamma}{\gamma - 1}}$$

$P'$ is found from $p/P' = \left[ 1 + \frac{\gamma - 1}{2} M'^2 \right]^{\frac{\gamma}{1 - \gamma}}$

and $M'$ is calculated using trigonometric functions and the measurements of U, $\beta$, P, and p.

$$\text{Stator:} \quad \overline{\omega} = \frac{P_3 - \overline{P}_4}{P_3 - p_3}$$

where:

$P_3$ = stator exit average freestream total pressure from wake rakes

$p_3$ = stator inlet static pressure calculated as described in data reduction procedures - Part 1

## DEFINITION OF VARIABLES (Continued)

**Equivalent Rotor Speed:**

$$N/\sqrt{\theta}$$

**Adiabatic Efficiency:**

Rotor: $$\eta_{ad} = \frac{\left(\overline{P}_3/\overline{P}_2\right)^{\frac{\gamma-1}{\gamma}} - 1}{\left(\overline{T}_3/288.2\right) - 1}$$

Rotor - Stator: $$\eta_{ad} = \frac{\left(\overline{P}_4/\overline{P}_2\right)^{\frac{\gamma-1}{\gamma}} - 1}{\left(\overline{T}_4/288.2\right) - 1}$$

IGV-Rotor-Stator, i.e., Stage: $$\eta_{ad} = \frac{\left(\overline{P}_4/\overline{P}_1\right)^{\frac{\gamma-1}{\gamma}} - 1}{\left(\overline{T}_4/288.2\right) - 1}$$

**Polytropic efficiency:**

Rotor: $$\eta_p = \frac{\frac{\gamma-1}{\gamma}\ln\left(\overline{P}_3/\overline{P}_2\right)}{\ln(\overline{T}_3/288.2)}$$

Rotor-Stator: $$\eta_p = \frac{\frac{\gamma-1}{\gamma}\ln\left(\overline{P}_4/\overline{P}_2\right)}{\ln(\overline{T}_4/288.2)}$$

IGV-Rotor-Stator, i.e., Stage: $$\eta_p = \frac{\frac{\gamma-1}{\gamma}\ln\left(\overline{P}_4/\overline{P}_1\right)}{\ln\left(\overline{T}_4/288.2\right)}$$

**Pressure Ratio:**

Rotor: $$\frac{\overline{P}_3}{\overline{P}_2}$$

## DEFINITION OF VARIABLES (Concluded)

Rotor-Stator: $\dfrac{\overline{P}_4}{\overline{P}_2}$

IGV-Rotor-Stator, i.e., Stage: $\dfrac{\overline{P}_4}{\overline{P}_1}$

Equivalent Flow:

$$\frac{W\sqrt{\theta}}{\delta}$$

Momentum Thickness Parameter:

Rotor: $$\frac{\overline{\omega}' \cos \beta'_3}{2\sigma} \left( \frac{\cos \beta'_3}{\cos \beta'_2} \right)^2$$

Stator: $$\frac{\overline{\omega} \cos \beta_4}{2\sigma} \left( \frac{\cos \beta_4}{\cos \beta_3} \right)^2$$

Peak Efficiency Surge Margin:

Rotor: $$\left[ \left[ \left( \frac{\overline{P}_3}{\overline{P}_2} \right) \Big/ \frac{W\sqrt{\theta}}{\delta} \right]_{surge} \Big/ \left[ \left( \frac{\overline{P}_3}{\overline{P}_2} \right) \Big/ \frac{W\sqrt{\theta}}{\delta} \right]_{\eta_{ad\ max}} \right] - 1$$

Rotor-Stator: $$\left[ \left[ \left( \frac{\overline{P}_4}{\overline{P}_2} \right) \Big/ \frac{W\sqrt{\theta}}{\delta} \right]_{surge} \Big/ \left[ \left( \frac{\overline{P}_4}{\overline{P}_2} \right) \Big/ \frac{W\sqrt{\theta}}{\delta} \right]_{\eta_{ad\ max}} \right] - 1$$

Pressure Rise Coefficient:

$$\text{Rotor, } \phi_R = J g_c \frac{c_p T \left[ \left( \frac{\overline{P}_3}{\overline{P}_2} \right)^{\frac{\gamma - 1}{\gamma}} - 1 \right]}{U_m^2}$$

$$\text{Rotor-Stator, } \phi_{R-S} = J g_c \frac{c_p T \left[ \left( \frac{\overline{P}_4}{\overline{P}_2} \right)^{\frac{\gamma - 1}{\gamma}} - 1 \right]}{U_m^2}$$

where T is NASA standard sea level temperature, i.e., 288.17°K (518.7°R)

## REFERENCES


1. "Aerodynamic Design of Axial Flow Compressor," (Revised), NASA SP-36, 1965.

2. Brent, J. A., J. G. Cheatham, and D. R. Clemmons, "Single-Stage Experimental Evaluation of Tandem-Airfoil Rotor and Stator Blading for Compressors, Part V - Analysis and Design of Stages D and E," NASA CR-121008, FR-5212, December 1972.

3. Brent, J. A., "Single-Stage Experimental Evaluation of Tandem-Airfoil Rotor and Stator Blading for Compressors, Part II - Data and Performance for Stage A," NASA CR-120804, PWA FR-4719, July 1972.

4. Steinolfson, R. S., Memo to B. A. Jones, "Secondary Flow and Axial-Velocity Ratio Corrections to 2-D Turning in Axial-Flow Compressor Blade Rows," 12 April 1971.

5. Schwenk, F. C., and G. W. Lewis, "Experimental Investigation of Transonic Axial Flow Compressor Rotor with Double Circular Arc Airfoil Blade Sections," Part III, NACA RME55F01, 25 July 1955.

6. Monsarrat, N. T., and M. T. Keenan, "Experimental Evaluation of Transonic Stators, Preliminary Analysis and Design Report," NASA CR-54620, 1967.

7. Keenan, M. J., K. G. Harvey, and G. A. Bogardus, "Experimental Evaluation of Transonic Stator, Data and Performance Report MCA Stator A," NASA CR-54621, 1968.

8. Keenan, M. J., and J. A. Bartok, "Experimental Evaluation of Transonic Stator, Data and Performance Report MCA Stator B," NASA CR-54622, 1968.

9. Monsarrat, N. T., M. J. Keenan, and P. C. Tramm, "High-Loading Low-Speed Fan Study, Design," NASA CR-72536, 28 July 1969.

10. Messenger, H. E., and E. E. Kennedy, "Two Stage Fan Aerodynamic and Mechanical Design," NASA CR-120859, January 1972.

11. Sulam, D. H., M. J. Keenan, and J. T. Flynn, "Single-Stage Evaluation of Highly-Loaded, High-Mach-Number Compressor Stages, Data and Performance MCA Rotor," NASA CR-72694, July 1970.